ASD-TDR-63-767

FINAL REPORT ON MANUFACTURING METHODS AND DESIGN PROCEDURES OF BRAZED REFRACTORY METAL HONEYCOMB SANDWICH PANELS

TECHNICAL DOCUMENTARY REPORT No. ASD-TDR-63-767

NOVEMBER 1963

ADVANCED FABRICATION TECHNIQUES BRANCH
MANUFACTURING TECHNOLOGY DIVISION
AND STRUCTURES DIVISION
FLIGHT DYNAMICS LABORATORY

AERONAUTICAL SYSTEMS DIVISION
AIR FORCE SYSTEMS COMMAND
UNITED STATES AIR FORCE
WRIGHT-PATTERSON AIR FORCE BASE, OHIO

ASD Project No. 7-937

(Prepared under Contract AF 33(657)-7276 by
Martin Marietta Corporation, Baltimore 3, Maryland;
J. W. McCown, C. R. Wilks, L. J. Gagola, A. Norton, M. Schwartz)

NOTICES

When Government drawings, specifications, or other data are used for any purpose other than in connection with a definitely related Government procurement operation, the United States Government thereby incurs no responsibility nor any obligation whatsoever; and the fact that the Government may have formulated, furnished, or in any way supplied the said drawings, specifications, or other data, is not to be regarded by implication or otherwise as in any manner licensing the holder or any other person or corporation, or conveying any rights or permission to manufacture, use, or sell any patented invention that may in any way be related thereto.

Qualified requesters may obtain copies of this report from the Defense Documentation Center (DDC), (formerly ASTIA), Cameron Station, Bldg. 5, 5010 Duke Street, Alexandria 4, Virginia

This report has been released to the Office of Technical Services, U.S. Department of Commerce, Washington 25, D.C., in stock quantities for sale to the general public.

Copies of this report should not be returned to the Aeronautical Systems Division unless return is required by security considerations, contractual obligations, or notice on a specific document.

300 - January 1964 - 162-22-392

FOREWORD

This Final Technical Documentary Report covers all work performed under Contract AF33(657)-7276 from 20 November 1961 to 20 September 1963. The manuscript was released by the authors on 20 September 1963 for publication as an ASD Technical Documentary Report.

This contract with the Martin Marietta Corporation, Baltimore, Maryland, was initiated under ASD Manufacturing Technology Division Project 7-937, "Manufacturing Methods for Brazed Refractory Metal Honeycomb Sandwich Panels." It was administered under the direction of B. E. Price, Manufacturing Technology Division, Advanced Fabrication Techniques Branch (ASRCT-4) and P. P. Plank, Flight Dynamics Laboratory, Structures Division (ASRMS-23).

Mr. James W. McCown of Martin Marietta's Structures and Materials Department was the engineer in charge. Others who cooperated in the research and in the preparation of this report were: C. R. Wilks, L. J. Gagola, A. M. Norton, J. F. Hughes, and M. J. Brown of the Structures and Materials Department; M. M. Schwartz, D. Buttermore, M. Wasilisin, C. Wirsing, C. Jenkins, P. D. Jacobson and J. Broderick, Advanced Manufacturing Technology Department; J. Miller and H. Kern, Quality Engineering Department.

All photomicrographs in this report reduced approximately 60% in reproduction.

ABSTRACT
Technical Documentary Report

ASD-TDR-63-767
20 September 1963

Final Report on the Manufacturing
Methods and Design Procedures of Brazed
Refractory Metal Honeycomb Sandwich Panels (U)

J. W. McCown
et al
Martin Marietta Corporation

Manufacturing methods and design procedures were developed for fabricating details and vacuum brazing of TZM (Mo-0.5Ti-0.07Zr) molybdenum and D-36 (Cb-10Ti-5Zr) columbium alloy honeycomb sandwich panels. These included the marforming of thin sheet, the welding and finishing of honeycomb core and the high temperature vacuum brazing of honeycomb sandwich panels. Panels simulating a heat shield and a structural application on aerospace vehicles were designed, fabricated and tested at temperatures up to 2600°F. The capability of fabricating, coating and utilizing brazed columbium sandwich panels on aerospace vehicles, with the required design procedures for application at temperatures up to 2400°F, was demonstrated. Only partial success was achieved with the TZM molybdenum alloy, because of the manufacturing problems created by severe welding problems, encountered in edge sealing of TZM panels. All joints could be electron beam welded, but sporadic cracking upon cooling could not be eliminated. The trouble was considered to stem from high weld restraint and metallurgical incompatibilities in braze alloy--TZM weldments.

- -

This report has been reviewed and is approved.

FOR THE COMMANDER:

JACK R. MARSH
Asst. Director
Manufacturing Technology Division
Air Force Materials Laboratory

W. A. SLOAN, JR., Col. USAF
Chief, Structures Division
Flight Dynamics Laboratory

CONTENTS

CONTENTS (continued)

I. INTRODUCTION

In the past, one key to success in aircraft development, and which now appears to be equally important in aerospace vehicle development, is the capability to design and fabricate high efficiency structures. Honeycomb construction, developed to provide maximum stiffness at a low weight, represents such a structure. It has been highly developed and widely applied using adhesive bonded aluminum. The advent of supersonic vehicles resulted in the requirement for structures to operate at 600° to 800° F. Brazed titanium and stainless steel honeycomb were developed to meet these requirements and are now in production.

Recently the advent of hypersonic and lifting re-entry vehicles has increased the desired operational temperatures to where only the refractory metals are feasible. This limitation has stimulated an extensive research and development effort in the field of refractory metal technology. Most of this effort has been extended toward the production of better alloys and oxidation protection coatings. Several laboratories have made independent studies toward developing braze alloys for refractory metals, but no concentrated effort had previously been made toward developing the complete technology for brazed sandwich panel fabrication of the refractory alloys.

Many problems had to be solved before such brazed systems could be successfully fabricated and proved acceptable for service on flight vehicles. These included braze alloy development, honeycomb core fabrication, braze tool and process development, oxidation protection coating development, and destructive testing to determine design properties and capabilities.

The state of the art in refractory metals and oxidation protection coatings had developed to the degree that it was appropriate for this program to be undertaken to develop the required brazing and associated technology for fabrication of practical honeycomb sandwich panels. The following pages present the results of such a program.

II. SUMMARY

A program was conducted to establish manufacturing methods and to develop design procedures for brazed refractory metal sandwich panels. The panel configurations selected were representative of two different structural concepts for aerospace vehicles; one was representative of a monocoque or semimonocoque application, the other represented a modular heat shield for a double-walled application.

Test panels were fabricated from D-36 (Cb-10Ti-5Zr) columbium and TZM (Mo-0.5Ti-0.07Zr) molybdenum. Thompson-Ramo-Wooldridge's Cr-Ti-Si oxidation protective coating was used on the D-36 panels, Pfaudler's PFR-6 coating on the TZM panels.

In addition to evaluating conventional braze alloys, a study was performed to develop higher remelt temperature braze alloys for vacuum brazing TZM and D-36. A Ti-8.5Si alloy showed considerable promise for TZM. This alloy could be brazed at 2550° F and, with proper diffusion heat treatment, it exhibited a remelt temperature above 3000° F. However, further development will be required for application to panel brazing. Palladium base alloys proved unsatisfactory for both TZM and D-36. Haynes 25 was selected as the braze alloy for the TZM structural panels and B-120 VCA titanium for all D-36 panels. No methods were developed for brazing TZM heat shield panels which would achieve the desired temperature capabilities.

Procedures were developed for welding and finishing TZM and D-36 honeycomb core. D-36 core was resistance welded with copper tooling. Special tools and techniques were developed for electron beam welding TZM core. D-36 core was finished by conventional sawing and sanding techniques. Diamond saw blades were required to cut the TZM core, and it was necessary to heat the TZM core to 200° F during sanding.

Marform techniques were developed for forming double stepped pans of TZM and D-36 for the heat-shield panel facings. The D-36 forming was done at room temperature, the TZM at 300° F.

U-channels were formed and welded into square frames for the structural panel edge members. The miter corner joints were electron beam welded. A special welding and stress relieving cycle was required to prevent cracking of TZM edge member frames.

Test panels (12 inches by 12 inches) were brazed in a high temperature vacuum furnace with ZrO_2 as a braze stop-off. Hard refractory metal tooling was used to support the panels during brazing. Electron beam welding was employed to edge-seal the D-36 structural panels and to install special load attachment strips. Special techniques were developed and design modifications made to seal the D-36 heat-shield panels.

Severe welding problems were encountered in edge sealing and in installing the load attachment strips to the TZM panels. About 50 different procedures were tried in unsuccessful attempts to solve these problems. All joints could be welded, but sporadic cracking upon cooling could not be eliminated. The trouble was considered to stem from high weld restraint and metallurgical incompatibilities in braze alloy-TZM weldments.

TZM heat-shield panels were not fabricated for test because material embrittlement, resulting from brazing well above the recrystallization temperature of the material, was so severe that the structural integrity of the panels would be inadequate for handling and meaningful test.

Edgewise shear and compression tests at room and elevated temperatures were accomplished on D-36 structural panels. Special test fixtures and systems were designed and assembled for these tests. Edgewise compression tests of coated TZM panels were attempted, but were unsuccessful because of the brittleness of the braze joints.

D-36 heat shield panels were tested in a dynamic hot gas environment at temperatures up to 2600° F. Panels successfully withstood exposures to temperatures up to 2400° F without coating failure.

Small specimens, cut from unfailed portions of the panels, were tested in a high temperature vacuum furnace to determine the honeycomb core properties. Special configuration tensile specimens were fabricated and coated for determining the fatigue properties of the facing materials at temperatures up to 2800° F.

The test results indicate that it is possible to design and fabricate columbium panels which have the required structural and thermal integrity for aerospace vehicle application. However, further development will be required before molybdenum alloys can be utilized for such an application.

III. MATERIALS AND COATINGS

Program requirements included the selection of one molybdenum and one columbium alloy, and an oxidation protective coating for each material. The material selections were basically limited to those which were immediately available, but strict insistence on previous production experience in thin sheet and foil gages would have restricted alloy selection seriously. Consideration was also given to alloys which had not been rolled to these gages in production quantities, where producers could provide assurance that no significant problems were expected and that schedule requirements could be met.

Alloys and coatings were reviewed in the literature (Refs. 1 through 31)* and in discussions with technical personnel of both the producers and other laboratories. The selections were based on information available during the first month of the program.

A. MATERIALS SURVEY AND SELECTION

1. Molybdenum Alloys.

Two molybdenum alloys were considered: Mo-0.5Ti and TZM (Mo-0.5Ti-0.07Zr). The tensile strengths of these alloys as a function of temperature are shown in Fig. 1. The directly comparable data which were available were obtained on bar rather than sheet, but they served to illustrate the higher strength and improved temperature resistance to recrystallization of the TZM alloy compared to Mo-0.5Ti.

Resistance to recrystallization was the primary consideration in the selection of the molybdenum alloy, contingent on availability in thin sheet and foil gages, to provide the best attainable temperature capabilities in the test panels. TZM was the more desirable alloy for service above 2000° F, if it could be obtained in the required gages. At the start of the program, only the Mo-0.5Ti alloy had been rolled to these gages in production quantities, but foil rolling of TZM had been demonstrated. The TZM alloy was selected for the program.

Material	Form	Data Source
TZM	Sheet	GE
TZM	Bar	Climax
Mo-0.5Ti	Bar	Climax
TZM	Sheet	Climax (suggested sheet specification)

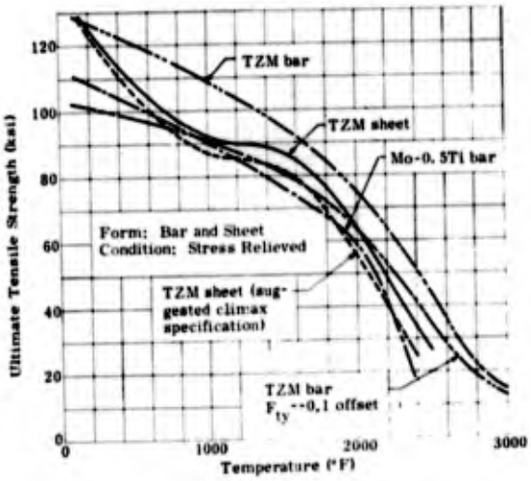

Fig. 1. Ultimate Tensile Strength Versus Temperature--Selected Molybdenum Alloys

2. Columbium Alloys

Six columbium alloys were considered: Cb-752 (Cb-10W-5Zr), F-48 (Cb-15W-5Mo-1Zr), FS-82 (Cb-33Ta-0.75Zr), D-14 (Cb-5Zr), D-36 (Cb-10Ti-5Zr), and B-33 (Cb-4V). The tensile strength and strength-to-weight data which were available on the six alloys are compared in Figs. 2 and 3.

Structurally, the stronger alloys were of primary interest, but the requirement for thin sheet and foil gages eliminated them from further consideration. Such gages were definitely beyond the state of the art for F-48. No insurmountable problems were envisaged for rolling these gages in Cb-752, but three to five months of development effort prior to production were anticipated.

Selection of the columbium alloys was thus restricted to the moderate strength alloys. These included FS-82 (Cb-33Ta-0.75Zr), D-14 (Cb-5Zr), D-36 (Cb-10Ti-5Zr) and B-33 (Cb-4V). Because similar strength-to-weight ratios characterize these alloys in the temperature range of interest (2100° to 2800° F), this factor could be largely discounted in the final alloy se-

*References will be found in Section XI.

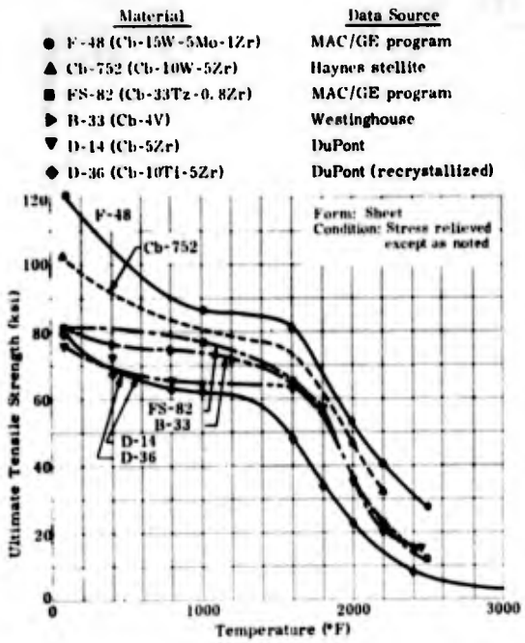

Fig. 2. Ultimate Tensile Strength Versus Temperature--Selected Columbium Alloys

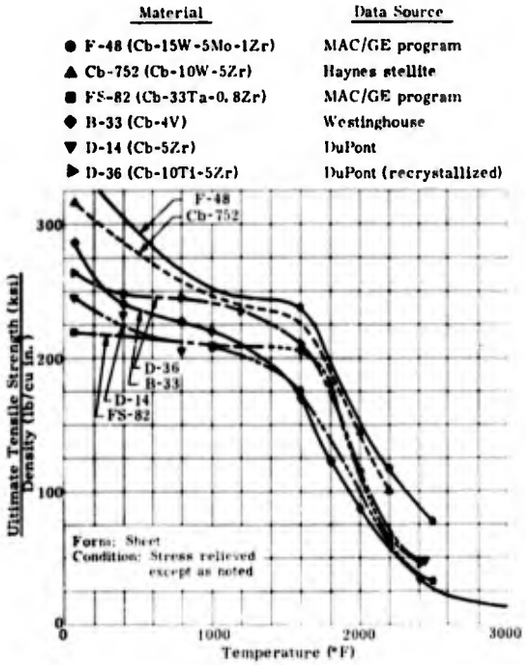

Fig. 3. Strength/Density Versus Temperature--Selected Columbium Alloys

lection. All of these alloys could be made in thin sheet and foil gages, but this has been accomplished only on a limited scale, except for the "older" FS-82 alloy. However, no real problems were anticipated for the other alloys.

FS-82 had the advantage of greater user and producer experience, but the lower densities of the new alloys (0.28 to 0.306 lb/cu in.) compared to FS-82 (0.37 lb/cu in.) enhanced their attractiveness, particularly where minimum gages characterized design. The heat shield panels were in this category; the lower density alloys provided a weight saving of 17 to 24% compared to FS-82.

The D-36 (Cb-10Ti-5Zr) was selected for the program. The improved oxidation coating capability of the alloy associated with its high titanium content was a dominant selection factor.

B. COATINGS SURVEY AND SELECTION

No attempt was made to review in detail all of the coating systems which were being developed for the protection of molybdenum and columbium alloys. A preliminary survey revealed that many of these were not pertinent to program requirements or were not sufficiently advanced for hardware application. A primary requirement was the availability of facilities adequate to coat 12- by 12-in. panels (16- by 16- in. with load attachment strips for structural panels).

1. Molybdenum Coatings

Coatings for molybdenum, applicable in the temperature range of interest on this program, were primarily silicides or complex silicides obtained by alloying with metallic additions. Such coatings included Pfaudler PFR-6 (Refs. 20 and 24), Vought II and IV (Ref. 22), Chromalloy W-2 (Refs. 22 and 29) and Chromizing Corporation Durak MG (Ref. 22). Sylcor 40S (Refs. 25 and 26), an Al-Sn coating system, was also considered.

The silicide types were generally proprietary coatings, applied by pack cementation. Comparative data for test conditions similar to those planned for this program were limited, but the reported performance of these coatings was considered to be generally adequate for the contemplated test

program. The Al-Si coating system, developed by Sylcor for tantalum, appeared also to have good potential for molybdenum. Coating reliability was more difficult to assess, particularly with reference to the correlation of test data on coupon-type specimens with performance on full-scale parts.

Pfaudler, Chromalloy and Sylcor responded to inquiries and indicated that facilities were available for coating the test panels. The Pfaudler PFR-6 coating, which was also being used on the High Temperature Fastener Program (AF33(616)-8104) at Republic Aviation Corporation, was selected for this program.

2. Columbium Coatings

Applicable coating systems for columbium were, as in the case of molybdenum, largely based on the use of silicides for protection. The systems were, in general, more involved, with multilayers of complex chemistry quite common. Such coatings included several developed by Pfaudler (Ref. 24), an experimental Chromalloy coating (Ref. 29), Chromizing Corporation K-S (Ref. 22), Thompson-Ramo-Wooldridge Cr-Ti-Si (Refs. 17 and 28), and Vought ICb and IICb (Ref. 27). The General Electric Al-Cr coating LB-2 (Ref. 6) was also considered.

Comparative data on the performance of six columbium coatings were reported on an ASD coating evaluation study (Ref. 17), with several of the coatings reportedly improved since the study was completed, The Thompson-Ramo-Wooldridge Cr-Ti-Si coating performed best under the test conditions employed in this study. The Pfaudler columbium coatings were not included.

Pfaudler, Chromalloy and Chromizing Corporation responded to inquiries and indicated that facilities were available for coating the test panels. Thompson-Ramo-Wooldridge indicated that new and larger facilities had already been planned and would be completed in time for the program. General Electric facilities were unavailable because of prior commitments.

The Thompson-Ramo-Wooldridge Cr-Ti-Si coating, which was also being used on the High Temperature Fastener Program (AF33 (616)-8104) at Republic Aviation Corporation, was selected for this program.

C. PROGRAM MATERIALS

1. TZM Panel Materials

The TZM molybdenum material was obtained from Universal Cyclops Steel Corporation. This included 0.002-in. foil, 0.008-, 0.012-, 0.025- and 0.040-in. sheet, and 5/16-in. tooling plate.

The material was purchased to Martin specification MMS 1633; pertinent chemical and mechanical property requirements are shown in Tables 1 and 2. Tensile requirements applied to sheet and strip ($\geq$ 0.006 in.) in the stress-relieved condition. The bend ductility requirement for sheet and strip up to 0.040 in. in thickness was a 2t radius bend through an angle of 105° at 65° to 85° F. A longitudinal flat bend on itself without cracking was required for foil gages (< 0.006-in. thickness). While more stringent flatness requirements were desired, actual requirements were limited generally to AMS 2242 (Tolerances, Corrosion and Heat Resistant Alloys, Sheet, Strip and Plate) to obtain vendor acceptance of the specification. The AMS 2242 variation from flat had to be further increased to 3/4 in. for material under 0.030 in. in thickness.

Table 1 summarizes the chemical compositions of the TZM heats from which the material for this program was processed. Mechanical properties are summarized in Table 2. Check tests made on one heat (KDTZM-518A) were in reasonable agreement with Universal Cyclops data.

Although the measured total tensile elongation of this sheet material ranged from 6 to 17%, Universal Cyclops indicated that the uniform elongation was considerably lower, on the order of 3%, and that the material was highly notch sensitive. Both of these limitations had to be considered in the fabrication of parts. Particularly important was edge preparation to remove any flaws which might be produced during shearing or cutting operations, to avoid cracking and brittle fracture during subsequent fabrication.

Universal Cyclops encountered major difficulties in the production of the 0.002-in. foil material. Initial deliveries were made approximately 2-1/2 months after promised dates, with subsequent deliveries to com-

TABLE 1

TZM Molybdenum Heat Analyses Reported by Universal Cyclops Steel Corporation

Heat Number	Chemical Analysis Ti%	Zr%	Fe%	Ni%	Si%	C%	O%	N%	H%	Mo%	Material Gages (in.)
Specification	.40 .55	.06 .12	.010 max	.002 max	.008 max	.010 .040	.003 max	.002 max	.001 max	Balance	
(MMS 1633) KDTZM											
-489A	.47	.11	.003	.001	.002	.040	.002	.002	.0001	Balance	.012
-518A	.47	.07	.002	.001	.001	.031	.002	.002	.0003	Balance	.012, .025
-741B	.44	.09	.005	.001	.004	.020	.0008	.0004	.0003	Balance	.008
-742B	.46	.09	.005	.002	.004	.021	.001	.0006	.0003	Balance	.008
-771B	.51	.06	.002	.001	.004	.027	.001	.0003	.0003	Balance	.008
-933A	.45	.11	.008	.002	.0035	.020	.0007	.0004	.0001	Balance	.312
-934B	.43	.09	.001	.001	.0035	.021	.002	.0002	.0001	Balance	.312
-936A	.46	.12	.0015	.002	.0035	.028	--	--	--	Balance	.002
-938A	.48	.11	.001	.001	.003	.032	.002	.0002	.0001	Balance	.040
-964	.48	.10	.0015	.003	.0035	.027	.002	.0003	.0002	Balance	.002

TABLE 2

TZM Molybdenum Sheet and Plate

Mechanical Properties Reported by Universal Cyclops Steel Corporation

Heat Number	Gage Thickness (in.)	Test Direction	Yield Strength (0.2% offset) (psi)	Ultimate Tensile Strength (psi)	Elongation in 2 Inches (%)	Room Temperature 105° Bend[a]	Vickers Hardness
Specification (MMS 1633)		Longitudinal	140,000 max	150,000 max	8 min	--	--
		Transverse	140,000 max	150,000 max	6 min	--	--
KDTZM -489A	0.012	Longitudinal	123,900	138,900	13.0	--	--
		Longitudinal	122,900	135,300	9.3	--	--
		Transverse	115,500	143,800	9.3	--	--
		Transverse	113,800	142,100	6.4	--	--
-518A	0.012	Longitudinal	118,200	135,400	13.5	--	--
		Longitudinal	121,000	137,500	10.5	--	--
		Transverse	136,800	141,900	11.5	--	--
		Transverse	130,500	140,800	10.5	--	--
518A*	0.012	Longitudinal	107,900	130,900	12.0	--	--
		45 deg	113,200	121,200	19.0	--	--
		Transverse	127,000	138,500	11.0	--	--
-518A	0.025	Longitudinal	122,800	140,300	14.5	2t	--
		Longitudinal	119,300	136,700	17.6	2t	--
		Transverse	128,900	145,300	11.3	2t	--
		Transverse	125,900	142,400	13.8	2t	--
-741B	0.008	Longitudinal	113,000	128,400	12.9	2t	--
		Longitudinal	113,900	132,300	17.4	2t	--
		Transverse	138,200	143,200	6.3	2t	--
		Transverse	136,400	143,100	8.7	2t	--
-742B	0.008	Longitudinal	106,900	124,600	14.8	2t	--
		Longitudinal	108,600	125,300	*10.0	2t	--
		Transverse	139,300	144,300	8.7	2t	--
		Transverse	132,500	140,300	8.5	2t	--
-771B	0.008	Longitudinal	108,600	131,000	11.4	2t	--
		Longitudinal	102,800	132,900	15.5	2t	--
		Transverse	128,200	141,700	9.3	2t	--
		Transverse	121,200	142,700	8.1	2t	--
-933A	0.312	Longitudinal	107,300	124,000	15.1	--	272
		Transverse	123,500	133,500	16.2	--	279
-934B	0.312	Longitudinal	112,300	130,300	17.1	--	284
		Transverse	127,400	138,500	13.4	--	267
-938A	0.040	Longitudinal	105,200	132,200	12.9	2t	--
		Longitudinal	101,600	129,300	13.4	2t	--
		Transverse	126,500	145,000	14.9	2t	--
		Transverse	126,600	143,700	11.3	2t	--

plete the order spread over a four-month period. The bend ductility of the foil was good. The majority of the material was flat with a minor herringbone surface finish pattern.

Sheet flatness was excellent, with no evidence of "oil-canning" which would have prevented the facing materials from making complete intimate contact with the core during panel brazing.

In the initial forming operation on the 0.008-in. material to produce double-step pans for heat shield facings, it became apparent that there was considerable variation in the fabricability of the material. Some sheets could be formed satisfactorily into pans; others, formed by identical procedures, would fracture or wrinkle at the panel corners. Visual examination provided no clue as to the cause of the difficulty. Some strangely appearing streaks were revealed by radiographic inspection, but these could not be correlated with the failure areas. Fabrication uniformity was significantly improved by stress-relieving in vacuum at 2200° F for one hour prior to forming. Sheets processed in this manner were formed with good corners. Subsequent stress-relieving and forming operations proved equally satisfactory. It was concluded that, even though this material was procured in the stress-relieved condition, the vendor operation was not sufficient to produce the necessary uniformity for these severe forming requirements.

2. D-36 Panel Materials

The D-36 columbium material was obtained from E. I. duPont deNemours and Company. This included 0.002-in. foil, 0.008-, 0.010-, 0.012-, 0.025- and 0.040-in. sheet, and 5/16-in. tooling plate.

The material was purchased to Martin specification MMS 1691; pertinent chemical and mechanical property requirements are shown in Tables 3 and 4. Tensile requirements applied to sheet and strip in the fully recrystallized condition. Foil (< 0.006-in. thick) was supplied in the as-rolled condition, and it was required that it have sufficient bend ductility to withstand a longitudinal flat bend on itself without cracking. While more stringent flatness requirements were desired, actual requirements were limited generally to AMS 2242 to obtain vendor acceptance of the specification. The AMS 2242 variation from flat had to be further increased to 3/4 in. for material under 0.030 in. in thickness.

Table 3 summarizes the chemical compositions of the D-36 heats from which the material for this program was processed. Mechanical properties are summarized in Table 4.

While the specification flatness requirements for sheet were met, the 0.008-in. D-36 columbium sheet exhibited sufficient waviness to cause problems in test panel brazing. The 0.008-in. material was marformed into double-step pans for the heat-shield panels. Even after the high pressure forming process, there was sufficient excess material in some facings to prevent complete intimate contact with the honeycomb core during the panel brazing operation. This caused blistered or unbrazed areas to remain on the panel after brazing. The blisters, which were found only on flat heat-shield panels, occurred along two adjacent panel edges.

A hot creep-flattening operation was attempted on several of the 0.008-in. heat shield facings. Each was placed in the brazing tool with additional pressure applied by tungsten weights, and the assembly was heated to 2200° F for one hour in vacuum. This "flattened" the sheet, but it also revealed the problem of excess material which caused blisters during the brazing process. Small blisters or "oil cans" appeared in the material at the same locations as were encountered during brazing. To remove the waviness or oil canning from the material by hot creep flattening, sufficient pressure would have had to be used to cause a compressive stress great enough to cause the material to creep. This was not possible, because the maximum pressure which could be obtained by dead weight loading was limited to about 1/2 psi.

No method was found for flattening these sheets. The problem was resolved by selecting a braze alloy system with sluggish flow characteristics to permit larger gaps to be bridged and acceptable, void-free panels to be produced.

3. TZM Molybdenum Bolts and Nuts

Four hundred TZM molybdenum shear-type bolts and nuts were procured from Voi Shan Manufacturing Company for attachment of shear test panels (flat structural panels) to the picture frame test jig. These fasteners were 1/4-in. diameter with 25 threads per inch. The threads on both the bolts and nuts were rounded for coating purposes, and there was extra clearance between the threads to allow for coating build-up. The PFR-6 coating was applied to the

TABLE 3

D-36 Columbium Heat Analyses
Reported by E. I. duPont de Nemours and Company

Heat Number	Chemical Analysis							Material Gages (in.)
	Ti%	Zr%	C%	O%	N%	H%	Cb%*	
Specification	9.0	4.0	0.01	0.04	0.01	0.0015	Balance	--
(SMS 1691)	11.0	5.0	maximum	maximum	maximum	maximum	Balance	--
36-002	11.0	4.7	0.0066	0.0425	0.0013	0.0022	Balance	0.002
36-097-02	10.5	4.9	0.0057	0.0317	0.0022	0.0015	Balance	0.025
36-098-03	10.5	4.8	0.0031	0.0214	0.0021	0.0004	Balance	0.040
36-099-02	10.6	4.8	0.0060	0.0230	0.0018	0.0015	Balance	0.025
36-099-03	10.5	4.4	0.0022	0.0213	0.0021	0.0004	Balance	0.040
36-100-01	10.5	4.9	0.0036	0.0207	0.0026	0.0005	Balance	0.025
36-100-02	10.6	4.9	0.0037	0.0233	0.0014	0.0001	Balance	0.025
36-142	10.3	4.6	0.0050	0.0183	0.0023	0.004	Balance	0.012
36-142-01	9.9	4.5	0.0048	0.0178	0.0021	0.0001	Balance	0.040
36-142-02	9.2	4.5	0.0050	0.0139	0.0020	0.0001	Balance	0.040
36-144-01	9.8	4.7	0.0024	0.0174	0.0013	0.0001	Balance	0.025
36-144-03	10.0	4.9	0.0024	0.0166	0.0017	0.0001	Balance	0.025
36-165-01	9.4	5.2	0.0039	0.0117	0.0024	0.0011	Balance	0.002
36-168	10.1	5.0	0.0035	0.0155	0.0023	0.0002	Balance	0.008
36-128	10.0	4.8	0.0074	0.0185	0.0014	0.0002	Balance	0.012, 0.040
36-168-01	9.9	4.7	0.0097	0.0247	0.0010	0.0017	Balance	0.002
36-168-04	10.3	5.3	0.0167	0.0419	0.0012	0.0022	Balance	0.002
36-308T086	9.6	5.4	0.0060	0.0237	0.0023	0.0002	Balance	0.010

*Columbium and tantalum plus trace impurities.

TABLE 4

D-36 Columbium Sheet and Plate

Mechanical Properties
Reported by E. I. duPont de Nemours and Company

Number	Gage Thickness (in.)	Test Direction	Yield Strength (0.2% offset) (psi)	Ultimate Tensile Strength (psi)	Elongation in 2 Inches (%)
Specification (SMS 1691)		Longitudinal	60,000 minimum	70,000 minimum	17 minimum
		Transverse	60,000 minimum	70,000 minimum	17 minimum
36-097-02	0.025	Longitudinal	66,400	74,200	24.0
		Transverse	68,200	76,700	24.0
36-098-03	0.040	Longitudinal	64,800	72,800	26.2
		Transverse	66,400	74,000	25.3
36-099-02	0.025	Longitudinal	67,200	74,200	25.0
		Transverse	68,200	74,300	26.1
36-099-03	0.040	Longitudinal	63,700	74,200	25.0
		Transverse	66,900	74,300	25.0
36-100-01	0.025	Longitudinal	65,600	71,800	26.0
		Transverse	66,400	73,400	25.0
36-100-02	0.025	Longitudinal	66,300	73,600	23.7
		Transverse	64,300	72,800	24.7
36-142	0.012	Longitudinal	63,600	72,300	22.9
		Transverse	63,800	71,000	19.0
36-142-01	0.040	Longitudinal	65,300	74,000	27.3
		Transverse	66,000	73,700	25.3
36-142-02	0.040	Longitudinal	66,500	73,300	26.1
		Transverse	65,100	74,600	28.2
36-144-01	0.025	Longitudinal	64,500	72,000	26.0
		Transverse	64,100	72,200	26.3
36-144-03	0.025	Longitudinal	65,400	72,100	27.5
		Transverse	66,900	73,900	26.0
36-168	0.012	Longitudinal	65,300	71,200	25.0
		Transverse	68,000	75,400	27.0
36-168	0.040	Longitudinal	67,800	74,200	34.0
		Transverse	68,700	73,900	33.0
36-168	0.008	Transverse	63,800	71,500	24.4
36-169	0.312	Longitudinal	Not reported		
		Transverse	Not reported		
36-308-T086	0.010	Transverse	70,300	78,100	19.8

bolts and nuts by Pfaudler. Figures 4 and 5 show cross-sectional photomicrographs of the threads of a coated bolt and nut, respectively.

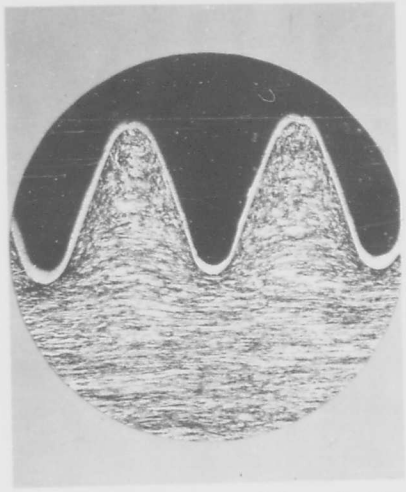

Fig. 4. Photomicrograph of Cross Section of Pfaudler PRF-6 Coated TZM Molybdenum Bolt Thread (75X)

Fig. 5. Photomicrograph of Pfaudler PFR-6 Coated TZM Molybdenum Nut (75X)

In general, these fasteners performed satisfactorily in tests. Most of the bolts were used as many as three times. In most cases, after two or three test exposures, the coating on the threads would become damaged to the extent that the TZM molybdenum would start to oxidize. During the thermal testing cycle, about 5 to 10% of the nuts would freeze to the bolts to such an extent that the bolts had to be broken to remove them from the test jig.

No incompatibility was noted between the Pfaudler PFR-6 coated TZM molybdenum bolts and nuts and the Thompson-Ramo-Wooldridge Cr-Ti-Si coated D-36 columbium test panels. The maximum temperature reached in the shear-strip attachments, where the fasteners were located, was about 1700° F. Actual panel test temperatures ranged up to 2400° F.

4. Recrystallization Behavior of TZM

Brazing studies in Phase I of the program were principally conducted on a small quantity of 0.013-in. thick TZM sheet received from Universal Cyclops prior to delivery of the material for test panel fabrication in Phase II. The Phase I material could be brazed at 2550° F for 15 minutes or at 2600° F for 5 minutes without recrystallization. The TZM molybdenum brazing studies were largely predicated on this behavior, since maximum brazing temperatures, consistent with avoidance of deleterious recrystallization effects, were desired to obtain optimum structural test panel capability.

Late in the brazing development study program, Phase II material was received. This material was found to be considerably less resistant to recrystallization than the Phase I stock and required a major change in the brazing temperature requirements which had previously governed the development work, if recrystallization was to be avoided. This had a major impact on the higher remelt temperature braze alloy studies.

Recrystallization studies which were made on both the Phase I and Phase II materials are summarized in Table 5 and presented graphically in Figs. 6 to 8. The studies encompassed reheating temperatures from 2200° to 2600° F and reheating times of 15, 30 and 60 minutes. Representative microstructures of the Phase II material

are shown in Figs. 9 and 10. No change in microstructure of the as-received 0.008- and 0.012-in. thick Phase II material was evident after 15 minutes at 2300° F. Evidence of slight recrystallization can be noted after 15 minutes at 2400° F. These gages were significantly recrystallized after 15 minutes at 2500° F.

Long-term structural capability for TZM in thin sheet form appears limited to 2200° to 2300° F unless processing schedules can be modified to provide more resistance to recrystallization. Original estimates had suggested that extended exposure to 2400° F without recrystallization might be possible. These estimates were based principally on the reported behavior of TZM bar material and on the short-time capabilities at 2550° to 2600° F of the 0.013-in. Phase I material. The Phase I material was deceptive to the extent that it could be exposed to short-time brazing cycles at these higher temperatures without recrystallization, yet had no long-term capability at 2400° F (cf. Table 5). With this additional information and the data on Phase II material, the original estimates were clearly optimistic.

TABLE 5

TZM Molybdenum Recrystallization Studies

Reheating Temperature (°F)	Reheating Time (min)	Phase I: Percent Recrystallization, 0.013-in. Sheet	Phase II: Percent Recrystallization, 0.008-in. Sheet (Heat T71B)	Phase II: Percent Recrystallization, 0.012-in. Sheet (Heat 516A)	Phase II: Percent Recrystallization, 0.025-in. Sheet (Heat 516A)	Phase II: Percent Recrystallization, 0.040-in. Sheet (Heat 936A)
2200	15		< 5	< 5		
2300	15		< 10	< 10		
2300	60		10	10		
2400	15		< 10	12		
2400	30	< 5*	30	20	< 5	< 2
2400	60	25*	85	75	15	10
2500	15		70	60		
2500	30	60*	90	85	60	60
2500	15	< 5**				
2600	5	< 5**				
2600	15		100	100	95	80

*Previously heated to 2700°F - 15 minutes (brazing studies)

**Brazing studies

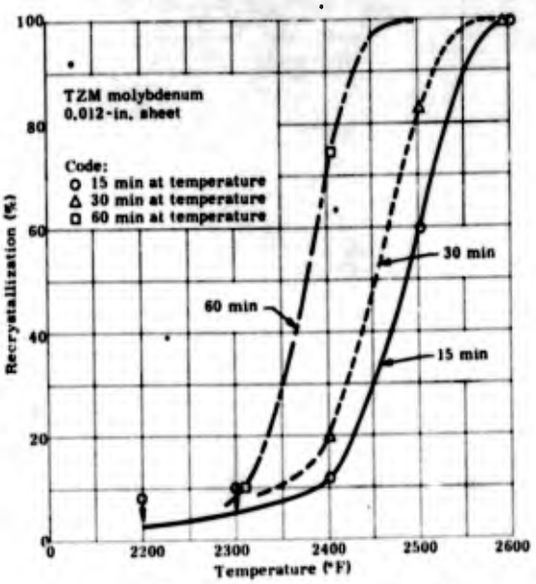

Fig. 7. Effect of Reheating Temperature and Time on Recrystallization of 0.012-in. TZM Molybdenum Sheet

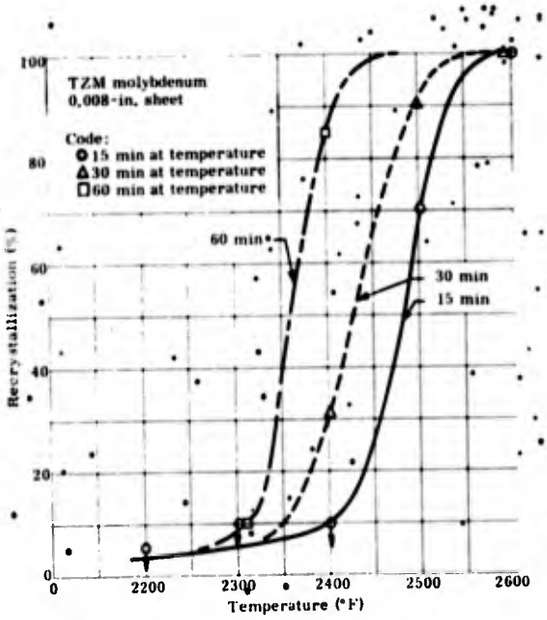

Fig. 6. Effect of Reheating Temperature and Time on Recrystallization of 0.008-in. TZM Molybdenum Sheet

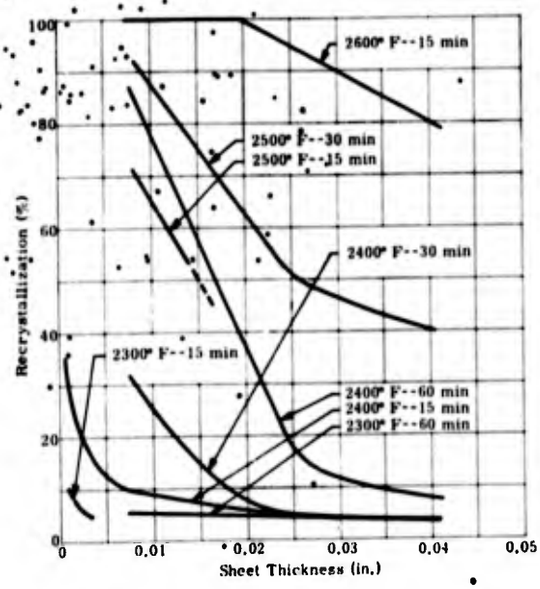

Fig. 8. Extent of Recrystallization of TZM Molybdenum Alloy Versus Sheet Thickness for Several Thermal Cycles

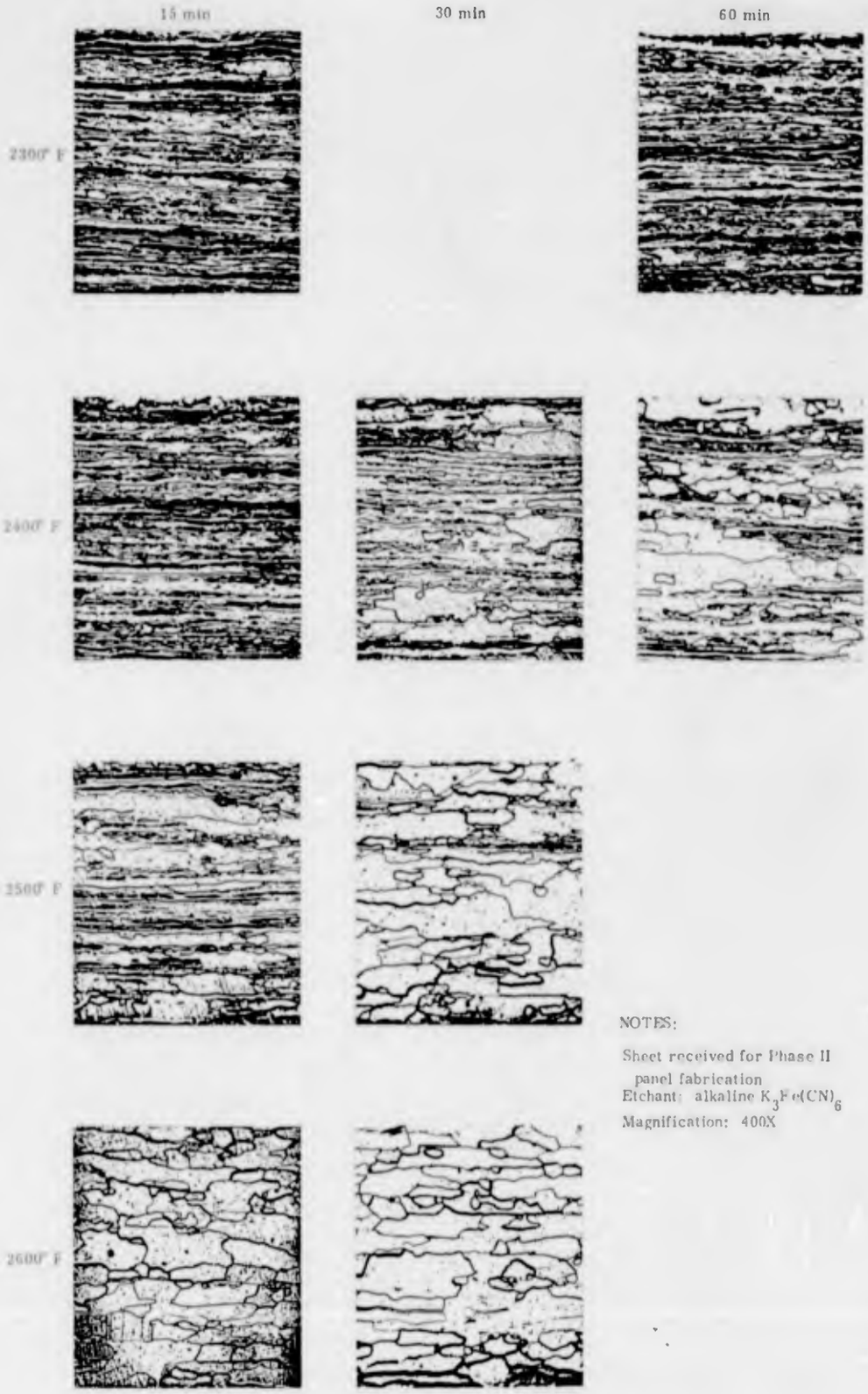

NOTES:

Sheet received for Phase II panel fabrication
Etchant: alkaline $K_3Fe(CN)_6$
Magnification: 400X

Fig. 9. Recrystallization Behavior of 0.008-in. TZM Sheet Versus Temperature and Time

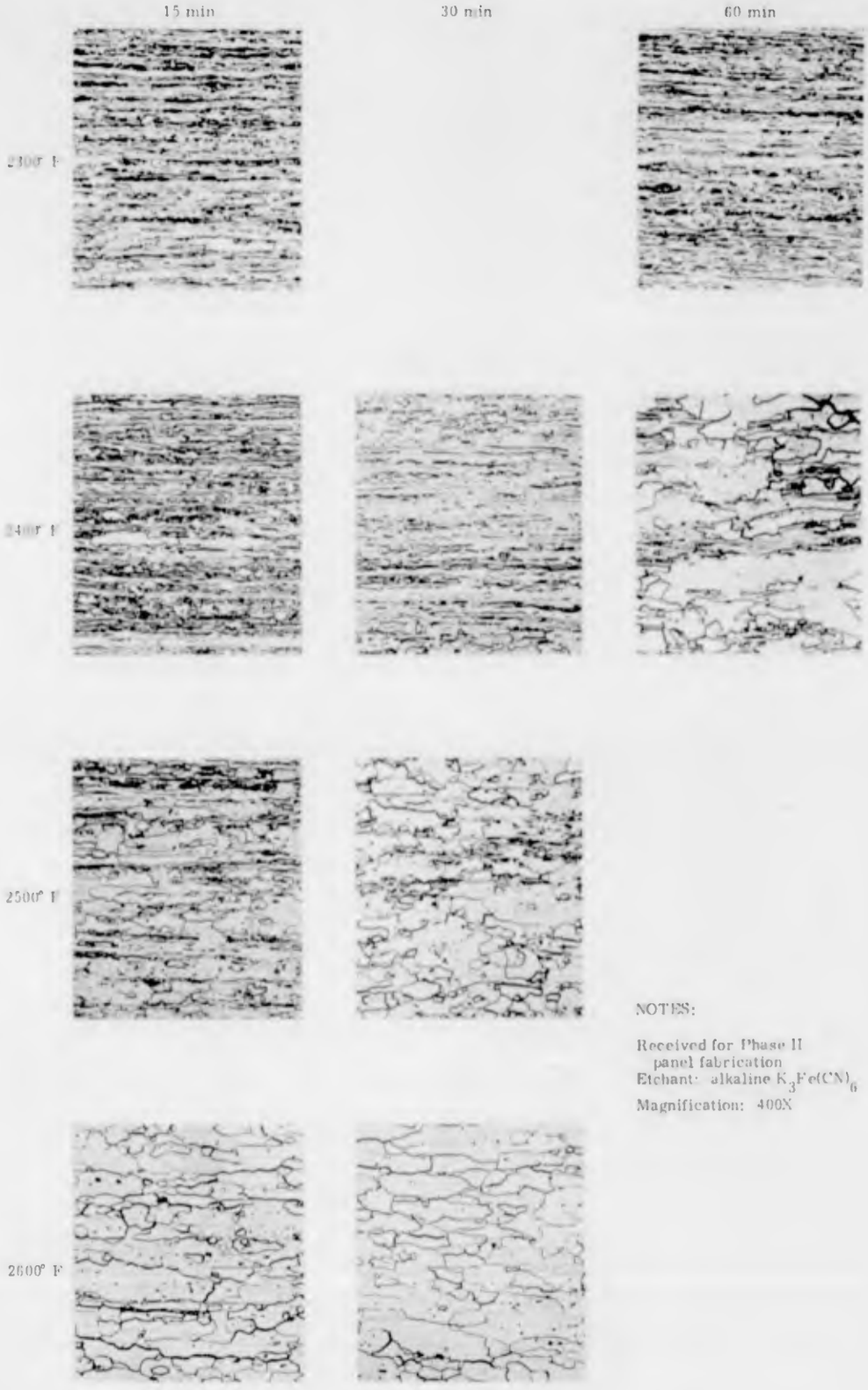

NOTES:

Received for Phase II panel fabrication
Etchant: alkaline $K_3Fe(CN)_6$
Magnification: 400X

Fig. 10. Recrystallization Behavior of 0.012-in. TZM Sheet Versus Temperature and Time

IV. PRELIMINARY DESIGN AND ANALYSIS STUDY

The purpose of the preliminary design and analysis study was to establish the test panel configurations. While a primary requirement was that these configurations be suitable for testing, they should also be representative of aerospace vehicle application. The test panels were designed to simulate two different types of vehicle applications:

(1) A load-carrying structural application for utilization as monocoque or semimonocoque structure.

(2) A modular-type radiation heat shield for a double-walled structural concept.

A. DESIGN CRITERIA

1. Structural Panels

In a monocoque structural application, the panels are subjected to in-plane loads due to the internal pressure requirements, flight maneuver loads and lateral loads due to aerodynamic pressures. Of the resulting panel stresses, the most severe design condition occurs when compression and shear loads are applied to the panels. These conditions, coupled with the panel size, provide the design requirements, such as thickness and strength, for the honeycomb core. No specific design conditions were available for the structural panels; these conditions are peculiar to the particular vehicle configuration, location and load factors. To provide a design that would simulate an actual application, a panel facing thickness representative of a structural application on a high lift reentry vehicle was arbitrarily selected. With the facing thickness fixed, an optimum core thickness could then be determined.

The edge members for the structural panels must also be representative of a practical application, yet suitable for testing. To meet these requirements, a U-channel edge member was selected because it represented a joint suitable for either welding or bolting.

Structural panel application temperatures are limited by the strength and ductility of the material, but, in general, panels should be capable of operation to temperatures of 2200° to 2400° F for aerospace application.

2. Heat Shield Panels

In a heat shield application, panel structural design is controlled by lateral pressure requirements. To provide a design that would be representative of a high lift re-entry vehicle application, a design condition of 1.2 psi at 3000° F was provided by ASD. With this condition fixed, the structural design could be determined.

The edges of the heat shield panels presented a peculiar design problem. The primary design requirements were to provide:

(1) A slip joint which will prevent entry of the hot boundary layer gases to the insulation area.

(2) A minimum weight design.

These could be best achieved by using a stepped joint with the step an integrally formed part of the panel facing. This provided the sealing requirements as well as a minimum weight design.

The panel supports should allow the panel to expand freely, with a minimum of thermal stresses generated in the panel. No particular effort was made to minimize heat transfer through the clip or to provide a support clip that represented an optimum design.

B. MATERIAL PROPERTIES

To accomplish the design study at the required time, it was necessary to select basic material performance data from available information. This information was used to establish facing strength and moduli, as well as a basis for predicting honeycomb core properties. Subsequent phases of the program determined these data experimentally.

1. Facing Properties

The material tensile strengths (Refs. 11 and 17) used for test panel design were those for D-36 sheet and TZM bar (Figs. 1 and 2). Ultimate shear strengths were estimated to be 50% of the ultimate tensile strength, and ultimate compressive strengths were assumed equal to the ultimate tensile strengths.

The stability design of the test panel required the use of an effective modulus of elasticity for design in the elastoplastic region. The effective modulus used in this study was

$$E' = \frac{2EE_t}{E + E_t}$$

where

E = Young's modulus of elasticity

E_t = tangent modulus of elasticity.

To determine the effective modulus at the temperatures required in test panel design, stress-strain curves at various temperatures were required. Stress-strain curves were reported up to 2400° F for TZM (Ref. 17). Young's modulus values were provided for D-36 by ASD, but stress-strain data were not available. Predicted stress-strain curves for D-36 were based on Young's modulus and the modulus and strengths at 0.001- and 0.002-in. strain and ultimate strengths reported (Ref. 11). The shape of the curves was chosen to be similar to that reported for FS-82 (Ref. 5).

2. Honeycomb Core Properties

The mechanical properties of D-36 columbium and TZM molybdenum honeycomb cores were predicted by means of simple theoretical formulas. The cores used for the test panel were square-cell welded honeycomb. Reduction factors were applied to core material properties to provide a reasonable margin of safety in core strength.

Honeycomb core densities were calculated from

$$\rho_c = \frac{2t_c}{s}\rho \qquad (1)$$

where

t_c = honeycomb foil thickness

s = honeycomb cell size (distance between parallel faces)

ρ = material density.

The shear strength of the honeycomb core was calculated from the formula

$$F_s = \frac{\rho_c}{\rho} F_{su} \qquad (2)$$

where

F_{su} = shear strength of the honeycomb core material.

The shear strength of the material was assumed to be 50% of the tensile yield strength at 0.1% offset for TZM, and 50% of the ultimate tensile strength for D-36. The yield rather than the ultimate strength of TZM was used to compensate for loss of properties because of partial recrystallization of the highly worked foils in subsequent fabrication. Although the shear strength should actually be closer to 60% of the tensile strength, a 50% factor was used to provide for other contingencies. For example, Eq (2) assumes that the honeycomb cell walls remain rigid to failure and do not buckle in a tension field web effect. In most honeycomb cores, the tension field web effect occurs prior to failure. Thus, the equation will generally indicate higher strength values than can be obtained in test. Also, the amount of braze node flow can vary the core shear strengths considerably.

The flatwise compressive strength of the honeycomb core was calculated from the equation

$$F_g = \frac{\rho_c}{\rho} F_{cy} \qquad (3)$$

where

F_{cy} = compressive yield strength of the honeycomb core material.

For the reasons previously discussed, the compressive yield strength of the material was assumed to be equal to tensile yield strength at 0.1% offset for TZM and equal to the tensile ultimate strength for D-36. Equation (3) will yield only approximate values for the flatwise compressive strength of the honeycomb core. In the equation it is assumed that the honeycomb cell walls remain rigid to failure, although the core wall will actually buckle at a fairly low stress and the material in the core nodes will take most of the load. The amount of braze node flow usually balances out the loss due to buckling.

The honeycomb core shear modulus was calculated from the equation

$$G_c = 0.6\frac{t_c}{s} G \qquad (4)$$

where

G = modulus of rigidity of the honeycomb core material.

The modulus of rigidity was derived from the relationship:

$$G = \frac{E}{2(1+\mu)}$$

where

Poisson's ratio μ was assumed to be 0.3.

Equation (4) gives only an approximate core shear modulus. The amount of braze node flow can make as much as a 50% difference in the core shear modulus. This not only makes the core shear modulus difficult to predict, but makes it almost impossible to get consistent test data for evaluation. The core shear modulus is one of the most important parameters in honeycomb design. To allow for unpredictable errors, a reduction factor of 0.6 is used in Eq (4) to provide honeycomb design values. The selection of this factor was based on the use of the equation with stainless steel core.

The flatwise compressive modulus of the honeycomb core was calculated from the equation

$$E_c = 0.4 \frac{\rho_c}{\rho} E \qquad (5)$$

where

E_c = modulus of elasticity of the honeycomb core material.

This formula generally gives spuriously high moduli because of the early buckling of the honeycomb cell walls. Again, for design purposes, a reduction factor of 0.4 is used.

The welded square-cell honeycomb core used for the test panel was assumed to be isotropic within the plane of its faces, a reasonable assumption for honeycomb core of this type. The nodal flow of the braze alloy decreases the variation of the core properties with ribbon direction. In general, this variation is within the normal scatter of results in honeycomb sandwich panel tests.

C. DESIGN PROCEDURES

In this discussion of the design procedures and information required for the structural design of the test panels, the information is presented in summary, and the major design curves and procedures are referenced from MIL-HDBK-23.

1. General Instability

The general design equation for panels with isotropic faces of similar material of equal thickness is

$$F_{cr} = \frac{\pi^2}{4} \frac{K}{\lambda} \left(\frac{h}{b}\right)^2 E' \qquad (6)$$

where

F_{cr} = critical stress

$K = K_f + K_m$

K_f = theoretical coefficient dependent on facing stiffness and panel aspect ratio

K_m = theoretical coefficient dependent on sandwich bending and shear rigidities and panel aspect ratio

$\lambda = 1 - \mu^2$

E' = effective compressive modulus of elasticity.

A direct solution of Eq (6) was impossible because of the dependency of E' on F_{cr}. To allow for a direct solution, the equation was modified to:

$$\frac{F_{cr}}{E'} = \frac{\pi^2 K}{4\lambda} \left(\frac{h}{b}\right)^2 \qquad (7)$$

The left side of Eq (7) is a function of the material properties and the right side is essentially a function of the panel geometry.

The general instability (Eq (7)) is applicable either to shear instability or compression instability. This is accomplished by using the proper coefficient "K" for either shear or compression. For determination of K, the test panels were assumed to have simply supported ends and edges, and an aspect ratio of 1.0. For the test panels, K_f was sufficiently small so that it was assumed to be equal to zero. The coefficient K_m is a function of the panel aspect ratio and the parameter

$$V = \frac{\pi^2 t_c t_f E'}{2\lambda b^2 G_c}$$

as given in Part III of MIL-HDBK-23.

The following iterative procedure was used to determine the required value of effective panel depth, h, to stabilize the panel. Curves required for the determination of K from V are given in Part III of MIL-HDBK-23. The term V was initially assumed to be zero and K was determined. Then Eq (7) was used to determine the value of h. Convergence was obtained in a few cycles of iteration.

Design plots were made for both shear and compression instability. These plots (Figs. 11 and 12) showed critical stress divided by panel weight versus core thickness at various temperatures. These plots were originally made using the rather limited material property data available in Phase I of the program. As a part of Phase III of the program, the basic theory (Eq (6)), utilizing the material properties obtained in Phase II, was compared with the actual panel test data.

A honeycomb panel failing in compression or shear instability will sometimes have a final failure in the form of a shear crimp (Fig. 13). This is a result of the panel buckling in short wave length, submitting the weak core to high shear stress. The core will fail in shear, relieving the stress in the facings. This will usually allow the remainder of the panel to return to its original shape, leaving the shear crimp as the only apparent failure. To ensure against this type of failure, the panels were designed to be stable at ultimate load.

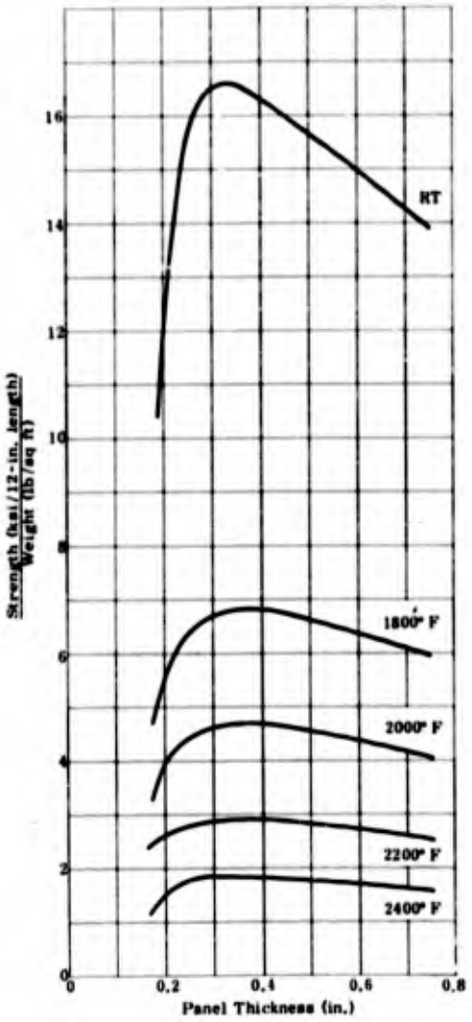

Fig. 11. D-36 Columbium--Strength-Weight Versus Panel Thickness (0.012-in. facing thickness)

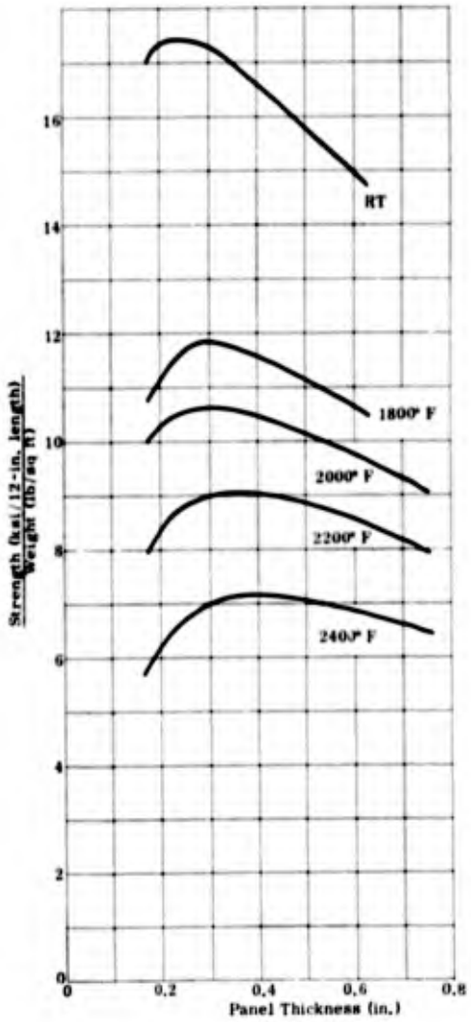

Fig. 12. TZM Molybdenum--Strength-Weight Versus Panel Thickness (0.012-in. facing thickness)

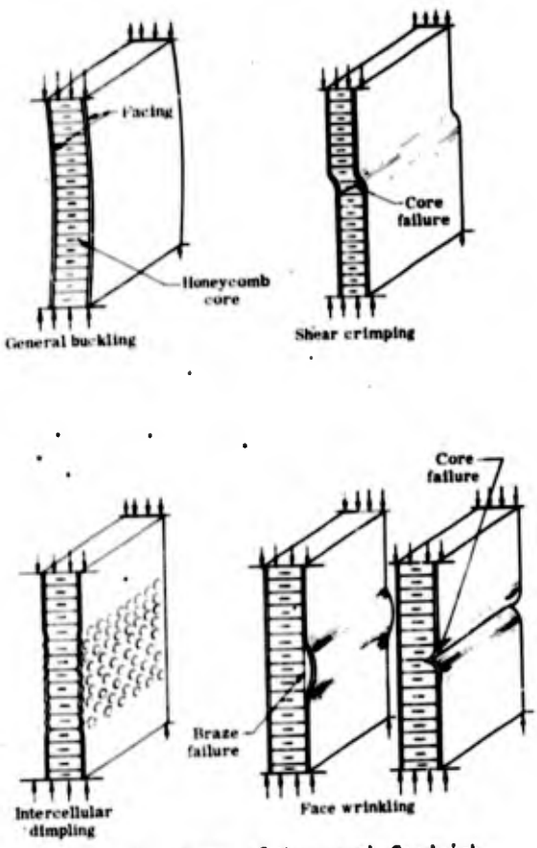

Fig. 13. Types of Honeycomb Sandwich Panel Failure

2. Local Instability

A local instability failure occurs when the braze or core fails, causing the facings to buckle at some limited or local area in the panel. This occurs because of a large core cell size, a weak honeycomb core or a weak braze alloy strength. The two basic types of failure that can occur are described below.

a. Intercellular dimpling

An intercellular dimpling failure occurs when the facing sheet buckles within the cell (Fig. 13). This type of failure is associated with thin skin and/or large core cell size. The critical facing stress at which dimpling will not occur is given by the equation

$$\frac{F_{c_{cr}}}{E'} = \frac{2}{\lambda}\left(\frac{t_f}{s}\right)^2 \qquad (8)$$

where

t_f = facing thickness

s = core cell size

$\lambda = 1 - \mu^2$.

This empirical equation represents a best fit curve to the available test data and is recommended in Part III of MIL-HDBK-23.

b. Face wrinkling

A face wrinkling failure occurs when the braze or core strength is insufficient to stabilize the facings. This type of failure usually occurs in a small local area, with the face buckling into the core if the core strength is insufficient, or with the facing buckling away from the core if the braze strength is insufficient (Fig. 13). This type of failure is associated with low braze or core strength. There are no completely acceptable design procedures for face wrinkling. The current recommendation in MIL-HDBK-23 calls for test to establish face wrinkling strength.

The face wrinkling strength is dependent on the braze strength and core compressive strength, and is directly dependent on the size of the braze fillet. Braze fillet affects the face wrinkling strength in two ways: first, by giving more braze contact area to resist tension, and, secondly, by adding better support to the honeycomb core so that it may be stressed to a higher load prior to buckling. It is exceedingly difficult to obtain uniform fillet size from panel to panel, making it almost impossible to obtain controllable test results with which an acceptable empirical equation could be written. Exactly what mechanism causes the first failure is also unknown. A usual case is where a thin face sandwich panel starts to have elastic or plastic dimpling of the facings. This causes increased stress in the core and braze alloy, which leads to a face wrinkling failure, while the original failure mechanism was that of intercellular dimpling.

Since there were no acceptable procedures to design for face wrinkling (between the time the panel design effort was completed and work reported in Chapter VII performed, Hoff's (Ref. 42) equation was approved for presentation in MIL-HDBK-23), the best practice was to make the ratio of the core density to facing thickness similar or larger than that found on brazed panels where there are sufficient data. If the core and braze strength are sufficiently high, the facing can be stressed to well above the yield strength before failure occurs. The problem was to determine "sufficiently high core strength." The core strength can be increased by using a denser or stronger core,

but, for a given temperature and braze alloy, the only way to increase the braze fillet strength is to decrease the core cell size, thus increasing the braze contact area.

A 3/16-in. square cell honeycomb core made from 0.002-in. thick foil was chosen for the test panel design. This was designed to provide sufficient core strength to prevent a local instability failure from crushing the core.

3. Thermal Stress

An investigation was conducted to determine the capability of a sandwich panel to withstand thermal stress caused by a thermal gradient through the panel. A configuration of a continuous sandwich panel over simple supports was assumed such as would be found on a vehicle surface of panels with moment continuity across supports at spars or bulkheads.

The following conditions were assumed:

(1) The covering was heated uniformly over the surface. Consequently, the only thermal gradient was through, not along, the sandwich panels. The thermal stresses, therefore, resulted only from the difference in uniform temperature between the inner and outer sandwich facings.

(2) Thermal bending of the sandwich panel was prevented by the clamped-edge effect of the moment continuity between adjacent panels.

(3) The supporting substructure did not prevent the heated panel from expanding in its plane. The compressive forces in the hotter outer facing were equilibrated by equal and opposite forces in the colder inner facing. Since the inner and outer facings both have the same thickness, their stresses were equal and opposite.

(4) Poisson's ratio "μ" was independent of strain and temperature and equal to 0.3 for both facings.

(5) The facings had isotropic material properties.

(6) There were no loads applied to the panel; hence, the stresses were only those resulting from the temperature distribution.

The plane-stress equations were written as

$$\epsilon_{x_{total}} = \alpha \Delta T + \frac{1}{E_S} (\sigma_x - \mu \sigma_y)$$

where

α = linear coefficient of thermal expansion (in./in. °F)

ΔT = difference between facing temperature and 70° F

E_S = secant modulus of the stress-strain curve of a facing at its specified temperature (psi).

Due to isotropy of the facings, their constraints and their temperatures,

$$\sigma_y = \sigma_x.$$

The total strains for the inner and outer facings became

$$\epsilon_i = \alpha_i \Delta T_i + (1 - \mu) \frac{\sigma_i}{E_{S_i}} \qquad (9a)$$

and

$$\epsilon_o = \alpha_o \Delta T_o + (1 - \mu) \frac{\sigma_o}{E_{S_o}}. \qquad (9b)$$

respectively.

The total strain of the inner facing equaled that of the outer facing according to assumption (2) above, so that Eqs (9a) and (9b) could be equated. The stress of the inner facing was equal and opposite to that of the outer facing, by assumption (3). Equations (9a) and (9b) were accordingly combined to give the thermal stress equation:

$$\sigma_o = - \left(\frac{E_{S_o} E_{S_i}}{E_{S_o} E_{S_i}} \right) \left[\frac{\alpha_o \Delta T_o - \alpha_i \Delta T_i}{1 - \mu} \right] \qquad (10)$$

Since E_{S_o} and E_{S_i} were functions of the strains, σ_o was not directly solvable from Eq (10). Equation (10) was solved by trial-and-error application of the stress-strain curves of the inner and outer facings at their various temperatures. The results were plotted as curves of stress versus outer facing

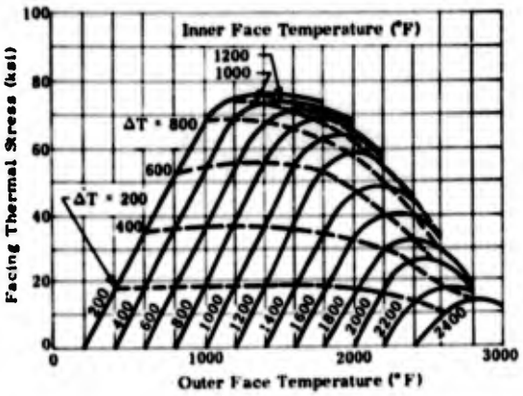

Fig. 14. Thermal Stress--TZM Molybdenum Honeycomb Sandwich Panels

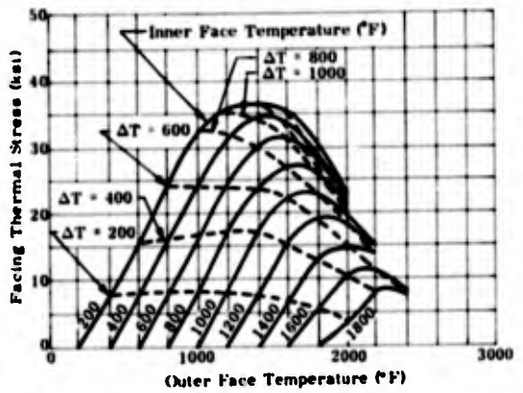

Fig. 15. Thermal Stress--D-36 Columbium Honeycomb Sandwich Panels

temperature for various inner facing temperatures in Figs. 14 and 15 for TZM and D-36, respectively.

It may be seen from Figs. 14 and 15 that the thermal stresses did not become high enough to rupture the inner facing. However, the stresses in the outer facing caused inelastic strains at the higher temperatures, which may be sufficiant to cause inelastic intercellular dimpling.

The panel thickness did not enter the thermal stress equation. However, the thermal strain differential ($\alpha_o \Delta T_o - \alpha_i \Delta T_i$) is greater for thicker panels, so it is expected that greater thermal stresses would occur in thicker panels.

D. TEST PANEL DESIGN

The structural test panel designs are shown in Drawings SK 46841 and SK 46842 of Appendix A of this report. The heat shield designs are shown in Drawings SK 46843 and SK 46844. The test panels were designed for simplicity and to simulate actual aerospace vehicle application.

A 0.5-in. core thickness for the structural test panels was selected because:

(1) This thickness was sufficient to stabilize the panels for shear and compression testing.

(2) Strength-to-weight studies indicate this core thickness to be near optimum (Figs. 11 and 12).

(3) Estimation of all factors and past experience indicates that any increase of core thickness over approximately 0.5 in. would have little, if any, effect on the test panel strength.

To minimize tooling cost and to provide an excellent comparison between TZM molybdenum and D-36 columbium, the test panel designs were identical for both alloys.

The heat shield panels were designed with support clips and access holes similar to those used by Bell in their double-walled structures program (Ref. 32). The holes in the panels are necessary to provide access to attachment fasteners to enable loosening of the fasteners for panel removal. These clips were preassembled and brazed with the panel.

All exposed braze joints and open panel edges were to be welded to seal the panels and protect the braze alloy.

E. TEST PANEL ANALYSIS

1. Structural Panels

The compression-test panels were designed to be stable to a compressive stress equal to ultimate tensile strength of the facing material (Figs. 1 and 2). Because of the testing at high temperature, either local instability or face wrinkling (with the face buckling away from the core) was considered to be the critical mode of failure. The shear-test panels were considered critical in the same manner.

The lack of sufficient material property data made it impossible to predict the ultimate strengths of the test panels accurately. Since there were no aerospace vehicle loads available with which to compare the strengths, margins of safety were not determined for the structural panels.

The critical dimpling stresses as calculated were lower than the general instability stress. The lowest critical stress was felt to be local stability or face wrinkling with a braze failure allowing the facing to buckle away from the core.

2. Heat Shield Panels

The primary structural load in the heat shield panel is caused by the dynamic pressure on the outer surface. This air pressure causes bending stress in the panel and shear and compression stress in the honeycomb core. A method of stress analysis for the heat shield panel was developed and is presented in Appendix B.

For test panel design purposes, a 1.2-psi airload of 3000° F was assumed. The following critical stresses were obtained:

(1) Facing stress: f_c = 3000 psi (Appendix B).

(2) Core stress: f_g = 50 psi (compression), f_s = 35 psi (shear).

The allowable stresses as could best be determined for this condition were:

(1) Facing stress:

TZM: F_{cy} = 6500 psi

D-36: F_{cu} = 3200 psi.

(2) Core stress:

Compression

TZM: F_g = 390 psi

D-36: F_g = 100 psi.

Shear

TZM: F_s = 180 psi

D-36: F_s = 50 psi.

The D-36 columbium heat shield panels were the most critical structural items. It was originally believed that the heat shield panels should be 0.25-in. thick instead of the 0.375 in. used, but the 0.25-in. thick panel resulted in negative margins.

V. TEST PANEL MANUFACTURING TECHNIQUES

A. HONEYCOMB CORE FABRICATION

1. Foil Corrugation

The TZM and D-36 foil materials were received in 4-in. wide coils of random lengths (TZM up to 6- to 8-ft lengths; D-36 up to 25-ft lengths). These were sheared with a paper cutter into 18.25-in. lengths to provide 14.2-in. strips after corrugation.

A match gear corrugating tool (Fig. 16) which had been used for stainless steel was found satisfactory for corrugating TZM and D-36; for D-36, it was only necessary to dress the 3/16-in. gear rollers and adjust the gear contact pressure to obtain the desired pitch; for TZM, best results were obtained by heating the gears and foil to about 200° F with heat lamps (Fig. 17).

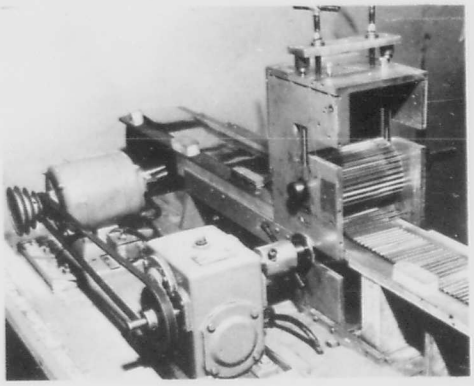

Fig. 16. Corrugation Tool for Fabricating Honeycomb Core

The D-36 foil strips were corrugated at room temperature, the TZM foil strips at 180° to 200° F. The corrugated foil was then sized in a renite (plastic) template to ensure that the configuration of each strip matched the core-welding tools. Nodal alignment was particularly important, since cumulative errors would eventually result in excessive mismatch so that nodes could not be joined.

After sizing, the corrugated foil was cleaned in a trichlorethylene vapor degreaser (Table 6) and stored until required for billet fabrication.

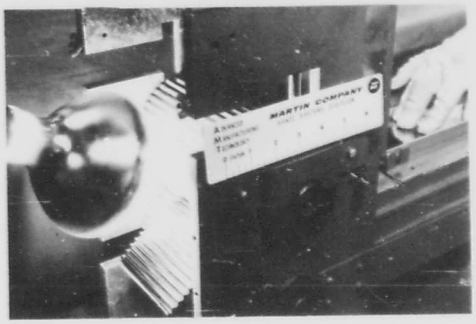

Fig. 17. Corrugating Foil for Honeycomb Core

TABLE 6

Summary of Cleaning Procedures Used for TZM Molybdenum and D-36 Columbium Parts

	Solvent Wiping (Acetone)	Vapor Degrease (Trichloroethylene)	Alkaline Cleaning	Chemical Cleaning (10 to 15% HF 40% HNO_3 balance H_2O ambient temperature)	Chemical Cleaning (15% H_2SO_4 4.5% HNO_3 0.5% HF 10.5 g/l Cr_2O_3 120° to 140° F)
D-36 corrugations		X			
D-36 straight channels	X			X	
D-36 curved channels	X			X	
D-36 core		X		X	
D-36 flat heat shield panels		X	X	X	
D-36 curved heat shield panels		X	X	X	
D-36 curved structural panels		X	X	X	
D-36 flat structural panels		X	X	X	
TZM corrugations		X			
TZM straight channels	X				X
TZM curved channels	X				X
TZM core		X			
TZM flat heat shield panels		X	X		X
TZM curved heat shield panels		X	X		X
TZM curved structural panels		X	X		X
TZM flat structural panels		X	X		X

2. Billet Fabrication

a. TZM molybdenum

The major technical problem in fabricating TZM molybdenum honeycomb core was in making the core node attachment. Conventional resistance spot-welding techniques, normally employed for core fabrication, are not adequate for molybdenum and its alloys.

Good structural welds are difficult to achieve by either resistance or fusion welding techniques. Cast weld zones exhibit a high ductile-brittle transition temperature and are relatively brittle at room temperature. This behavior is further aggravated if interstitial levels are raised during the welding process. Electron beam welding does not eliminate the basic welding problem, but cast and heat-affected zones can be closely controlled to minimum levels.

Three methods for making the TZM core node attachment were considered: (1) diffusion bonding, (2) spike welding and (3) electron beam welding.

(1) Diffusion bonding. The diffusion bonding technique metallurgically would provide an ideal joining method. However, it was evident, from the literature and in discussions with technical personnel of other laboratories, that the state of the art had not yet advanced to the point where the honeycomb core for this program could be fabricated. With the extensive development effort indicated, no experimental evaluation of this technique was made.

(2) Spike welding. Spike welding (high voltage, high current, short duration impulse spot welding) was briefly investigated. This technique had been used for heavier gage material but had not been evaluated on foil. Efforts to obtain satisfactory foil joints were not successful; only burn-throughs and nonfusion of foil layers occurred. The primary problem was associated with electrode configuration. Standard electrodes were not satisfactory for the thin refractory metal foil.

(3) Electron beam welding. A Hamilton-Zeiss electron beam welder was used to establish the feasibility of electron beam welding the TZM honeycomb core. A prototype tool was designed and built to position the corrugated foil for welding, and two small billets (2-1/2 by 2-1/2 by 4 in.) of 3/16-in. square cell core were fabricated. While the joints are not ductile at room temperature, the fabricated core had sufficient structural integrity so that it could be processed for fabrication into brazed panel assemblies. With feasibility demonstrated, the electron beam welding technique appeared to be the best available method and was selected to produce the TZM core for the program.

At this point in the program, a new model, high voltage Hamilton-Zeiss electron beam welder (Fig. 18) was installed to provide the necessary work area for fabricating 14- by

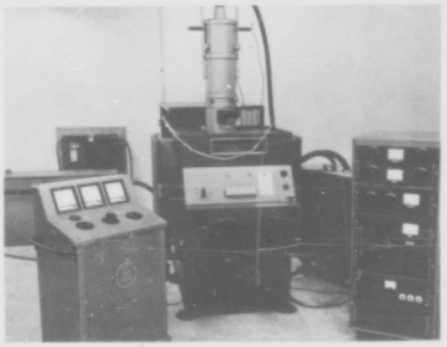

Fig. 18. Electron Beam Welder

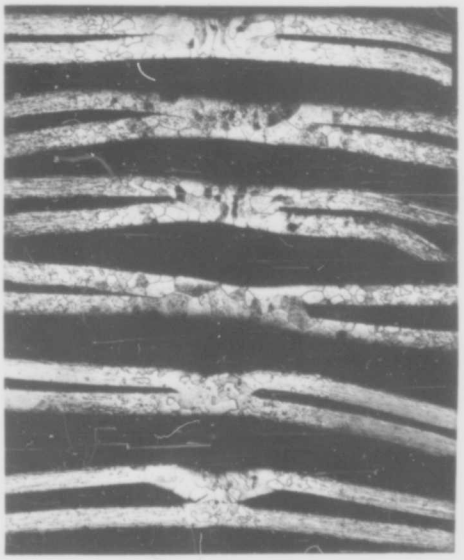

Effect of welding speed on weld microstructure of electron beam welded 0.002-in. TZM molybdenum honeycomb core. (200X)

Welding speed

a. 27.5 in./min
b. 39.0 in./min
c. 39.5 in./min
d. 44.0 in./min
e. 48.5 in./min
f. 58.0 in./min

Fig. 19. Effects of Welding Speed on TZM Foil Welds

14- by 4-in. billets. This machine is capable of producing weldments at speeds up to 100 in./min. Various parameters were evaluated to determine the optimum welding conditions for fabricating TZM honeycomb core. These included voltage and amperage settings, and welding speed. The best welds were produced with machine settings of 90 kv and 0.75 ma. Welding speeds of 27.5 to 58.0 in./min were evaluated, with 40.0 in./min selected as the optimum speed for honeycomb core fabrication. The effect of welding speed on joint microstructure is shown in Fig. 19.

A tool (Figs. 20 and 21) was made to produce 14- by 14- by 4-in. TZM honeycomb core billets. This tool, similar to the prototype tool, included two sets of mandrels which held the corrugated strips of foil in place for welding. A hold-down plate with localized pressure pins rested on the top of the upper set of mandrels to exert a constant pressure on the foil to produce uniform nodal contact. The lower set of mandrels supported the nodes and reacted to the contact pressure of the upper set of mandrels. This contact was necessary to produce a continuous nodal weld. If continuous nodal contact was not maintained, the foil was severed by the electron beam and no weld was formed.

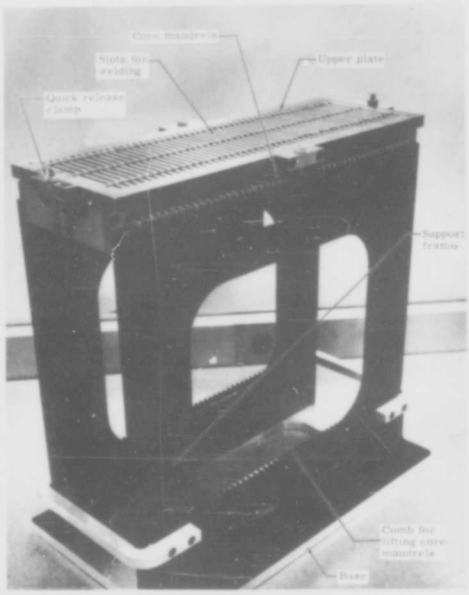

Fig. 20. Electron Beam Weld Tools for Honeycomb Core

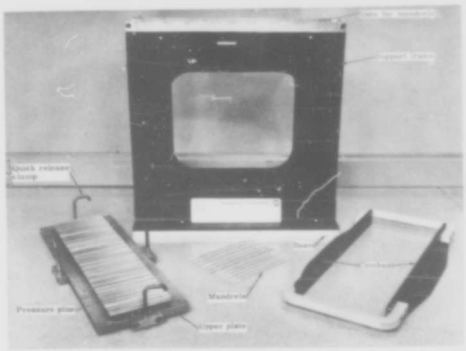

Fig. 21. Electron Beam Weld Tools for Honeycomb Core

The billets were built up layer-by-layer. As each layer of corrugated foil was electron beam welded (electron beam weld settings shown in Fig. 22), a careful inspection was made to verify the soundness of each weld joint. Necessary repairs were made with standard techniques (replacing of damaged cells with new cells resistance tack welded in place, and similarly welding separated nodes). A thin titanium foil interlay was used in the joints to facilitate welding.

After the welding of each layer of corrugation was completed, the hold-down plate was removed and the mandrels lifted from the base fixture with a special set of combs. The lower set of mandrels could then be removed, the next layer of corrugated foil laid in place, the removed set of mandrels placed in position above the other set of mandrels, and the next line of nodal welds made. This process was repeated until welding of the billet was completed.

b. D-36 columbium

Preliminary tests confirmed that conventional resistance welding techniques could be used to fabricate the D-36 honeycomb core. Resistance welds in sample lots of both 0.001- and 0.002-in. thick foil (Fig. 23) exhibited good strength and ductility. Some copper pickup from the welding wheel electrode was noted, but this had no effect on the joint and was easily removed by a nitric acid etch.

In the fabrication of the 14- by 14- by 4-in. billets, two staggered rows of copper fingers were used to support the foil (Fig. 24). The first operation, after each layer of foil

Summary of Electron Beam Welds

	Detail	Material	Table Speed	Weld Angle	KV	ma
a	Core	D-36	Resistance welded			
		TZM	40 in./min	90°	90	0.75
b	Attachment clip assembly	D-36	25 in./min	12°	105	4
		TZM	25 in./min	12°	130	7
c	Attachment clip to panel	D-36	20 in./min	90°	50	1.65
		TZM	20 in./min	90°	70	2.00
d	Access hole insert	D-36	20 in./min	90°	50	1.65
		TZM	20 in./min	90°	70	2.00
e	U-channel assembly	D-36	25 in./min	90°	100/98	8/11
		TZM	40 in./min	90°	85	3
f	Shear strip to panel	D-36	25 in./min	90°	110	5
		TZM				
g	Sealing structural curved panel	D-36	Variable	90°	No precise setting established	
		TZM	Variable	90°		
h	Sealing heat shield panel	D-36	Variable	90°	90	0.8
		TZM				

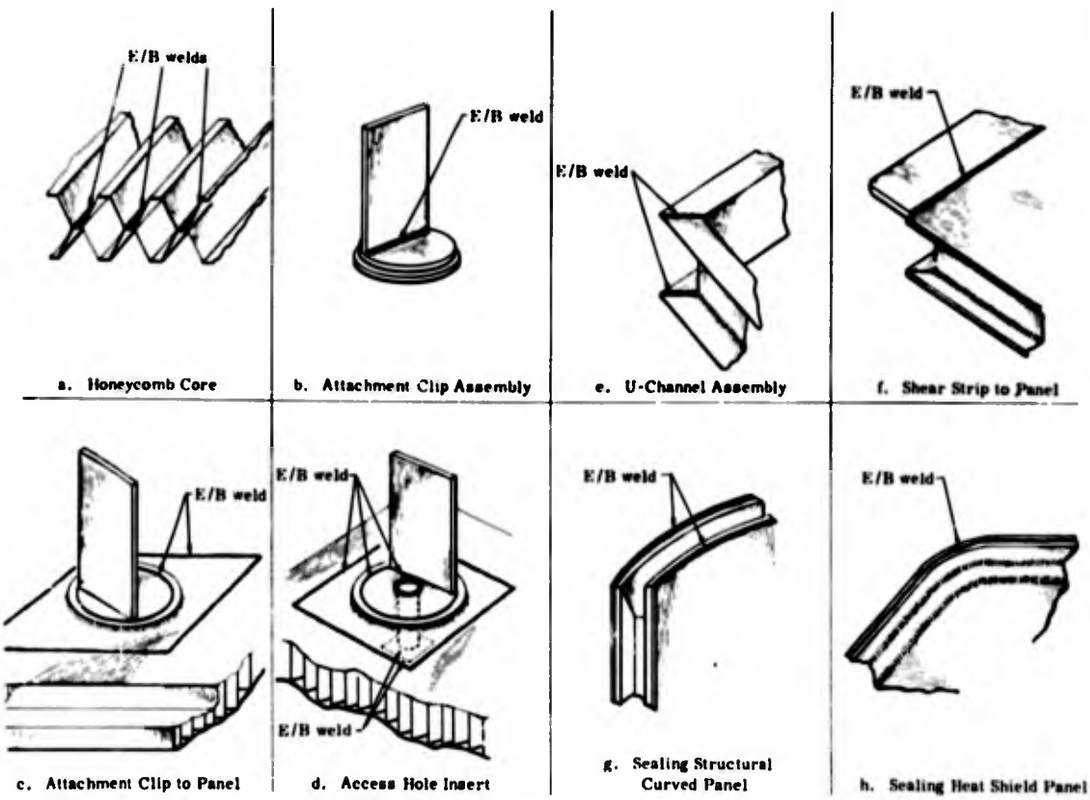

a. Honeycomb Core
b. Attachment Clip Assembly
e. U-Channel Assembly
f. Shear Strip to Panel
c. Attachment Clip to Panel
d. Access Hole Insert
g. Sealing Structural Curved Panel
h. Sealing Heat Shield Panel

Fig. 22. Detail Configuration for Electron Beam Welding

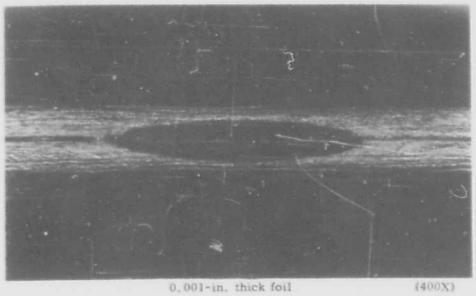

0.001-in. thick foil (400X)

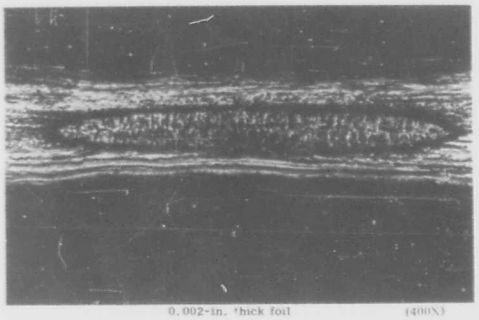

0.002-in. thick foil (400X)

Fig. 23. Resistance Welded D-36 Columbium Foil

Fig. 24. Tooling for Resistance Welding of D-36 Columbium Honeycomb Core

was added, was to tack-weld the end of each row of cells into place (Fig. 25). This held the foil in the proper position for welding. A water-cooled copper roller wheel was used to stitch-weld the core foil at a rate of about 10 spots per second (Fig. 26). Successive

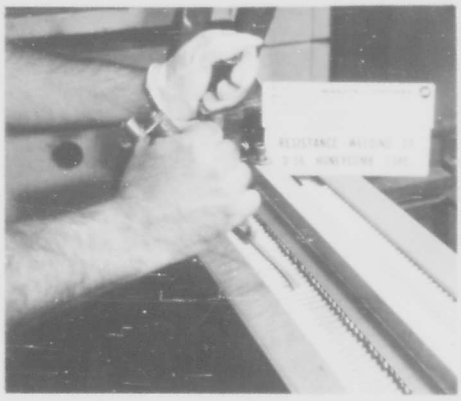

Fig. 25. Tack-Welding Ends of Corrugations in Place

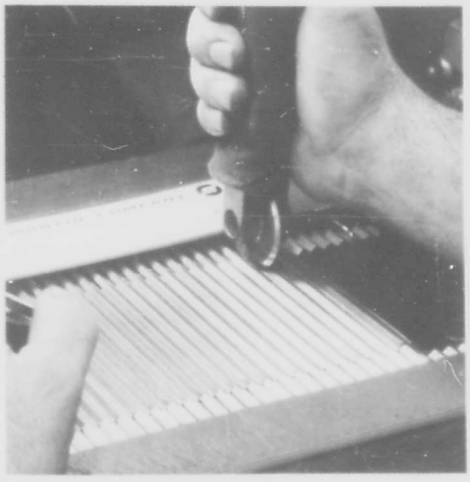

NOTE:
A water-cooled copper roller wheel is used.

Fig. 26. Welding Nodes of D-36 Columbium Honeycomb Core

layers of the corrugated foil were welded until the billet was completed (Fig. 27). Few repairs were needed, but were made by conventional tack-welding techniques where required.

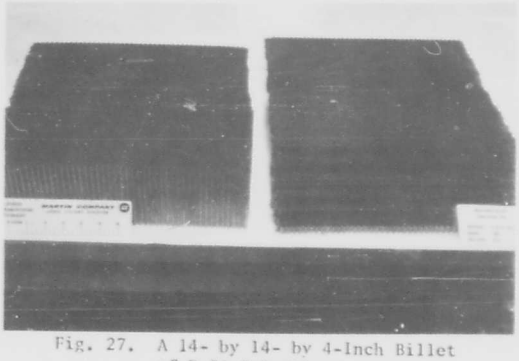

Fig. 27. A 14- by 14- by 4-Inch Billet of D-36 Columbium Honeycomb Core

3. Slabbing and Sanding

a. TZM molybdenum

Slabbing procedures were evaluated on the two 2-1/2- by 2-1/2- by 4-in. billets. These were sawed into 1/2-in. thick slabs on a Tannewitz high speed band saw (10,000 surface ft/min) (Fig. 28). Of several types of blades which were evaluated, only a 120-grit diamond impregnated blade proved satisfactory. The frictionally generated heat as the blade cut through the core was found to be sufficient to keep the recrystallized nodal weld above the ductile-brittle transition temperature, and thus prevented major cracking. However, some minor cracking or tearing occurred during sawing, and sufficient stock must be provided in the rough cut slab (approximately 1/16 in. over required finished thickness) so that these defective areas can be removed during the finishing operation.

Three techniques for finishing TZM honeycomb core to the required thickness tolerance of ±0.0015 in. were evaluated in the initial studies:

(1) Disc cutting.

(2) Hand or machine sanding.

(3) Filling and sanding.

The use of a disc- or mushroom-type cutter to trim the core produced tears in the core material and was quickly discarded as

Fig. 28. Sawing Billet of TZM Honeycomb Core with Diamond Blade

a possible finishing technique. Both hand and machine sanding were found capable of providing an acceptable finish and the required tolerances on these small samples. Further accuracy could be obtained with the filling and sanding technique, which involved filling the billet with an acrylic plastic prior to slabbing and removal of the acrylic with acetone after final sanding, but this method was considerably more time consuming. The latter was considered only as a backup procedure, if tolerances over larger expanses of core could not be maintained with sanding alone. It was recognized that, in any case, hand sanding would not be adequate, and that machine sanding would be necessary to meet the tolerances.

While the smaller core samples were sanded cold, this technique produced extensive cracking in almost all of the honeycomb cell walls on slabs cut from full-scale 14- by 14- by 4-in. billets. Two additional techniques, hot sanding and the Anocut process, were investigated. Both proved satisfactory for finishing core. The hot sanding technique, which involved heating both the core and the sander to about 200° F, was selected for finishing the honeycomb core for the test panels.

Sanding was accomplished with resin-abrasive cloth belts designated as Type 6, 120-grit, 45-degree flex, single-splice, medium velvet carborundum. The core was rough sanded to within about 0.040 in. of the

required thickness and then inspected to determine if any repairs were required. Repairs were made before sanding to final thickness. After repair, the slabs were sanded to the required thickness with ±0.0015-in. tolerance.

b. D-36 columbium

The D-36 billets were similarly sliced into slabs. High strength steel blades were satisfactory; diamond impregnated blades were not required.

The sanding was accomplished as for TZM, except that heating was not required.

4. Sizing and Stepping

The core for the panels was rough-cut to size (X-Y dimension) with a band saw and then finished to the proper dimensions with a belt sander.

The core for the curved structural panels was curved by placing the core between the curved braze tools and heating to 2200° F for one hour in a vacuum furnace. This was all the preparation needed for the structural panel core.

The core for the heat shield panels was stepped to fit the heat shield facing pans. This was accomplished on D-36 by holding the core in a special tool and cutting the step with a carbide disc cutter (Fig. 29). The heel of the step was cut to full depth in one pass, and the horizontal cuts were made in increments not exceeding 0.050 in. The rate of travel of the cutter was about 4 in./min. Rough or high spots were removed by sanding with a carborundum stone.

The same procedures were utilized for TZM; however, it was found necessary to fill the core with sodium thiosulphate to stabilize the cell walls during cutting (Fig. 30). Adequate filling was obtained by heating the sodium thiosulphate to 140° F and pouring into the core cells along the edges where the core step was to be cut. After the cutting was accomplished, the sodium thiosulphate was removed with hot water.

5. Cleaning

After sizing and stepping were completed, all of the core slabs were trichlorethylene vapor degreased (Table 6). This completed the cleaning of the TZM core; however, it was necessary to acid etch (Table 6) the D-36 core slabs to remove the copper deposit

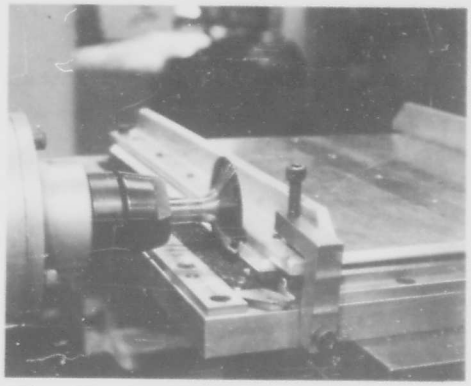

Fig. 29. Cutting Step in D-36 Columbium Honeycomb Core for Heat Shield Panels

that occurred during welding. After cleaning, the slabs were placed in polyethylene bags and stored until they were used.

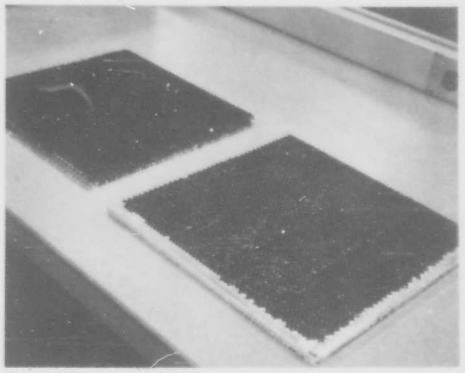

Fig. 30. TZM Honeycomb Slab Filled with Sodium Thiosulphate for the Stepping Operation

B. PANEL DETAIL FABRICATION

1. Heat Shield Panel Facings

The heat shield panels consisted of two formed double-stepped pans trimmed along certain lines and fitted together to form a stepped-edge module-type panel (Dwg Nos. SK-46843 and SK-46844, Appendix A). Three basic pans were formed--a flat pan, a convex pan and a concave pan.

The double step facings presented special forming problems, and an investigation was

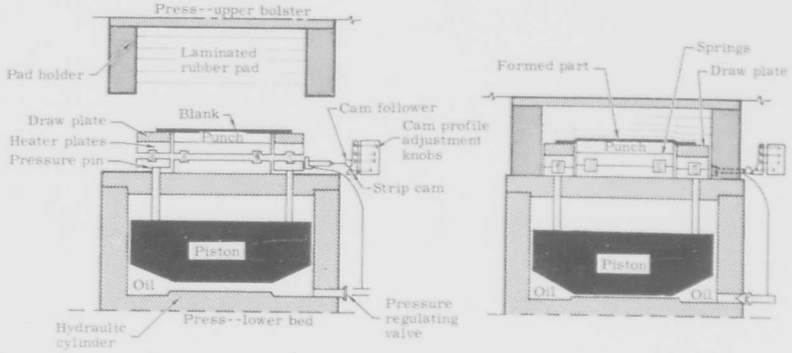

Procedure:

1. The blank to be formed is placed on the punch-draw plate assembly.
2. As the upper head descends, the rubber pad grips the blank against the punch-draw plate assembly, and the heater plate insulator spring is then fully compressed.
3. Further descent of the head forces the draw plate downward while the punch remains stationary.
4. The blank, gripped between the rubber and the draw plate, is drawn over the punch and formed without wrinkles.

Fig. 31.- The Marform Process

conducted to develop suitable manufacturing procedures, using the Marform process.

The Marform process (Fig. 31) involves forming with hard metal tools against high pressure (6000 psi) rubber. The material to be formed is gripped between the rubber and draw plate, then drawn over the punch and formed. To form these facings, it was necessary to determine forming temperatures and to develop special underlay and overlay procedures and lubrication techniques to prevent cracking or wrinkling of the material at the facing corners.

a. Tooling

The dies shown in Figs. 32 and 33 are typical of those which were made. Three sets of dies, each consisting of two punches, two draw plates and two radius plates, were required to form the three heat shield facing pan configurations. Checkout tests were made with PH 15-7 Mo steel sheet. The dies functioned properly, and satisfactory steel facings were formed.

Heater units were added later to provide for elevated temperature forming. These units contained Cal-Rod resistance heaters, with variac control of power to the heaters. The punch-draw plate assembly temperature was monitored with a thermocouple.

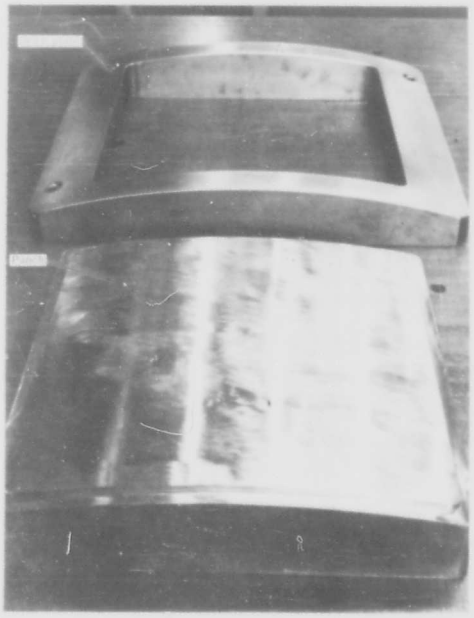

Fig. 32. Second Step Curved Heat Shield Panel Marform Dies

Several small springs served to raise the heater units off the press base plate during the heatup and layup operation to provide an air gap between the heater and tooling and the base plate. This served to insulate the base plate from the heater and tooling so that most of the heat generated was conducted into the tooling where it was needed. When the upper head of the press was lowered and pressure applied, the springs were compressed into small circular recesses in the heater units, so that the tool rested directly on the base plate of the press.

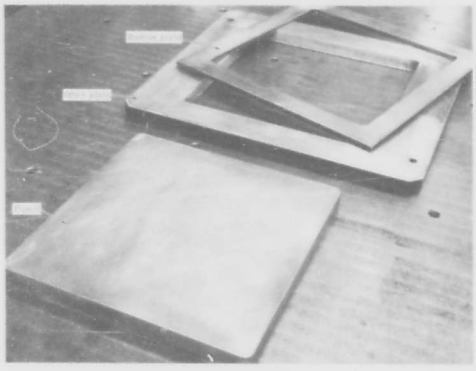

Fig. 33. Second Step Flat Heat Shield Panel Marform Dies

b. Forming development

TZM molybdenum. Small 4- by 4-in. TZM blanks were used in the initial studies to develop forming procedures for the panel corners.

The dies were initially fabricated with 0.030-in. edge radii. These radii were satisfactory for the steel checkout material, but poor results were obtained in attempts to form TZM corners at room temperature. The TZM material cracked and shattered, with little or no forming actually taking place. In the next series of tests, the dies were heated in a furnace to 300° F, and two out of six pieces were formed without cracking. Figures 34 and 35 show a cracked and a successfully formed corner, respectively. Only the first step forming operation was evaluated in this series of tests.

The edge radii on the dies were changed to 0.050 in., and several other forming aids were used in efforts to form the panel corners. By using a stainless steel foil overlay and underlay on the TZM blank and forming at temperatures of 175° to 250° F, some double-stepped panel corners were formed successfully (Fig. 36).

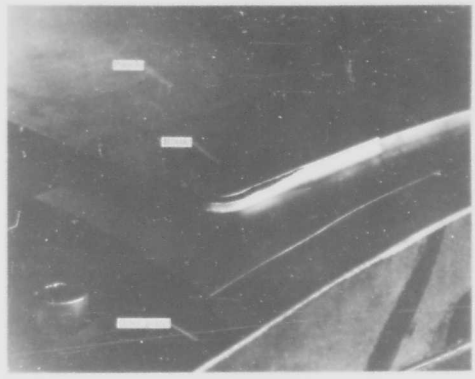

Fig. 34. TZM Heat Shield Corner Blank Cracked in First Step Forming Operation

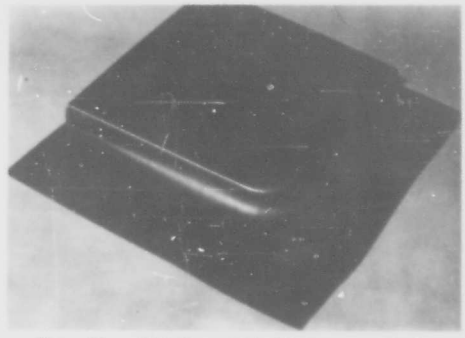

Fig. 35. TZM Heat Shield Corner Blank Formed in First Step Forming Operation

In scaling up to full-scale heat shield panel facings, it was found that lubricants had to be added and temperature increased to 300° F to avoid cracking. Additional experiments were therefore conducted to develop improved procedures.

The best results were obtained by forming the first step in two operations. The initial operation included the addition of a 0.032-in. aluminum filler plate under the punch, and a light film of lubricant was applied to the face of the draw plate. This formed the first step with a larger radius bend and 0.032 in. deeper than required. The filler plate and underlay were removed,

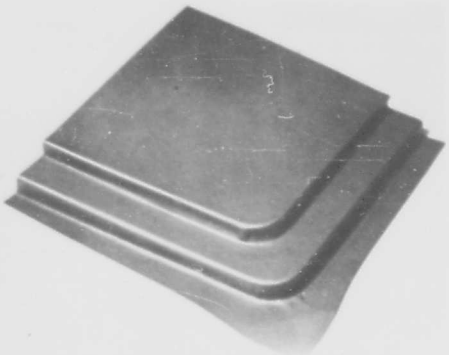

Fig. 36. TZM Heat Shield Panel Corner Completely Formed

the radius plate installed, and lubricant applied to the top and bottom surfaces of the TZM blank in the second operation to form the bend radius and step depth to final dimensions. This technique reduced the excessive localized deformation and resultant cracking that occurred when this first step was formed in a single forming operation. The second step was formed in one operation with no underlay or overlay, with lubricant sprayed on the top and bottom surfaces of the TZM blank.

As discussed in Section III, there was considerable variation in the fabricability of the starting 0.008-in. TZM sheet material for the heat shield panel facings. Fabricating uniformity was significantly improved by stress relieving this material in vacuum at 2200° F prior to forming.

D-36 columbium. It was anticipated that forming of the D-36 heat shield panel facings would not present any major problems, and that the procedures developed for TZM would be more than adequate for D-36. However, some modifications were found necessary. Lubrication was a particularly sensitive variable.

Heating to 400° F did not improve the forming characteristics of D-36. Some facings were formed at temperatures to 400° F during the checkout period, but the majority were formed successfully at room temperature.

The best results were obtained by forming the first step in two operations as used for TZM, but with an overlay as well as an underlay and with a heavy film of lubricant sprayed on the top side of the overlay (side formed against rubber) and no lubricant on the draw plate. The overlay and underlay were removed and the radius plate used in the second operation as for TZM. A very light film of lubricant was applied on the top surface of the D-36 blank at the four corners.

Forming of the second step was accomplished by using the Marform tool and radius plate to draw the material as shown schematically in Fig. 37. The corners of the D-36 blank were rounded to within 3/8 in. of the final step dimension. A medium amount of lubricant was then applied to the top and bottom surfaces of the facing and to the flange area. This technique produced smooth crack-free corners on D-36.

c. Forming procedures

TZM. The following forming procedures were utilized for the TZM molybdenum. These procedures applied to the flat, concave and convex facings.

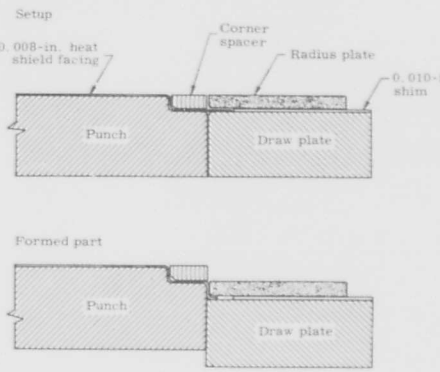

Procedure:

1. Lay up facing over second step marform punch and draw plate.
2. Insert space blocks on four corners and install shim 0.002-in. thicker than skin being formed.
3. Set radius plate.
4. As the upper head descends, the rubber pad grips the blank against the punch-draw plate assembly.
5. Further descent of the upper head forces the draw plate downward while the punch remains stationary.
6. The facing is drawn around the draw plate, forming the heat shield facing.

Fig. 37. Second Step Marform Operation for the D-36 Columbium Heat Shield Facings

(1) The 0.008-in. TZM material with a 0.003-in. stainless steel underlay was sheared to provide 14.5- by 14.5-in. square blanks. The stainless steel underlay was used in the forming operation.

(2) The Marform press was prepared for the first step operations with a 0.032-in. filler plate placed under the punch assembly. The filler plate was required initially to form the first step 0.032 in. deeper than required.

(3) The forming tools were heated to 300° ± 25° F.

(4) A thin film of lubrication was applied to the face of the draw plate.

(5) The first forming operation on the first step was completed with the full press pressure of 6000 psi being exerted.

(6) The 0.003-in. stainless steel underlay and the 0.032-in. filler under the forming punch were removed.

(7) Lubricant was applied to the top and bottom surface of the TZM blank, and the radius plate placed in position.

(8) The second operation on the first step was completed with a pressure of 1500 psi.

(9) The top and bottom surfaces of the TZM blank were sprayed with a light film of lubricant.

(10) The second step was formed at 6000 psi (Fig. 38).

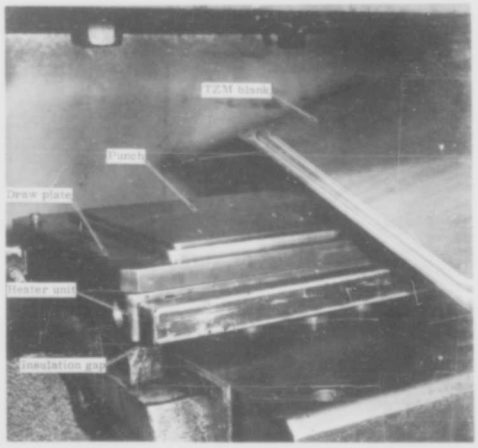

Fig. 38. Second Step Marform Operation for Heat Shield Panel Facings--TZM Molybdenum Blank and Heater Units Shown

D-36. The following forming procedures were utilized for the D-36 columbium. These procedures applied to the flat, concave and convex facings.

(1) The 0.008-in. D-36 columbium sheet and two 0.003-in. stainless steel sheets were sheared to 14.5- by 14.5-in. square blanks and wrapped in paper (these stainless steel blanks were used as overlays and underlays in the forming process).

(2) The Marform press was prepared for the first step operation. A 0.032-in. filler plate was placed under the punch assembly.

(3) A heavy film of lubricant was sprayed on the top side of the laminated blank only (the side formed against the rubber).

(4) For the concave facing pan only, a 0.5- by 2- by 11.75-in. rubber pad was centered over the blank.

(5) The first step forming operation was completed at a pressure of 6000 psi.

(6) The 0.003-in. overlay and underlay were removed. The 0.032-in. filler plate was removed from under the punch.

(7) A very light film of lubricant was applied to the top surface of the four corners of the D-36 blank.

(8) The radius plate-forming operation was completed at a pressure of 1500 psi.

(9) The corners of the D-36 blank were rounded to within 3/8 in. of the final step dimension.

(10) A medium amount of lubricant was applied to the top and bottom surfaces of the pan and to the flange area.

(11) The second step operation radius plate was located with the four corner spacers on the punch assembly (Fig. 37).

(12) The forming was completed at a pressure of 1500 psi.

d. Finishing

Hand shearing of the D-36 facings to approximate final dimensions was a simple operation but, because of the notch sensitivity of TZM, it was found necessary to trim the TZM facings at 200° to 300° F to prevent cracking. The trimming was done on a hot plate, and the shears were also heated to temperature.

Some hand work was required to sharpen the edge angles and the corner lips, and a small drum sander sufficed for finishing to required dimensions.

The pans were hand fitted in pairs to ensure against gaps and poor fitting corners. The TZM pans were stress relieved at 2200° F for one hour to provide as much ductility as possible for this operation. The TZM pans were straightened at about 200° to 300° F.

2. Structural Panel Facings

The sheets for the curved panel facings were hand wrapped to fit the curve. This was sufficient to complete the operation; however, in most instances the facings were placed in the vacuum furnace at the time the structural panel core was curved to assure proper contact.

3. U-Channel Edge Members

The principal development effort was devoted to determining a satisfactory corner joint configuration and the matching tolerances required to electron beam weld these corners. A mitered corner joint selected in the test panel design proved acceptable and could be welded if the channels were machined to within 0.002-in. tolerance. Initial studies were performed with stainless steel, since neither refractory alloy was available. A welded stainless steel U-channel is shown in Fig. 39.

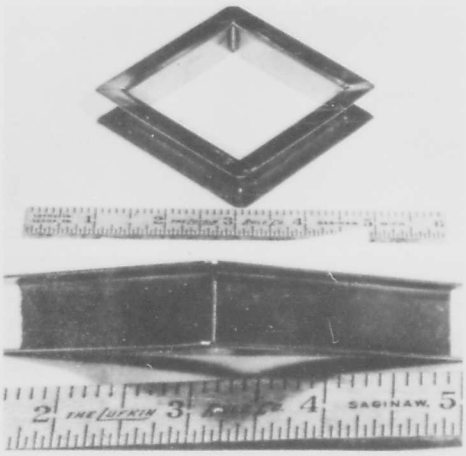

Fig. 39. Simulated Edge Members in Stainless Steel-Electron Beam Welded

a. Tooling

Two tools were made to form the straight U-channel members to the required tolerance: a Marform tool to form the channel and a female sizing die (Fig. 40) to control the outside width of the channel to ±0.0015 in. as required for panel brazing.

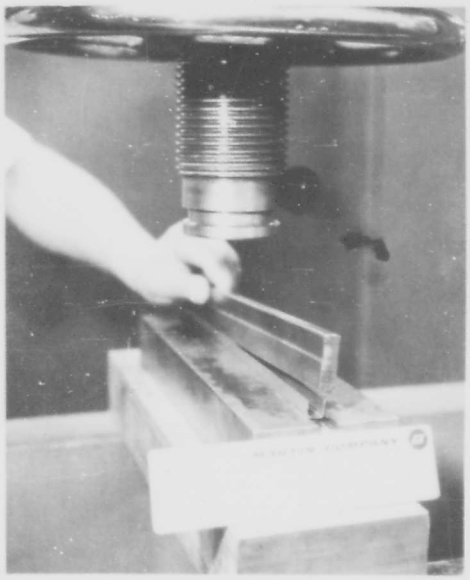

Fig. 40. Tool for Second Forming Operation on Structural Panel U-Channels

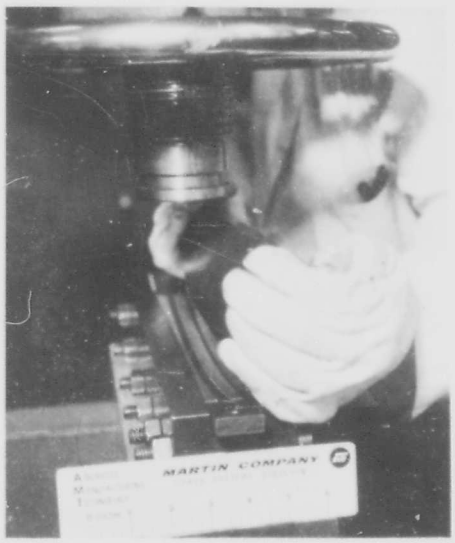

Fig. 41. Bending U-Channels for Curved Structural Panels

Two additional tools were constructed to bend the channels to the proper radius for the curved panels. A hydraulic press tool (Fig. 41) was made to curve the straight channels, which were first fitted over soft steel shims of the proper thickness. A special male tool was made for the second operation which involved Marform sizing to the exact curvature.

Special tools were made to hold the U-channels for welding. These were constructed so that all joints could be welded before removing the U-channel picture frame. Figure 42 shows the tool for flat U-channel frames. A similar tool was made for curved U-channel frames.

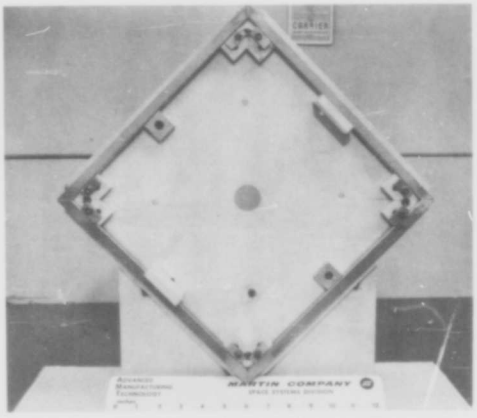

Fig. 42. Matching the Straight U-Channels to the Tool for Electron Beam Welding of the Miter Joint

b. Mitering

The U-channels were first rough sawed to a length slightly longer than required and then ground (Fig. 43) to the proper dimension. A carborundum Type II grind wheel was used in the grinding operation, in which about 0.001 to 0.002 in. of material was removed per pass. Individual sets of frames were ground to match the tool shown in Fig. 42. The required fit tolerances were +0.000 and -0.002 in.

The ends of the curved U-channels were finished in the same manner as the straight channels. However, special holding tools were utilized to provide the required correction for the different curvatures of the inner and outer leg of the channel.

The TZM and D-36 U-channels were finished by the same procedure, except that the TZM channels were processed at about 200° F.

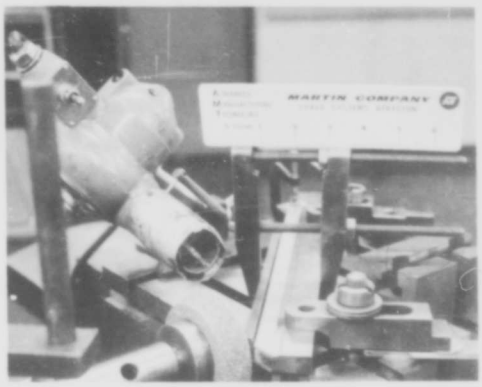

Fig. 43. Grinding the Ends of the U-Channels for the Picture Frame Miter Joints of the Structural Panels

A hot air blower shown in Fig. 43 was used to heat the U-channels during grinding.

c. Welding

D-36. The D-36 U-channels were joined into a frame by welding. The tool shown in Fig. 42 was used to hold the channels during welding. A similar tool was used for the curved panel frames. All U-channels were cleaned according to the requirements of Table 6 before they were welded.

The flats of the U-channel corner joints were electron beam welded. The welding was accomplished progressively on alternate sides and corners to prevent residual stresses caused by welding from opening up the unwelded corner joints. Weld settings (Fig. 22) were developed for these joints.

The vertical joints (the joint perpendicular to the parallel legs of the channel) were initially electron beam welded. This required special tilting of the frames, several pump-down cycles for welding and hand manipulation of the part during welding. A TIG welding process, using filler wire, was evaluated and found more desirable because of the simplicity and ease of application.

TZM. Special elevated temperature welding and stress relieving procedures were necessary to prevent cracking. The following procedures were developed for the TZM frames:

(1) The TZM U-channels were matched to the welding frame shown in Fig. 42. Special allowances were made in the dimensions

to ensure that the channels would fit when the jig and frames were heated to 250° F.

(2) The weld jig and frames were heated to 250° F in an oven, then matched in the jig and placed in the electron beam weld chamber.

(3) Two corner flat welds were made.

(4) Steps (2) and (3) were repeated until all flat joints were welded.

(5) After the start of Step (2) and until Step (6) was completed, the frames were not allowed to cool below 200° F. During the time the parts were not in the weld chamber, they were stored in the oven at 250° to 300° F.

(6) The welded frames were stress-relieved at 2200° F for one hour in the high temperature vacuum (2×10^{-5} torr) furnace.

(7) The vertical joints of the U-channel frames were TIG welded.

(8) The frames were stored in an oven at 250° to 300° F until they could be stress-relieved again by the same procedure shown in Step (6).

***

After welding, both the D-36 and TZM frames were inspected for pin holes or cracks and reworked if necessary. Any rework to remove excess weld metal from the frames was done at room temperature on the D-36 and about 200° F on the TZM.

4. Heat Shield Panel Support Clips

The heat shield panel support clips (Dwg Nos. SK-46843 and SK-46844, Appendix A) were fabricated by electron beam welding. The discs (support pad) were blanked from 0.025-in. sheet stock. The legs were sheared, then machined to exact size. The blanking and shearing were performed at 300° F for TZM; all other operations on both alloys were performed at room temperature.

Initially, the discs were machined with a 3:1 bevel on the outer edge; however, because of sealing difficulties that occurred later in the program, this bevel was changed to a step.

A special tool (Fig. 44) was used to hold the discs and legs in position for electron beam welding. The legs were welded on one side, then turned 180 degrees and welded on the other side; weld settings are shown in

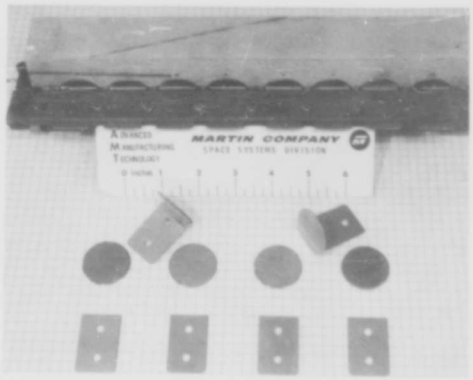

Fig. 44. Heat Shield Support Clips and Electron Beam Welding Tools

Fig. 22. Small tungsten targets were placed at the edge of each leg, so that, when end of the leg was reached, the beam would run onto the target and not burn a hole through the disc.

Photomicrographs of typical joints are shown in Figs. 45 and 46. The TZM joint, while brittle, had sufficient structural integrity for handling and testing. This was demonstrated qualitatively by breaking several welded clips. The D-36 joints were ductile.

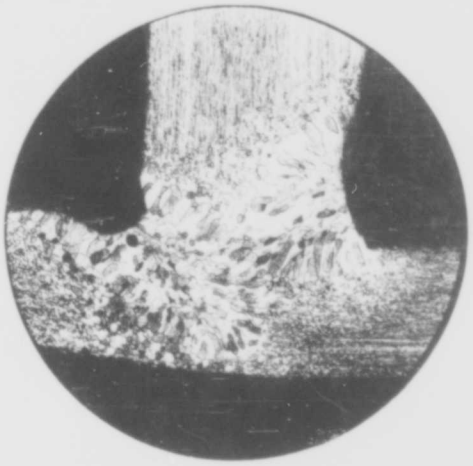

Fig. 45. Photomicrograph of Electron Beam Welded T-Joint of TZM Molybdenum Showing Recrystallization in Weld Zone (75X)

After welding, a hand operation (with a hammer and block) was used to flatten any

warped discs. Again, this operation was performed at about 200° F on TZM.

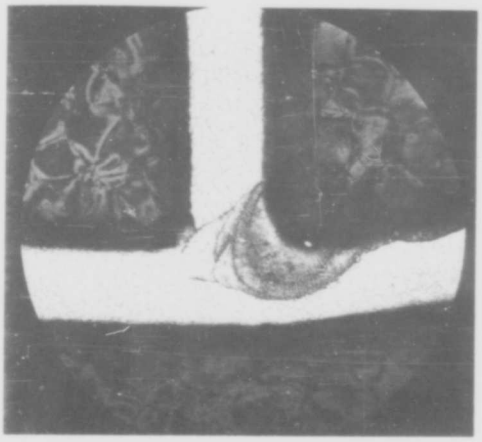

Fig. 46. Photomicrograph of Electron Beam Welded T-Joint of D-36 Columbium Showing Grain Refinement in the Weld Zone (75X)

C. BRAZING

1. Braze Alloy Development, Evaluation and Selection

For structural applications, the TZM and D-36 alloys are effectively limited to temperatures of 2300° to 2600° F maximum. Recrystallization of molybdenum alloys, which produces both weakening and embrittlement, limits the temperature capabilities of TZM. While the D-36 alloy is not similarly embrittled, strength at higher temperatures is inadequate for an efficient structure. For heat shield applications, service operational temperatures should approach 2600° to 3000°F for the panels to serve as efficient radiators. These temperatures are consistent with the capabilities of the selected oxidation protective coatings and with the material properties.

Based on these considerations, the following brazing objectives were established:

(1) D-36 columbium structural panels. Brazements should be capable of resisting structural loads to 2300° to 2600° F.

(2) D-36 columbium heat shield panels. Brazements should be capable of resisting small structural loads at 2800° to 3000° F.

(3) TZM molybdenum structural panels. Brazements should be capable of resisting structural loads to 2400° F; the brazing cycle should not recrystallize the TZM molybdenum alloy.

(4) TZM molybdenum heat shield panels. Brazements should be capable of resisting small structural loads at 2800° to 3000° F.

It was recognized that commercially available brazing alloys would not completely satisfy the TZM panel requirements. With brazing temperatures for structural panels limited to 2400° to 2600° F maximum to avoid recrystallization, braze strength at 2400° F would be inadequate, and TZM heat shield panels would be recrystallized in brazing above 3000° F to provide the desired operational temperature capability. The latter might be tolerable because the TZM panels would eventually be recrystallized in service; however, the recrystallization which occurred during brazing would increase the difficulty of handling the panels without damage during subsequent fabrication, coating and testing.

The original intent of the program was to use available materials and processes for test panel fabrication. However, some braze alloy development appeared desirable in view of the inadequacy of available alloys to provide maximum utilization of the capabilities of the TZM molybdenum alloy. Consideration was given to brazing systems in which higher remelt temperatures could be obtained by modification of brazement chemistry subsequent to brazing. The concepts for higher remelt temperature alloys were not new, but only a limited amount of the reported work was relevant to the specific materials and requirements of this program.

Of three higher remelt temperature techniques--volatilization, exothermic reaction brazing, and diffusion alloying--only diffusion alloying was considered as an immediate feasible approach to the vacuum brazing of honeycomb sandwich panels. Volatilization techniques were not applicable because the panels were to be vacum brazed and contained nonperforated core (Ref. 33). Exothermic brazing, while potentially attractive, was in the early developmental stages when this program was initiated and was not considered further (Ref. 34).

The diffusion alloying technique involves adding elements such as silicon and boron to the basic filler alloy to depress the liquidus temperature (e.g., by the formation of a low melting eutectic). The melting point is then

raised by altering the chemistry of the brazement by diffusion heat treatments (Refs. 35 and 36). For example, the platinum-3.5% boron eutectic composition melts at a temperature approximately 1500° F below that of platinum. Braze-remelt temperatures as high as 3800° F have been reported for this system in the brazing of tungsten (Ref. 35).

Principal efforts in the diffusion alloying higher remelt studies were directed to the platinum-boron, platinum-silicon, palladium-silicon, palladium-aluminum and titanium-silicon systems--all of which exhibit low melting eutectics.

a. Braze alloy evaluation techniques

For the initial braze alloy study, T-joint, laminate, and sandwich panel specimens, as shown in Fig. 47, were used to evaluate selected brazing alloy systems. The T-joint specimens provided a simple screening test with which brazements could be evaluated both visually and metallographically. These specimens were used to determine the brazing characteristics of all filler alloys with respect to wetting, filleting action, alloying and erosion.

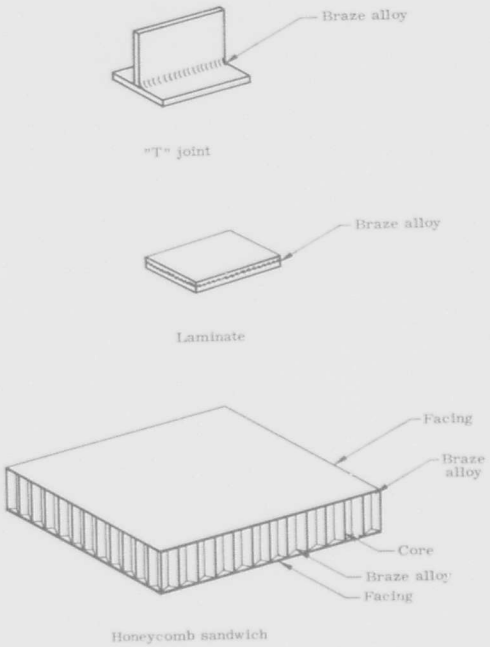

Fig. 47. Specimen Configurations for Braze Alloy Evaluation and Selection

Laminate specimens were useful in determining the wetting action of braze alloys over large faying surface areas. These were representative of actual edge-member-to-panel skin joints and were used to evaluate further those alloys which provided satisfactory T-joints. Finally, honeycomb sandwich specimens were used for evaluation of the most promising alloys. These small sandwich panels were checked visually and metallographically to determine the action of the filler alloy on the thin foil core.

All brazing was accomplished in a cold wall, high temperature vacuum furnace (Fig. 48), which was used to fabricate the test panels. Operating pressures generally ranged between 10^{-4} and 10^{-5} torr. All test specimens were chemically cleaned prior to brazing. The following solutions were utilized:

Molybdenum	Columbium
95% H_2SO_4	10 to 15% HF
4.5% HNO_3	60% HNO_3
0.5% HF	H_2O balance
18.8 g/l Cr_2O_3	

These solutions were used at 120° to 140° F; immersion times varied between two and five minutes.

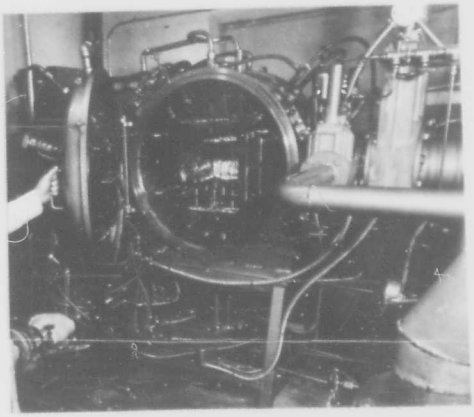

Fig. 48. Cold-Wall Vacuum Brazing Furnace

b. Initial braze alloy studies

The braze alloys selected for initial evaluation with TZM and D-36 and the results obtained are summarized in Table 7. Of the four braze alloys selected for evaluation with TZM, two (Haynes 25 and Inconel) had flow temperatures at or below the anticipated recrystallization temperature of TZM for the brazing time cycle required for panel fabrication. Haynes 25 exhibited the best brazing characteristics (Fig. 49) and provided ductile joints. These brazing studies were conducted on TZM material which exhibited greater resistance to recrystallization than the material received later for fabrication of the test panels. The original test material could be heated to 2600° F for short periods without recrystallizing, as shown in Fig. 49. As a result of this study, it was assumed that Haynes 25 would be satisfactory for fabricating the TZM structural test panels. However, the effects of extended high temperature exposure on these brazements were not evaluated at this time.

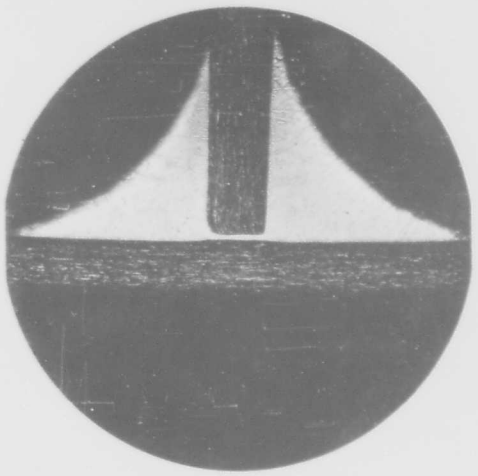

TZM T-joint brazed with Haynes 25 alloy at 2600° F. Some alloying has occurred with negligible erosion of base material. (75X)

Fig. 49. TZM Brazed T-Joint--Haynes 25

Laminate specimens (approximately 1 by 3 in.) of the original TZM test material were prepared to evaluate edge closure sealing. Haynes 25 and commercially pure titanium braze alloys provided satisfactory void-free laminates, which were anticipated and indicative of the excellent wetting action of both braze materials. A laminate brazed with Haynes 25 is shown in Fig. 50.

TZM-Haynes 25 brazed laminates were selected for studying techniques to seal the test panels hermetically and prohibit possible deleterious interactions between the brazing alloy and the protective coating. Electron

TABLE 7

Braze Alloys Initially Evaluated for TZM Molybdenum and D-36 Columbium

Braze Alloy	Nominal Composition	Brazing Temp (°F)	Braze Study Results with TZM Molybdenum	Braze Study Results with D-36 Columbium
Haynes 25	55% Co, 20% Cr, 15%W, 10% Ni	2600	Excellent wetting and filleting characteristics; ductile joint	Not evaluated
Inconel	80% Ni, 14% Cr, 6% Fe	2550	Excellent wetting and filleting. Brittle joint due to brittle intermetallic phase	Not evaluated--low melting eutectic forms between columbium and nickel
Palladium	100% Pd	2900	Good filleting and wetting. Ductile joint. Base metal recrystallized and extremely brittle	Excellent filleting and wetting. Severe alloying with base metal occurred. Ductile joint
Pd-Cu	60% Pd, 40% Cu	2250	Not evaluated	Excellent filleting and wetting. Severe alloying with base metal. Ductile joint
Titanium	Commercially pure titanium	3100	Excellent filleting and wetting. Braze joint showed some ductility, but recrystallized base alloy extremely brittle	Good wetting and marginal filleting. Excellent joint ductility. Severe alloying above 3100° F, but with improved filleting

beam welding was selected as the best technique to effect the closure seals for edge-member-to-skin brazements on the test panels. Weld parameters were established utilizing the small test laminate specimens. As shown in Fig. 51, the laminate edges were successfully sealed and there appeared to be no detrimental effects on the welded joints as a result of braze alloy dilution with the parent material. The electron beam weld sealing technique was selected for all closure seals on the test panels and also for the attachment of shear load strips required on some test panels.

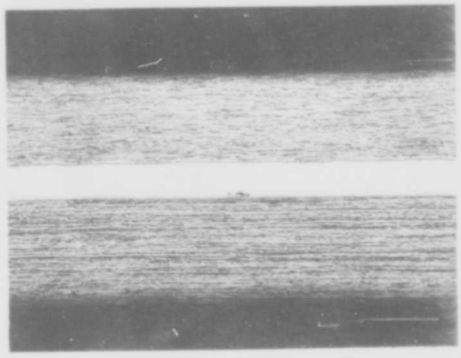

TZM laminate brazed with Haynes 25 alloy at 2600° F. The lack of void areas indicates the excellent wettability of the braze alloy.

Fig. 50. TZM Brazed Laminate (65X)

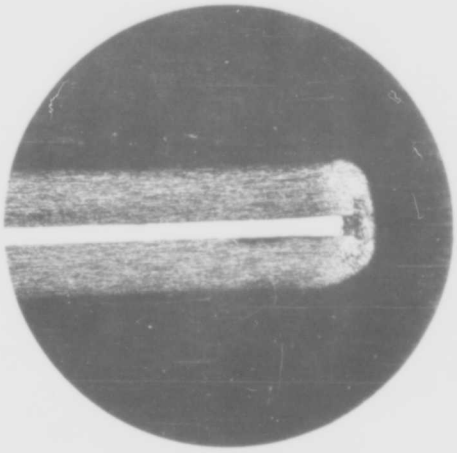

A photomicrograph of a TZM laminate brazed with Haynes 25 alloy and subsequently electron beam welded on an edge. (75X)

Fig. 51. TZM Brazed Laminate

Although these preliminary weld tests were satisfactory, major problems were encountered in welding and sealing the fabricated test panels. These problems are discussed in detail in Section V-F on panel sealing.

Pure palladium and titanium were evaluated as possible braze alloys for TZM heat shield panels. Both braze metals exhibited exceptional filleting and wetting characteristics. However, the parent TZM material was recrystallized and extremely brittle (Figs. 52 and 53).

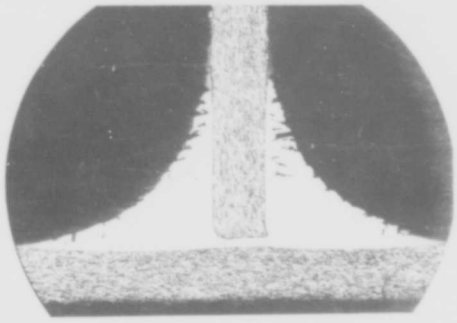

A TZM T-joint brazed with pure palladium at 2900° F. The voids shown in fillet are shrinkage voids. Very little alloying and erosion have occurred. (75X)

Fig. 52. TZM T-Joint--Pure Palladium Braze

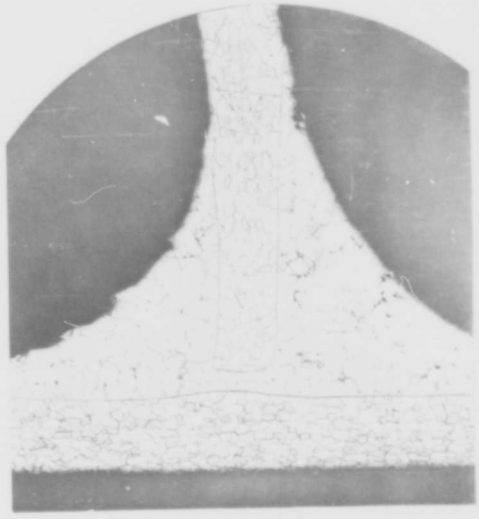

A TZM T-joint brazed with commercially pure titanium at 3100° F. An alloy bond is evident with slight erosion of the parent metal. (75X)

Fig. 53. TZM T-Joint--Pure Titanium Braze

Commercially pure titanium produced a satisfactory braze on D-36, although fillets were small and some erosion occurred even at 3100° F which is the minimum flow temperature for pure titanium (Fig. 54). Increasing the brazing temperature to 3200° F for optimum flow resulted in severe erosion of the parent D-36 material as shown in Fig. 55.

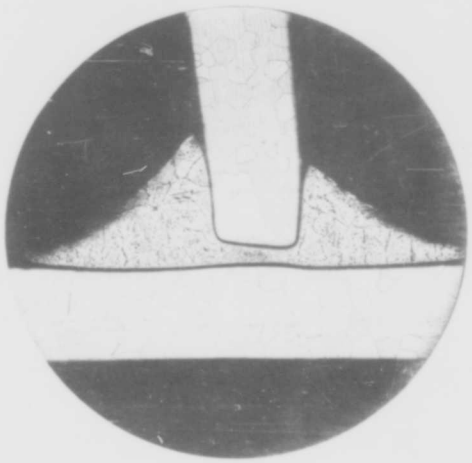

A photomicrograph of a D-36 T-joint brazed with commercially pure titanium at 3100° F. Filleting action of the braze alloy is marginal at this temperature. (75X)

Fig. 54. D-36 T-Joint--Pure Titanium Braze

Difficulties with severe erosion and alloying were also experienced with palladium and palladium base brazing alloys on D-36. As shown in Fig. 56, pure palladium alloyed severely with D-36 columbium. Prior brazing experience with palladium in conjunction with unalloyed columbium and the D-31 (Cb-10%Ti-10%Mo) alloy indicated no adverse effects. T-joint specimens were prepared and brazed with pure palladium at 2900° F to verify prior test results. Photomicrographs of these T-joints are shown in Figs. 57 and 58. Very little alloying or erosion was noted for the columbium-palladium brazement. However, some alloying and erosion of D-31 were obtained with pure palladium. In neither case was the alloying and/or erosion as severe as with the D-36-palladium combination. Similar results were obtained on D-36 in brazing with a 60%Pd-40%Cu alloy (Fig. 59).

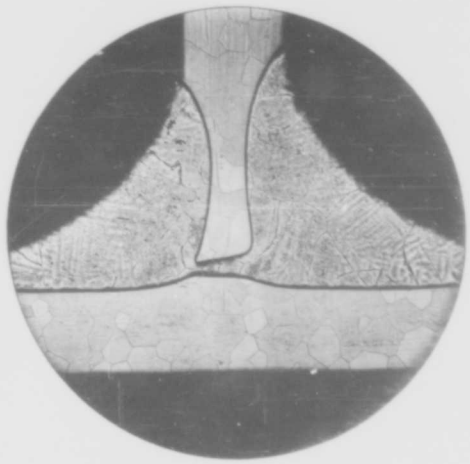

D-36 T-joint brazed with commercially pure titanium at 3200° F. Erosion of the base alloy has occurred as a result of braze temperature increase to improve filleting characteristics. (75X)

Fig. 55. D-36 T-Joint Brazed with Titanium at 3200° F

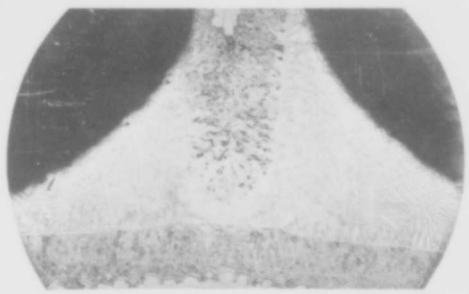

A D-36 T-joint brazed with pure palladium at 2900° F. Severe alloying has occurred between the base and filler material. This reaction has not been evidenced with either pure columbium or Cb-10Ti-10Mo. (75X)

Fig. 56. D-36 T-Joint--Pure Palladium Braze

The cause of this severe alloying was not investigated, but it was evident that palladium, or palladium-base alloys, could not be used with D-36. One possible contributing factor to the apparent sensitivity of D-36 columbium to both brazing alloys and temperature is the relatively low melting point of D-36 (3500° F) in comparison with unalloyed columbium (4474° F) and the D-31 alloy (4100° F).

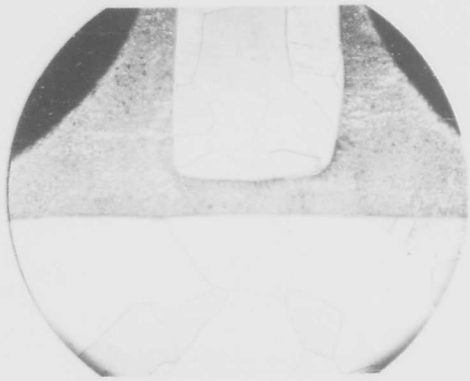

Photomicrograph of a pure columbium T-joint brazed with pure palladium at 2900° F. A very narrow alloy zone is indicated with no erosion of the base material (75X)

Fig. 57. Pure Columbium T-Joint--Pure Palladium Braze

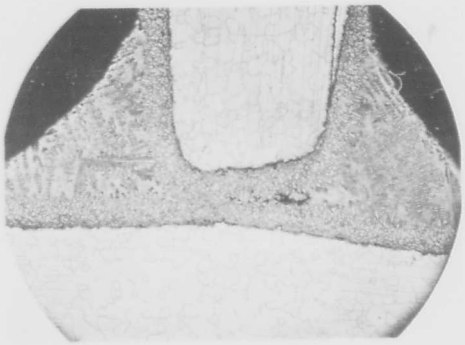

A photomicrograph of a Cb-10Ti-10Mo T-joint brazed with pure palladium at 2900° F. Alloying has occurred but is not as severe as noted in Fig. 56. (75X)

Fig. 58. Cb-Ti-Mo T-Joint--Pure Palladium Braze

While braze alloys which depend on volatilization to achieve higher remelt temperatures were not considered applicable for vacuum brazing, one alloy of this type--TZB (48%Ti-48%Zr-4%Be)--was briefly investigated. This alloy, developed by the Metallurgy Division of Oak Ridge National Laboratory, was reported to flow at approximately 2000° F in an inert atmosphere. Brazing tests conducted in vacuum indicated, as anticipated, that volatilization of the beryllium during heating raised the initial melt temperature to at least 2550° F.

This alloy had poor wetting and filleting characteristics when used to braze TZM. However, although some erosion occurred, the TZB alloy exhibited good filleting and wetting characteristics on D-36 columbium (Fig. 60). Attempts to attain a higher remelt temperature by subjecting these D-36 brazements to diffusion treatments at 2000° to 2200° F were unsuccessful.

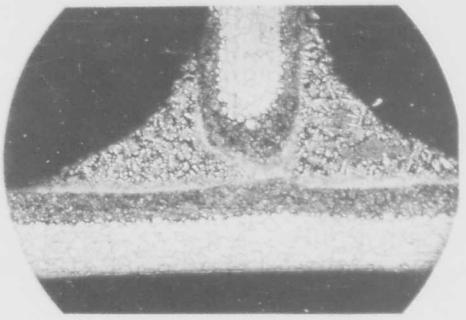

Photomicrograph of a D-36 T-joint brazed with 60Pd-40Cu at 2250° F. Again, severe alloying with the base material is evidenced, which indicates the possibility of a low melting eutectic reaction occurring between the ternary Cb-Ti-Zr and Pd-Cu. (75X)

Fig. 59. D-36 T-Joint--Pd-Cu Braze

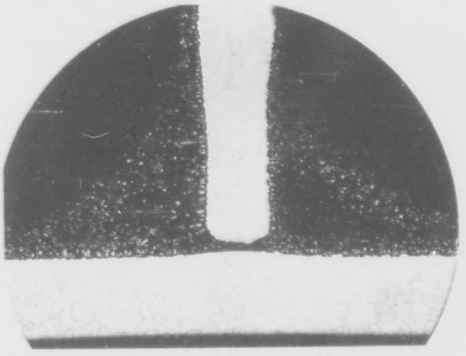

A D-36 T-joint brazed with 48Ti-48Zr-4Be at 2550° F. Erosion of the parent material is evidenced but is not considered severe. Specimen was etched to bring out grain structure of base metal. (75X)

Fig. 60. D-36 T-Joint--Ti-Zr-Be Braze

c. Higher remelt braze alloy evaluation

Because of the shortcomings of available conventional braze alloys, especially for the TZM molybdenum test panels, emphasis was then placed on the evaluation and development of higher remelt temperature braze alloy systems. A number of braze alloy systems were reviewed with which higher remelt temperatures might be

achieved by either the diffusion alloying or volatilization techniques. The alloys selected for evaluation on TZM and D-36 and the results obtained are summarized in Tables 8 and 9.

Of the alloys listed in Tables 8 and 9, two (93%Pd-7%Al and 97%Pd-3%Be) depended on volatilization to achieve higher remelt. Although attempts to braze the TZB alloy in vacuum were unsuccessful, it was hoped

TABLE 8

Brazed Alloy Systems Evaluated for Higher Remelt Capabilities on TZM Molybdenum

Braze Alloy Nominal Composition	Braze Alloy Flow Temperature (°F)		Brazing Characteristics	Remelt Capability Based on Separation Temperature Check
	Estimated	Actual		
48% Ti, 48% Zr, 4% Be	2000	2550--due to volatilization of beryllium	Poor filleting and wetting. No joint strength	
96.5% Pt, 3.5% B	1600	1800	Excellent flow and filleting. Braze joint extremely brittle	No increase by diffusion heat treatment and addition of base metal powder to braze alloy
95.5% Pt, 4.5% Si	1550	2050	Good flow and filleting. Braze joint extremely brittle	
93% Pd, 7% Al	2000	2600--volatilization of aluminum (?)	Good flow and filleting. Braze joint extremely brittle	
97% Pd, 3% Be	1750	2600--due to volatilization of beryllium	Good flow and filleting. Braze joint shows little or no ductibility	
95% Pd, 5% Si	1500	2100	Fair flow and filleting. Braze joint shows good ductility	
91.5% Ti, 8.5% Si	2450	2550	Fair flow and filleting. Braze joint shows good ductility	Diffusion treatment raised separation temperature above 3000° F with addition of base metal powder

TABLE 9

Brazed Alloy System Evaluated for Higher Remelt Capabilities on D-36 Columbium

Braze Alloy Nominal Composition	Braze Alloy Flow Temperature (°F)		Brazing Characteristics	Remelt Capability Based on Separation Temperature Check
	Estimated	Actual		
48% Ti, 48% Zr, 4% Be	2000	2550--due to volatilization of beryllium	Excellent filleting and wetting. Slight erosion of base metal. Good joint ductility	No increase after heat treat for 2 hours at 2200° F
96.5% Pt, 3.5% B	1600	1800	Good filleting and wetting. Braze joint extremely brittle	No increase by diffusion heat treatment and addition of base metal powder to braze alloy
95.5% Pt, 4.5% Si	1550	2050	Good flow and filleting. Braze joint extremely brittle	
93% Pd, 7% Al	2000	2600--volatilization of aluminum (?)	Excellent filleting and wetting. Braze joint extremely brittle	
97% Pd, 3% Be	1750	2600--due to volatilization of beryllium	Marginal flow and filleting. Some joint ductility	
95% Pd, 5% Si	1500	2100	Good flow and filleting. Braze joint extremely brittle	
91.5% Ti, 8.5% Si	2450	2550	Good flow and filleting. Excellent joint ductility	Diffusion treatment raised separation temperature above 2800° F with addition of base metal powder

hat carefully controlled brazing cycles would permit brazing at the estimated flow temperatures for these systems. Maximum heating rates and minimum hold times at brazing temperature were employed in an effort to avoid rapid volatilization of the high vapor pressure constituents, but without success. No further effort was made to utilize the volatilization technique for attaining higher remelt temperatures.

The higher remelt temperature braze alloys selected for evaluation were prepared in a standard arc-melting furnace. The 50- to 75-gm arc-melted buttons were given homogenizing heat treatments, then crushed or filed and ground into powders. Testing of these alloys was conducted on T-joint specimens, and visual and metallographic examinations were made to evaluate the brazing characteristics of each with respect to wetting, filleting action, alloying, erosion, etc. Tests were conducted to define the remelt temperature (based on separation under a small load) of some of the selected alloy systems.

Consideration was given to the possibility that the remelt temperature of Haynes 25 might be raised by longer holding times at brazing temperature or by a subsequent diffusion treatment. The primary advantage of utilizing Haynes 25 as a brazing alloy was its availability in foil form. Foil material is easily preplaced for brazing, whereas powdered braze alloys such as Ti-8.5%Si and Pt-3.5%B would present problems in preplacement during panel assembly prior to brazing.

T-joint specimens of TZM were brazed with Haynes 25 and held at the brazing temperature for various times. Additional specimens were subsequently diffusion heat treated. No increase in remelt temperature was achieved for the TZM-Haynes 25 combination (Table 10). However, it was noted that extended times at the brazing temperature or extended diffusion treatments at high temperatures (2200° F) embrittled the TZM-Haynes 25 braze joints.

An evaluation was conducted of several platinum- and palladium-base alloy systems with which higher remelt temperatures might be achieved by diffusion alloying of the brazement with the base material. Boron and silicon were used as liquidus temperature depressants. These alloy systems were not suitable for the structural joining of TZM or D-36. The flow and filleting characteristics

TABLE 10

Summary of Braze Alloy Remelt Tests

Base Metal Braze Combinations	Test Load (gm)	Test Temperature (°F)						
		2750	2850	2900	2950	3100	3150	3250
TZM, Ti-8.5% Si								
As brazed	10	--	--	--	Failed	--	--	--
Diffused 3 hr at 2200° F	10	--	--	--	No failure	--	No failure	Failed
	20	--	--	--	No failure	--	No failure	Failed
	30	--	--	--	No failure	--	Failed	--
Diffused 6 hr at 2200° F	10	--	--	--	No failure	--	No failure	Failed
Diffused 3 hr at 2300° F	10	--	--	--	No failure	--	No failure	Failed
Diffused 3 hr at 2400° F	10	--	--	--	No failure	--	No failure	Failed
TZM, Haynes 25								
As brazed--no hold time	10	Failed	--	--	--	--	--	--
As brazed--15-min hold	10	Fail d	--	--	--	--	--	--
Diffused 3 hr at 2200° F	10	Failed	--	--	--	--	--	--
D-36, Ti-8.5% Si								
As brazed	10	--	Failed	--	--	--	--	--
Diffused 3 hr at 2200° F	10	--	--	No failure	--	Failed	--	--
	20	--	--	No failure	--	--	--	--
D-36, B-120VCA								
As brazed	10	--	--	--	--	Failed	--	--

of these braze systems were generally satisfactory, but the brazed joints were extremely brittle and often cracked (Figs. 61 and 62).

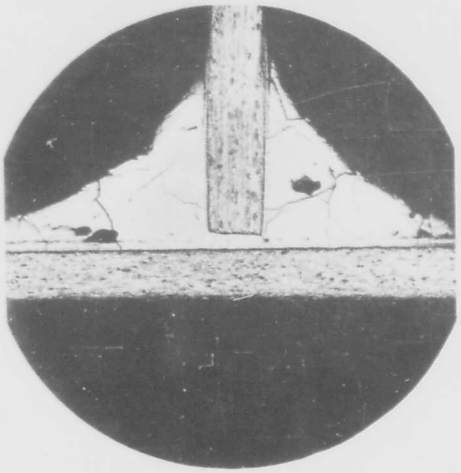

Fig. 61. TZM T-Joint--Pt-3.5% B Braze (75X)

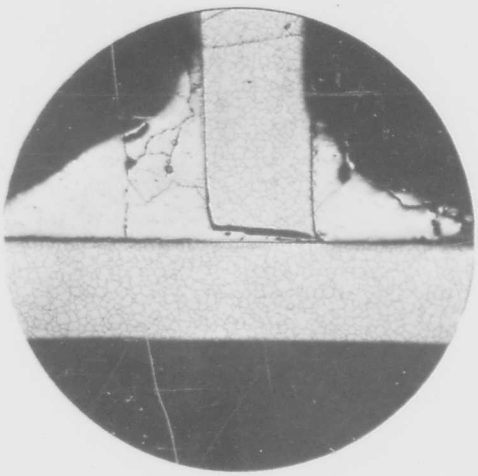

Fig. 62. D-36 T-Joint--Pt-3.5% B Braze (75X)

Attempts were made to circumvent the brittleness problems experienced with the platinum- and palladium-base alloys through process variations. T-joint specimens of TZM molybdenum-Pt-3.5%B were brazed and subsequently diffusion heat treated in a single cycle, to avoid cooling to room temperature before diffusion heat treatment. This processing cycle did not alleviate the brittleness problem. Molybdenum powder additions to the braze alloy also did not help to reduce the brittleness. Additional effort to resolve the brittleness problems experienced with the higher remelt temperature precious metal braze alloys was discontinued in view of the more promising results which were concurrently being obtained on the titanium-silicon system.

The titanium-silicon system (Ref. 36) showed promise. The 8.5%Si eutectic composition melts at approximately 2425° F--some 600° F below the melting point of pure titanium. Brazements exhibited excellent filleting and wetting, and were ductile and free from cracks.

Studies were conducted to determine if the remelt temperature of Ti-8.5%Si brazements could be increased to 3000° F or higher by diffusion heat treatment. T-joint specimens were prepared, with molybdenum powder added to the brazing alloy powder, and brazed at 2550° F. These were exposed to various heat treatment cycles and checked for remelt temperature, as manifested by joint separation under a small load. The maximum capabilities achieved with a 2200° F, three-hour diffusion heat treatment were 3150° F for joint loads up to 2 psi and 2950° F for a joint load of 6 psi, with no joint separation (Table 10).

The addition of molybdenum powder to the filler alloy provided greater assurance of the completeness of the reaction between the braze alloy (Ti-8.5%Si) and the base metal. A ratio of braze alloy to refractory metal powder of 4:1 was found to be optimum. Excessive additions retarded flow and required a further increase in the brazing temperature.

The changes in the microstructure as a result of diffusion alloying are evident in Figs. 63 and 64. Figure 63 shows a TZM T-joint brazed at 2550° F with molybdenum powder added to the Ti-8.5%Si filler alloy. Very little alloying of the filler with the base material and molybdenum powder occurred. The matrix is of eutectic composition, with a dispersion of molybdenum powder. After a three-hour diffusion heat treatment at 2200° F, definite alloying occurred at the base-metal-braze-alloy interface. There was also diffusion alloying of the braze alloy and the molybdenum powder. The structure is essentially the same as that shown in Fig. 64, after diffusion treatment and subsequent exposure under a small load at 2950° F. There was no evidence of melting at this temperature.

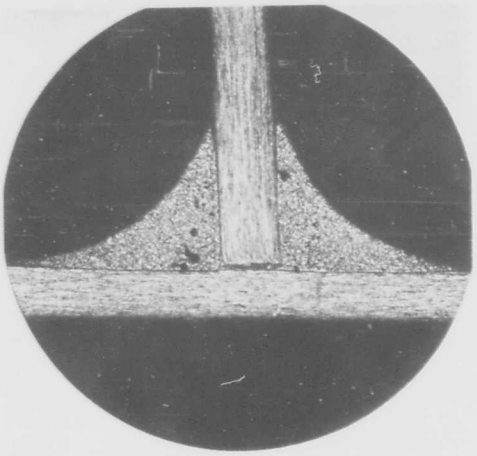

Fig. 63. TZM T-Joint--Ti-8.5% Si Braze (75X)

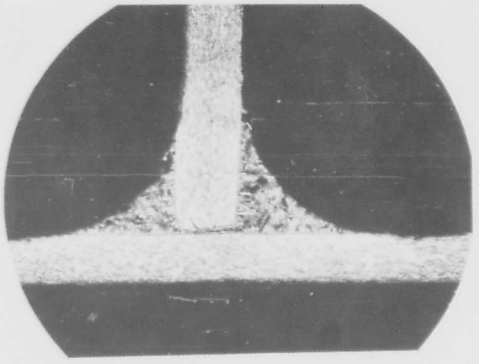

Fig. 64. TZM Brazed Joint After Test at 2950° F (75X)

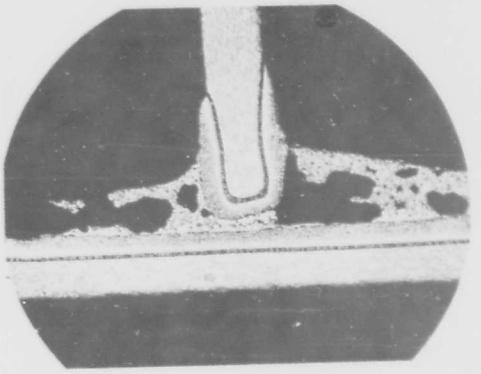

Fig. 65. TZM Molybdenum Brazed with Ti-8.5% Si After Separation Test at 3150° F (75X)

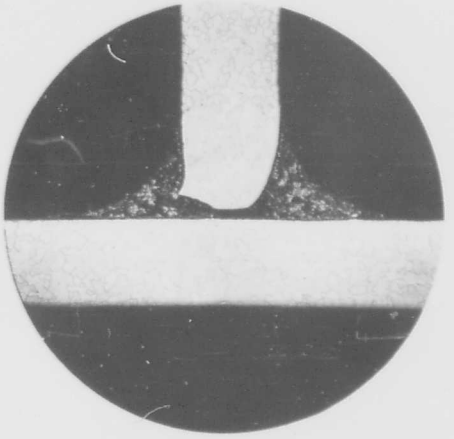

Fig. 66. D-36 T-Joint--Ti-8.5% Si Braze (75X)

Figure 65 shows a T-joint specimen heated to 3150° F without separation. However, some fillet area melting of the braze alloy occurred, indicating gross heterogeneity in the composition of the brazement. Additional development effort will be required to reduce this heterogeneity, including refinements in powder preparation and blending techniques.

The Ti-8.5%Si system provided excellent, ductile fillets on D-36 (Fig. 66), and, with the addition of powder filler metal and diffusion heat treatment, the separation temperature was increased slightly (Table 10).

d. Braze alloy selection

At this point in the study program, the TZM sheet material for test panel fabrication was received. Braze alloy tests conducted with the new TZM material indicated that it rapidly recrystallized at 2550° F. Figure 67 shows the new TZM material brazed with Ti-8.5%Si at 2550° F and held at brazing temperature for 15 minutes; the parent material is essentially fully recrystallized. The original test material (cf Fig. 63) could be held at 2600° F for 5 minutes without re-

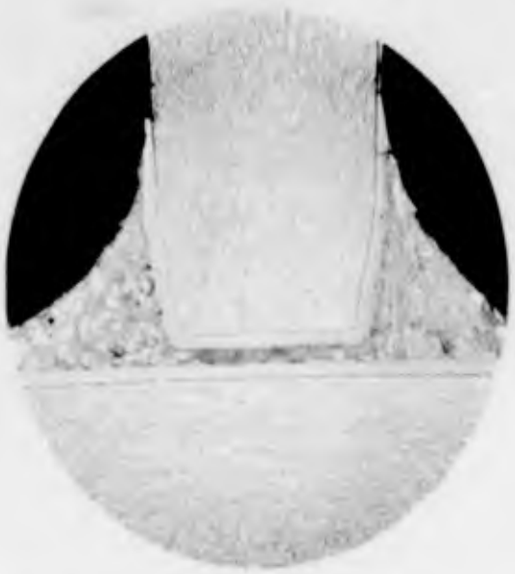

Fig. 67. TZM Molybdenum Sew Material Brazed with Ti-8.5% Si at 2550° F and Diffusion Treated at 2400° F for Four Hours (75X)

crystallizing. The Ti-8.5%Si higher remelt alloy system was being developed on the premise that the 2550° F braze cycle would not cause any recrystallization of the TZM material. Further development of this specific alloy was discontinued when the material to be used in the test panel fabrication was found to recrystallize at this brazing temperature.

Because of the increased operational temperature benefits that could be gained with higher remelt alloys, an effort was made to modify the Ti-8.5%Si system to permit brazing at or below 2400° F. The modified alloys evaluated are summarized in Table 11. Tests were conducted to establish whether a braze temperature of 2400° F or less could be realized. Three alloys exhibited good flow at 2400° F: 64.5%Ti-27.5%V-8%Si, 78%Ti-13.5% Cr-8.5%Si, and 48.5%Ti-48.5%Zr-3%Si. The wetting and filleting characteristics of these three alloys were evaluated. They showed satisfactory wetting action, but produced very thin brittle joints. Further development of these alloy systems was stopped when it became evident that an extended effort would be required to develop a satisfactory higher remelt alloy for the TZM panel material.

At this time, conventional palladium-base braze alloys that flow between 2200° and 2400° F were evaluated. These included 60%Pd-40%Cu, 70%Pd-30%Cu, 60%Pd-40%Co, 70%Pd-30%Ag, and 54%Pd-10%Cr-36%Ni. All

TABLE 11

Flow Characteristics of Modified Ti-Si-Alloy Powders

Braze Alloy	Flow Characteristics	
	2400° F	2450° F
B120VCA Titanium-8.5% Si		Good
B120VCA Titanium-9% Si		Poor
B120VCA Titanium-9.5% Si		Poor
B120VCA Titanium-10% Si		Good
B120VCA Titanium-10.5% Si		Good
65% Ti-27.5% V-7.5% Si	No flow	
64.5% Ti-27.5% V-8% Si	Good	
64% Ti-27.5% V-8.5% Si	No flow	
78% Ti-13.5% Cr-8.5% Si	Excellent	
76.5% Ti-13.5% Cr-10% Si	No flow	
74.5% Ti-13.5% Cr-12% Si	No flow	
48.5% Ti-48.5% Zr-3% Si	Excellent	
47% Ti-47% Zr-6% Si	Marginal	
46% Ti-46% Zr-8% Si	Marginal	

produced uniform ductile fillets when joints were held at the brazing temperature for very short times (up to one minute). However, when longer brazing cycles were employed or when the brazements were subjected to temperatures just below the flow point for more extended periods (Pd-Cr-Ni system only), the alloys diffused extensively into the TZM alloy, and complete recrystallization of the parent metal occurred in these areas.

The time-temperature relationships for the palladium-copper system when utilized to braze TZM proved very critical. Figure 68 shows a TZM T-joint brazed with 60%Pd-40%Cu at 2250° F and held approximately 1 minute at temperature. No evidence of recrystallization can be seen. However, when the brazing temperature was increased 50° F, the 60%Pd-40%Cu alloy diffused into the parent TZM material and almost complete recrystallization was obtained (Fig. 69). Tests were conducted with the 60%Pd-40%Cu alloy on TZM to determine the effects of holding times of 1, 5, 10 and 15 minutes at the recommended 2250° F flow temperature for the system. With holding times longer than 1 minute, recrystallization of the TZM was increasingly effected through diffusion of the braze alloy in the parent material (Fig. 70). Maximum depth of the recrystallized zone was reached after a 10-minute hold time (approximately 0.003 in.). Similar, but strikingly more detrimen-

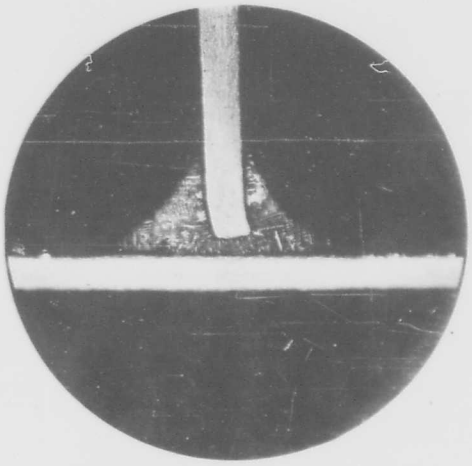

Fig. 68. TZM Molybdenum Brazed at 2250° F with 60% Pd-40% Cu Braze Alloy (1 min at braze temperature (75X)

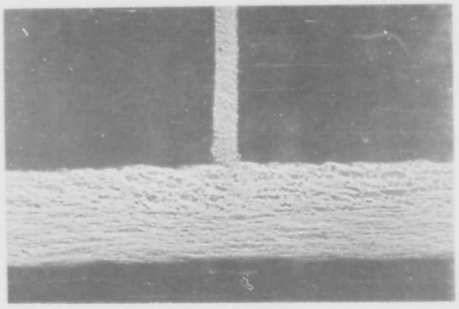

Fig. 69. Photomicrograph of TZM Sheet and Core Brazed with 60% Pd-40% Cu at 2300°F (200X)

tal, results were obtained with the 70%Pd-30%Cu alloy. The higher brazing temperature (2400° F) produced complete recrystallization of the TZM sheet and core material as shown in Fig. 71.

Figure 72 shows the microstructure of a T-joint specimen brazed with Premabraze 101 (54%Pd-10%Cr-36%Ni) at 2350° F, in which recrystallization started at the braze alloy-parent metal interface. A companion T-joint specimen was heated at 2200° F for 15 minutes and subsequently heated to 2400° F under a small load. Joint separation did not

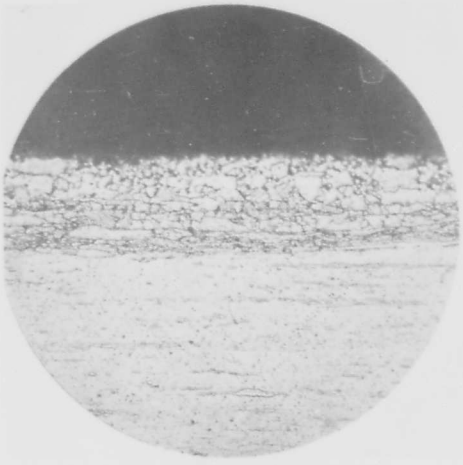

Fig. 70. TZM-0.008-in. Foil Brazed with 60% Pd-40% Cu at 2250° F with 10-Minute Hold Time (525X)

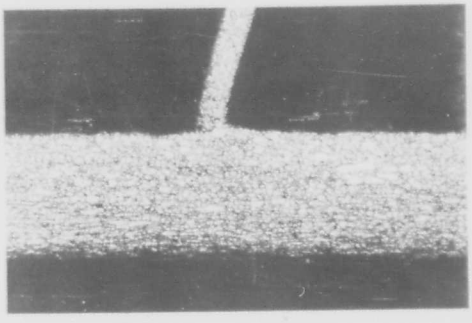

TZM honeycomb core to skin joint brazed with 70% Pd-30% Cu at 2400° F for 8 min. Specimen was extremely brittle with all the braze alloy diffusing into the base metal (200X).

Fig. 71. TZM Molybdenum Specimen Brazed with 70% Palladium-30% Copper

occur but the parent material was completely recrystallized (Fig. 73) and there was severe erosion, primarily as a result of nickel diffusion.

From these studies, it was evident that none of the palladium-base alloys with flow temperatures in the range of 2300° to 2400° F was acceptable. It was also evident that considerable additional development would be

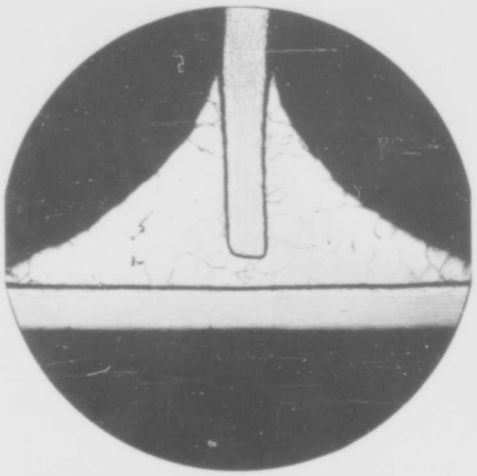

Recrystallization at braze alloy-material interface. (75X)

Fig. 72. TZM Molybdenum Brazed with Prema-braze 101 (54% Pd-10% Cr-36% Ni) at 2350° F

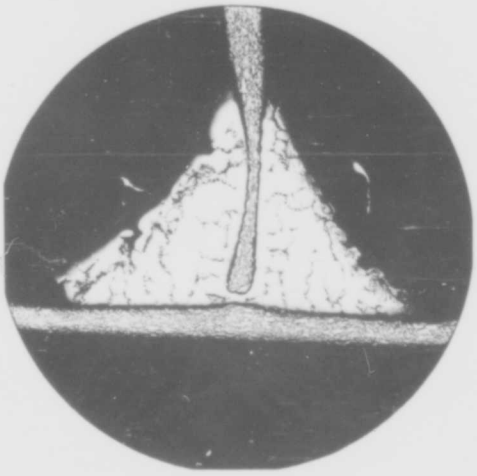

Braze made at 2350° F and then subsequently exposed to 2200° F for 15 min, 2300° F for 15 min and 2400° F for 15 min under a small load. (75X)

Fig. 73. TZM Molybdenum Brazed with Prema-braze 101 (54% Pd-10% Cr-36% Ni)

necessary to provide an acceptable alloy which would flow in the 2300° to 2400° F range.

It was concluded, at this time, that the best resolution of this brazing problem was to select a braze alloy that did not diffuse rapidly into the base metal and produce immediate and complete recrystallization, even if this involved brazing at temperatures slightly above those which recrystallized the TZM material. In making this decision, it was necessary to accept some recrystallization. However, if the maximum temperature and the time above 2400° F were held to a minimum, the extent of recrystallization could be limited.

Haynes 25 met these requirements and was selected as the braze alloy for TZM structural panels. This alloy has excellent filleting and node flow characteristics (Fig. 74). Test strips of TZM, which were brazed for 5 minutes at 2550° F, had sufficient room temperature ductility so that cold bends could be made without fracturing the strips. However, based on the results of extended exposure at the braze temperature and on the diffusion heat treatment cycles evaluated in conjunction with the higher remelt temperature studies, the total time at these higher temperatures must be restricted to avoid serious embrittlement.

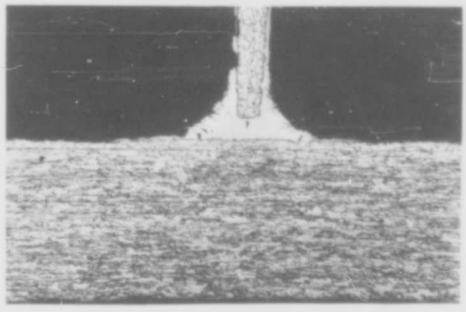

Photomicrograph of cross section of 0.012-in. TZM skin to core brazed with Haynes 25 at 2550° F for 5 min. No stop-off was used. (200X)

Fig. 74. TZM Molybdenum Core to Skin Brazed with Haynes 25

The high braze temperatures required for pure titanium and B-120 VCA titanium completely recrystallize TZM. However, it was not known how seriously this em-

brittlement would affect handling, testing and possible vehicle application. Therefore, it was decided to braze two panels with these alloys before the final decision on the TZM heat-shield panel was made.

Since D-36 columbium structural panel brazing temperatures were not similarly restricted, no direct effort was made toward finding a higher remelt temperature alloy for D-36. From the initiation of the study, it was considered that titanium or titanium alloys could be used to braze D-36. The D-36 study consisted of checking the TZM braze alloys on D-36. None of these alloys showed any advantages over titanium. Titanium and B-120 VCA, a chromium-vanadium-aluminum-titanium alloy, were selected for D-36 test panel brazing. The latter alloy flows at 2950° F and is somewhat more sluggish than commercially pure titanium, thus permitting the brazing of relatively wider gaps. This alloy was used advantageously in fabricating the D-36 heat shield panels, where problems arose in the fabrication of the heat shield pans with adequate flatness.

A D-36 columbium T-joint brazed with B-120 VCA titanium is shown in Fig. 75. The microstructure shows metallurgical bonding along the braze alloy-base metal interface and complete alloying of the braze alloy with the honeycomb foil. The joint is ductile and can be bent double without fracture. A pure titanium-D-36 columbium braze joint has a similar structure but exhibits less alloy bonding and diffusion.

e. Braze stop-off evaluation

During the braze alloy evaluation studies, TiO_2 (titanium dioxide), in a suitable lacquer binder, was used to retard the flow of the braze materials. Relatively small amounts of this stop-off material were required. No adverse effects were noted in parent metal behavior which could be attributed to the use of the TiO_2 stop-off.

Prior to actual panel fabrication, several large sandwich panels were brazed to check both the stop-off material and the test panel tooling. It was found that the TiO_2 stop-off material, which was suitable for brazing small specimens, severely contaminated the D-36 columbium alloy when brazed at 2900° to 3200° F, and made it extremely brittle at room temperature (Fig. 76). This embrittlement was attributed to the fact that TiO_2 was not entirely chemically inert at these temperatures and pressures.

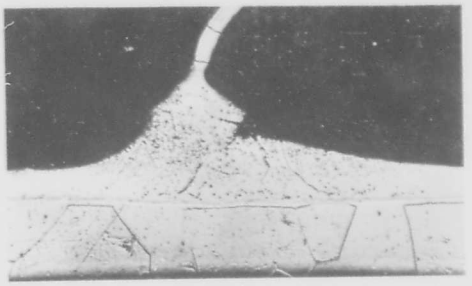

Braze made at 2950° F for 15 min. Specimen was ductile and could be bent without fracture. (200X)

Fig. 75. D-36 Columbium Specimen Brazed with B-120 VCA Titanium

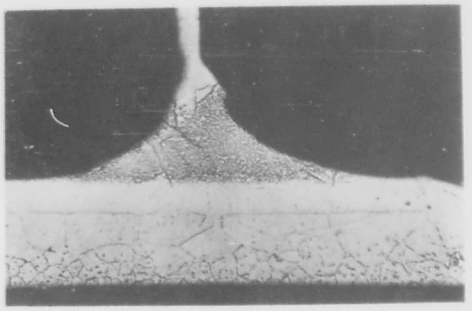

Braze made at 2950° F for 15 min in presence of TiO_2 stop-off. Specimen was extremely brittle. Note retarded grain growth and pronounced grain boundaries on the surface exposed to the stop-off. (200X)

Fig. 76. D-36 Columbium Brazed with B-120 VCA Titanium

Several additional materials which might serve as stop-off agents were evaluated. These included alumina (Al_2O_3), magnesia (MgO), zirconia (ZrO_2), silicon carbide (SiC), and graphite cloth. Tests were made to determine whether any of these had the necessary stop-off characteristics, namely, chemical inertness at the temperatures and pressures to be used, and restriction of braze flow. The results of these tests are summarized in Table 12.

None of these materials was completely satisfactory as a stop-off agent. Zirconia was sufficiently inert and served as an effective separating agent, but it was not

TABLE 12

Stopoff Evaluation Summary

Stop-Off Material	Test Temp (°F)	Base Material	Braze Alloy	Effects Upon Base Material
TiO_2	2950	D-36	B-120VCA Titanium	Serious embrittlement
Al_2O_3	2950	D-36	B-120VCA Titanium	Embrittlement
MgO	2950	D-36	B-120VCA Titanium	Embrittlement
SiC	2950	D-36	B-120VCA Titanium	Very slight embrittlement. Very difficult to remove
Nicrobraz Red	2950	D-36	B-120VCA Titanium	Embrittlement
Graphite cloth	2950	D-36	B-120VCA Titanium	No embrittlement. Material picks up carbon. Extremely difficult to remove
Graphite cloth	3150	D-36 TZM	A-55 Titanium	Same as above
ZrO_2	2400	TZM	70% Pd-30% Cu	None visible.
ZrO_2	2950	D-36	B-120VCA Titanium	None visible. No embrittlement
ZrO_2	3150	TZM	A-55 Titanium	As above.
ZrO_2	3150	D-36	A-55 Titanium	None visible. No embrittlement

completely effective in restricting braze alloy flow. The other materials contaminated and, in most cases, severely embrittled the D-36 alloy. D-36 columbium brazed in the presence of ZrO_2 stop-off showed no evidence of contamination (Fig. 77).

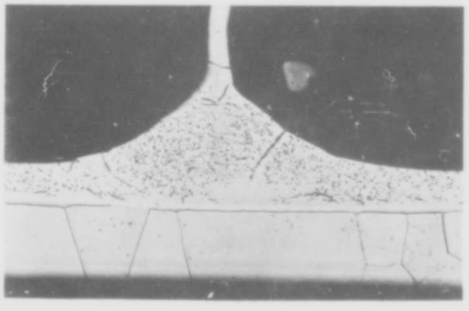

Braze made at 2950° F for 15 min in presence of ZrO_2 stop-off. Specimen was ductile and could be bent without fracture. (200X)

Fig. 77. D-36 Columbium Specimen Brazed with B-120 VCA Titanium

As a result of these studies, zirconia was selected for use as a stop-off agent in the fabrication of the TZM molybdenum and D-36 columbium test panels.

2. Braze Tooling

Exploded views of test panel braze tooling, which was fabricated for a curved heat shield panel and a flat structural panel, are shown in Figs. 78 and 79. Similar tools were made for flat heat shield and curved structural panels. To avoid thermal expansion mismatch problems, tools were made from both TZM and D-36.

Tooling details were made from 5/16-in. TZM and D-36 plate and were heliarc welded in an argon dry box. Columbium filler wire was used for both TZM and D-36.

After the plate stiffeners and the edge member details were welded, each tool was stress relieved at 2200° F. To avoid cracking, the TZM tools were preheated to 200° F before welding and maintained at this temperature until stress relieving. Some warpage occurred as a result of welding and stress-relieving. Each tool was straightened on a brake press and re-stress relieved; this cycle was repeated until dimensional

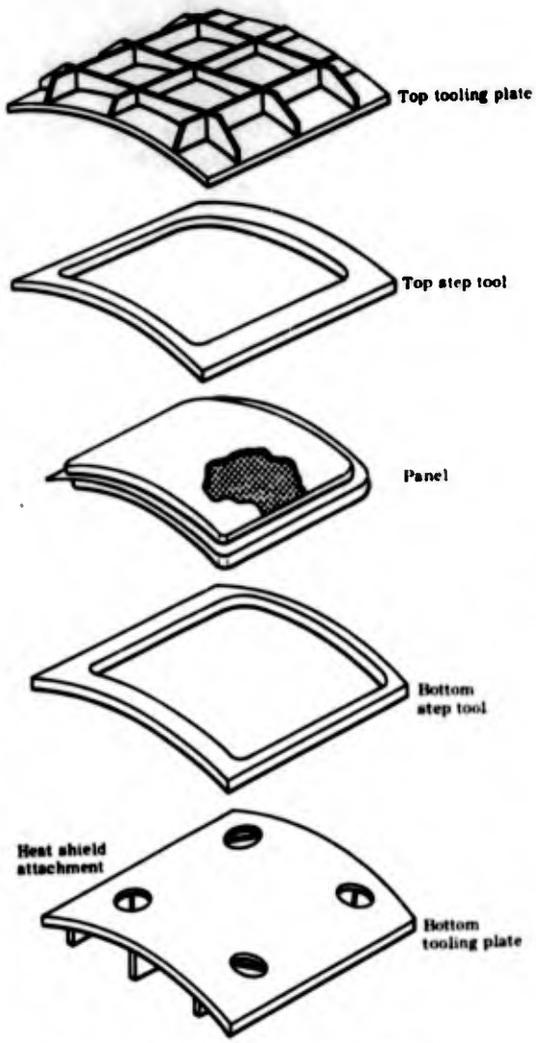

Fig. 78. Curved Refractory Metal Structural Panel (D-36 and TZM)

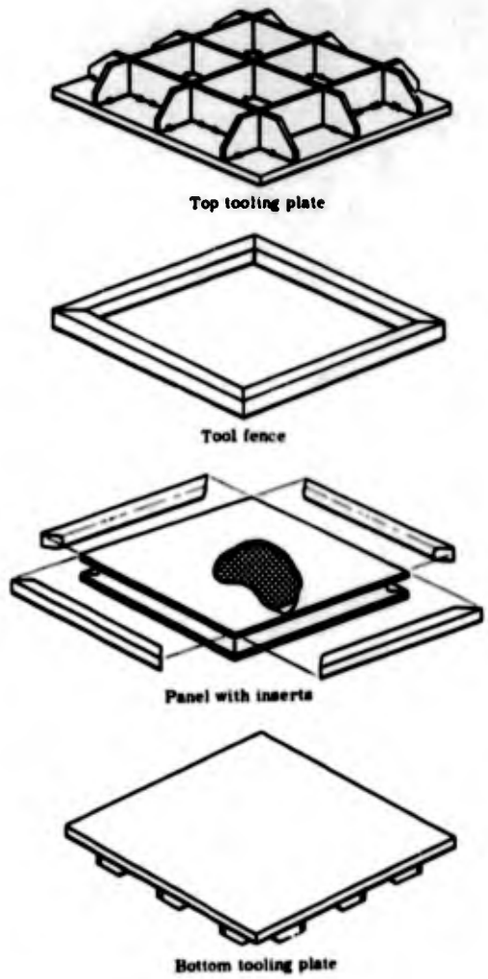

Fig. 79. Flat Refractory Metal Structural Panel (D-36 and TZM)

stability was attained. The mating surfaces were then machined and the tool again stress relieved; this cycle was repeated if necessary. Curved tools were turned to shape on a King vertical turret lathe, and flat surfaces were ground (±0.0005-in. tolerance). Each tool was then subjected to a simulated thermal brazing cycle and refinished and recycled, if necessary, until dimensional stability was obtained.

Recesses and slots were cut into the heat shield bottom tooling plates to provide space for the support clips and doubler discs. The top and bottom step tools served as spacer rings which were machined to fit around the steps in the heat shield panels. These served to apply pressure for brazing in the step areas. Inserts or spacer bars, built up as laminates from sheet stock and placed in the U-channels of the structural panels, were used to ensure proper brazing contact pressure between the U-channel and the skin, and to prevent crushing of the U-channel.

The same top and bottom tooling plates were used for the flat structural and flat heat shield panels. The curved structural and heat shield panels were designed with the same outer radius so that the same top tooling plate could be used. Because of the different panel thicknesses, separate bottom tooling plates were required for the curved structural and heat shield panels.

3. Panel Brazing

Test panel brazing was accomplished in a cold wall vacuum furnace. The furnace has a 13- by 13- by 13-in. heating zone with tantalum-strip heater elements (Fig. 48), with the work supported in the center of the furnace on nine 1/2-in. diameter tungsten pins. Furnace temperature was monitored with two tungsten-rhenium thermocouples. Heating was manually controlled to ensure that the proper vacum (2×10^{-5} torr) was maintained during the total braze cycle.

a. Panel assembly

Braze alloy. The structural panel braze alloy foil was trimmed 3/16 in. smaller (in width and length) than the facings (Fig. 80). Small strips, 0.45 in. wide, were cut to fit along the inner legs of the U-channel edge member.

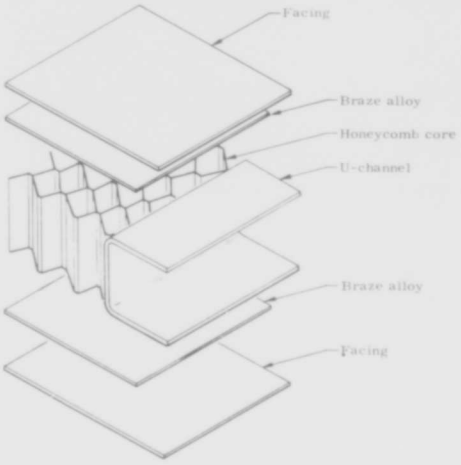

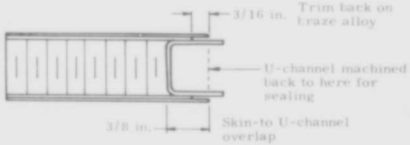

Fig. 80. Trimming Back Braze Alloy from Edge of Panel to Prevent Excess Flow from Joint

The heat shield panel braze alloys were marformed over the same tools used for the heat shield facing. This provided excellent fit and eliminated the trimming and handling of many small pieces. The titanium brazing alloys were formed at 300° F. After forming, the braze alloy was trimmed 3/16 in. smaller (in width and length) than the heat shield facing pan.

Cleaning. All panel details were cleaned (Table 6) and placed in polyethylene bags. All handling of cleaned panel details was accomplished with clean white cotton gloves.

Assembly. The structural panel braze alloy was tack-welded to the inner surface of the facing and the U-channel. The core was slipped in place in the frame and the facings were tack-welded to the U-channel. A complete structural panel layup is shown in Fig. 81.

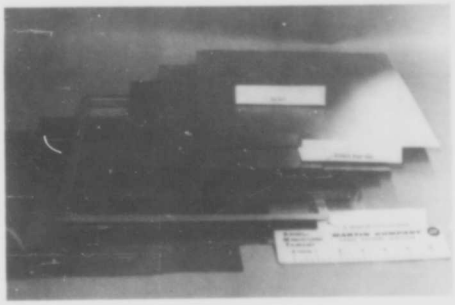

Fig. 81. Panel Buildup for Brazing Showing Flat D-36 Columbium Structural Panel (B-120 VCA braze alloy titanium)

The heat shield panel braze alloy was tack-welded to the inner surface of the facing. The core was then placed on one facing and the other facing placed on top. The facings were slipped into place and held with small clamps. The overlapping lips around the edges of the panel were resistance-tack-welded together; any copper pickup was removed by light sanding. The braze alloy disc was then tack-welded to the inner face of the support clip.

To facilitate the tack-welding of the TZM panels, 1/8- by 1/8- by 0.002-in. pieces of titanium were used as an interlay.

Application of stop-off. The surfaces of the braze tools were coated with ZrO_2 stop-off in a suitable nitrocellulose lacquer (Raffi and Swanson No. 1830). Thin separator sheets were used between the braze tools and the panel. The surfaces in contact with the panel were coated with stop-off. These separator sheets were used to prevent panel-to-tool

bonding as a result of excessive braze alloy flow.

For the structural panels, the outer surfaces of the laminated U-channel inserts were coated with stop-off. For the heat shield panels, the spacer rings were coated with stop-off.

All stop-off coated parts were placed in an oven at 300° to 400° F for about one hour to accelerate drying of the lacquer.

Panel brazing. The assembled panels were placed on the braze tools (Figs. 82 and 83) and then placed inside the vacuum furnace (Fig. 84).

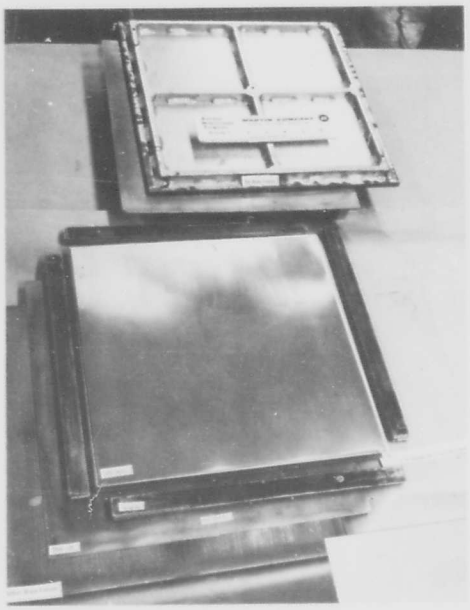

Fig. 82. Braze Tool Buildup for Brazing Flat D-36 Columbium Structural Panels

The furnace was evacuated to 10^{-4} torr before the power was turned on. Furnace power was regulated until a temperature of 1000° to 1100° F was reached. The furnace was maintained in this temperature range to permit outgassing of the load until the pressure dropped to 2×10^{-5} torr. This operation usually took about 5 to 15 minutes.

Fig. 83. Braze Tool Buildup for Curved D-36 Columbium Heat Shield Panel

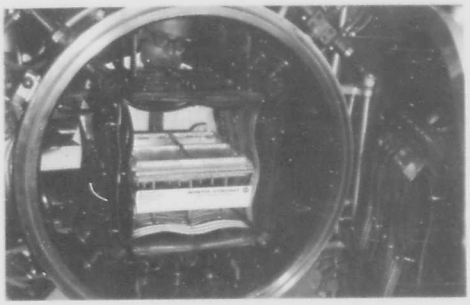

Fig. 84. Flat D-36 Columbium Braze Tools in Furnace

During the panel braze cycle, a 2150 ± 50° F step was used to provide time for the braze-tool temperature to stabilize, to prevent any nonuniform temperature distribution from warping the braze tools. This step also provided extra time for any outgassing that occurred above the 1100° F plateau. All brazing was done at a vacuum of 2×10^{-5} torr or less.

Four distinct thermal cycles were used for panel brazing: Haynes-25-TZM panel system (Fig. 85); pure titanium braze cycle for both TZM and D-36 (Fig. 86); B-120 VCA titanium with D-36 (Fig. 87); and B-120 VCA titanium with TZM (Fig. 88). For the TZM panels, the time above 2200° F was held to a minimum to limit recrystallization.

Two problems were encountered in the test panel brazing. One was a result of the oilcans in the D-36 material, the other the out-of-curvature of the TZM U-channel frames.

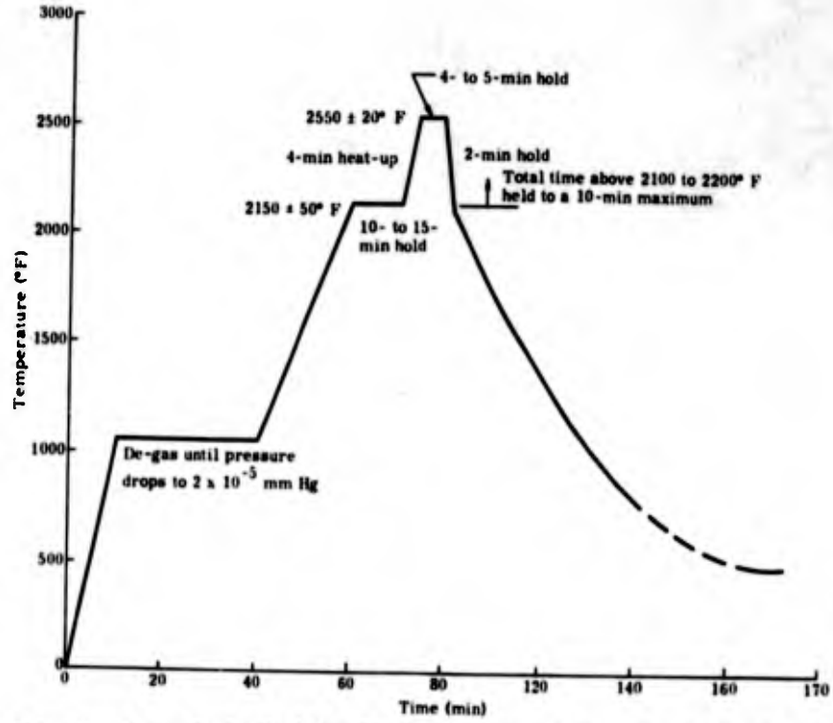

Fig. 85. Braze Cycle Used for T2M Structural Panels (Haynes 25 braze alloy)

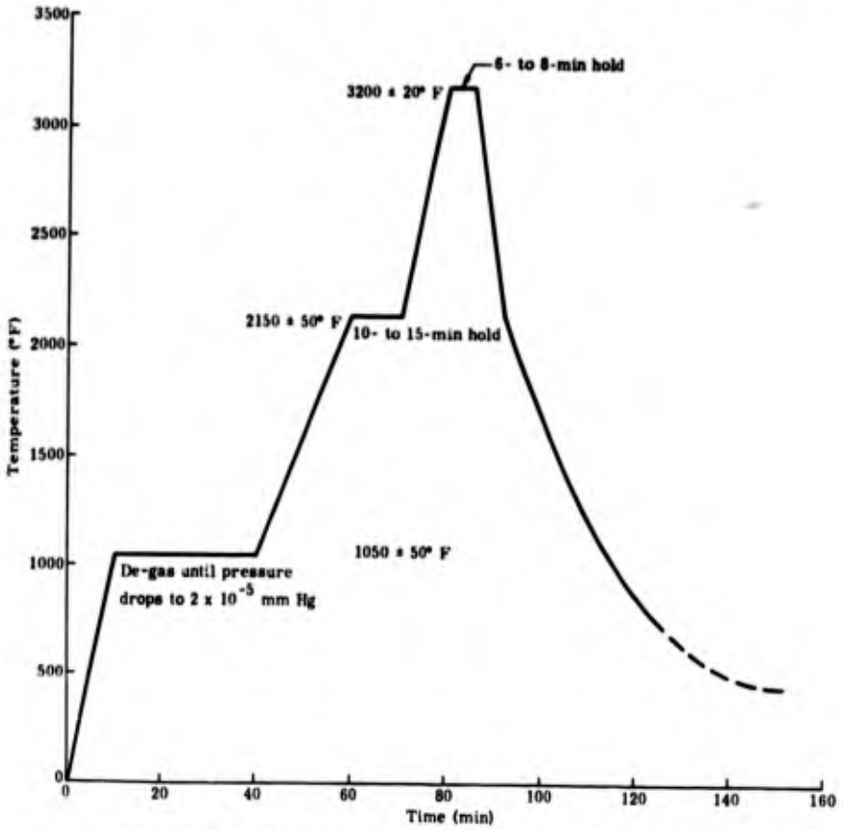

Fig. 86. Braze Cycle Used with A-55 Titanium Braze Alloy

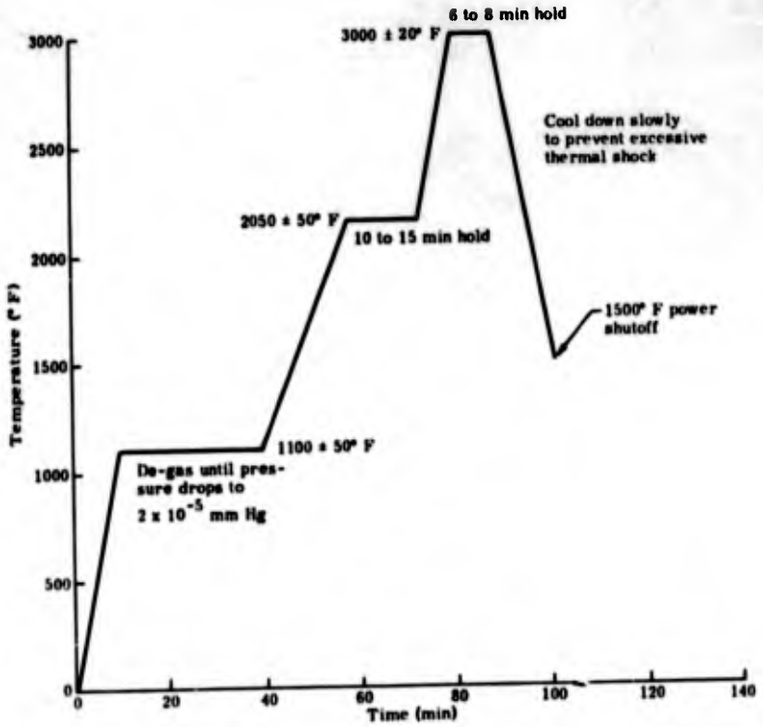

Fig. 87. Braze Cycle Used on D-36 Panels (B-120 VCA titanium braze alloy)

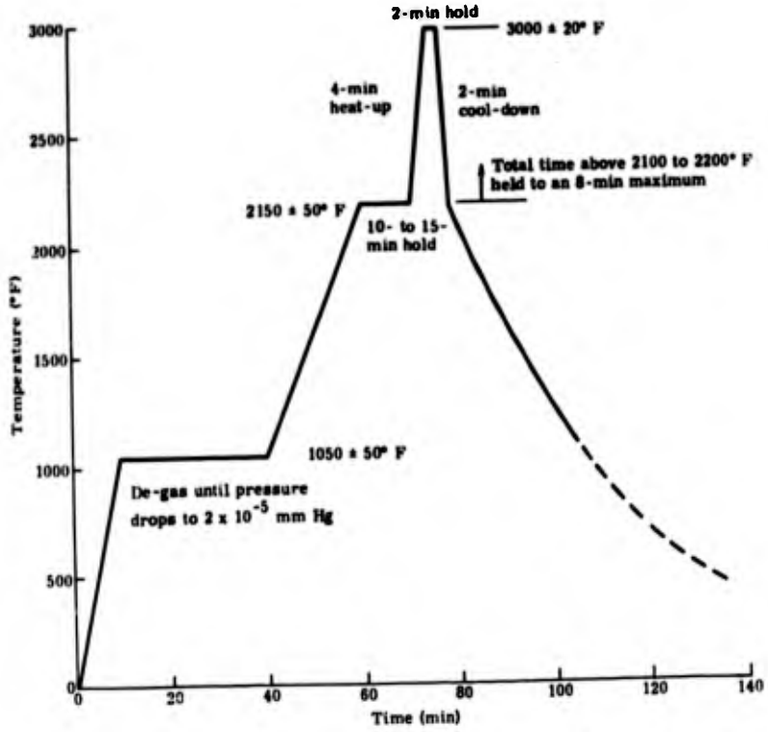

Fig. 88. Braze Cycle Used for TZM Heat Shield Panel (B-120 VCA titanium braze alloy)

The 0.008-in. D-36 sheet material had oilcans that caused severe problems in brazing the heat shield panels. The panels would braze satisfactorily but would have blisters along two edges, due to the oil-canning. Creep flattening the sheets for one hour at 2200° F in vacuum and utilizing B-120 VCA titanium as the braze alloy (instead of pure titanium) virtually eliminated blistering. The B-120 VCA titanium braze alloy provided larger fillets and was capable of bridging larger gaps between the core and facing than the pure titanium.

In brazing curved TZM panels, it was necessary to have an extremely close match between the braze tool curvature and the U-channel frame curvature, if braze voids were to be eliminated. This was not the case with D-36. It was considered that, at the 3000° F braze temperature, the D-36 U-channel frame was so weak that it would rapidly creep to fit the stiffer braze tools, thus assuring the contact required for brazing. However, the TZM frames at the 2550° F braze temperature still had sufficient strength to bridge any existing mismatches, resulting in braze voids. This was corrected by reworking the frames, where necessary, to assure proper contact before brazing.

Cleaning. Any traces of stop-off adhering to the panels were removed with a soft brush or very fine emery paper. In Fig. 89, a flat structural panel is shown after removal from the braze furnace, and a heat shield panel is shown in Fig. 90. The panels were bright and clean when taken from the furnace. The panels did not have the characteristic dimpling that is associated with panels brazed under a uniform static pressure.

Any excess flow of braze alloy was removed by lightly sanding the contaminated area.

Fig. 89. Flat TZM Molybdenum Structural Panel

Fig. 90. Curved D-36 Columbium Heat Shield Panel Showing Support Clips

D. PANEL FINISHING

The principal finishing operation, prior to coating, was electron beam welding to make various closure seals. This was done to prevent possible deleterious reactions between the braze alloy and the oxidation protection coating. Attachment strips were also electron beam welded to the flat structural panels.

The feasibility of making the required joints was checked out on small prototype specimens, with specific attention to welding in the presence of braze alloy at closure seals. No problems were apparent. However, major difficulties were encountered when attempts were made to scale-up these techniques to the test panels. Only limited design changes were possible because panel details were already fabricated, and a considerable number of the panels had already been brazed.

1. Structural Panels

a. D-36 columbium

The edges of the D-36 structural panels were machined straight and parallel. The curved panel corners were rounded to a 1/8-in. radius, the edge radii to a minimum radius of 0.010 in.

Eight 0.040-in. load attachment strips, 12- by 1.25-inch strips for each flat structural panel, were sheared to rough size and machined to final size. The three edges and two corners of the strips that were not to be welded to the panel were rounded and smoothed. The panels and strips were trichlorethylene vapor degreased and stored in polyethylene bags.

Welding parameters were established for the load attachment strips and edge sealing (Fig. 22). A simple tool was fabricated to hold the panels for welding the special load attachment strips to the shear test panels. This consisted of an insert bar and a plate which were held in place by a clamp.

The strips were electron beam welded to the flat panel edges as shown in Fig. 45. A typical weld is shown in Fig. 91. The first two panels were welded without tacking the ends of the strip to the panel, and excessive mismatch caused pinholes and unwelded gaps. Attempts to repair these by both TIG and electron beam welding were unsuccessful. Tacking at each end eliminated the problem and the remaining eleven panels were successfully welded. The welds were inspected by painting a fluorescent dye on the weld surface at the inner leg of the U-channel and then examining the outer surface of the weld under ultraviolet light. If there had been any cracks or pinholes that went through the entire weld, the dye could have been seen on the outer surface of the weld. None of the panels sent to the coating facility for test purposes had any such cracks or pinholes.

Fig. 91. Photomicrograph of Electron Beam Welded D-36 Columbium Joint Attachment Strip to Panel Weld (Magn 75X)

A drill template was made for locating the holes in the attachment strips (Fig. 92). This template was made from the fixture used for the panel shear test. The holes were drilled and then reamed to 0.257-in. diameter. All edges were rounded.

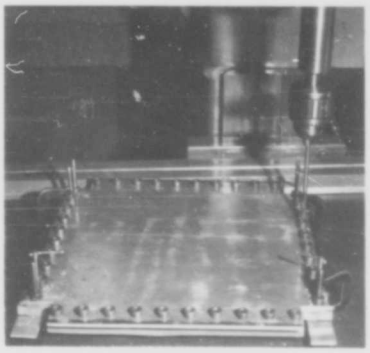

Fig. 92. Reaming Holes to Size in Shear Strips of a D-36 Flat Structural Panel

All eight edges of the curved panels were sealed by electron beam welding.

After welding, the panel edges were inspected to determine if there were any weld defects. A fluorescent dye penetrant check was made and any defects were repaired. All panels selected for coating passed this check without any defects. The welded edges were examined to determine if the welding caused any roughening of the surface that might cause a weak spot in the coating. Any questionable areas were smoothed by sanding.

All panels were again trichlorethylene vapor degreased and placed in a polyethylene bag. The completed panels were placed in individual boxes and then boxed in lots of five. These lots were then shipped to Thompson-Ramo-Wooldridge for application of the Cr-Ti-Si coating.

Upon receipt of the panels at Thompson-Ramo-Wooldridge for coating, they were vapor degreased, given an acid etch and inspected for flaws. Some very small intergranular cracks were discovered in some of the flat structural panels with load attachment strips. The cracks extended from the attachment strip weld into the panel and were usually normal to the welds (Fig. 93). The cracks did not go through the entire weld, but, apparently, just penetrated to the brazed joint.

Such cracks could not be repaired by welding with any consistency. Accordingly, repair of these cracks was not attempted, and all panels, including those that contained these small cracks, were coated. The cracks could not be detected after coating, indicating that the coating either filled in or bridged

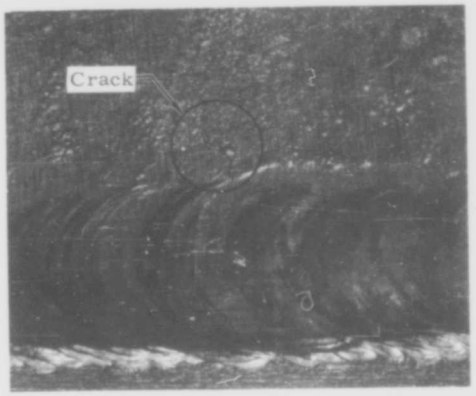

Fig. 93. Intergranular Crack in Electron Beam Welded D-36 Columbium Structural Panel (Magn 10X)

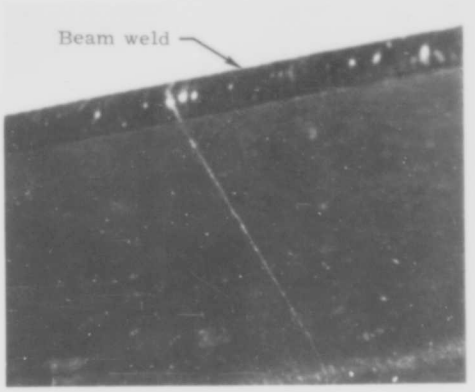

Fig. 94. Typical Crack on TZM Structural Panel Edge

over these imperfections. No oxidation or structural flaws that could be attributed to these cracks were observed in subsequent testing at temperatures up to 2400° F.

b. TZM molybdenum

Serious problems were encountered both in welding the load attachment strip and in edge sealing. Weld settings were developed for these joints, but severe cracking of the welds and adjacent material could not be eliminated.

In welding the miter joints of the U-channel frames for the TZM structural panels, it was necessary not only to stress relieve at 2200° F after welding, but to weld at 250° F and store at 250° to 300° F without intermediate cooling prior to stress relief. A similar welding and stress relieving cycle was used to edge-seal a TZM panel. Cracks were found on two edges after the complete heat treat cycle (Fig. 94). A second panel in storage at 250° F, awaiting the 2200° F stress relief treatment, was also found to be cracked. Cracks were normal to the weld and 1/4 to 1 in. in length.

Welding study. About 50 welding schedules, which involved various combinations of preheating, postheating, welding speed, welding voltage, welding amperage and stress relief, were evaluated in an unsuccessful attempt to determine a procedure which would prevent weld cracking.

Welds on one panel were planished (10% reduction in thickness) to introduce residual compression stresses in the weld areas. None of the planished welds cracked, but one edge cracked in storage at 250° to 300° F prior to planishing. It was evident that planishing, while helpful, would not eliminate the basic cracking problem. None of the procedures which were tried eliminated the basic problem of cracking prior to stress-relief.

Metallographic study. These studies indicated that the basic problems of welding molybdenum under high restraint were further aggravated by the presence of braze alloy in both closure seal and load attachment strip welds. Two contributing mechanisms were indicated: (1) the development of small intergranular cracks during solidification of the weld nugget and (2) the formation of a second phase between the molybdenum and the braze alloy in the weld zone.

Small intergranular cracks were found in the weld nuggets (Fig. 95). These probably occurred because of the large differences in the solidification temperatures of the nugget constituents. The braze alloy (Haynes 25-55Co-20Cr-15W-10Ni), or new compounds which formed, collected in most of these cracks, but some remained void. A microhardness survey (Fig. 96) indicated that an intermetallic compound had formed along some grain boundaries. Intercrystalline penetration and random entrapment of the braze metal in the parent weld metal were also observed.

The second phase in the molybdenum occurred in the form of a precipitate. Indications were that most of it formed during cooling after welding (Fig. 97), although

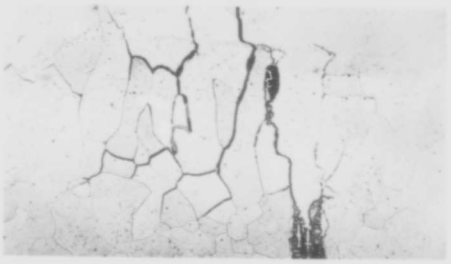

Fig. 95. TZM Molybdenum Structural Panel Electron Beam Edge Seal

Photomicrograph of electron beam weld nugget showing edge of nugget with braze joint. Material is in as-welded plus stress-relieved at 2200° F for one hour condition. Tukon microhardness (150-gm load) check indicates the highly alloyed zone is three times harder than parent metal. (350X)

Fig. 96. TZM Molybdenum Structural Panel Electron Beam Edge Seal

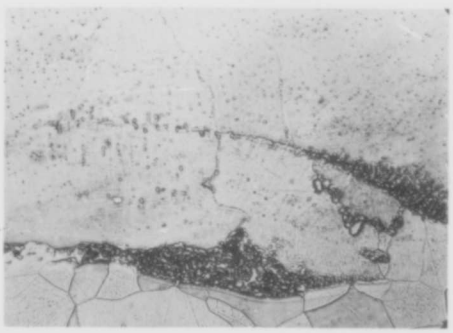

Photomicrographic of electron beam weld nugget showing the precipitation of the second phase of the molybdenum alloy. Lower part of picture shows highly alloyed zone between the braze alloy (55Co-20Cr-15W-10Ni) and the base metal. (700X)

Fig. 97. TZM Molybdenum Structural Panel Electron Beam Edge Seal

more precipitation did occur after a one-hour, 2200° F stress relief cycle (Fig. 93). A volume change is usually associated with the formation of a precipitate. Additional stresses will occur with a differential volume change between the weld and the parent material.

With small intergranular cracks in the welds, as well as an extremely brittle weld due to the presence of intermetallic compounds, normal welding stress, with or without those caused by the formation of the precipitate, will cause the welds to develop major cracks. Any subsequent loading or handling stresses will only aggravate this cracking. Because of the formation of the brittle intermetallic compound, the cracking could occur at any feasible storage temperature or during any subsequent thermal aging or treatment of the panel.

Once the microcracks and embrittled conditions in the weld exist, cracking will eventually occur, even though some treatment might postpone immediate cracking. The only way that cracking from this source can be prevented is by not welding in the presence of the braze alloy or by having braze alloys that form only single phase solid solution alloys with the base metal. The basic problem of making these high restraint welds per se may be difficult to solve.

In the test panels, all welding was designed to be of a secondary structural nature and was primarily to effect a hermetic seal which would protect the braze alloy from the oxidation protection coating. Only in the strips attached to the flat structural panel for load application purposes would any weld be required to sustain more than a very small stress. However, welds of this type must be able to withstand the stresses that will be incurred when the panels are used on any type of aerospace vehicle. It was concluded that structural TZM panels which involved welding could not be produced with sufficient structural integrity for satisfactory test. Major developments, both in improved alloys and welding techniques, would be required to produce acceptable molybdenum hardware of this type for both test and structural applications. Some panels, which were not edge sealed, were coated for testing in compression. No feasible technique for shear testing of the panels was available.

The TZM panel finishing consisted of machining the edges straight and parallel, rounding the corners and smoothing the edges. Machining was performed at about 250° F, by utilizing a setup in which the heat

was supplied by an electric heating blanket (Fig. 98). The panels were then cleaned (Table 6), wrapped and shipped to Pfaudler for application of the PFR-6 coating.

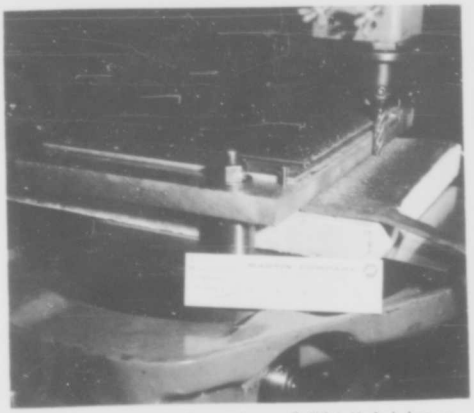

Fig. 98. Machining Edge of TZM Molybdenum Structural Panel

2. Heat Shield Panels

The heat shield panels required hermetic sealing around the panel periphery, at the access tube inserts and around the edges of the support clips.

a. D-36 columbium

After the panels were brazed, the access tube holes were drilled through the center of the support clip disc. A template was utilized in drilling these holes to assure proper location (Fig. 99). After drilling, these holes were reamed to fit 0.25-in. diameter, 0.010-in. wall tubing.

A rotary weld tool was made for electron beam welding the thin metal tubes in place to form the access holes in the heat shield panels. A photograph of the tool in the weld chamber is shown in Fig. 100.

The upper plate of this tool was supported above the lower plate on ball bearings and rotated on adjustable eccentric gears. The eccentricity could be changed to permit adjustment of the circular path to be welded. Rotary motion was provided by coupling the gears to the drive mechanism of the welder. It was also planned to use this tool to weld around the brazed doubler disc of the heat shield panel support clip so that no braze alloy would remain exposed.

NOTE:

D-36 columbium heat shield panel with access holes drilled and tube inserts shown.

Fig. 99. Tool for Locating Access Hole in Curved Heat Shield Panels

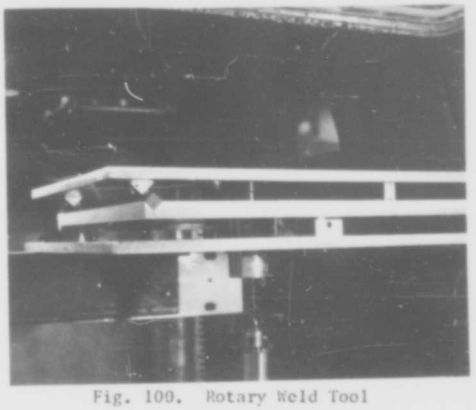

Fig. 100. Rotary Weld Tool

Another simple tool was also fabricated to hold the panels for welding around the periphery to seal all brazed joints. This consisted of a T-stand and a clamp.

The overlap edges of the heat shield panel facing were reworked prior to sealing. This was necessary to be sure that the facing edge, where the weld was to be made, was in contact with the other facing. Rework was accomplished by hand rubbing and resistance-tack-welding in the areas where elastic properties prevented closure (spring-type action of thin edge). All copper deposits were removed prior to welding.

The basic weld techniques required to seal these panels were checked out early in

the program on simulated specimens; but when they were first attempted on a full-scale panel, the results were unsatisfactory. The major problems occurred in sealing the support clip and the access hole tube insert. This welding caused pinholes, burn-through or cracking in the panel skins. The problem seemed to stem from having to make welds in an area of the sandwich panel facing over the honeycomb core. The primary difficulty was encountered in welding around the edge of the support clips and in welding the insert tubes to the external facing of the panel. When the electron beam was started around one of these joints, the titanium braze metal just ahead of the weld fusion zone started to melt and wet the surface of the two parts being sealed. As soon as this happened, the metal melted, but the braze alloy seemed to contaminate the surfaces so that the two parts did not fuse. The viewing system of the electron beam welder was used in making these observations.

When these difficulties were encountered, two supplementary studies were initiated. One was to conceive design modifications that would allow sealing of the joint in an area removed from the braze alloy; the other was to establish optimum electron beam weld parameters.

Design modification. Since the problems had arisen from welding along an exposed braze surface, it was considered necessary to make a panel design modification so the necessary sealing operation could be performed without any effects from the braze alloy. The panels were already brazed, so the best solution appeared to be the addition of a thin disc around the support clip and the tube insert (Fig. 101). This would allow the seal weld to be made on the panel skin away from the exposed braze joint. These discs would be nonstructural and would be used only to effect a seal.

Electron beam welding studies. A study was made to determine the effects of the variables encountered in welding the test panels and to establish optimum weld settings and weld joint configuration. This study started with simple D-36 sheet material and progressed to making welds on test panels. The D-36 columbium material utilized in this study was given a thermal treatment identical to that used in the test panel brazing to provide material comparable to that in the test panels.

The first welding investigation consisted of evaluating 14 different combinations of weld conditions on a sheet of 0.008-in. D-36.

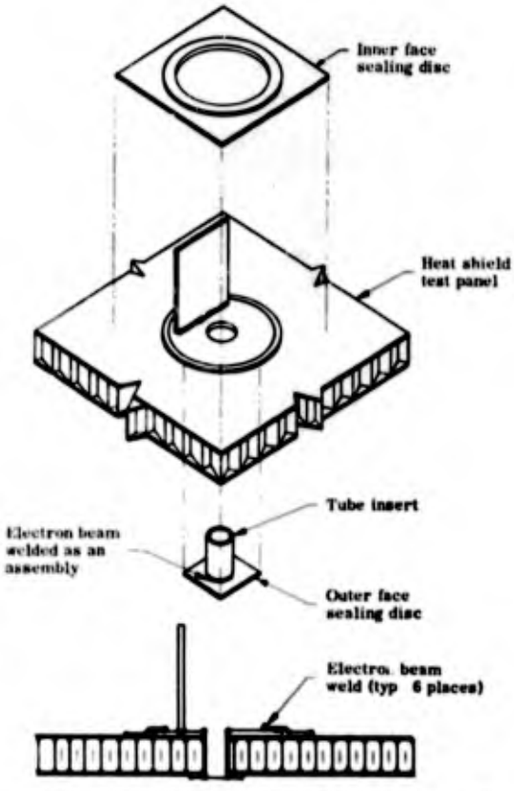

Fig. 101. Design Modification Made to D-36 Columbium Heat Shield Panels

Two voltage settings, nine amperage settings and two weld speeds were tried. Two settings were established that provided 100% penetration without cutting:

(1) 50 kv, 1.75 ma, 20-in./min weld speed.

(2) 80 kv, 1.00 ma, 40-in./min weld speed.

A wider weld nugget was obtained with the first setting because of the higher amperage and slower speed.

Nineteen different welding conditions were evaluated on two sheets of 0.008-in. D-36 columbium. These sheets were made to simulate a test panel facing (i.e., bare on one side and coated with B-120 VCA or pure titanium on the other (Fig. 102). The weld settings evaluated consisted of three voltages, 11 amperages and 3 weld speeds. The best weld settings were the same as those selected for the bare material.

Lap-type edge welds and overlay-type burn-through welds (Fig. 102) were evaluated on 0.008-in. D-36 columbium sheet material.

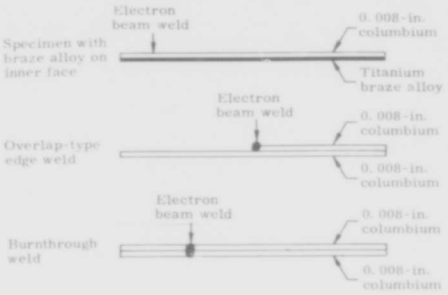

Fig. 102. Specimens Used in Electron Beam Welding Study

Fourteen specimens were made with these types of joints. The welding conditions evaluated consisted of 2 voltage settings and 8 amperage settings, at a welding speed of 20 in./min. The best welding conditions for the burn-through weld were 50 kv, 2.35 ma and 20-in./min weld speed; for the edge-type weld, 50 kv, 1.65 ma and 20 in./min.

To evaluate the effects of various welding conditions on an actual honeycomb panel, welds with various power and speed settings were made on the surface of a 0.008-in. D-36 facing brazed to a piece of 3/16-in. cell honeycomb core (Fig. 103). The optimum settings for making these welds were found to be close to those selected as optimum for welding the bare D-36 skin (50 kv, 1.65 ma and 20 in./min). It was found that, in most cases, a weld discontinuity occurred at the point where the weld passed over the core cell (Fig. 103). The discontinuity was usually in the form of a pinhole and a change in the width of the weld zone.

To determine if the settings established in these studies could be used to attach the sealing details in place, sixteen 1.25-in. and 0.5-in. squares were welded to the surface of one of the brazed panels. Weld settings of 50 kv, 1.65 ma and a speed of 20 in./min were used to attach these square patches. Of the 64 welds required to attach the patches to the panel, only 8 were found to have pinholes. These welds were inspected

Weld settings

Weld No.	17	16	15	14	13	12	11	10	9	8	7	6	5	4	3	2	1
kv	80	80	80	80	50	50	50	50	50	50	50	50	50	80	80	80	80
MA	1.25	1.25	1.25	1.25	1.75	1.75	1.75	1.75	1.75	1.5	1.25	1.0	.75	1.0	1.25	.75	.5
ipm	80	60	40	20	80	60	40	20	40	40	40	40	40	40	40	40	40

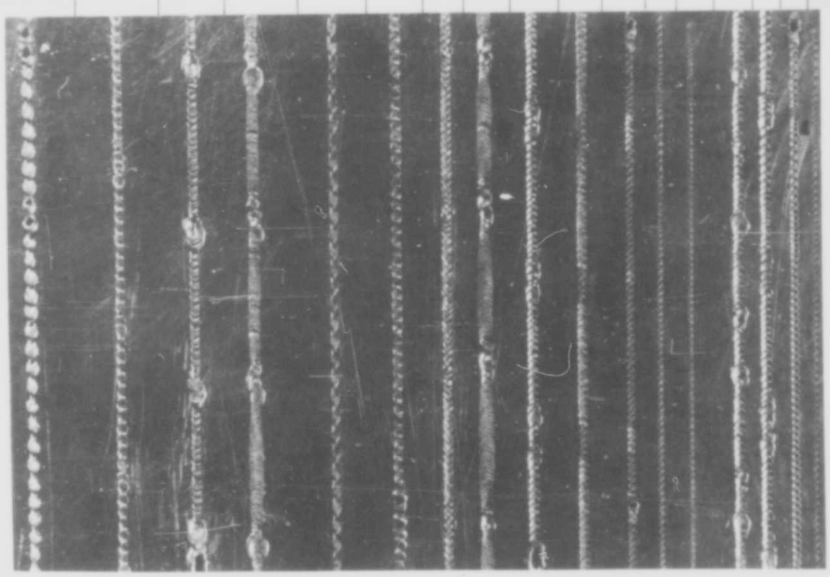

Fig. 103. Electron Beam Test Welds on D-36 Columbium Panel

by the Zyglo process (fluorescent dye penetrant). In general, the welds were of good quality and it was considered that, with proper control procedures and detail fit, a high percentage of good welds could be made, and any pinholes could be eliminated by rework.

Some sporadic cracking of D-36 welds was also encountered and, despite all efforts, could not be completely eliminated. This was true of the edge closure welds, which otherwise presented no major difficulties, as well as the clip and tube insert welds which have been discussed in detail. Some cracks were also found in the structural panels as previously noted. While not known at that time, it is now reported that other users are experiencing similar difficulties with the D-36 alloy, despite the high ductility of the material.

All cracking observed has been intercrystalline. Undoubtedly accentuating the cracking problem in this program was the large grain size that resulted from the thermal treatment to which the alloy was subjected during the brazing cycle prior to welding. Some grains were huge, occupying, in many cases, the full cross section of the facing material (Fig. 104).

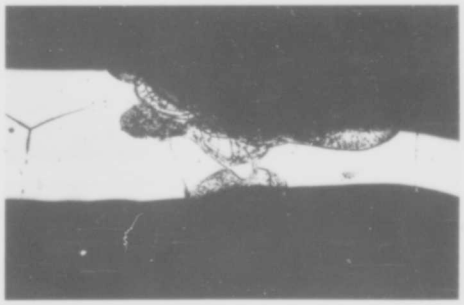

Fig. 104. Electron Beam Seal Weld--D-36 Heat Shield Panel (Magn 100X)

The cracking mechanism was not investigated at this time but was later considered to be associated with low grain boundary strength, which probably resulted from segregation of alloy constituents to produce lower melting areas at or adjacent to grain boundaries. Titanium segregation is a natural suspect.

Several repair or rework techniques were attempted with only partial success. The most successful technique was to take a small sliver of D-36 and press it tightly into the pinhole and then reweld. If the sliver of material fitted tightly, the reweld process would usually work; but if it did not, the sliver would either drop through the hole or fly out as the electron beam passed across the area. (TIG welding on the surface of the panel was considered since it would be possible to add material .o fill in the hole; however, this proved unsatisfactory because of the extreme cracking that occurred around the weld area.) In several cases, it was possible to run the beam back and forth over small cracks and seal them, but in most cases the cracks would recur after the welding was completed.

In summary, panels for test were sealed by electron beam welding, using the settings shown in Fig. 22. Some of the excessive corner gaps that could not be electron beam welded were successfully TIG welded. All pinholes were repaired by electron beam welding or TIG welding. However, if the TIG welding spot was allowed to become larger than about 0.050 in. in diameter, some fine intergranular cracking occurred.

The support clip sealing details (Fig. 101) were fabricated from 0.008-in. D-36 sheet stock and 1/4-in. OD, 0.010-in. wall thickness Cb-1Zr tubing. The outer face and inner face square details were formed, machined and then passed through a thermal cycle similar to the panel braze cycle. The outer face detail was then electron beam welded to the tube.

The outer face detail tube assembly was electron beam welded to the panel. The tube was electron beam welded to the doubler disc. The inner face detail was welded to the skin and then to the doubler disc (Figs. 105 and 106). This order is required or such severe mismatch will occur that the outer edge cannot be welded. The weld settings utilized for all these operations were 50 kv, 1.65 ma and a speed of 20 in./min. Special copper tools were made to hold the sealing details firmly in place against the panel surface during welding. In some cases, the sealing details were resistance tack-welded to the panel surface. This was found to be the best method of ensuring proper fit and contact. Any copper deposits were removed prior to electron beam welding.

Most of the required welds were made very satisfactorily, but in spite of the extensive studies which were made and the exacting processes that were maintained, some intergranular cracks and pinholes occurred persistently. Using the most exacting controls possible, a series of good

welds could be made; then, in a completely random pattern, a pinhole or a crack would occur.

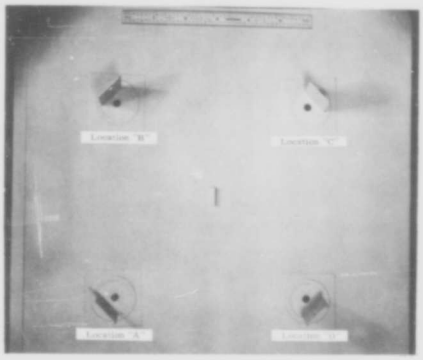

Fig. 105. Inner Face Sealing Details and D-36 Columbium Heat Shield Panel

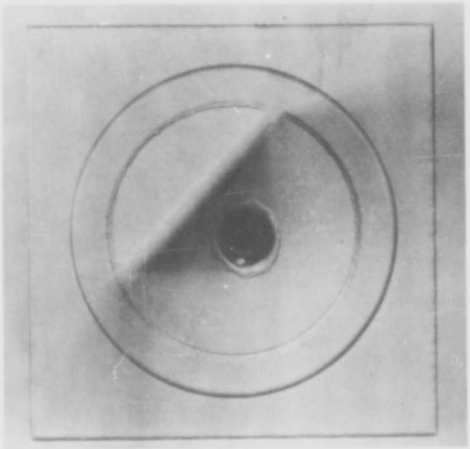

Fig. 106. Inner Face Support Clip Sealing Disc

Electron beam repairs were attempted on all discrepancies. For the worst cracks and all unrepairable pinholes, the sealing details were removed and new ones installed. With these operations all visible pinholes and some intergranular cracks were repaired. However, some of the microscopic pinholes and intergranular cracks could not be repaired. Since it was impossible to eliminate all of the imperfections in these D-36 heat shield panels, it was necessary to coat some panels, which contained minor cracks, for the test program. Imperfections were carefully documented so that they could be correlated with panel performance.

The panels selected for test were cleaned (Table 6), wrapped and shipped to the coater.

b. TZM molybdenum

Basic welding problems were further aggravated because the TZM heat shield panels were fully recrystallized during brazing and were extremely brittle.

The first TZM heat shield panel was brazed with pure titanium braze alloy. The panel was so brittle that one corner was broken in removing it from its storage container. The core material crumbled easily.

Because of this extreme brittleness, the next panel was brazed with B-120 VCA titanium, utilizing an extremely rapid braze cycle to keep grain growth to a minimum. The panel seemed to have more toughness but was still brittle. The edges of the panel were sealed (Figs. 107 and 108) by electron beam welding, but the corners, where the metal bends had opened up during the brazing cycle, could not be bent back without cracking. Three of these corners were successfully TIG welded, but the fourth cracked after welding.

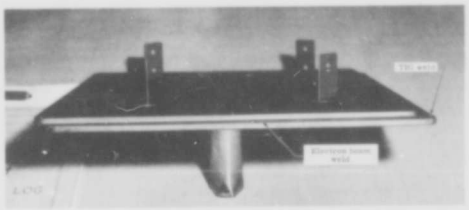

Fig. 107. TZM Molybdenum Flat Heat Shield Panel Brazed with B-120 VCA Titanium at 3000° F

Because of the difficulties encountered in sealing the disc and tubes on the D-36 columbium heat shield, the required sealing operations on TZM were attempted on only a limited scale. All the welds made on the surfaces of these panels either cracked or caused cracking in the parent material around the weld.

All panel brazing was stopped while a welding study was conducted to determine if most or all of the disc and tube sealing welds could be accomplished before panel brazing.

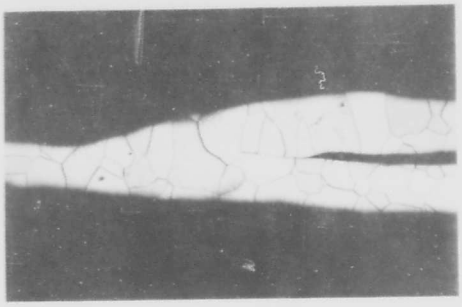

Fig. 108. Photomicrograph of Electron Beam Welded Edge Seal on TZM Molybdenum Heat Shield Panel (100X)

A welding study similar to that accomplished on D-36 columbium was performed on 0.008-in. TZM material. The optimum settings for penetration of the 0.008-in. TZM sheet were 70 kv, 2.00 ma and a speed of 20 in./min. For burn-through welds the best settings were 70 kv, 3.00 ma and a speed of 20 in./min. The best settings for the overlap-type edge weld were 70 kv, 2.00 ma and a speed of 20 in./min. These settings were higher than those utilized for D-36 because of the higher melting temperature of TZM.

To evaluate the possibility of making all welds before brazing, a clip assembly and tube were welded to a 4- by 4- by 0.008-in. sheet. This was done to check the amount of warpage that occurred and to determine optimum welding parameters for acceptable welds. It was found that any flexing or bending of the specimens would cause the welds to crack. The welding study was terminated with the conclusion that it would be extremely difficult to develop any reliable process for welding the TZM heat shield panels prior to brazing.

In any case, the more basic problem of these TZM heat shields is their extreme brittleness if the brazing is accomplished at temperatures well above those which cause recrystallization. It was concluded that no additional TZM heat shield panels should be produced since such panels would not have sufficient structural integrity to accomplish the test program successfully. They could not, in any case, be considered flightworthy components.

E. QUALITY ASSURANCE PROGRAM AND PANEL FABRICATION DATA

A Quality Assurance program was established for the inspection and evaluation of all details and completed panels. The program was divided into two major sections:

(1) Panel in-process control.

(2) Nondestructive evaluation of brazed panels.

1. Panel In-Process Control

During the fabrication of the panel details, each operation was monitored and each detail inspected for compliance to design criteria. Fabrication log books were maintained for each panel, which contained a step-by-step breakdown of pertinent manufacturing operations and quality evaluation. These data were recapped in a summary sheet for use in the testing and analysis phases.

2. Nondestructive Evaluation of Panel Integrity

Primarily, nondestructive evaluation techniques were used for braze line, core, and coating integrity determinations. While X-radiography is normally used for the evaluation of the braze line and core, this technique was found to be inadequate for brazed D-36 and TZM panels because of the nature of the panel facing materials and braze alloys. To detect the presence of the braze alloy with X-radiography, the absorption coefficient of the braze alloy must be higher than the facing material. The opposite condition exists in the brazed panels on this program, with the braze alloys having a lower absorption coefficient than the facing materials. Therefore, X-radiography could not be employed for braze line evaluation, although it was employed for the evaluation of the honeycomb core uniformity. Each panel was X-radiographed to establish the existence of core defects such as cracked, crushed or deformed cores (Tables 13 through 19). No core defects were found.

For the determination of braze line integrity, two different inspection techniques were evaluated: (1) ultrasonics and (2) thermography. The thermographic technique was simple and rapid and was more economical for the evaluation of the braze line integrity with adequate isolation of defects than the ultrasonic techniques. It was used for braze line evaluation.

The thermographic system utilizes a specially formulated heat-affected fluid. When the fluid is applied to the honeycomb panel and heat is applied, a temperature differential causes the fluid to be repelled from all

(warm) areas and coalesce in the core cell (cool) areas. This temperature differential is created because the core partitions act as heat sinks. Where there is lack of braze, no pattern will appear; where the core is deformed, the pattern duplicates the irregularities. A thermographic pattern for a brazed columbium structural honeycomb panel is shown in Fig. 109.

In the absence of any satisfactory nondestructive coating evaluation techniques, only visual examination was possible under 10-power magnification to ensure against any obvious coating defects.

3. Test Panel Fabrication Summary

Test panel fabrication is summarized in tabular form: D-36 panel data are presented in Tables 13 through 16; TZM panel data are presented in Tables 17 through 19.

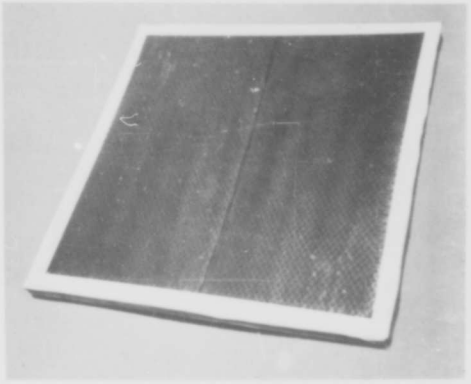

Fig. 109. Thermograph of D-36 Columbium Panel

TABLE 13

Summary of Flat D-36 Columbium Structu

Panel Number	Panel Type	Total Panel Weight (lb)	Panel Thickness (in.)	Panel Facing Material Heat No.	Panel Facing Thickness (in.)	Braze Temperature (°F)	Pressure in Braze Furnace (mm Hg)	Braze Alloy	Waviness
1	D-36 flat structural	2.116	0.5171 to 0.5204	36-168-03	0.0115 to 0.0125	3000	2×10^{-5}	B-120 VCA Titanium	None
2	D-36 flat structural	2.107	0.519 to 0.523	36-168-03	0.0118 to 0.0125	3000	2×10^{-5}	B-120 VCA Titanium	None
3	D-36 flat structural	2.067	0.5168 to 0.5194	36-168-03	0.0115 to 0.0125	3000	1.6×10^{-6}	B-120 VCA Titanium	None
4	D-36 flat structural	2.136	0.518 to 0.520	36-168-03	0.0115 to 0.0125	3000	1.0×10^{-5}	B-120 VCA Titanium	None
5	D-36 flat structural	2.116	0.519 to 0.525	36-168-03	0.012 to 0.0125	3000	1.2×10^{-5}	B-120 VCA Titanium	None
6	D-36 flat structural	2.138	0.519 to 0.5245	36-168-03	0.0119 to 0.0126	3000	1.8×10^{-5}	B-120 VCA Titanium	None
7	D-36 flat structural	2.156	0.519 to 0-5225	36-168-03	0.0118 to 0.0125	3000	1.2×10^{-5}	B-120 VCA Titanium	None
8	D-36 flat structural	2.156	0.518 to 0.5196	36-168-03	0.0115 to 0.0125	3000	1.2×10^{-5}	B-120 VCA Titanium	None
9	D-36 flat structural			36-168-03	0.0115 to 0.0125	3000	2.2×10^{-5}	B-120 VCA Titanium	None
10	D-36 flat structural	2.163				3000		B-120 VCA Titanium	None
11	D-36 flat structural	2.132				3000		B-120 VCA Titanium	None
12	D-36 flat structural	2.125				3000		B-120 VCA Titanium	None
13	D-36 flat structural	2.137				3000		B-120 VCA Titanium	None

TABLE 13

Summary of Flat D-36 Columbium Structural Panel Quality Control Data

Panel Facing Thickness (in.)	Braze Temperature (°F)	Pressure in Braze Furnace (mm Hg)	Braze Alloy	Waviness	Warpage (in 12-in. wavelength)	Face Indentations	Visual Inspection	X-ray Results	Thermography Results	Panel Quality	Finished for Coating
0.0115 to 0.0125	3000	2×10^{-5}	B-120 VCA Titanium	None	0.0015 to 0.005	None	Clean--no questionable areas	No crushed core	No detectable braze voids	Acceptable	Sealed and shipped to TRW
0.0118 to 0.0125	3000	2×10^{-5}	B-120 VCA Titanium	None	0.0015 to 0.005	None	Clean--one spot where skin might have had hole	No crushed core	No detectable braze voids	Acceptable	Sealed and shipped to TRW
0.0115 to 0.0125	3000	1.6×10^{-6}	B-120 VCA Titanium	None	0.001 to 0.009	None	Clean--no questionable areas	No crushed core	No detectable braze voids	Acceptable	Sealed and shipped to TRW as coating test part
0.0115 to 0.0125	3000	1.0×10^{-5}	B-120 VCA Titanium	None	0.002 to 0.006	None	Clean--no questionable areas	No crushed core	No detectable braze voids	Acceptable	Sealed and shipped to TRW
0.012 to 0.0125	3000	1.2×10^{-5}	B-120 VCA Titanium	None	0.0015 to 0.006	None	Clean--minor scratches on one skin	No crushed core	No detectable braze voids	Acceptable	Sealed and shipped to TRW
0.0119 to 0.0126	3000	1.8×10^{-5}	B-120 VCA Titanium	None	0.0015 to 0.007	None	Clean--no questionable areas	No crushed core	No detectable braze voids	Acceptable	Sealed and shipped to TRW
0.0118 to 0.0125	3000	1.2×10^{-5}	B-120 VCA Titanium	None	0.0015 to 0.006	8 small dents 6--0.0004 in. deep, 2--0.002 in. deep	Clean--minor dimples only	No crushed core	No detectable braze voids	Acceptable	Not finished
0.0115 to 0.0125	3000	1.2×10^{-5}	B-120 VCA Titanium	None	0.001 to 0.005	None	Clean--minor scratches from handling, otherwise okay	No crushed core	No detectable braze voids	Acceptable	Not finished cutup
0.0115 to 0.0125	3000	2.2×10^{-5}	B-120 VCA Titanium	None		None	Clean--one spot has questionable area	No crushed core	No detectable braze voids	Acceptable	Sealed and shipped to TRW
	3000		B-120 VCA Titanium	None	0.0015 to 0.008	None	Clean--no questionable areas	No crushed core	No detectable braze voids	Acceptable	Sealed and shipped to TRW
	3000		B-120 VCA Titanium	None	0.001 to 0.018	None	Clean--no questionable areas	No crushed core	No detectable braze voids	Acceptable	Sealed and shipped to TRW
	3000		B-120 VCA Titanium	None	0.0015 to 0.008	None	Clean--no questionable areas	No crushed core	No detectable braze voids	Acceptable	Sealed and shipped to TRW
	3000		B-120 VCA Titanium	None	0.0015 to 0.009	None	Clean--no questionable areas	No crushed core	No detectable braze voids	Acceptable	Sealed and shipped to TRW

TABLE 14

Summary of Flat D-36 Columbium Heat Shield Panel Q

Panel Number	Total Panel Weight (lb)	Panel Thickness (in.)	Facing Material Heat No.	Facing Thickness (in.)	Braze Temperature (°F)	Time at Braze Temperature (min)	Vacuum Pressure (mm Hg x 10^{-5})	Braze Alloy	
1				0.008 to 0.008	3200	8		A-55 Titanium	
2				0.008 to 0.008	3200	8		A-55 Titanium	Se ar of
3	1.375	0.3810 to 0.3850	36-168-02	0.008 to 0.008	3200	8	6.2	A-55 Titanium	Cl qu ar
4				0.008 to 0.008	3200	8		A-55 Titanium	Sr ar of ex fl
5				0.008 to 0.008	3200	8		A-55 Titanium	Sr on ne
6	1425	0.3830 to 0.3900	36-168-02	0.008 to 0.008	3025	8	2.4	B-120 VCA Titanium	Cl se de
7	Panel not brazed because of crack in heat-shield facings								
8	1.362	0.3811 to 0.3877	36-168-02	0.008 to 0.008	2950	8	3.0	B-120 VCA Titanium	Cl no ab
9	1.368	0.3708 to 0.3870	36-168-02	0.008 to 0.008	3000	8	3.2	B-120 VCA Titanium	Cl no ab
10		0.380 to 0.389		0.008 to 0.008	3000	8		B-120 VCA Titanium	Or ou fa
11	1.342	0.3790 to 0.3810	36-108-02	0.008 to 0.008	3000	8	2.4	B-120 VCA Titanium	Cl no ab

TABLE 14

Summary of Flat D-36 Columbium Heat Shield Panel Quality Control Data

Braze Temperature (°F)	Time at Braze Temperature (min)	Vacuum Pressure (mm Hg x 10^{-5})	Braze Alloy	Visual Inspection Results	X-ray Results	Thermography Results	Panel Flatness (in./16 in. ℓ. min max)	Panel Quality	Finished for Coating
3200	8		A-55 Titanium						
3200	8		A-55 Titanium	Several voids around edge of panel		Several voids around edge of panel			
3200	8	6.2	A-55 Titanium	Clean--no questionable areas	No crushed core	Small void areas--one side	Not measured	Acceptable	
3200	8		A-55 Titanium	Small damage area on edge of panel from excess braze flow					
3200	8		A-55 Titanium	Small voids--one corner needs rework					
3025	8	2.4	B-120 VCA Titanium	Clean--several small dents	No crushed core	Two small braze voi	0.0025 to 0.0025	Acceptable	
ield facings									
2950	8	3.0	B-120 VCA Titanium	Clean--no questionable areas	No crushed core	No questionable areas	0.000 to 0.060	Acceptable	
3000	8	3.2	B-120 VCA Titanium	Clean--no questionable areas	No crushed core	Two small braze voids	0.000 to 0.025	Acceptable	
3000	8		B-120 VCA Titanium	One void on outer surface			0.000 to 0.040		
3000	8	2.4	B-120 VCA Titanium	Clean--no questionable areas	No crushed core	No questionable areas	0.014 to 0.019	Acceptable	

TABLE 15

Summary of Curved D-36 Columbium Heat

Panel Number	Total Panel Weight (lb)	Panel Thickness (in.)	Facing Material Heat No.	Facing Thickness (in.)	Braze Temperature (°F)	Time at Braze Temperature (min)	Vacuum Pressure (mm Hg x 10^{-5})	Braze Alloy
1	Not meas-ured	Not meas-ured		0.008 to 0.008	3000	8		B-120 VCA Titanium
2	1.425	0.3745 to 0.3803	36-168-02	0.003 to 0.008	2950	8	2.8	B-120 VCA Titanium
3	1.325	0.3775 to 0.3795	36-168-02	0.008 to 0.008	3000	8	2.4	B-120 VCA Titanium
4	1.312	0.3775 to 0.3830	36-168-02	0.008 to 0.008	3000	8	1.7	B-120 VCA Titanium
5	In progess	In progess			3000	8	1.4	B-120 VCA Titantium
6	1.375	0.3780 to 0.3815	36-168-02	0.008 to 0.008	2950	8	2.8	B-120 VCA Titanium

TABLE 15

Summary of Curved D-36 Columbium Heat Shield Panel Quality Control Data

Braze Temperature (°F)	Time at Braze Temperature (min)	Vacuum Pressure (mm Hg x 10^{-5})	Braze Alloy	Visual Inspection Results	X-ray Results	Thermography Results	Panel Flatness (in. / 12 in. min max)	Panel Quality	Finished for Coating
3000	8		B-120 VCA Titanium	One edge was damaged when excess flow of braze alloy stuck the panel to the support ring				Scrapped	Not finished
2950	8	2.8	B-120 VCA Titanium	Clean--no questionable areas	No crushed core	No questionable areas	0.000 to 0.055	Acceptable	In progress
3000	8	2.4	B-120 VCA Titanium	Clean--one scratch	No crushed core	No questionable areas	0.008 to 0.015	Acceptable	In progress
3000	8	1.7	B-120 VCA Titanium	Clean--few small dents	No crushed core	No questionable areas	0.007 to 0.014	Acceptable	In progress
3000	8	1.4	B-120 VCA Titantium	Clean--no questionable areas	No crushed core	No questionable areas	In progress	Acceptable	In progress
2950	8	2.8	B-120 VCA Titanium	Clean--no questionable areas	No crushed core	No questionable areas	0.006 to 0.019	Acceptable	In progress

TABLE 16

Summary of Curved D-36 Columbium Structural Pane

Panel Number	Total Panel Weight (lb)	Panel Thickness (in.)	Facing Material Heat No.	Facing Thickness (in.)	Braze Temperature (°F)	Time at Braze Temperature (min)	Vacuum Pressure (mm Hg x 10^{-5})	Braze Alloy
1	2.12	0.515 to 0.520	36-168-03	0.0125 to 0.0126	3000	8	1.8	B-120 VCA Titanium
2	Not recorded	Not recorded	36-168-03	Not recorded	3000	8	2.4	B-120 VCA Titanium
3	Not recorded	Not recorded	36-168-03	Not recorded	3000	8	2.5	B-120 VCA Titanium
4	2.137	0.5127 to 0.5204	36-168-03	0.0127 to 0.0128	3000	8	2.3	B-120 VCA Titanium
5	No weight	0.511 to 0.5165	36-168-03	0.0122 to 0.0125	3000	8	2.8	B-120 VCA Titanium
6	2.00 Panel edges machined prior to weighing	0.5133 to 0.5192	36-168-03	0.0122 to 0.0123	3000	8	1.8	B-120 VCA Titanium
7	2.05 (as above)	0.5139 to 0.5201	36-168-03	0.0121 to 0.0126	3000	8	1.3	B-120 VCA Titanium
8	2.12	0.5124 to 0.5120	36-168-03	0.0123 to 0.0124	3000	8	1.2	B-120 VCA Titanium
9	2.085	0.5135 to 0.5193	36-168-03	0.0122 to 0.0122	3000	8	1.2	B-120 VCA Titanium
10	2.15	0.5160 to 0.5245	36-168-03	0.0123 to 0.0129	3000	8	1.8	B-120 VCA Titanium
11	2.087	0.5165 to 0.5200	36-168-03	0.0120 to 0.0122	3000	8	1.0	B-120 VCA Titanium

TABLE 16

Summary of Curved D-36 Columbium Structural Panel Quality Control Data

Braze Temperature (°F)	Time at Braze Temperature (min)	Vacuum Pressure (mm Hg x 10^{-5})	Braze Alloy	Visual Inspection Results	X-ray Results	Thermography Results	Panel Flatness (in. /12 in. min max)	Panel Quality	Finished for Coating
3000	8	1.8	B-120 VCA Titanium	Clean-- minor dent in one corner	No crushed core	No questionable areas	0.000 to 0.018	Acceptable	Sealed and shipped to TRW
3000	8	2.4	B-120 VCA Titanium	Clean-- no questionable areas	No crushed core	No questionable areas	Not measured	Acceptable	Sealed and shipped to TRW
3000	8	2.5	B-120 VCA Titanium	Clean-- no questionable areas	No crushed core	No questionable areas	Not measured	Acceptable	Sealed and shipped to TRW
3000	8	2.3	B-120 VCA Titanium	Clean-- minor dents on one side	No crushed core	No questionable areas	0.000 to 0.033	Acceptable	Panel dented during machining--not selected for coating
3000	8	2.8	B-120 VCA Titanium	Clean-- no questionable areas	No crushed core	No questionable areas	0.007 to 0.024	Acceptable	Sealed and shipped to TRW
3000	8	1.8	B-120 VCA Titanium	Clean-- one shallow dent	No crushed core	No questionable areas	0.009 to 0.054	Acceptable	Sealed and shipped to TRW
3000	8	1.3	B-120 VCA Titanium	Clean-- small oxide spots	No crushed core	No questionable areas	0.006 to 0.007	Acceptable	Sealed and shipped to TRW
3000	8	1.2	B-120 VCA Titanium	Clean-- no questionable areas	No crushed core	No questionable areas	0.012 to 0.016	Acceptable	Sealed and shipped to TRW
3000	8	1.2	B-120 VCA Titanium	Clean-- no questionable areas	No crushed core	No questionable areas	0.010 to 0.010	Acceptable	Sealed and shipped to TRW
3000	8	1.8	B-120 VCA Titanium	Clean-- no questionable areas	No crushed core	No questionable areas	0.009 to 0.039	Acceptable	Sealed and shipped to TRW
3000	8	1.0	B-120 VCA Titanium	Clean-- no questionable areas	No crushed core -- one core repair	No questionable areas	0.005 to 0.035	Acceptable	Sealed and shipped to TRW

TABLE 17

Summary of Flat TZM Molybdenum Structural Pan

Panel Number	Total Panel Weight (lb)	Panel Thickness (in.)	Facing Material Heat No.	Facing Thickness (in.)	Braze Temperature (°F)	Time at Braze Temperature (min)	Vacuum Pressure (mm Hg x 10^{-5})	Braze Alloy
1	2.578	0.5123 to 0.5148	KDTZM 518A	0.0123 to 0.0135	2550	5	2.0	Haynes 25
2	2.550	0.5090 to 0.5169	KDTZM 518A	0.0127 to 0.0128	2550	5	2.0	Haynes 25
3	2.631	0.5130 to 0.5155	KDTZM 489A	0.0130 to 0.0133	2500	5	2.2	Haynes 25
4	2.612	0.5110 to 0.5130	KDTZM 518A	0.0129 to 0.0133	2500	5	2.1	Haynes 25
5	2.625	0.5132 to 0.5180	KDTZM 489A	0.0131 to 0.0133	2550	5	3.0	Haynes 25
6	2.600	0.5110 to 0.5140	KDTZM 489A	0.0127 to 0.0130	2500	5	2.3	Haynes 25
7	2.625	0.5120 to 0.5145	KDTZM 489A	0.0128 to 0.0129	2500	5	2.5	Haynes 25
8	2.531	0.5117 to 0.5200	KDTZM 489A	0.0121 to 0.0122	2580	5	1.1	Haynes 25
9	2.581	0.5009 to 0.5169	KDTZM 518A	0.0115 to 0.0125	2580	5	1.2	Haynes 25
10	In progress							
11	2.618	0.5141 to 0.5196	KDTZM 489A	0.0129 to 0.0137	2580	5	1.2	Haynes 25

TABLE 17

Summary of Flat TZM Molybdenum Structural Panel Quality Control Data

Braze Temperature (° F)	Time at Braze Temperature (min)	Vacuum Pressure (mm Hg x 10^{-5})	Braze Alloy	Visual Inspection Results	X-ray Results	Thermography Results	Panel Flatness (in. / 12 in. min max)	Panel Quality	Finished for Coating
2550	5	2.0	Haynes 25	Clean--no questionable areas	No crushed core--a few core repairs	No questionable areas	0.003 to 0.003	Acceptable	
2550	5	2.0	Haynes 25	Clean--no questionable areas	No crushed core--a few core repairs	No questionable areas	0.006 to 0.006	Acceptable	
2500	5	2.2	Haynes 25	Clean--no questionable areas	No crushed core--a few core repairs	No questionable areas	0.002 to 0.005	Acceptable	
2500	5	2.1	Haynes 25	Clean--no questionable areas	No crushed core--a few core repairs	No questionable areas	0.007 to 0.008	Acceptable	
2550	5	3.0	Haynes 25	Clean--no questionable areas	No crushed core--a few core repairs	No questionable areas	0.009 to 0.012	Acceptable	
2500	5	2.3	Haynes 25	Clean--no questionable areas	No crushed core--a few core repairs	No questionable areas	0.008 to 0.018	Acceptable	
2500	5	2.5	Haynes 25	Clean--no questionable areas	No crushed core	No questionable areas	0.007 to 0.009	Acceptable	
2580	5	1.1	Haynes 25	Clean--no questionable areas	No crushed core	No questionable areas	0.003 to 0.012	Acceptable	
2580	5	1.2	Haynes 25	Clean--no questionable areas	No crushed core	No questionable areas	0.004 to 0.006	Acceptable	
2580	5	1.2	Haynes 25	Clean--no questionable areas	No crushed core	No questionable areas	0.009 to 0.012	Acceptable	

TABLE 18

Summary of Curved TZM Molybdenum Structural

Panel Number	Total Panel Weight (lb)	Panel Thickness (in.)	Facing Material Heat No.	Facing Thickness (in.)	Braze Temperature (°F)	Time at Braze Temperature (min)	Vacuum Pressure (mm Hg x 10^{-5})	Braze Alloy
1	2.531	0.5115 to 0.5215	KDTZM 489A	0.0111 to 0.0127	2580	5	1.4	Haynes 25
2			KDTZM 489A	0.0129 to 0.0112	2580	5	1.4	Haynes 25

TABLE 19

Summary of Flat TZM Molybdenum Heat Shield

Panel Number	Total Panel Weight (lb)	Panel Thickness (in.)	Facing Material Heat No.	Facing Thickness (in.)	Braze Temperature (°F)	Time at Braze Temperature (min)	Vacuum Pressure (mm Hg x 10^{-5})	Braze Alloy
1				0.008 to 0.008	3300	8	2.1	A-55 Titanium
4	1.637	0.379 to 0.3835		0.008 to 0.008	3008	2		B-120 VCA Titanium

TABLE 18

Summary of Curved TZM Molybdenum Structural Panel Quality Control Data

Braze mperature (° F)	Time at Braze Temperature (min)	Vacuum Pressure (mm Hg x 10^{-5})	Braze Alloy	Visual Inspection Results	X-ray Results	Thermography Results	Panel Flatness (in./12 in. min max)	Panel Quality	Finished for Coating
2580	5	1.4	Haynes 25	Clean--no braze defects; one possible crack in U-channel	No crushed core. Few core repairs	One small braze void	0.005 to 0.007	In progress	
2580	5	1.4	Haynes 25	Several blisters and questionable braze areas	Possible damaged core. Several core repairs	Several braze voids and questionable areas		Not acceptable	

TABLE 19

Summary of Flat TZM Molybdenum Heat Shield Panel Quality Control Data

Braze nperature (° F)	Time at Braze Temperature (min)	Vacuum Pressure (mm Hg x 10^{-5})	Braze Alloy	Visual Inspection Results	X-ray Results	Thermography Results	Panel Flatness (in./12 in. min max)	Panel Quality	Finished for Coating
3300	8	2.1	A-55 Titanium	Good braze--one corner damaged in removal from braze tools					
3008	2		B-120 VCA Titanium	Good--no questionable areas		No questionable areas	0.007 to 0.008		

VI. TEST PROGRAM

The overall objectives of the test program were to determine the strength and thermal characteristics of the panel materials and panel assemblies for correlation with design procedures. To accomplish these objectives, room and elevated temperature tests were performed to determine the ultimate edgewise compression and shear strengths of the structural panels. The D-36 columbium heat shield panels were subjected to simulated re-entry environments in a dynamic gas facility. Material property tests were performed on small honeycomb core and panel facing specimens.

The test program was divided into four sections: (1) high temperature instrumentation studies, (2) structural panel testing, (3) heat shield panel testing, and (4) small specimen testing.

A. HIGH TEMPERATURE INSTRUMENTATION STUDIES

The purpose of the instrumentation study was to determine thermocouple configurations and installation techniques suitable for measuring the temperatures of the coated D-36 columbium and TZM molybdenum panels during test. The study was divided into two phases: configuration determinations and installation techniques.

The initial phase of the study consisted of evaluating thermocouple configurations and their thermal response at varying temperature rise rates. Five thermocouple configurations were selected for the evaluation (Fig. 110). For simplicity and economy, a 0.010-in. thick stainless steel sheet, insulated with fiberfrax, was used as the test specimen. Chromel-alumel thermocouple wire was used for all of the configurations since the maximum test temperature for this phase of the study was 1600° F. The sheath thermocouples used in this phase were fabricated by inserting the thermocouple wire in an MgO filled Inconel sheath. The different configurations were attached to the test specimen in a circular pattern around a spot-welded standard thermocouple (Fig. 111). Mounting in this manner allowed the same thermal environment to be imposed on all of the configurations at the same time, so that relative comparisons could be easily obtained. Constant rise rates ($\Delta T/\Delta t$) of 5°, 10°, 20°, 30°, 35° and 40° F/sec were imposed on the test specimen from ambient temperature to 1600° F by using a quartz lamp radiant heater unit

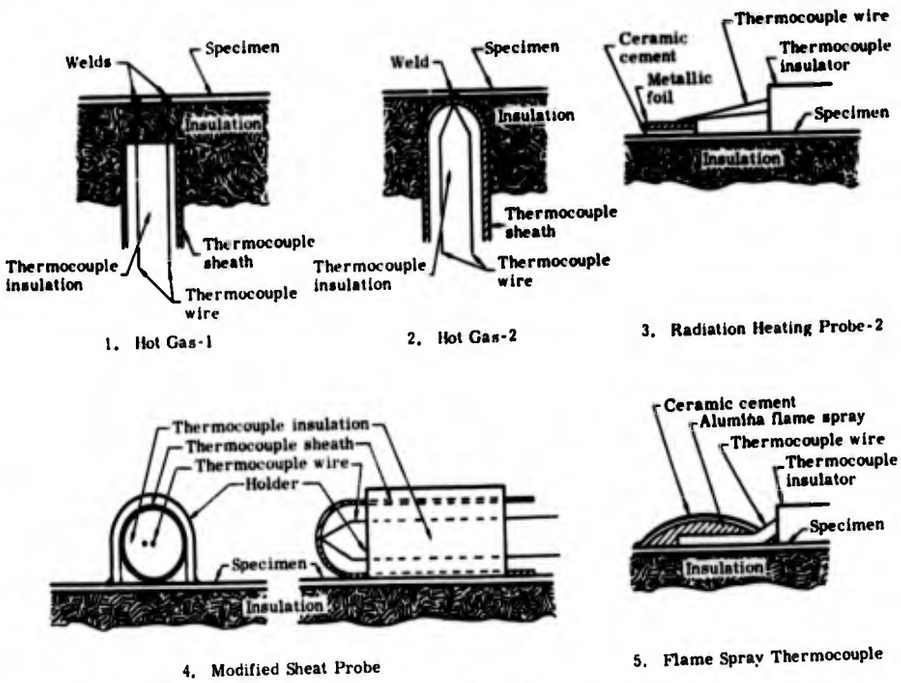

1. Hot Gas-1
2. Hot Gas-2
3. Radiation Heating Probe-2
4. Modified Sheat Probe
5. Flame Spray Thermocouple

Fig. 110. Thermocouple Installation Configuration

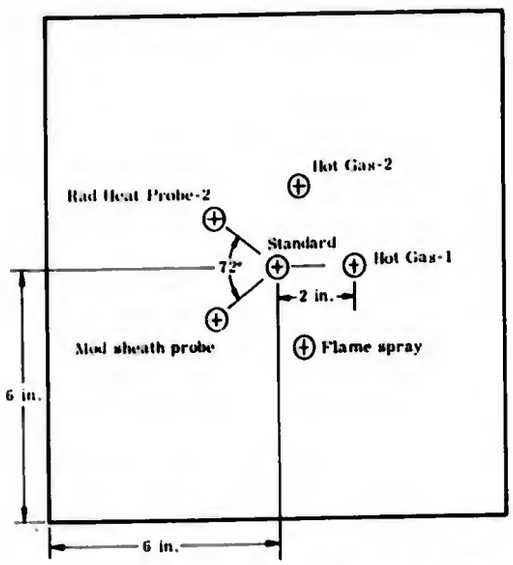

Fig. 111. Test Specimen Thermocouple Layout

and an ignitron power regulator and controller.

The results of these tests are plotted for three conditions- $\Delta T/\Delta t = 5°$, 20° and 40° F/sec (Figs. 112, 113 and 114). In general, the data showed that the hot gas-1 and radiation heat probe-2 were satisfactory throughout the rise rate range (5° to 40° F/sec). The modified sheath probe performed satisfactorily up to a rise rate of 20° F/sec, after which its indicated temperature lag became excessive. However, this was the only thermocouple that ever matched the standard thermocouple during the steady-state portion of the profile. The hot gas-2 thermocouple exhibited the poorest performance. This was caused by the thermal mass of the sheath acting as a heat sink. If a sufficient length of the sheath (2 in. or more) could have been maintained at temperature, this thermocouple would perform more satisfactorily. This was demonstrated by the modified sheath probe which had about 4 in. of the sheath under the direct influence of the thermal input. The flame spray thermocouple data represented an average of all configurations.

Two of the thermocouple configurations were eliminated as a result of their mediocre thermal response characteristics (hot gas-2 and flame spray). The hot gas-1 configuration was also eliminated because considerable difficulty was encountered in obtaining a satisfactory weld between the thermocouple wire (Cr-Al) and the control specimen (stain-

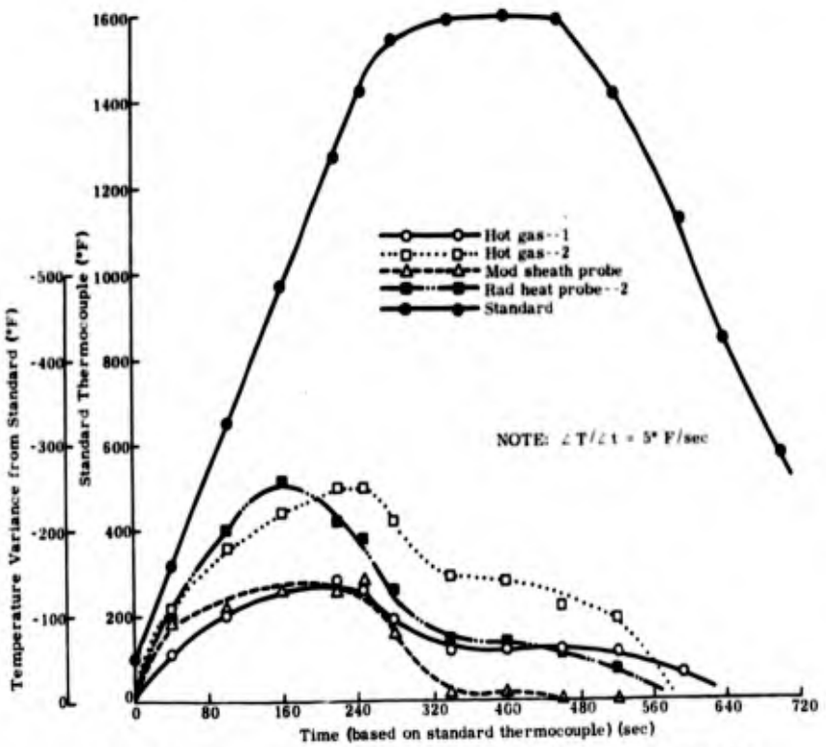

Fig. 112. Temperature Variance from Standard Thermocouple

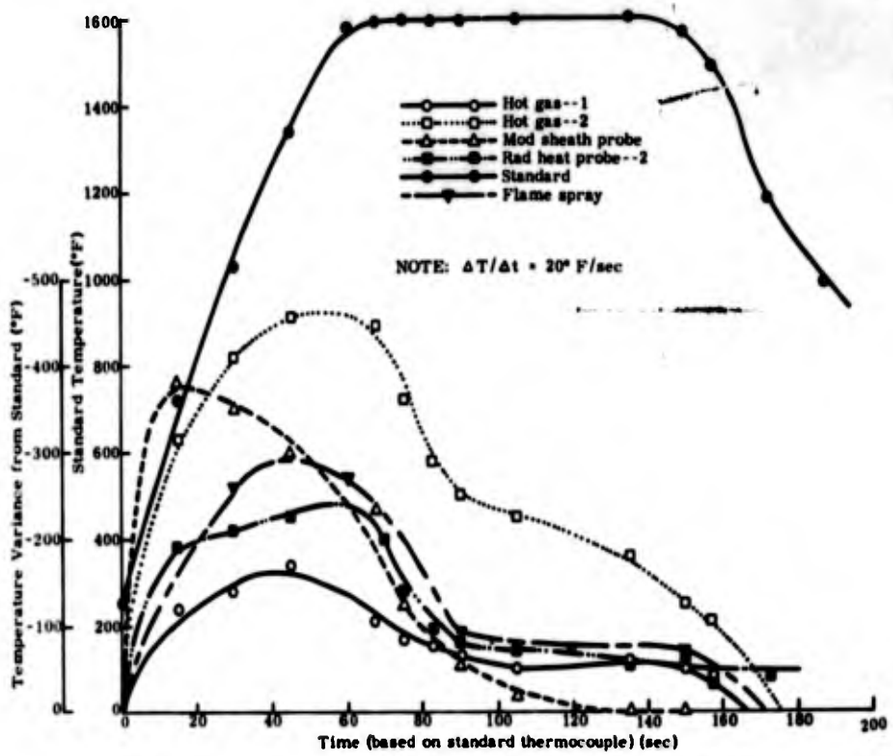

Fig. 113. Temperature Variance from Standard Thermocouple

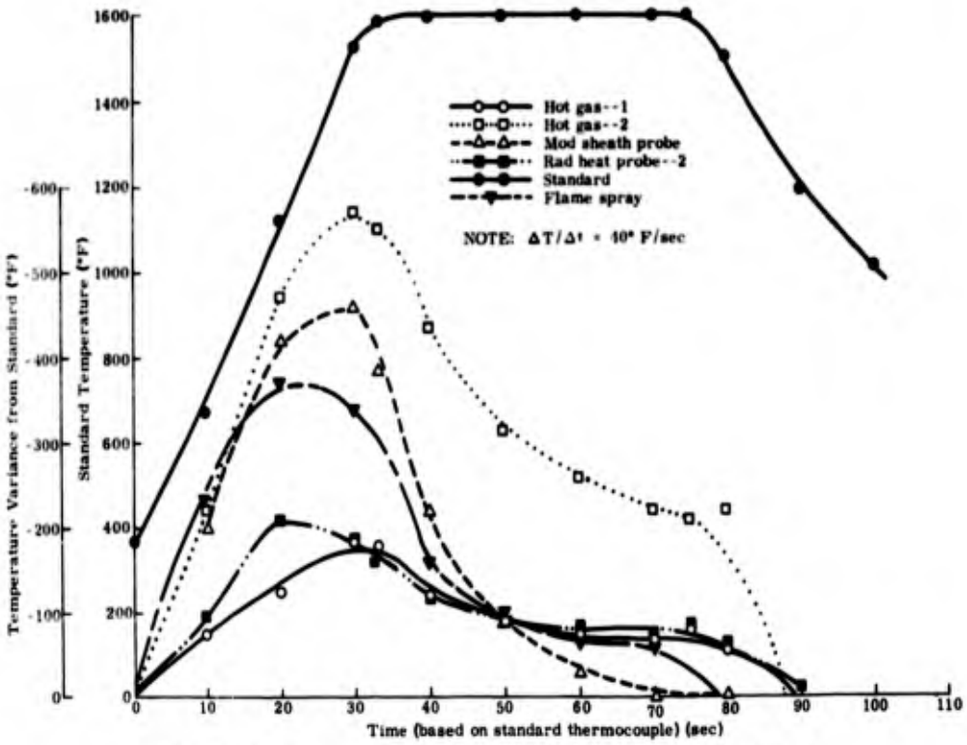

Fig. 114. Temperature Variance from Standard Thermocouple

less steel). Also, since tungsten-rhenium thermocouple wire would be used for tests with temperature environments above 2400° F (platinum reacts with the disilicide coatings), even more difficulty would be encountered in welding the W-Re wire to the coated D-36 and TZM.

Different attachment techniques were investigated for the two remaining configurations (modified sheath probe and the radiation heating probe-2). Early in the evaluation, it was decided that the modified sheath probe would be used for the hot gas tests because of its inherent ability to withstand a vibratory environment, and the radiation heating probe-2 would be used only for the structural panels because of its apparent inability to withstand a dynamic environment. (Subsequent heat shield tests verified these decisions.) The modified sheath probe consisted of a hot-grounded junction columbium sheath thermocouple inserted in an integral holder which was welded to the panel facing. The major disadvantage of this configuration is that the thermocouple holder must be installed on the panel during the manufacturing process (Fig. 115).

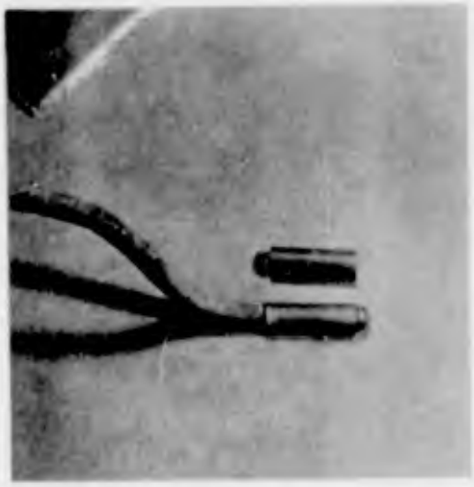

Fig. 115. Modified Sheath Probe Thermocouple Installation on D-36 Columbium Panel--Backup Sheath Used on Panel

A problem was encountered when two 12-in. long 0.125-in. OD, 0.012-in. wall columbium sheath thermocouples (W-5% Re versus W-26% Re thermocouple wires) were coated with a Cr-Ti-Si oxidation protective coating. The coating process embrittled the thermocouple wires because of the relatively long (8 hours) soak time at 2300° F, therefore making the attachment of thermocouple lead wires to the thermocouple extremely difficult. Therefore, an Al-Sn coating was tried on the columbium sheath thermocouples. This coating does not require an extended elevated temperature treatment. Subsequent heat shield tests using the modified sheath probe were performed with Al-Sn coated thermocouples with complete success.

The radiation heating probe-2 was used in the structural panel tests. The problems with this configuration were the selection of the foil material and the cement needed to bond the thermocouple to the panel surface. The problem of selecting the proper foil material arose from several factors:

(1) Compatibility with the silicide coating.

(2) Matching thermal characteristics with surface material.

(3) Compatibility with the thermocouple wire.

(4) Capability of withstanding temperatures in excess of 2000° F.

Three different foil materials were tried: platinum, platinum-rhodium and titanium. The platinum foil reacted with the coating and the cement was gradually eaten away. The titanium oxidized rapidly above 1500° F and, consequently, completely disintegrated. No serious reactions occurred with the platinum-rhodium foil, however, during extended exposure tests at 2400° F, the foil eventually reacted with the coating and cement. The platinum-rhodium system was not evaluated at temperatures higher than 2400° F.

A special study was conducted to determine the best cement which could be used to bond the radiation heating probe-2 to the heated surface. Several different mixtures were evaluated with varying degrees of success:

Mixture	Adhesive Properties
Molybdenum disilicide + silicon carbide	Good
Molybdenum disilicide + titanium carbide	Good
Aluminum phosphate	Fair
"Savereisen" No. 1	Poor

Of the cements tried, the molybdenum disilicide mixtures exhibited the best adhesive

properties. These mixtures were prepared by mixing sodium silicate and distilled water (a 1 to 1 mixture by volume), and then adding enough molybdenum disilicide to obtain a thin paste consistency. The silicon carbide (or titanium carbide) was also mixed with distilled water to a thin paste consistency. The thermocouple was cemented to the specimen by first applying a thin coating of the silicon carbide, then applying a thick coating of the molybdenum disilicide mixture. After the thermocouple had been cemented to the specimen, a temperature curing cycle was used to evaporate the water from the cement. The temperature cure also seemed to affect the adhesive qualities of the bond. Several temperature cures were tried; the best results were obtained with a 1000° F temperature soak for one-half hour. Generally, this thermocouple configuration performed satisfactorily during the structural panel tests.

B. STRUCTURAL PANEL TESTS

The edgewise compression and shear strengths of the structural panels were determined for five basic test conditions:

(1) Room temperature with single-cycle ultimate load.

(2) Single-cycle temperature with single-cycle ultimate load.

(3) Multiple temperature cycles with single-cycle ultimate load.

(4) Multiple temperature cylces with multiple load cycles.

(5) Single-cycle temperature gradient with single-cycle ultimate load.

These conditions represented a comprehensive spectrum of possible load and temperature environments that the structural honeycomb panels might encounter in actual application. Twenty-three structural panels were tested (20 D-36 columbium, 3 TZM molybdenum).

1. Test Equipment

A special structural panel test fixture was assembled, which consisted of two major systems, one for loading and one for heating the panels.

a. Loading system

The loading system was an automatic closed-loop servomechanism electrohydraulic mechanism (Fig. 116) which programmed, applied, controlled and recorded the test loads. Such a system was necessary so that the applied load would be independent of the temperature of the panel. The load device must be capable of reacting with the thermal expansion of the panel to prevent thermal stresses from building up when heating the panel.

Another portion of this system was a special loading jig designed and fabricated to apply loads to the panels. The basic construction of the loading jig consisted of two columns mounted in a base and connected at the top by a frame. A center loading beam with frictionless rollers was installed between the two columns and allowed to move freely in the vertical direction. The load cells and hydraulic actuators were attached to each end of the loading beam. The shear tests were performed in the bottom portion of the loading jig, and the compression tests were performed in the top portion. A maximum deflection microswitch was used in both test setups to automatically dump the test load, so that excessive secondary damage to the panel would be minimized.

Special load fittings were designed to apply the test loads to the panels at elevated temperatures (Figs. 117 and 118). A picture frame load application jig was used for the shear panel tests. A major problem in the design of the loading fixture was to minimize thermal stresses. This was accomplished by closely matching the thermal expansion of the fixture to that of the panels so that the differences were minimized. Rene' 41 was selected as the shear fixture material because of its favorable coefficient of thermal expansion (greater than Cb or Mo) and its strength at temperature. Since the fixture temperature would be lower than that of the panel, due to the heat sink effect of its greater thermal mass, the thermal expansion criterion was achieved. An analysis of the allowable fixture temperature versus panel temperature for both materials is presented in Appendix C. These curves were derived so that the thermal stresses introduced by the relative expansions of the two materials would be kept at a minimum (30% of the design ultimate panel tensile stress). This meant that the shear fixture temperature would be monitored and controlled so that its temperature was always in the safe range.

The shear fixture was designed so that each edge of the frame could be inserted between the panel attachment strips, and the ends were stepped so that end joints could be

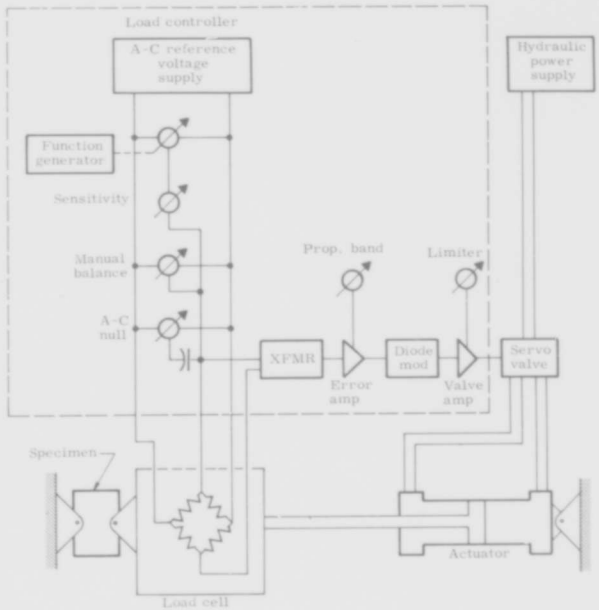

Fig. 116. Block Diagram, Load Control System

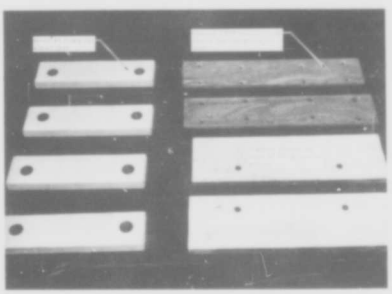

Fig. 117. Special Test Parts for High Temperature Test Fixtures

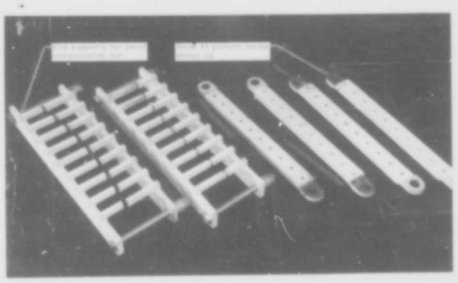

Fig. 118. Fixtures for High Temperature Structural Panel Test

pinned together (Fig. 118). The shear frame was flame-sprayed with alumina (low thermal absorptivity) to protect it from the direct radiation of the heating lamps.

The curved panels were to be loaded in axial compression, so it was necessary to design special end and edge supports to prevent premature or irrelevant failures. The end fixture consisted of four sets of steel fingers with tips of various lengths cut to fit the curvature of the panels. The finger fixture was flame-sprayed with alumina for radiation protection. One set of fingers was placed on the convex side of the panel, and a matching set was placed on the concave side (both top and bottom). The finger fixtures were then positioned on the panel so that the finger tips were located at the intersection of the core and the U-channel. This prevented the U-channel flanges from bending outward. However, during the first elevated

temperature compression test, the channel flanges bent inward. Consequently, stainless steel filler strips were placed inside the U-channels to prevent the inward motion of the channel flanges. The vertical edge stabilization members were steel strips flame-sprayed with alumina and made to slide freely into the U-channels. Special coated columbium compression plates were used to transmit the test load from the loading beam to the panel. These plates were insulated from the loading beam with fiberfrax.

b. Heating system

The heating system comprised two 360-kw single-phase Research, Incorporated ignition power regulators and controllers, two heater assemblies and associated instrumentation support equipment. The heater assemblies were made of thick copper plates, with grooves machined in the surface and gold plated. The lamps fitted snugly into these grooves, so that the quartz envelopes were cooled by conduction (Fig. 119). Higher operating temperatures are possible with this arrangement because of the positive action of water cooling used in the reflector system. The two radiant heaters were fitted with 3200-watt T-3 radiant heating lamps (16 in. long).

2. Preliminary Tests

Four preliminary tests were conducted to determine the stress and temperature distributions of the structural panels. Specifically, these tests were:

(1) Shear panel room temperature stress distribution.

(2) Shear panel temperature distribution (no load).

(3) Compression panel room temperature stress distribution.

(4) Compression panel temperature distribution (no load).

To determine the efficiency of the picture frame loading system, a room temperature proof test was performed on a D-36 columbium panel. This panel was instrumented with 12 AR-1 (paper) rosette strain gages and mounted in the Rene 41 picture frame shear fixture (Fig. 120). An 8000-lb load was applied to the panel in 1000-lb increments. Strain readings were recorded, reduced to stresses, and compared to the calculated applied stress. The calculated applied stress was derived by dividing the applied load by the panel shear area:

$$\tau_{applied} = P/A$$

where

P = applied load = 7000 lb (representative increment)

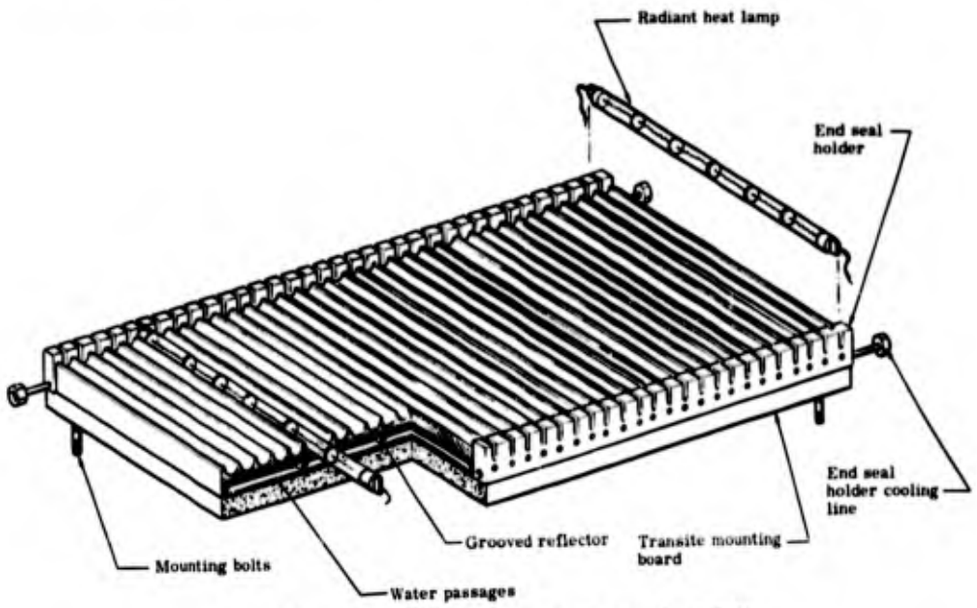

Fig. 119. Quartz Lamp Radiant Heater Assembly

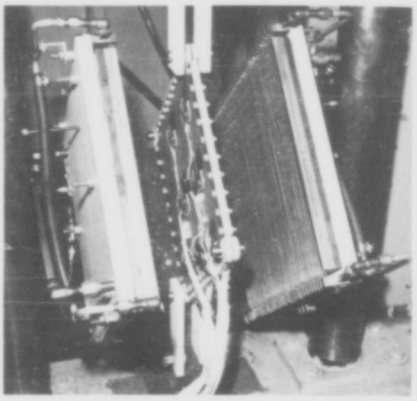

Fig. 120. Stress Distribution Test--D-36 Columbium Structural Shear Panel

A = shear area = panel side length x $\sqrt{2}$ x (facing thickness + braze alloy thickness) x 2 = 0.475 sq in.

$\tau_{applied}$ = average shear stress = 14,750 psi.

The actual panel stresses were obtained from the strain measurements by using the formula

$$\tau_{max} = \left[\frac{E}{2(1+\mu)}\right]\left[(\epsilon_a - \epsilon_c)^2 + 2\epsilon_b - (\epsilon_a + \epsilon_c)^2\right]^{1/2}$$

where

E = Young's modulus = 14.8×10^6 psi

μ = Poisson's ratio = 0.3

ϵ_a = strain reading of "a" leg of strain gage

ϵ_b = strain reading of "b" leg of strain gage

ϵ_c = strain reading of "c" leg of strain gage.

A representative stress distribution is presented in Fig. 121 as isoclinic stress lines. The measured stresses in the upper and lower corners of the panel were higher than the applied stresses. However, the stresses over the main portion of the panel are within 5% of the calculated stress.

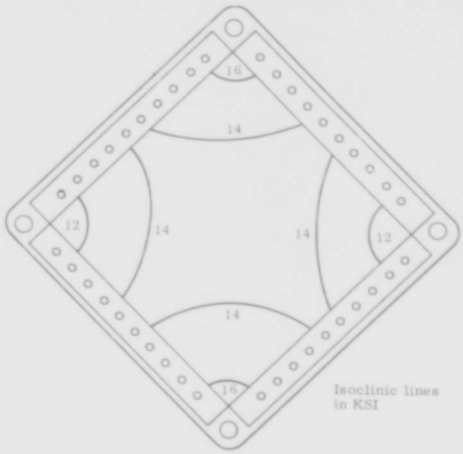

Fig. 121. Structural Shear Panel Stress Distribution

A 2300° F temperature test was performed on a coated D-36 columbium structural panel instrumented with seven chromel-alumel thermocouples. This test was performed to determine the imposed temperature distributions on the panel and René 41 loading fixture (Fig. 122). In this plot, the boundaries of the temperature isotherms were approximated between the thermocouples by the discoloration of the panel surface (a green tint of Cr_2O_3 forms at 2000° F). The general area of the panel influenced by the core was 2300° F. The corners of the panel were approximately 300° F lower. This was caused by the heat sink effect of the René 41 fixture and the attachment pins. While the center of the panel was at 2300° F, the shear strips were at 1600° F and the René 41 picture frame was at 1310° F, which was within the temperature limits for matching thermal expansions of the fixture and the panel. Consequently, the temperature distributions imposed on the panel by the radiant heaters were considered satisfactory.

A room temperature proof test was also accomplished for the compression panel and its loading arrangement (Fig. 123). Again, 12 AR-1 rosette strain gages were bonded to a compression panel. A 15,000-lb compression load was applied to the panel in 3000-lb

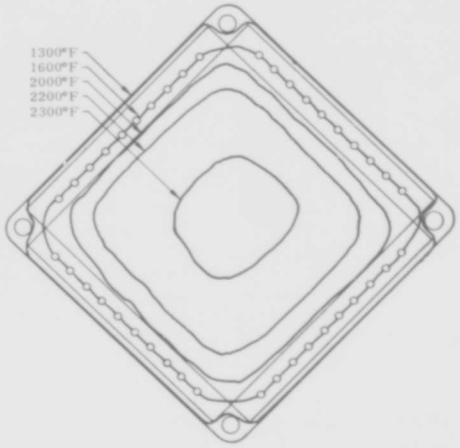

Fig. 122. Temperature Isotherms for 2300° F Shear Panel Temperature Distribution Test

increments. The strain gage readings were recorded, reduced and compared to the calculated applied stress which was

$$\sigma = P/A$$

where

P = applied load = 15,000 lb

A = compression area = (facing thickness + braze alloy thickness) x developed skin length x 2 + U-channel cross-sectional area x 2 = 0.377 sq in.

σ = applied compression stress = 39,800 psi.

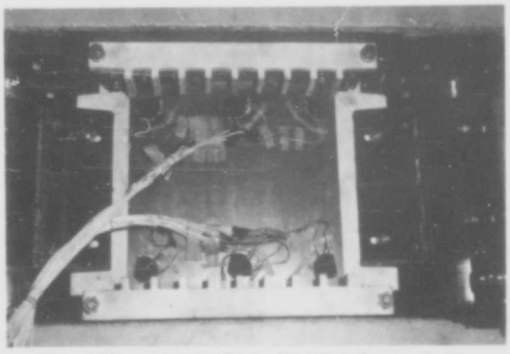

Fig. 123. Stress Distribution Test--D-36 Columbium Compression Panel

The measured panel stresses were obtained from the strain measurements by using the formula

$$\sigma_{calculated} = \epsilon E$$

where

ϵ = strain measurement in in./in.

E = Young's modulus = 14.8×10^6 psi.

The average measured stress on the convex face of the panel was 37,860 psi and the average stress on the concave face was 35,150 psi. These stresses were within 5 and 12%, respectively, of the calculated applied stress and were within 7% of one another. The horizontal leg of the strain gages along the panel edges indicated the Poisson effect, while at the center of the panel, the horizontal strain gages indicated no strain which is indicative of a plane strain condition.

A 2000° F temperature distribution test was also performed on a D-36 compression panel instrumented with four thermocouples (Fig. 124). The center of the U-channel was at 1660° F while the main portion of the panel was at 2020° F. This was caused by the heat sink effect of the finger fixture. All portions of the core area of the panel were within 50° F of the panel center temperature.

Fig. 124. Temperature Isotherms for 2000° F Compression Panel Temperature Distribution Test

3. Test Procedures

The general procedures used for both the shear and compression tests were:

(1) Instrument the test panel with thermocouples.

(2) Mount the panel between the two heater units.

(3) Preset the maximum deflection "dump" to the appropriate setting.

(4) Preload the panel approximately 200 lb to eliminate linkage slack.

(5) Apply the appropriate load and temperature profiles (Fig. 125).

(6) In the case of the shear tests only, apply the test load only when the shear fixture temperature was within allowable limits.

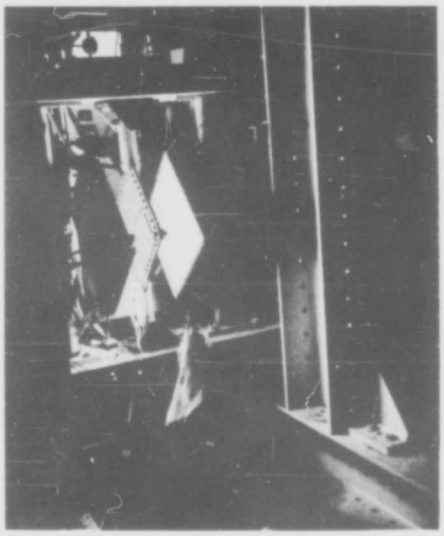

Fig. 125. D-36 Columbium Structural Panel Shear Test

The instrumentation for the structural panel tests was developed during the high temperature instrumentation study. The deflection limit switch was normally preset to allow the shear panels to diagonally deflect approximately 3/8 in. before dumping the test load. This was necessary to minimize secondary failures, since the panels were to be cut into small specimens for future tests. The setting for the compression tests was approximately that same as that for the shear panel test.

The load and temperature programs were started simultaneously. For the single-cycle temperature-load tests, the panel temperature was raised at a rate of 10° F/sec until the desired test temperature was reached. The panel was then soaked at this temperature for a minimum of two minutes (or, in the case of the shear tests, until the shear test fixture temperature was within safe limits). The test load was then applied at a rate of 400 lb/sec until the panel failed. After failure, the load was automatically released by the deflection switch, and the temperature gradually decreased to room temperature. This gradual temperature decay was necessary to keep the relative thermal expansions of the fixtures and panels from increasing the damaged area of the failed panels.

4. Test Results

Ten D-36 columbium flat structural panels were subjected to ultimate shear tests. The results of these tests are presented in Figs. 126 through 135. Generally, the mode of failure of these panels was local face wrinkling, intercellular dimpling (prevalent for the higher temperature tests) and intergranular tensile fracturing. However, Panel Nos. 6 and 13 exhibited general material failure. Panel No. 4 failed due to thermal stresses alone. This was caused by a heater power failure created by the loss of the control thermocouples. The resulting temperature differential between the panel and the shear fixture (the panel cooled faster than the shear fixture) created thermal stresses large enough to rupture the facings of the panel.

Ten D-36 columbium curved structural panels were tested in axial compression. The results of these tests are presented in Figs. 136 through 145. General instability was the primary mode of failure of all panels. Some of the high temperature test panels also had intercellular dimpling failures.

Three TZM molybdenum structural panels (two curved, one flat) were also tested. However, because of the extreme brittleness of these panels and the lack of an effective hermetic seal, no complete tests were accomplished (all panels were to be tested in compression). Curved Panel No. 6 was evidently damaged during installation in the test jig. The flange of the U-channel was probably cracked when the stabilization strips were installed (observed after the test). Curved Panel No. 10 failed because of a complete braze failure of the facing core at an ex-

MATERIAL Columbium alloy, D-36
PANEL NO. 9
TYPE OF TEST Shear
MAX TEST TEMP 1960° F
TIME AT MAX TEMP 140 sec
FAILING LOAD 16,600 lb
ULT STRESS 34,500 psi
RENÉ JIG TEMP 1170° F

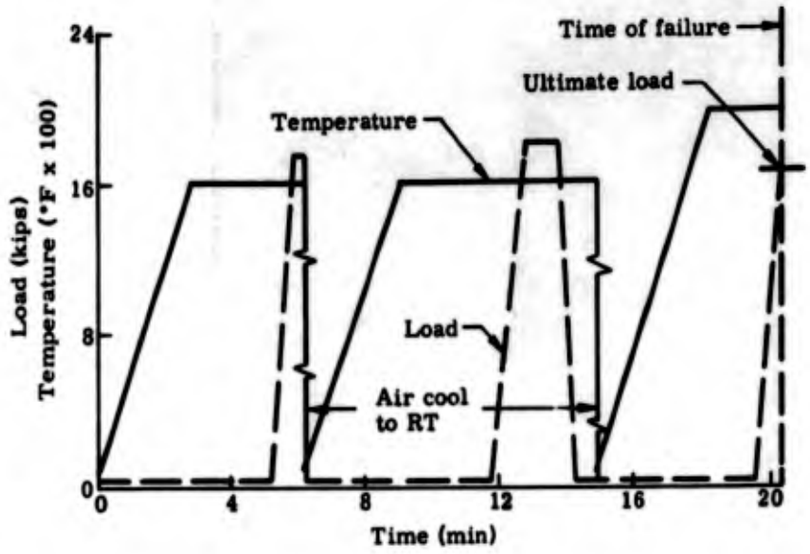

Fig. 126. Shear Test, D
Panel No. 9

MATERIAL Columbium alloy, D-36
PANEL NO. 5
TYPE OF TEST Shear
MAX TEST TEMP 2315° F
TIME AT MAX TEMP 240 sec
FAILING LOAD 9200 lb
ULT STRESS 19,400 psi
RENÉ JIG TEMP 1310° F

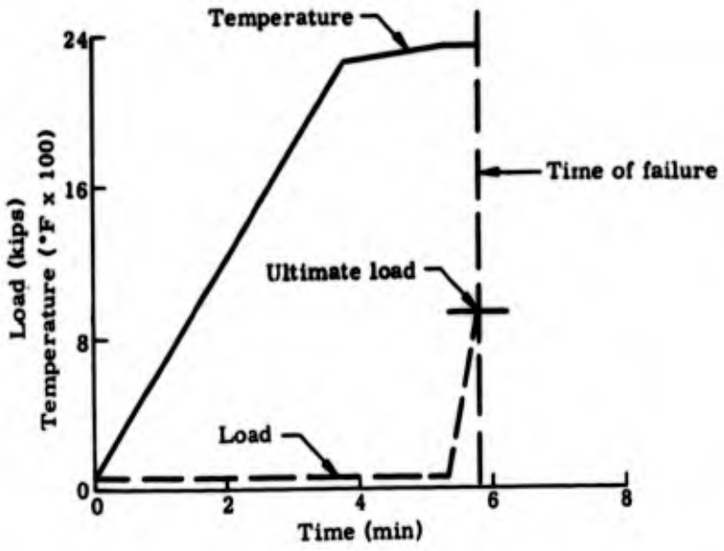

Fig. 127. Shear Test, D
Panel No. 5

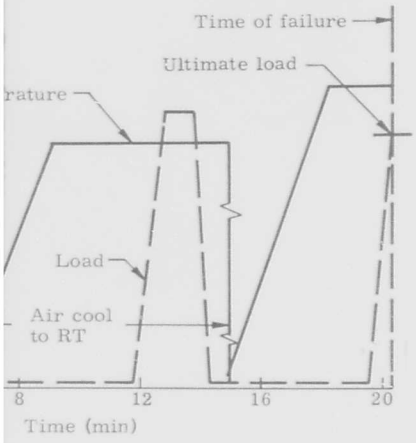

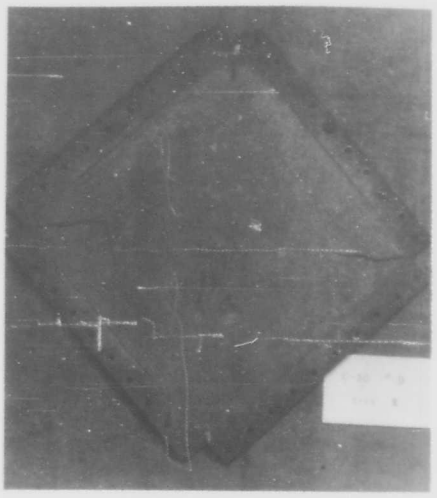

Fig. 126. Shear Test, D-36 Structural Panel No. 9

DESCRIPTION OF PANEL FAILURE
Local instability. Face wrinkling.

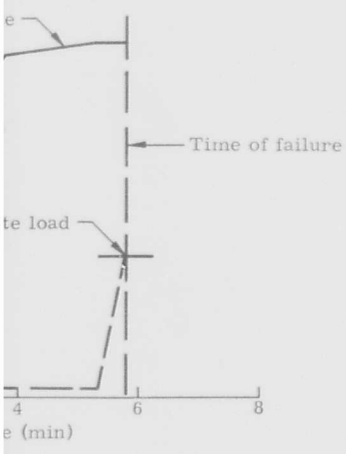

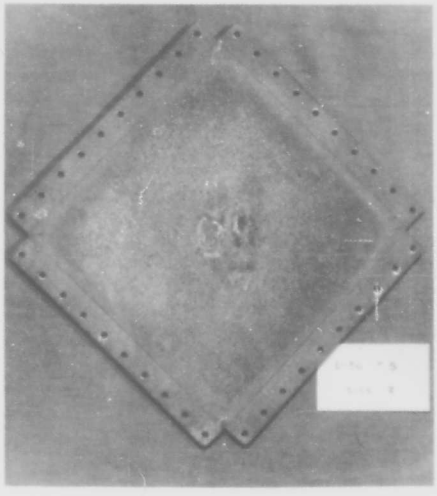

Fig. 127. Shear Test, D-36 Structural Panel No. 5

DESCRIPTION OF PANEL FAILURE
Local instability. Face wrinkling.

MATERIAL Columbium alloy, D-36
PANEL NO. 7
TYPE OF TEST Shear
MAX TEST TEMP 2340° F--outer face 2140° F--inner face
TIME AT MAX TEMP 90 sec
FAILING LOAD 10, 600 lb
ULT STRESS 22, 200 psi
RENÉ JIG TEMP 1330° F

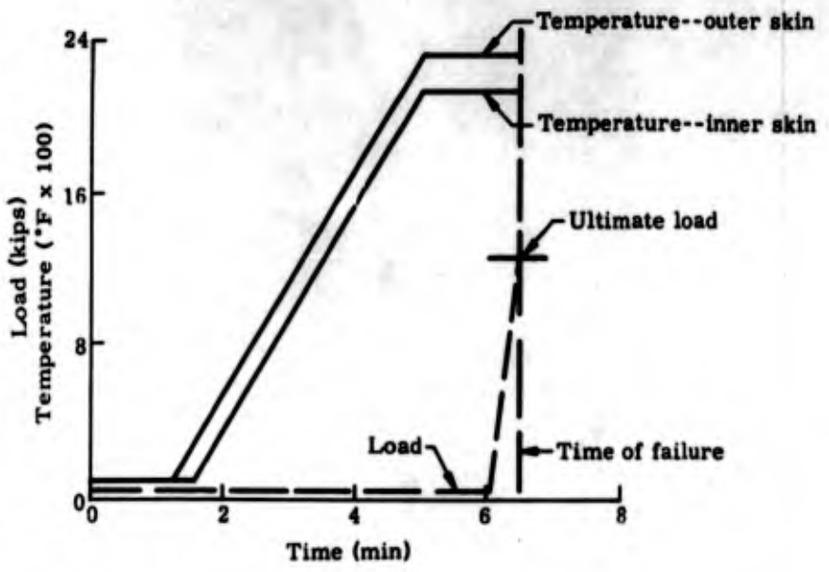

Fig. 128. Shear Test, D-36 Str
No. 7

MATERIAL Columbium alloy, D-36
PANEL NO. 11
TYPE OF TEST Shear
MAX TEST TEMP 2350° F--outer face 1950° F--inner face
TIME AT MAX TEMP 100 sec
FAILING LOAD 13, 000 lb
ULT STRESS 27, 300 psi
RENÉ JIG TEMP 1270° F

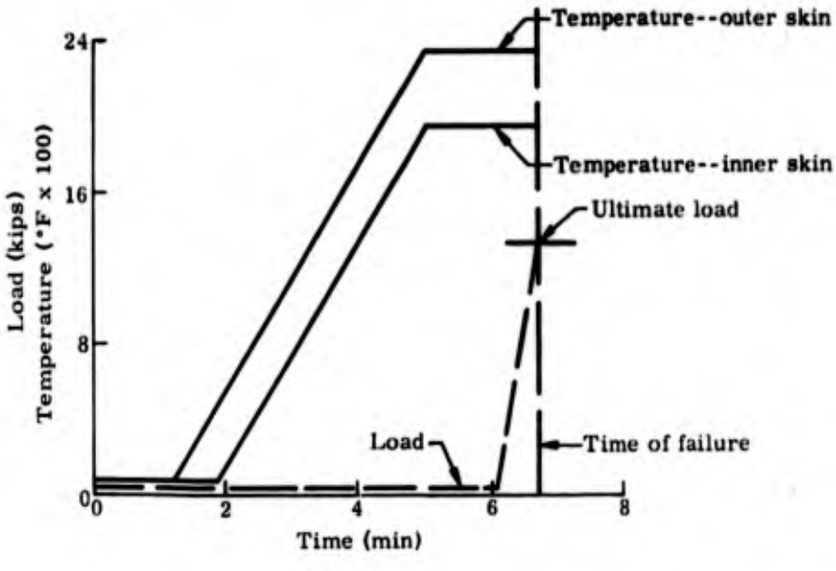

Fig. 129. Shear Test, D-36 St
No. 11

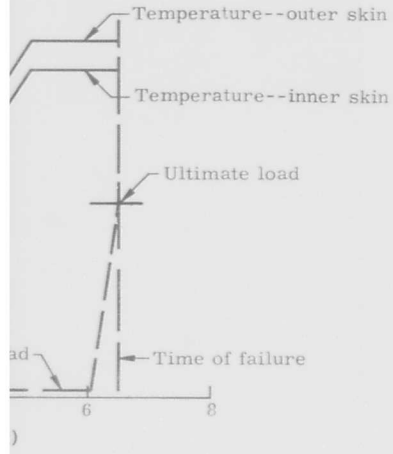

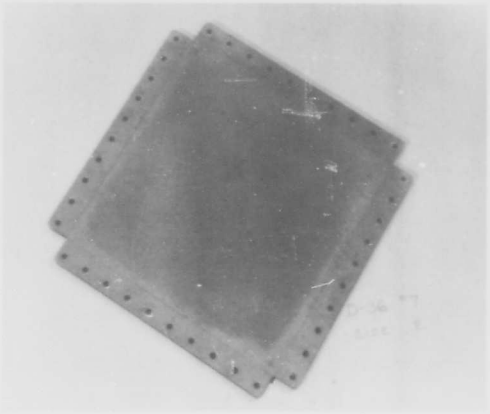

Fig. 128. Shear Test, D-36 Structural Panel No. 7

DESCRIPTION OF PANEL FAILURE
Local instability face wrinkling and intercellular dimpling. Plastic crown existed in panel from thermal gradient.

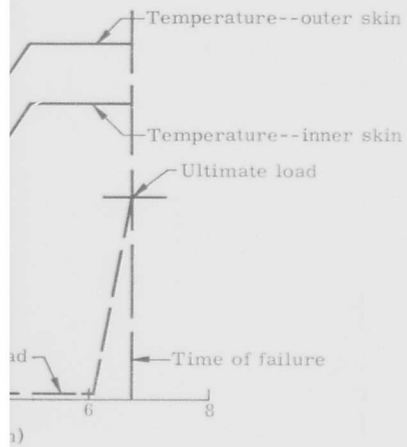

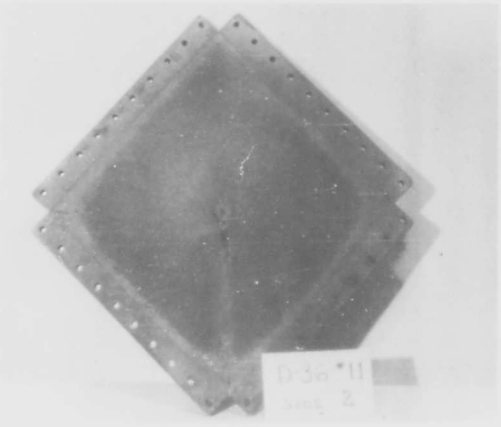

Fig. 129. Shear Test, D-36 Structural Panel No. 11

DESCRIPTION OF PANEL FAILURE
Local instability face wrinkling and intercellular dimpling. Plastic crown existed in panel from thermal gradient.

MATERIAL Columbium alloy, D-36
PANEL NO. 1
TYPE OF TEST Shear
MAX TEST TEMP 1980° F
TIME AT MAX TEMP 1602 sec
FAILING LOAD 15,800 lb
ULT STRESS 32,100 psi
RENÉ JIG TEMP 1180° F

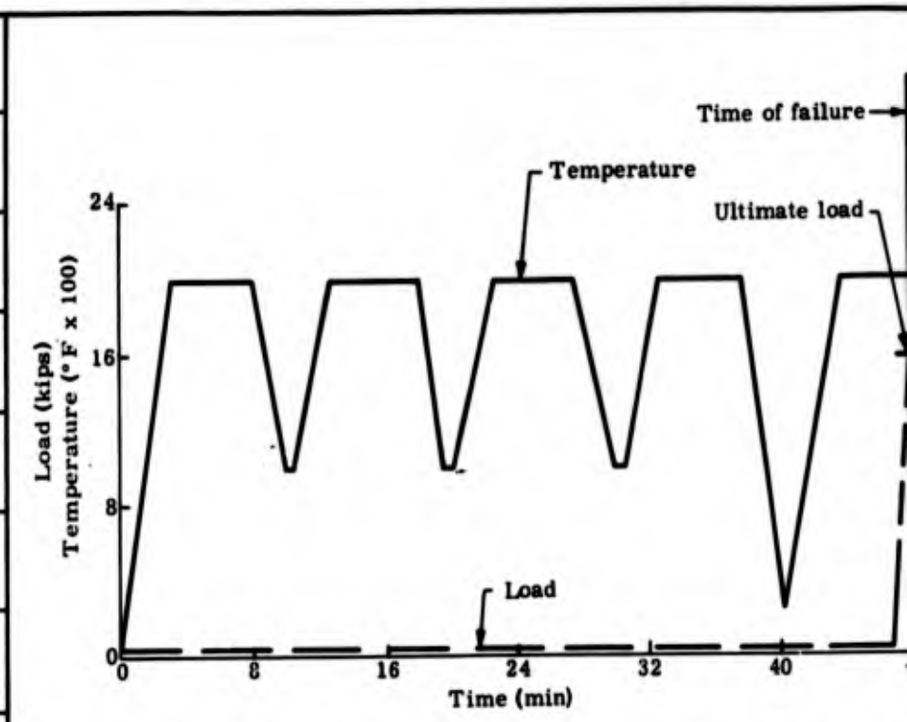

Fig. 130. Shear Test, D-36 No. 1

MATERIAL Columbium alloy, D-36
PANEL NO. 2
TYPE OF TEST Shear
MAX TEST TEMP 2400° F
TIME AT MAX TEMP 1520 sec
FAILING LOAD 7650 lb
ULT STRESS 15,800 psi
RENÉ JIG TEMP 1440° F

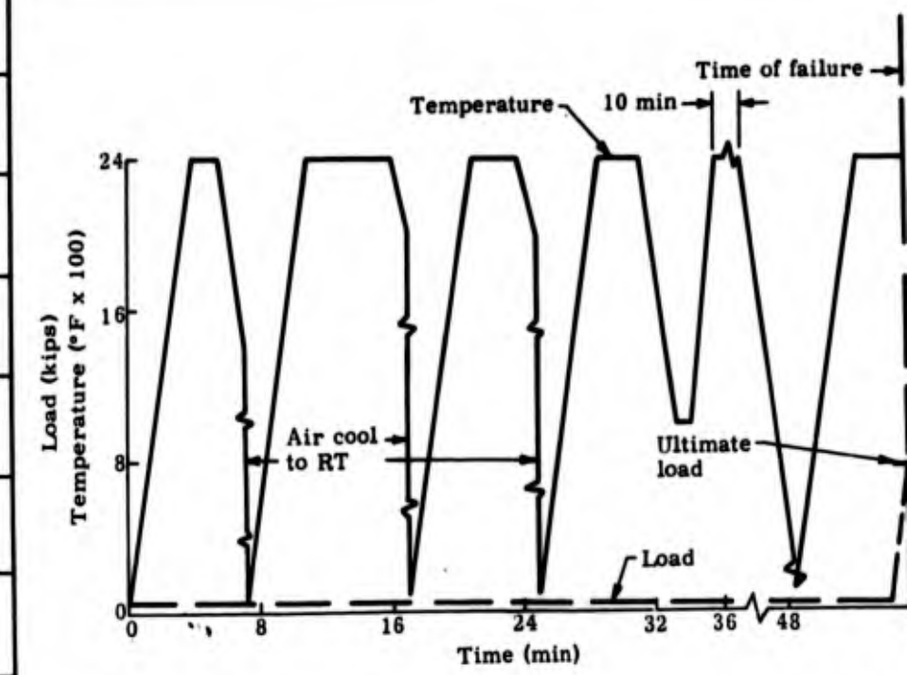

Fig. 131. Shear Test, D-36 No. 2

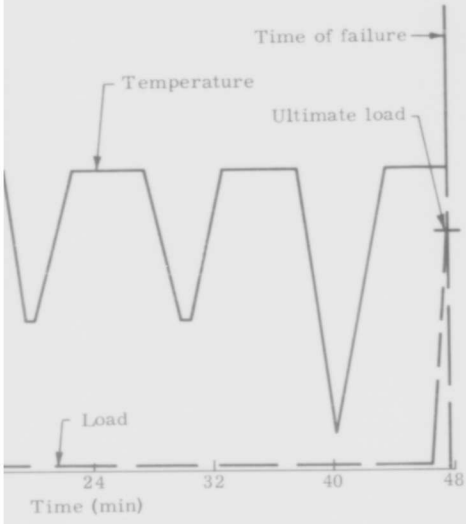

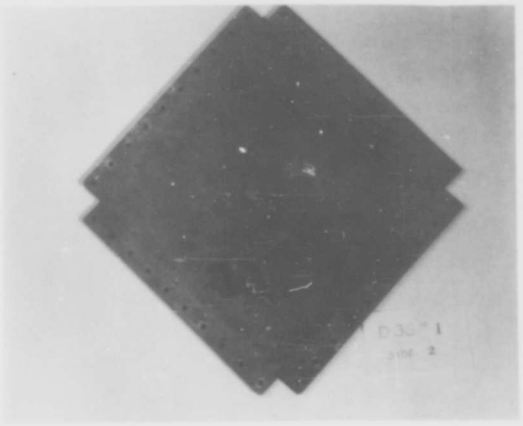

DESCRIPTION OF PANEL FAILURE
Local instability face wrinkling.

Fig. 130. Shear Test, D-36 Structural Panel No. 1

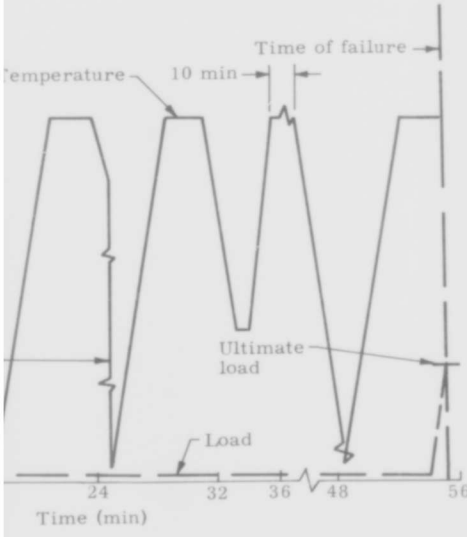

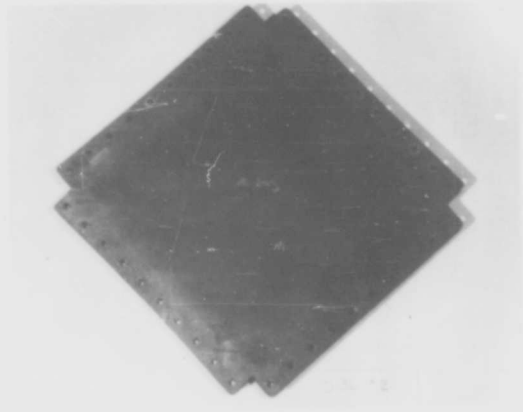

DESCRIPTION OF PANEL FAILURE
Local instability intercellular dimpling.

Fig. 131. Shear Test, D-36 Structural Panel No. 2

MATERIAL Columbium alloy, D-36
PANEL NO. 13
TYPE OF TEST Shear
MAX TEST TEMP 1625° F
TIME AT MAX TEMP 1536 sec
FAILING LOAD 24,800 lb
ULT STRESS 51,700 psi
RENÉ JIG TEMP 920° F

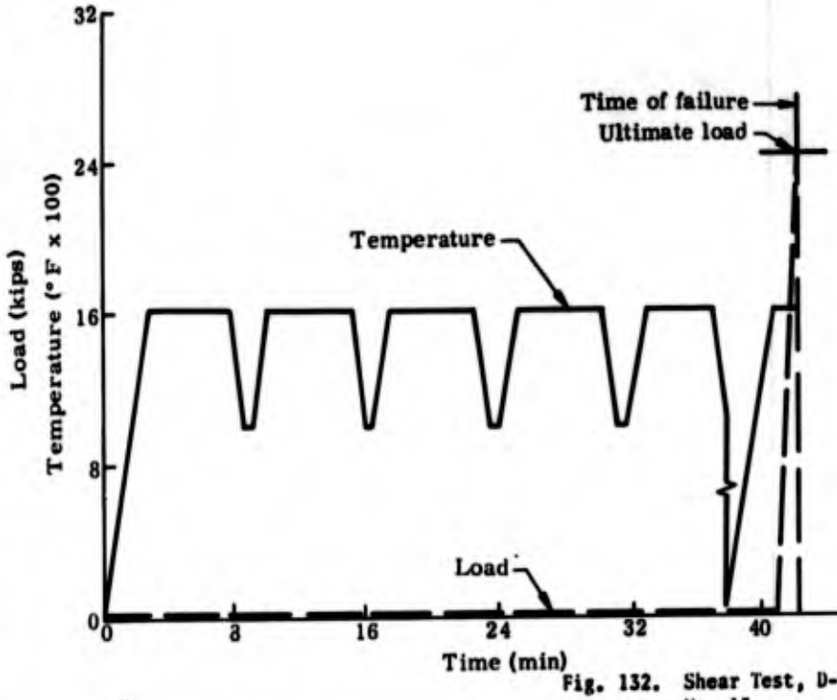

Fig. 132. Shear Test, D-36 St
No. 13

MATERIAL Columbium alloy, D-36
PANEL NO. 6
TYPE OF TEST Shear
TIME AT MAX TEMP RT
FAILING LOAD 38,000 lb
ULT STRESS 78,300 psi
RENÉ JIG TEMP

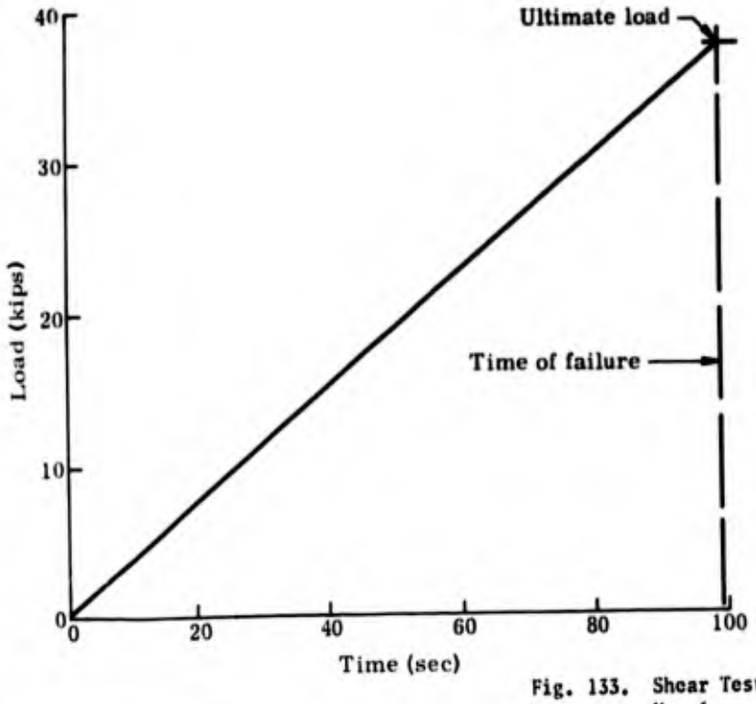

Fig. 133. Shear Test, D-36 S
No. 6

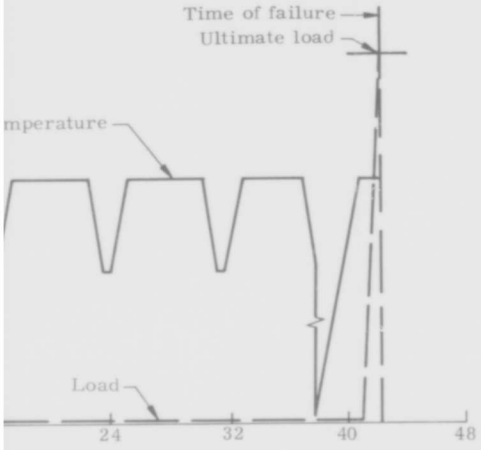

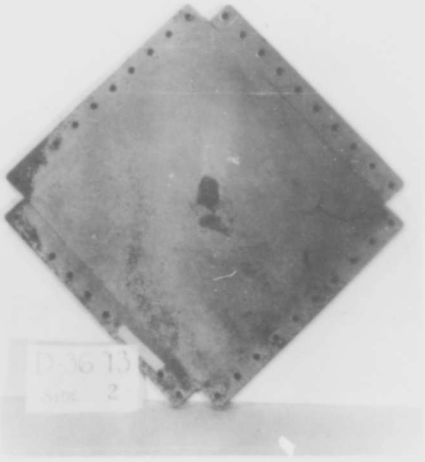

Fig. 132. Shear Test, D-36 Structural Panel No. 13

DESCRIPTION OF PANEL FAILURE
Ultimate material failure--coating spalled off.

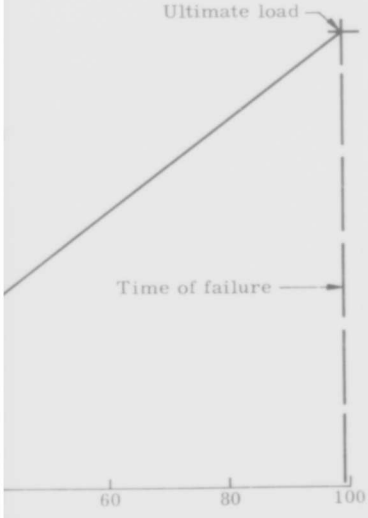

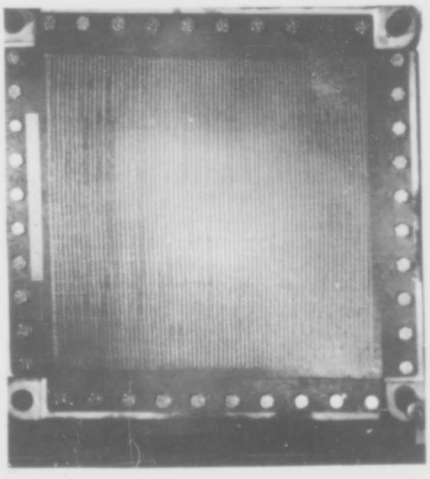

Fig. 133. Shear Test, D-36 Structural Panel No. 6

DESCRIPTION OF PANEL FAILURE
Ultimate material failure--coating acted as a stress-coat--spalled off on evenly spaced lines.

MATERIAL Columbium alloy, D-36
PANEL NO. 12
TYPE OF TEST Shear
MAX TEST TEMP 2300° F
TIME AT MAX TEMP 840 sec
FAILING LOAD 5000 lb--max 500 lb--min
ULT STRESS 10, 500 psi--max 1, 050 psi--min
RENÉ JIG TEMP 1250° F

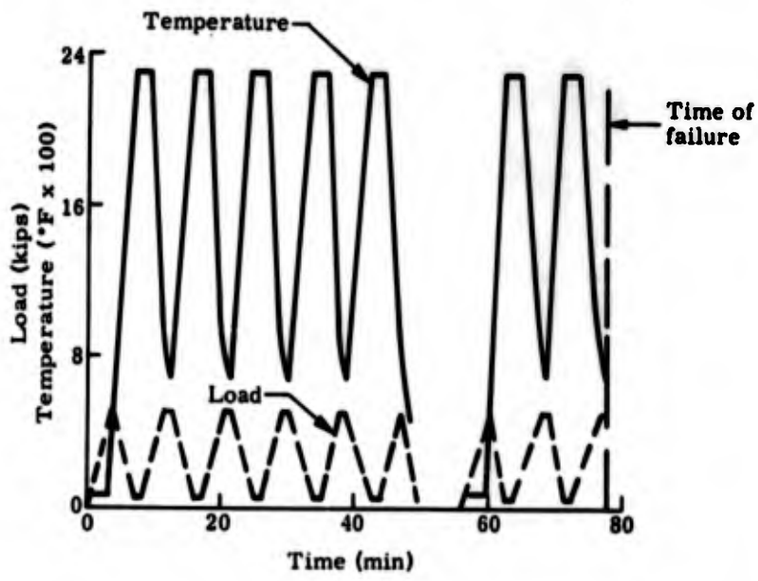

Fig. 134. Shear Test, D-36 ... No. 12

MATERIAL Columbium alloy, D-36
PANEL NO. 4
TYPE OF TEST Shear
MAX TEST TEMP 2350° F
TIME AT MAX TEMP 260 sec
FAILING LOAD
ULT STRESS
RENÉ JIG TEMP Shown

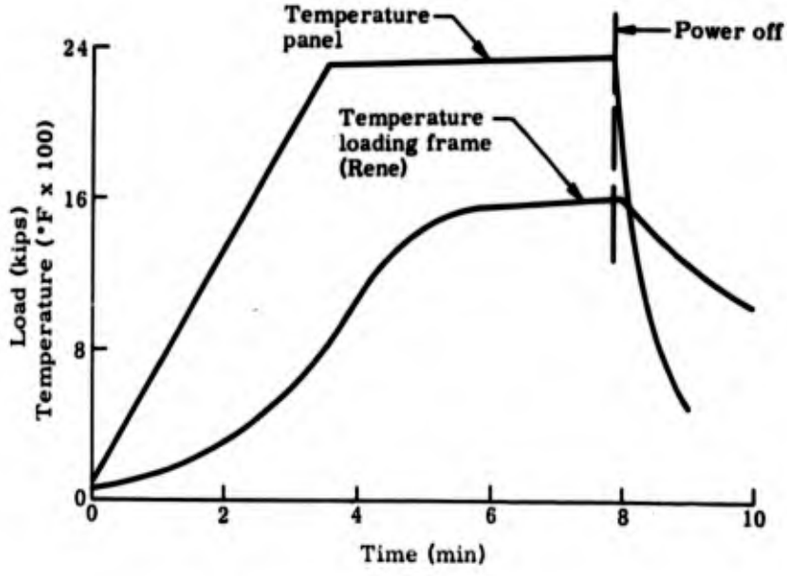

Fig. 135. Shear Test, D-36 ... No. 4

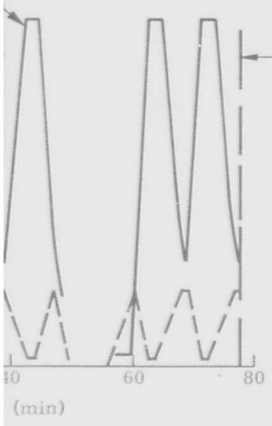

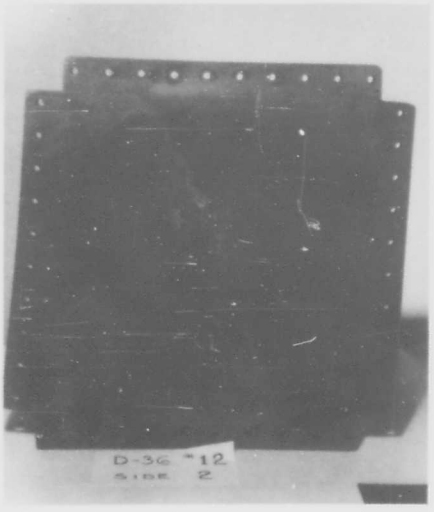

DESCRIPTION OF PANEL FAILURE
Local instability face wrinkling, intercellular dimpling.

Fig. 134. Shear Test, D-36 Structural Panel No. 12

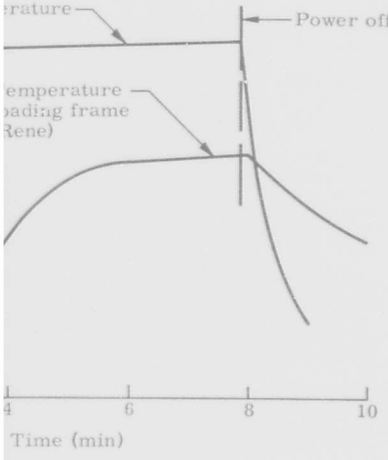

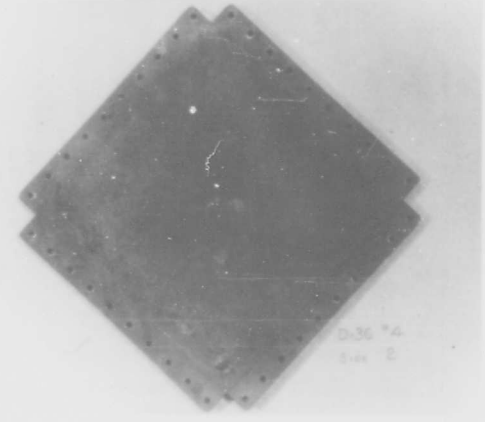

DESCRIPTION OF PANEL FAILURE
Tension failure due to thermal stresses imposed when loss of power to radiant lamps allowed specimen to cool much more quickly than the René 41 frame. (No applied mechanical load.)

Fig. 135. Shear Test, D-36 Structural Panel No. 4

MATERIAL Columbium alloy, D-36	
PANEL NO. 1	
TYPE OF TEST Compression	
MAX TEST TEMP 2000° F	
TIME AT MAX TEMP 288 sec	
FAILING LOAD 20,000 lb	
ULT STRESS 53,000 psi	
RENÉ JIG TEMP	

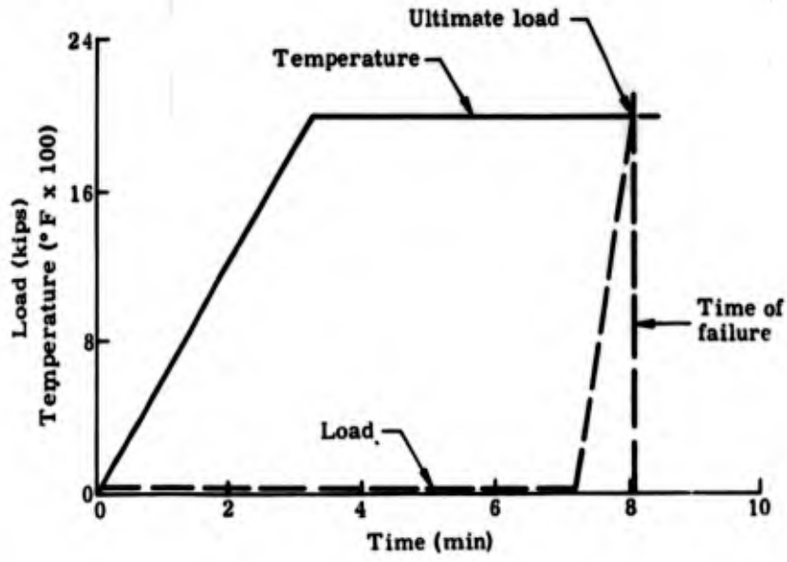

Fig. 136. Compression Test, D-3
Panel No. 1

MATERIAL Columbium alloy, D-36	
PANEL NO. 2	
TYPE OF TEST Compression	
MAX TEST TEMP 2400° F	
TIME AT MAX TEMP 270 sec	
FAILING LOAD 9000 lb	
ULT STRESS 23,100 psi	
RENE JIG TEMP	

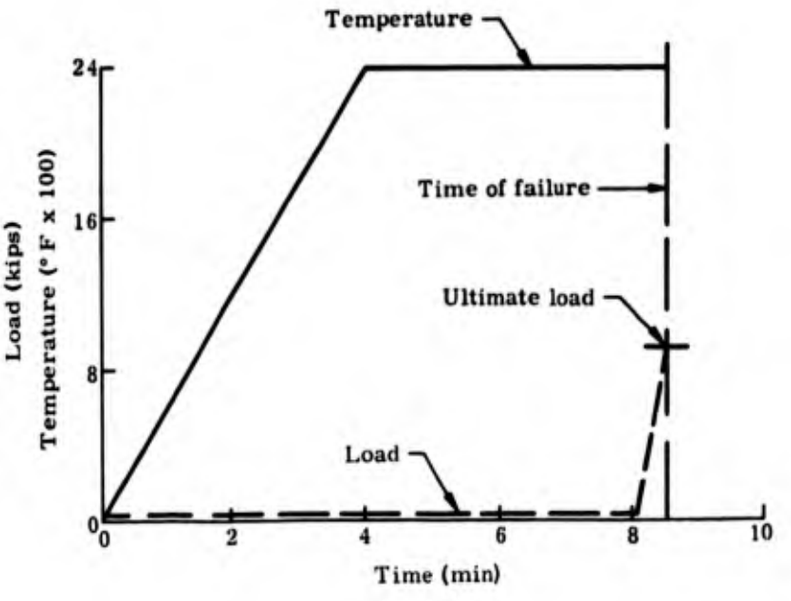

Fig. 137. Compression Test, D-3
Panel No. 2

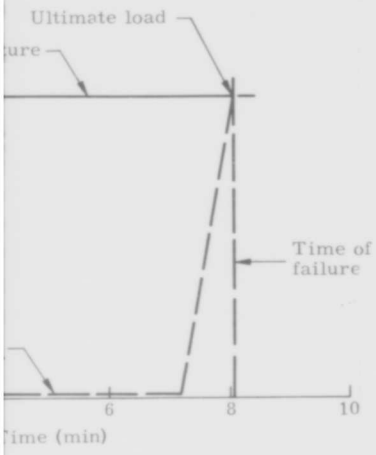

Fig. 136. Compression Test, D-36 Structural Panel No. 1

DESCRIPTION OF PANEL FAILURE
General instability. Permanent crown in center of panel. Failure of bottom "U" channel vertical legs.

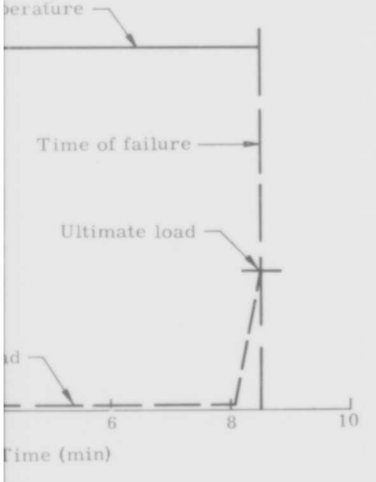

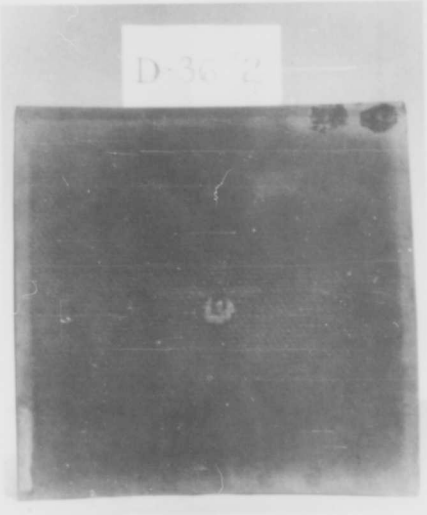

Fig. 137. Compression Test, D-36 Structural Panel No. 2

DESCRIPTION OF PANEL FAILURE
General instability. Secondary local failure--intercellular dimpling and face wrinkling. Load was prematurely released before maximum failure stress was obtained.

MATERIAL Columbium alloy, D-36
PANEL NO. 3
TYPE OF TEST Compression
MAX TEST TEMP 2300° F
TIME AT MAX TEMP 600 sec
FAILING LOAD 9000 lb--max 1600 lb--min
ULT STRESS 23, 800 psi--max 4, 250 psi--min
RENÉ JIG TEMP

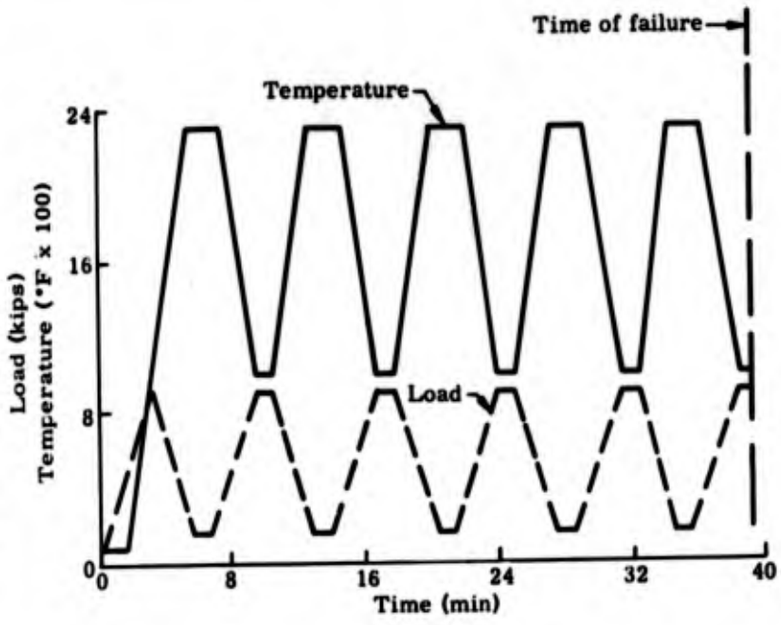

Fig. 138. Compression Test, Panel No. 3

MATERIAL Columbium alloy, D-36
PANEL NO. 5
TYPE OF TEST Compression
MAX TEST TEMP 2000° F
TIME AT MAX TEMP 1686 sec
FAILING LOAD 19, 400 lb
ULT STRESS 52, 000 psi
RENÉ JIG TEMP

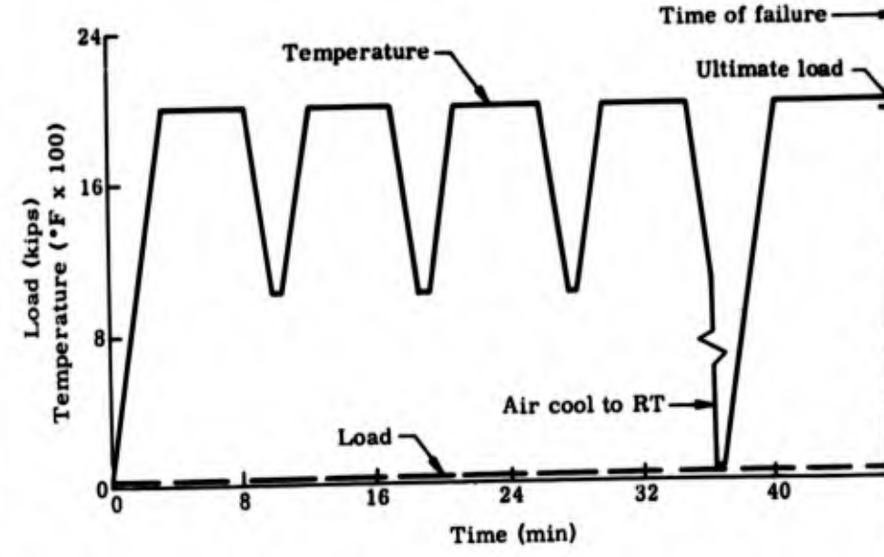

Fig. 139. Compression Test, Panel No. 5

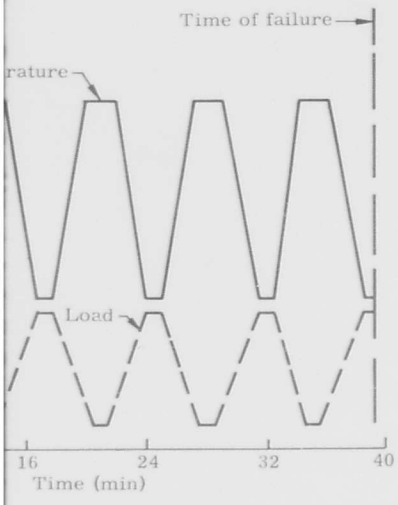

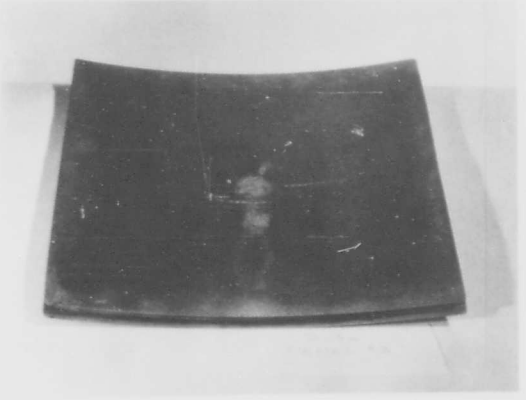

Fig. 138. Compression Test, D-36 Structural Panel No. 3

DESCRIPTION OF PANEL FAILURE
General instability. Creep failure during sixth loading cycle.

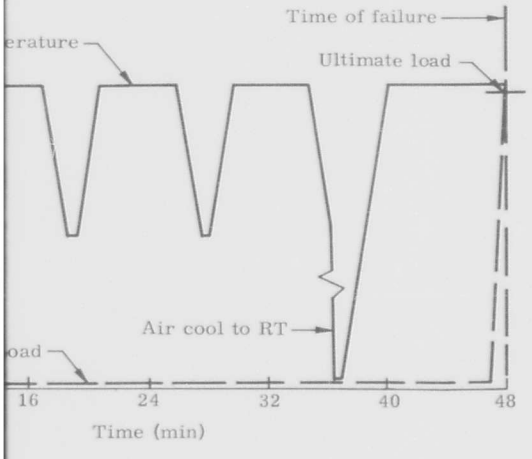

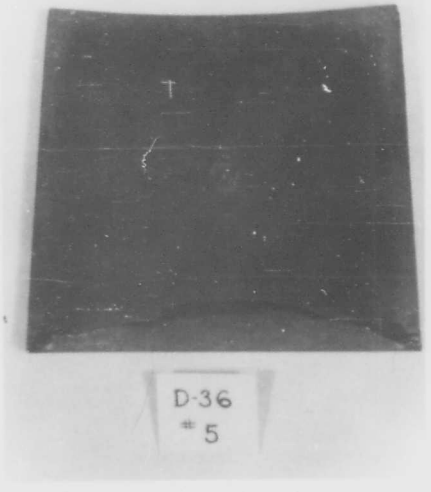

Fig. 139. Compression Test, D-36 Structural Panel No. 5

DESCRIPTION OF PANEL FAILURE
General instability. Crown in panel. Secondary failure--shear crimp.

MATERIAL Columbium alloy, D-36
PANEL NO. 10
TYPE OF TEST Compression
MAX TEST TEMP 1620° F
TIME AT MAX TEMP 150 sec
FAILING LOAD 27, 400 lb
ULT STRESS 72, 800 psi
RENÉ JIG TEMP

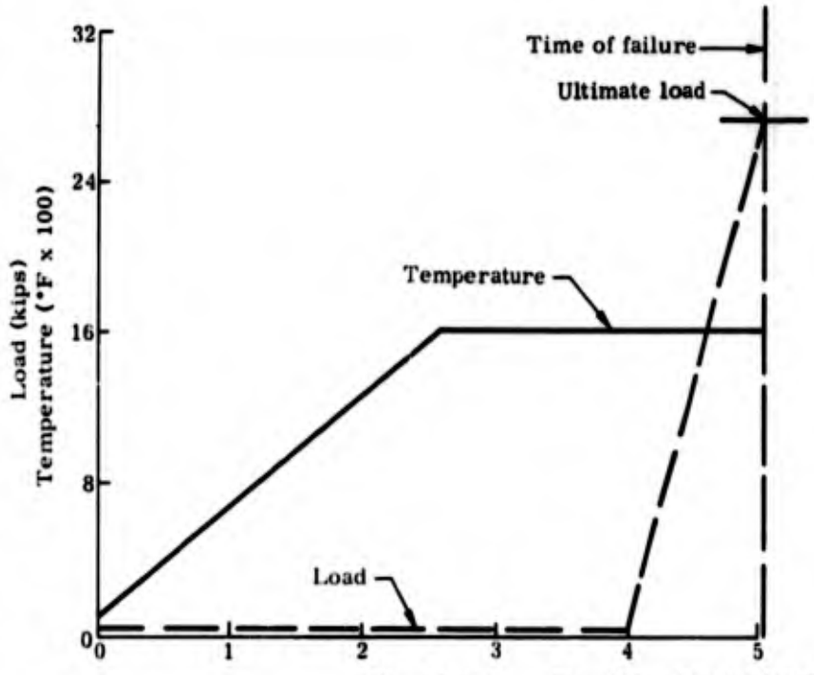

Fig. 140. Compression Test, D-36
Panel No. 10

MATERIAL Columbium alloy, D-36
PANEL NO. 11
TYPE OF TEST Compression
MAX TEST TEMP 1600° F
TIME AT MAX TEMP 1510 sec
FAILING LOAD 26, 800 lb
ULT STRESS 73, 000 psi
RENÉ JIG TEMP

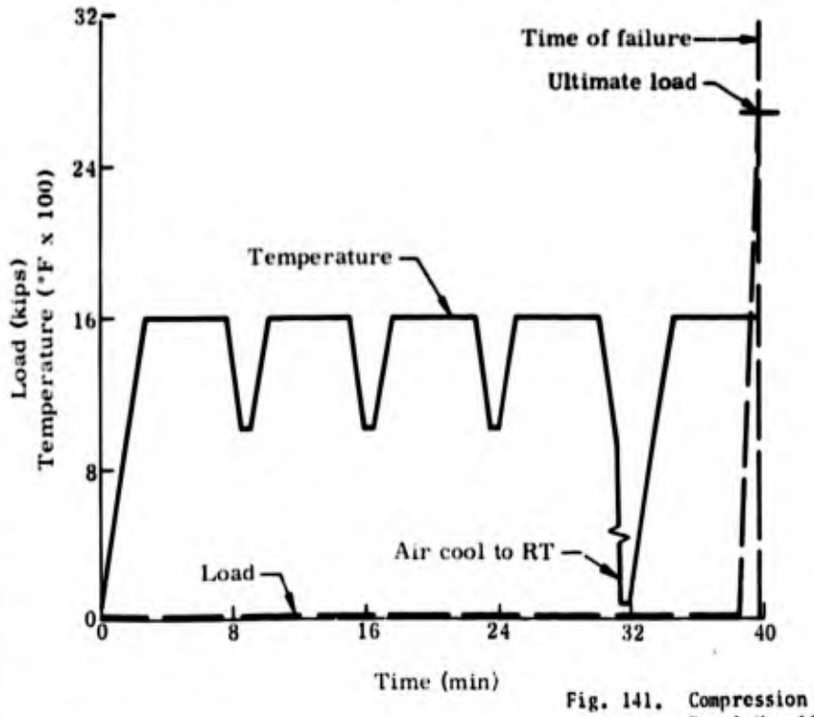

Fig. 141. Compression Test, D-3
Panel No. 11

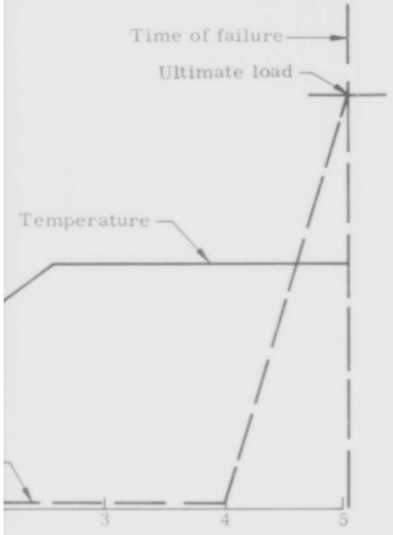

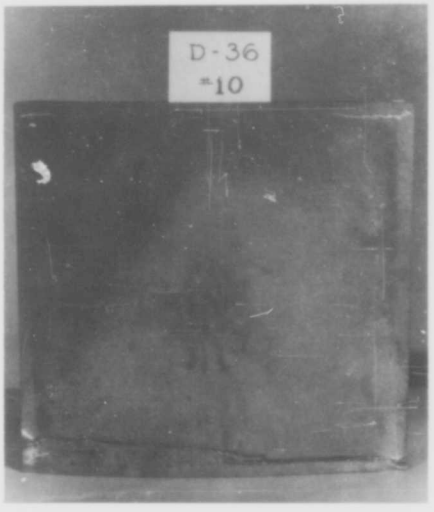

Fig. 140. Compression Test, D-36 Structural Panel No. 10

DESCRIPTION OF PANEL FAILURE
General instability crown in panel.

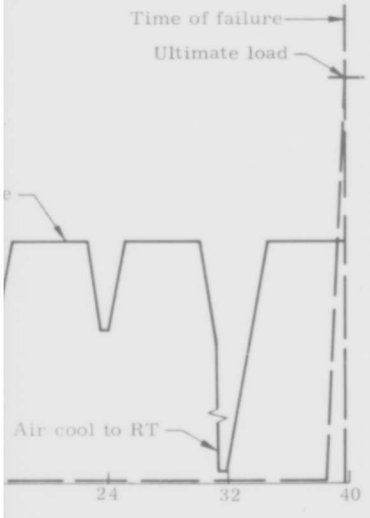

Fig. 141. Compression Test, D-36 Structural Panel No. 11

DESCRIPTION OF PANEL FAILURE
General instability crown in panel.

MATERIAL Columbium alloy, D-36	
PANEL NO. 8	
TYPE OF TEST Compression	
MAX TEST TEMP 2350° F--outer face 2140° F--inner face	
TIME AT MAX TEMP 307 sec	
FAILING LOAD 14,700 lb	
ULT STRESS 39,400 psi	
RENÉ JIG TEMP	

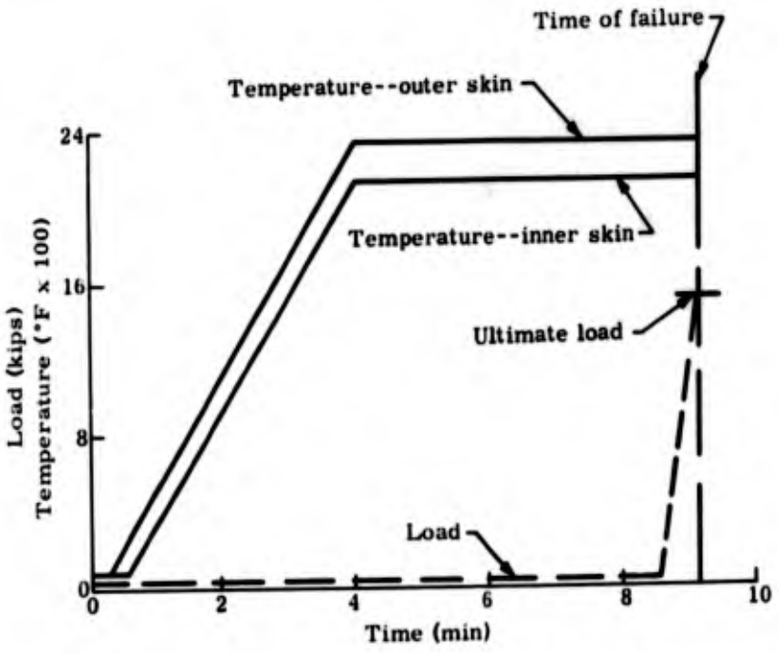

Fig. 142. Compression Test Panel No. 8

MATERIAL Columbium alloy, D-36	
PANEL NO. 7	
TYPE OF TEST Compression	
MAX TEST TEMP 2350° F--outer face 1950° F--inner face	
TIME AT MAX TEMP 315 sec	
FAILING LOAD 16,400 lb	
ULT STRESS 44,000 psi	
RENÉ JIG TEMP	

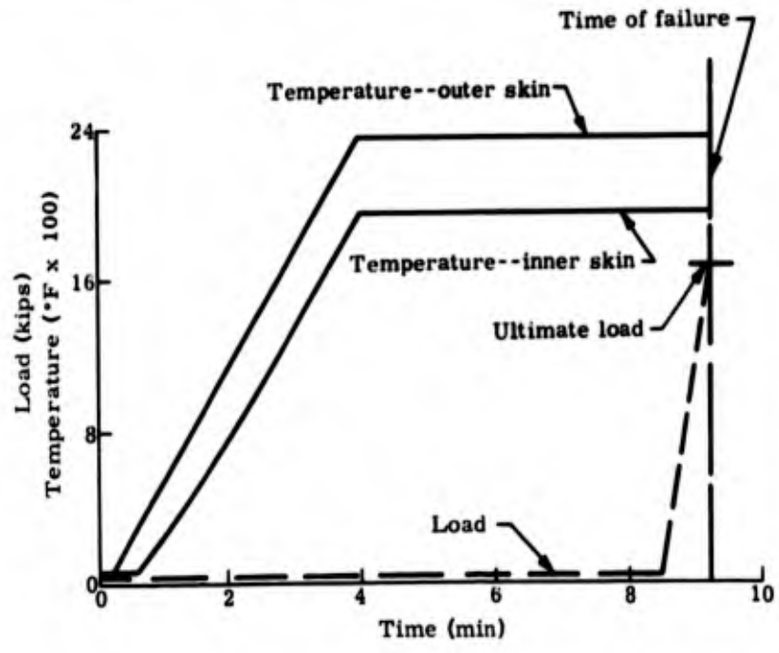

Fig. 143. Compression Test Panel No. 7

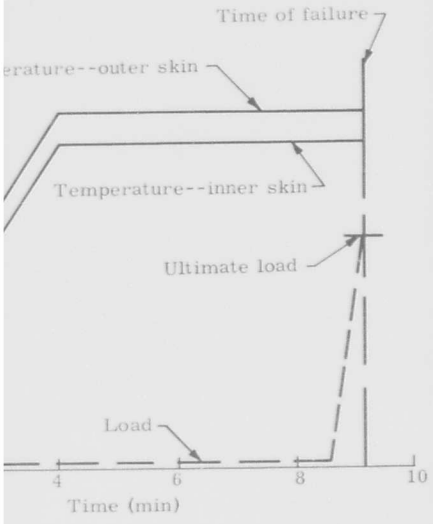

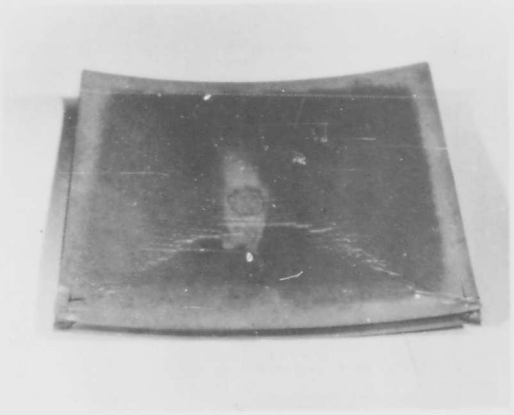

DESCRIPTION OF PANEL FAILURE
General instability. Face wrinkling on lower temperature face after panel crowned.

Fig. 142. Compression Test, D-36 Structural Panel No. 8

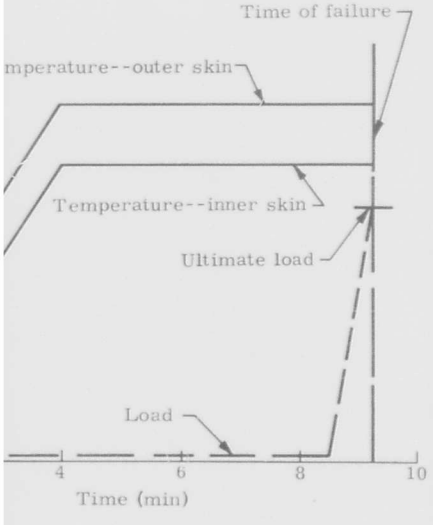

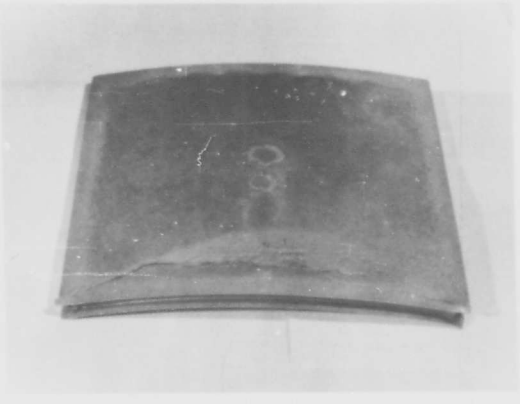

DESCRIPTION OF PANEL FAILURE
General instability. Face wrinkling on lower temperature face after panel crowned.

Fig. 143. Compression Test, D-36 Structural Panel No. 7

MATERIAL Columbium alloy, D-36
PANEL NO. 6
TYPE OF TEST Compression
MAX TEST TEMP 2400° F
TIME AT MAX TEMP 1200 sec
FAILING LOAD 12, 000 lb
ULT STRESS 32, 400 psi
RENÉ JIG TEMP

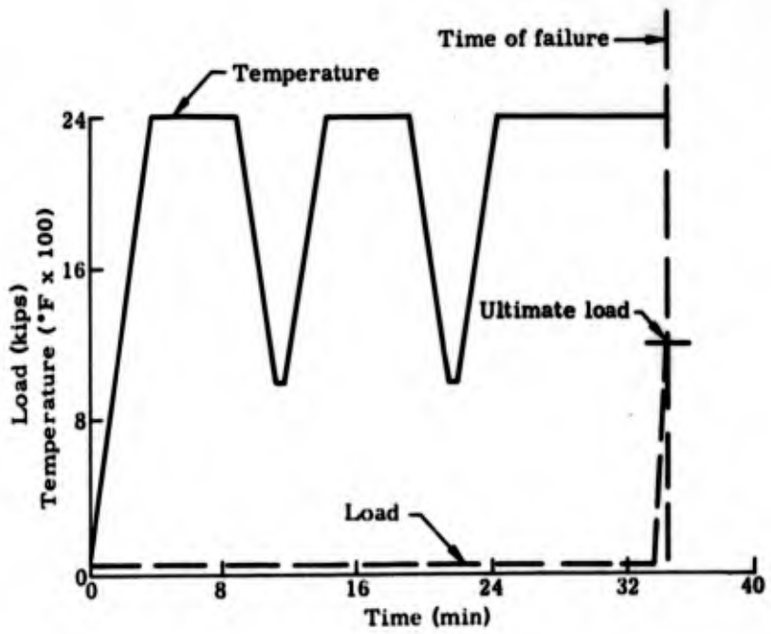

Fig. 144. Compression Test, D-3
Panel No. 6

MATERIAL Columbium alloy, D-36
PANEL NO. 9
TYPE OF TEST Compression
TIME AT MAX TEMP RT
FAILING LOAD 36, 000 lb
ULT STRESS 97, 700 psi
RENÉ JIG TEMP

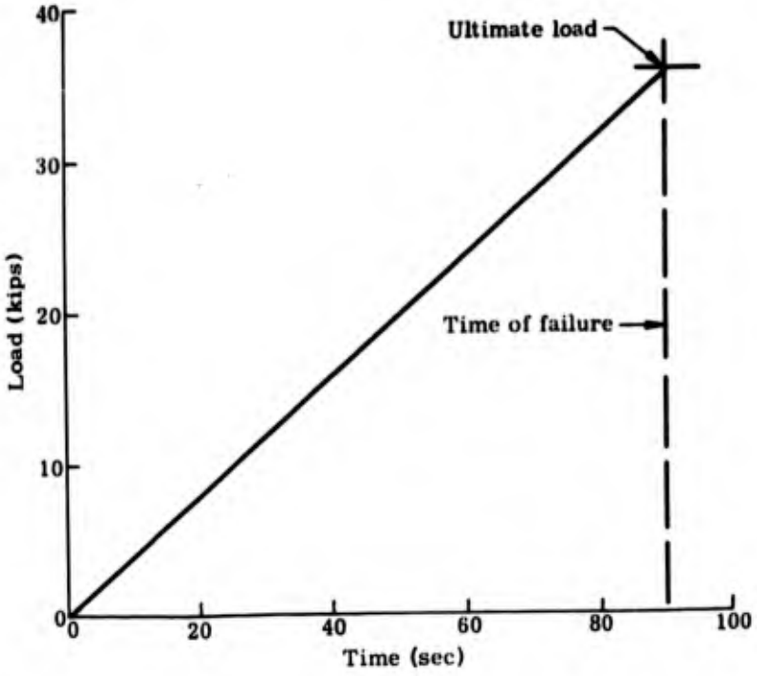

Fig. 145. Compression Test, D-
Panel No. 9

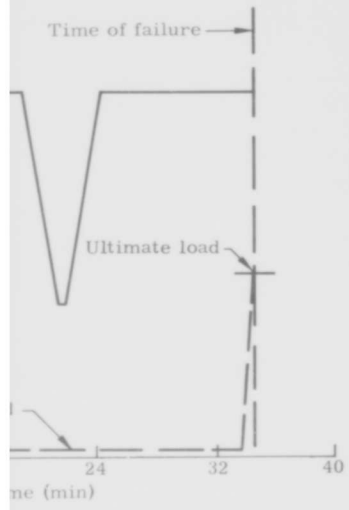

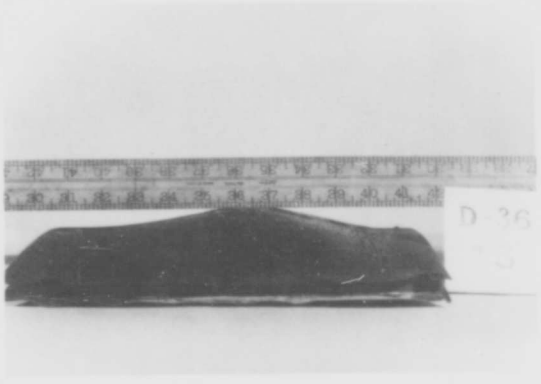

Fig. 144. Compression Test, D-36 Structural Panel No. 6

DESCRIPTION OF PANEL FAILURE
General instability crown in panel. Secondary failure--face wrinkling, warped edges.

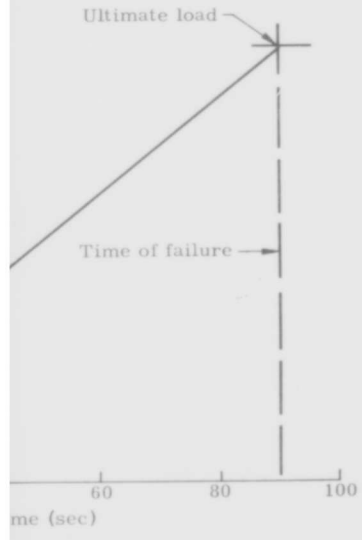

Fig. 145. Compression Test, D-36 Structural Panel No. 9

DESCRIPTION OF PANEL FAILURE
General instability crown in panel. Secondary failure--"U" channel flange crimping.

tremely low stress level. Flat Panel No. 8 exploded during heating because of expansion of entrapped air.

C. HEAT SHIELD TESTS

The objective of the heat shield test program was to determine the capability of the heat shield panels to withstand simulated re-entry conditions. To achieve this, three basic test conditions were selected:

(1) Maximum thermal life.

(2) Typical re-entry.

(3) Repeated thermal exposure.

The maximum life test consisted of maintaining a panel at temperature for a sustained period until the panel failed. These tests determined the maximum single exposure time at temperature for the heat shield panels. The typical re-entry tests qualified the panels for representative re-entry environments (provided by ASD). The repeated exposure tests determined the panel capability for repeated usage.

Ten D-36 columbium heat shield panels were subjected to these test conditions. Eight of the panels were tested in the hot gas facility and two were tested in the quartz lamp radiant heating facility.

1. Test Equipment

The dynamic gas environment for the heat shield test was supplied by a 14-in. hot gas facility which consisted of:

(1) Air compressors to furnish air to the burner cans.

(2) A conventional jet engine burner can used to preheat oxygen-enriched air.

(3) An afterburner section which produces a stream of hot air and gaseous combustion products by igniting propane and oxygen.

(4) A 14-in. convergent exit nozzle which directs the hot gaseous stream.

(5) A movable specimen mounting carriage on a 25-ft track.

(6) Associated instrumentation and control equipment (Fig. 146).

Basically, three facility operating conditions (14-A-1, 14-B-1 and 14-C-1) were used

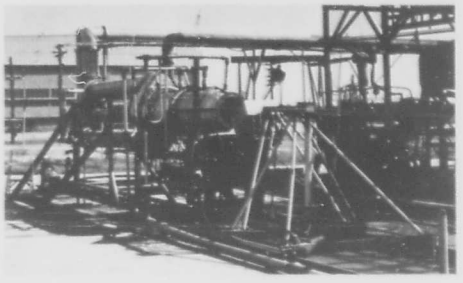

Fig. 146. Hot Gas Facility

for imposing the simulated re-entry environments on the heat shield panels (Table 20). Condition 14-A-1 represents the maximum stream conditions of the facility, while Conditions 14-B-1 and 14-C-1 represent the minimum and intermediate stream conditions used on this program (Fig. 147).

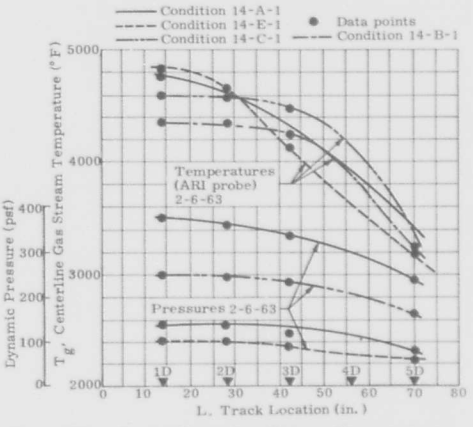

Fig. 147. Centerline Gas Stream Temperatures and Dynamic Pressures, Two Conditions

Two panel holders were designed and fabricated for the heat shield tests in the hot gas facility (Fig. 148). The only difference between the two holders was that the external face of each holder was fabricated to match the curvature of the specimen. Essentially, the holder design was comprised of an insulated box in a water-cooled jacket. The test specimen was mounted in the insulated box by bolting the panel attachment legs to a stainless steel bracket which was attached to a water-cooled steel mounting plate. Fiberfrax insulation was inserted between the inner face of the panel and the steel mounting

Fig. 148. Hot Gas Facility with Flat Heat Shield Panel Test Fixture

plate. The sides of the insulated box were an integral part of the jacket and protected the specimen and insulation from the water sprayed on the holder for cooling purposes. Two nickel fairing strips were welded to the edges of the holder cutout to prevent adverse flow in the area of the panel steps. The panel holders also had the provision of variable angle of attack with the hot gas stream centerline. This mounting procedure closely approximated a cooled, double-wall installation technique.

The radiant heating system was generally the same as described in Section C, Structural Panel Tests. The primary differences in the test setup were that only one heater was used to heat the panel and that the inner side of the panel was backed with fiberfrax insulation. Columbium sheath thermocouples (previously described) were used to monitor the panel temperatures.

2. Preliminary Tests

Several preliminary tests were performed in the hot gas facility to determine the pressure distributions on the heat shield panels. The initial tests were performed using a flat, water-cooled steel plate of the same size as the flat heat shield panel mounted in the panel holder. Seven wall pressure pickups connected to seven vertical manometers were mounted in the steel plate in a pattern suitable for determining the pressure distribution over the simulated panel area. A total pressure probe was installed in the stream to monitor the stream pressure. Three test runs were performed with only the facility air compressors operating, to qualitatively determine the panel pressure distribution at various angles of attack (20, 30 and 60 deg). With this information, the 30-deg angle-of-attack attitude was chosen for a "hot" run (Condition 14-A-1) to quantitatively determine the pressure distribution on the simulated flat panel (Fig. 149). The results of this test indicated that the 30-deg angle of attack represented the best compromise between uniformity and desired pressure (1.2 psi). Later tests on an independent program also indicated that an α of 30 deg for a flat plate produced a near maximum facility heating rate with uniform heating distribution (Ref. 37). Consequently, the α = 30-deg attitude was initially chosen for all panel tests. However, during two of the curved heat shield tests, structural tension failures of the panel upper attachment legs occurred. A pressure distribution test at an α = 30 deg was performed on a curved plate (similar to the flat plate described above). The results from this test indicated that the failures were caused by an adverse pressure distribution on the panel (negative pressure at the top of the panel to positive pressure at the bottom of the panel). Consequently, a new angle of

TABLE 20

Operating Parameters of the Hot Gas Facility

Parameter	Condition 14-A-1	Condition 14-B-1	Condition 14-C-1	Units
Type of flow	Turbulent	Turbulent	Turbulent	--
Flow velocity	0.45	0.30	0.40	Mach No.
Mass flow rate	14.0	8.1	11.6	lb/sec
Dynamic pressure	320.0	144.0	250.0	psf
Sound pressure level	162.0	162.0	> 150	db
Gas temperature	4360.0	4780.0	4600.0	°F
Stagnation enthalpy	1350.0	1370.0	1320.0	Btu/lb

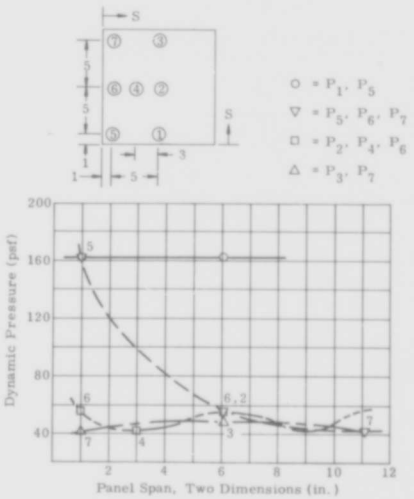

Fig. 149. Simulated Flat Heat Shield Panel Pressure Distribution

attack and facility operating condition had to be obtained for the curved panels. A 90-deg angle of attack was selected for pressure uniformity, and a facility operating condition with a dynamic stream pressure of 250 psf was used to obtain panel pressures less than 2 psi and temperatures up to 2400° F.

3. Test Procedures

The actual tests on the heat shield panels in the hot gas facility were generally accomplished by the following procedure:

(1) Instrument specimen with a control thermocouple.

(2) Mount specimen in the holder.

(3) With the carriage at the end of the track and the stream deflection shield up, start and then stabilize the afterburner.

(4) Drop the stream deflection shield.

(5) Using the specimen's thermocouple as a control device (up to 2000° F), move the specimen toward or away from the nozzle exit according to the desired time-temperature profile.

(6) At temperatures above 2000° F, use the Pyro-650 optical pyrometer as the temperature control.

The results of the high temperature instrumentation study indicated the use of a sheath thermocouple for the hot gas tests (dynamic environment). Consequently, a columbium sheath tungsten-rhenium thermocouple was used for thermal control. The thermocouple was attached to the center of the inner face of the specimen by means of an integral mechanical panel holder (Fig. 115). Several flat heat shield panels did not have this holder and the thermocouple was bonded to the specimen with molybdenum disilicide cement. These thermocouples failed during the tests.

After the installation of the control thermocouple, the panel was mounted in the panel holder as previously explained. However, since these panels had access holes, several attempts were made to fill the holes in order to prevent adverse flow and subsequent hot spots. The first attempt was the insertion of fused silica plugs into the holes, flush with the exposed surface. During the first heat shield test, the plug became too hot and consequently expanded, causing a failure of the access hole tube. The next attempt proved to be the most successful. It consisted of "stuffing" fiberfrax insulation into the holes until the exposed panel surface was aerodynamically smooth. Generally, the insulation would stay in the holes, but during several tests, it was removed by the air stream. The loss of these plugs caused local hot spots around the holes (Fig. 150).

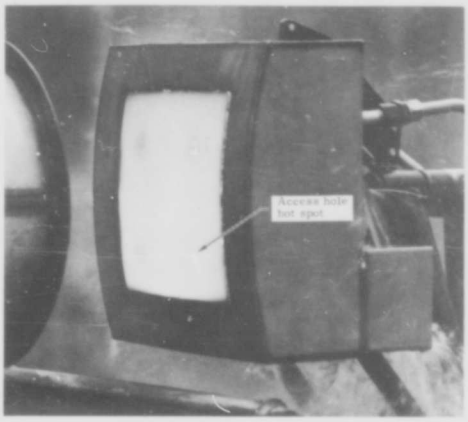

Fig. 150. Local Hot Spot Created by Heat Shield Panel Access Hole

During the actual performances of these tests, constant visual monitoring (including photographic documentation), as well as thermocouple and optical pyrometer monitoring, was accomplished. Qualitative information concerning panel deflection, heat distribution and coating appearance was obtained by the visual monitoring sources. The thermocouple and optical pyrometer supplied the quantitative temperature data during the tests.

The two tests in the radiant heating facility were performed in a manner similar to the structural panel tests with the exception that no load was applied to the panels.

4. Test Results

Two flat D-36 columbium heat shield panels (Nos. 9 and 7) were subjected to the maximum life condition. This consisted of a minimum temperature test (2200° F) and a maximum temperature test (2600° F) (Figs. 151 and 152). Panel No. 9 failed in the access hole area because of the fused silica plugs, thus rupturing the tube and the outer skin. However, even though this premature failure occurred approximately 15 min after the start of the test, the panel continued to withstand the imposed environment for another 15 min without any additional failures.

MATERIAL Columbium alloy, D-36
PANEL NO. 7
TYPE OF TEST Hot gas flat heat shield
MAX TEST TEMP (AVG) 2640° F
TIME ABOVE 2400° F 750 sec
TEST ANGLE 30 deg
DYNAMIC PRESSURE 370 psf

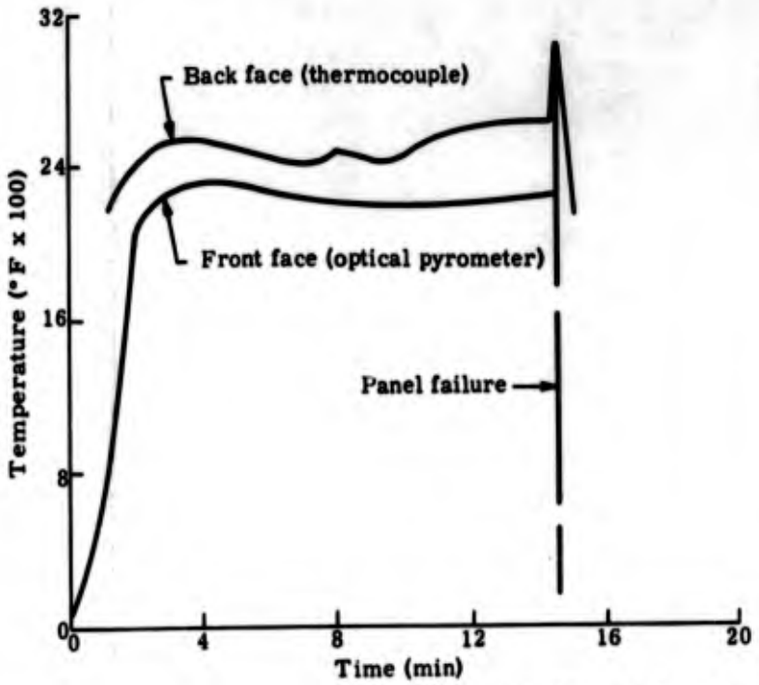

Fig. 151. Hot Gas Test, D-36 Fla
Panel No. 7

MATERIAL Columbium alloy, D-36
PANEL NO. 9
TYPE OF TEST Hot gas flat heat shield
MAX TEST TEMP (AVG) 2360° F
TIME AT MAX TEMP 870 sec
TEST ANGLE 30 deg
DYNAMIC PRESSURE 144 psf

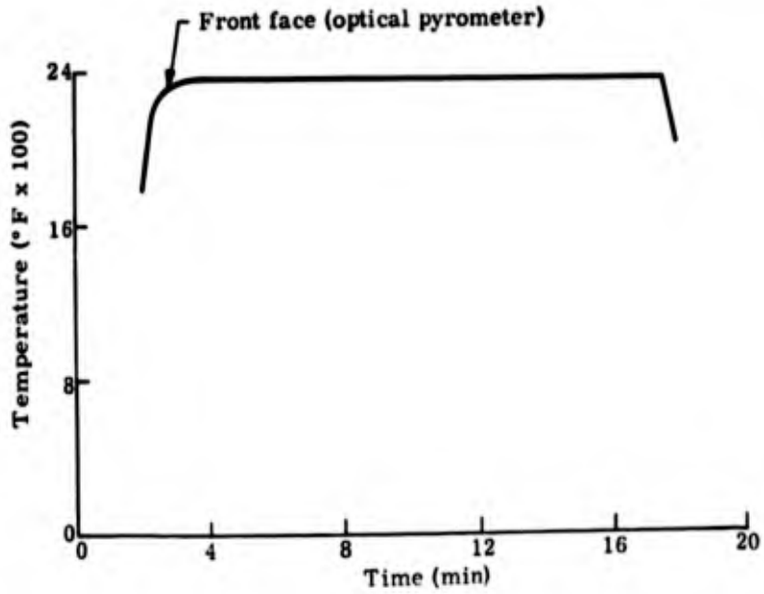

Fig. 152. Hot Gas Test, D-36 Fl
Panel No. 9

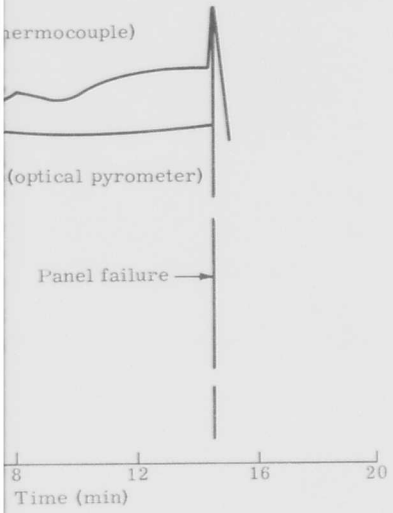

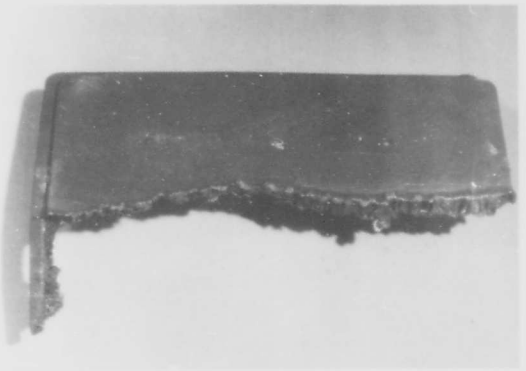

Fig. 151. Hot Gas Test, D-36 Flat Heat Shield Panel No. 7

DESCRIPTION OF PANEL FAILURE
Local failure occurred at hot spots on lower right edge due to lower lip deflecting into the air stream after sustained operation at 2600° F and a high dynamic pressure.

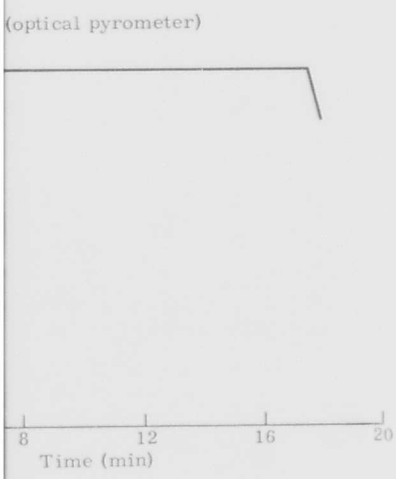

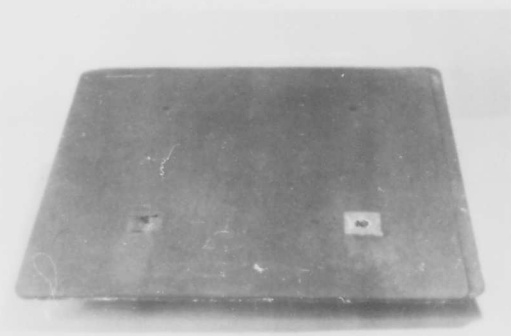

Fig. 152. Hot Gas Test, D-36 Flat Heat Shield Panel No. 9

DESCRIPTION OF PANEL FAILURE
Panel failed at both upper attachment surface patches due to hole filler inserts pushing out.

Panel No. 7 successfully withstood the maximum condition of the facility (14-A-1) for 12 min before a local hot spot developed causing the eventual failure of the panel two minutes later. The hot spot developed along the lower edge of the panel when this edge protruded into the gas stream creating a local stagnation condition. An optical pyrometer reading of 2800° F was obtained in the general area of the hot spot, but this reading was lower than the maximum temperature of the local area because of the pyrometer's wide field of vision.

The typical re-entry tests were accomplished by imposing various re-entry time-temperature profiles (provided by ASD) on the heat shield panels. Four D-36 columbium panels were subjected to two re-entry conditions. Panel Nos. 3 (Fig. 153) and 4 (Fig. 154) (both curved panels) were tested with the 2600° F re-entry trajectory. Both of these panels failed prematurely because of an adverse pressure distribution causing the failure of the upper right attachment leg (see preliminary tests) (Fig. 155). However, even after the attachment leg failed, the panel continued to support the loads and temperatures until the unsupported corner deflected into the air stream, creating a hot spot. Two panels (curved No. 2 and flat No. 5) (Figs. 156 and 157, respectively) successfully withstood a lower temperature (2200° F) re-entry profile without incident. Panel No. 5 was also tested at a steady-state condition of 2200° F for 17 additional minutes without any damage.

Four panels were tested for the repeated exposure (cyclic) condition. Panel Nos. 5 and 6 (both curved) were tested in the hot gas facility while Panel Nos. 4 and 11 (both flat) were tested in the radiant lamp facility (Figs. 158 through 161). Panel No. 6 had a local failure of a sealing detail after being exposed to four five-minute cycles at 2150° F. Panel No. 5 failed in the upper corner after three five-minute cycles at 2400° F. Panel No. 4 was subjected to the same time-temperature profile as Panel No. 5 in the radiant facility. However, Panel No. 4 withstood five thermal cycles before severe oxidation occurred along the panel edges and sealing details. These two tests in the two different facilities gave a qualitative evaluation on the comparative severity of the two types of thermal environment. Panel No. 11 failed due to a sealing detail becoming detached, exposing an uncoated area on the panel face during the second cycle at 2600° F.

D. SMALL SPECIMEN TESTS

The small specimen test portion of the test program was concerned with determining the mechanical properties of the D-36 and TZM panel honeycomb core and facing materials. Specifically, the desired properties were:

Core	Facing
Shear strength and modulus	Tensile ultimate and yield strengths, modulus of elasticity, elongation
Flatwise compression strength and modulus	Column compression strength
	Creep strength
	Fatigue strength

All of these properties were determined at elevated temperature.

1. Test Equipment

A high temperature cold-wall vacuum test furnace and a 150,000-lb universal testing machine were used for all of the core properties tests and the facing tensile ultimate, yield strength and fatigue strength tests. A 4000° F vacuum furnace and an arcweld creep rack were used for the facing creep tests.

The cold-wall vacuum test furnace is capable of attaining temperatures of 3500° F at 10^{-5} torr. The 5- by 6- by 12-in. furnace test chamber consists of 14 sets of W-shaped 1/4-in. diameter tantalum rod elements on four sides, surrounded by six-layer tantalum-columbium heat shield packs on six sides (Fig. 162). The test loads were applied through the upper and lower shield packs by water-cooled stainless steel load rods. These rods are vacuum-sealed by stainless steel bellows and each is capable of a ± 1-in. displacement from the neutral position. The external end of the bottom rod was attached to the movable loading head of the test machine, and the upper rod was attached to the fixed cross beam of the test machine. Special tungsten rod end fittings were used for the transition from ambient to elevated temperature zones.

The facing creep tests were performed in a high temperature vacuum furnace located on an arcweld creep rack (Fig. 163). This furnace is capable of attaining 4000° F at a vacuum of 5×10^{-5} torr. Radiant heat is supplied to the specimen by two curved tantalum elements. The creep rack employs a 20:1 mechanical advantage for indirect loading of

MATERIAL Columbium alloy, D-36
PANEL NO. 3
TYPE OF TEST Hot gas curved heat shield
MAX TEST TEMP (AVG) 2520° F
TIME ABOVE 2200° F 690 sec
TEST ANGLE 30 deg
DYNAMIC PRESSURE 370 psf

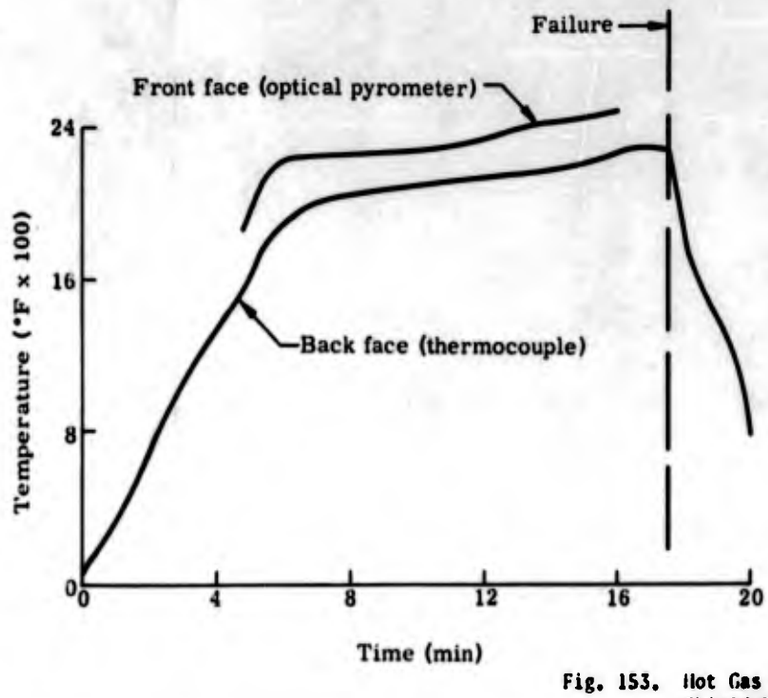

Fig. 153. Hot Gas Test, D-36
Shield Panel No. 3

MATERIAL Columbium alloy, D-36
PANEL NO. 4
TYPE OF TEST Hot gas curved heat shield
MAX TEST TEMP (AVG) 2525° F
TIME ABOVE 2400° F 390 sec
TEST ANGLE 30 deg
DYNAMIC PRESSURE 370 psf

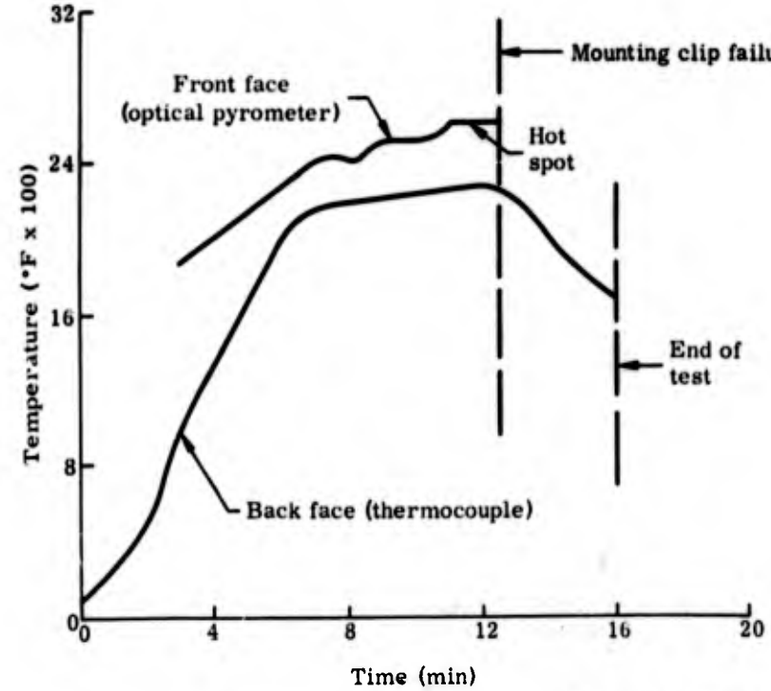

Fig. 154. Hot Gas Test, D-36
Shield Panel No. 4

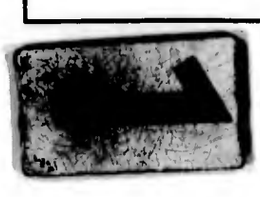

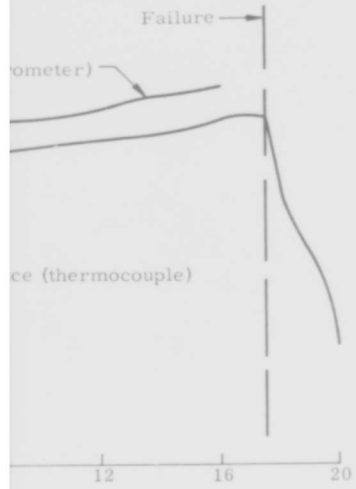

Fig. 153. Hot Gas Test, D-36 Curved Heat Shield Panel No. 3

DESCRIPTION OF PANEL FAILURE
After eleven minutes, upper right attachment failed at the back face. Resultant load redistribution caused overloading and subsequent failure of lower attachment leg test bolts (stainless steel). Resultant deflection caused upper portion of panel to protrude into gas stream.

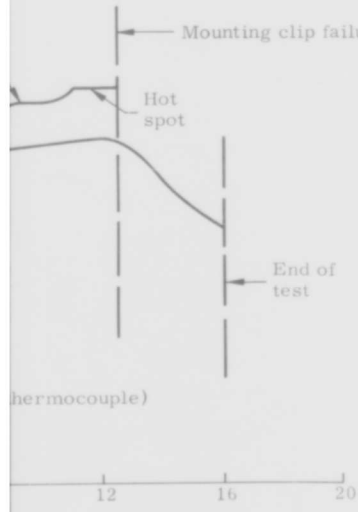

Fig. 154. Hot Gas Test, D-36 Curved Heat Shield Panel No. 4

DESCRIPTION OF PANEL FAILURE
Upper right attachment failed at 12 minutes and a hole developed in that area. Resultant redistribution of loading caused lower attachment clips to crush core. Added deflection caused upper LH corner (intersection of stepped edges) to protrude into gas stream.

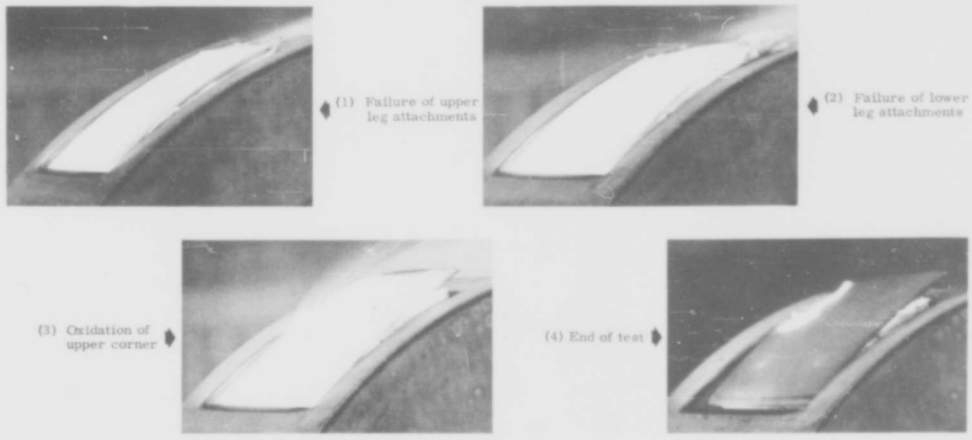

Fig. 155. Curved B-36 Columbium Heat Shield Panel No. 3 Failure Sequence

the specimen. Calibrated weights were used to apply precise constant loads to the specimen.

Tungsten test fixtures were fabricated for the honeycomb core properties tests. These fixtures were designed so that the appropriate mode of failure could be obtained from the core specimens. Various modifications to the fixtures were accomplished as a result of the preliminary tests and some of the initial tests. (Details describing these modifications are described under Subsection 4, Test Procedures.) Figures 164 through 167 depict the final test setups for the three honeycomb specimen test conditions: shear, column compression and flatwise compression. The core shear (flexure) fixtures included two sets of simple beam supports (one with an 8-in. span and one with a 4-in. span). The column compression fixtures included specimen edge support members to prevent crushing of the specimen edges. Rocker pads were also used to ensure the proper alignment of the load in relation to the specimen. All of the appropriate fixture surfaces for the three setups were machined flat and parallel for proper loading alignment (e.g., compression block upper and lower surfaces, compression table upper and hole bottom surfaces).

2. Instrumentation

The major effort in this area was expended on deflection measuring devices for the core properties and facing tensile tests. For the core properties tests, the deflections of the specimens were obtained by measuring the head motion of the test machine with a deflectometer. This method was used because of its simplicity and reliability, since all of the measuring equipment was located external to the furnace, thereby eliminating any vacuum and temperature effects on the measuring sensor. Also, because the test loads were relatively small and the test machine and fixtures were large and structurally stiff, the deflection in the system was negligible. The movement of the machine head was checked with both deflection dial gages and the deflectometer during the preliminary tests, and the results of both measuring devices compared extremely well with one another.

The measuring system for the tensile ultimate and yield tests was much more complex than that used for the core properties tests. Head motion could not be used for these tests since the gage length of the specimen must be known to obtain strain. Consequently, an optical measuring system was used to determine the specimen deflections (Fig. 168). The primary components of this system were tantalum slide rule gages, tantalum and Inconel gage clamps (tantalum clamps became unusable after the first temperature test due to the bonding of the holding screws), a bifilar telemicroscope and two 16-mm movie cameras. The system was operated by sighting on the slide rule gage (scribed every 0.020 in.), located on the specimen, through the furnace sight port with the bifilar telemicroscope. One 16-mm movie camera, located at the eyeglass end of the telemicroscope was used to record the rela-

MATERIAL Columbium alloy, D-36
PANEL NO. 2
TYPE OF TEST Hot gas curved heat shield
MAX TEST TEMP (AVG) 2260° F
TIME AT MAX TEMP 300 sec
TEST ANGLE 30 deg
DYNAMIC PRESSURE 144 psf

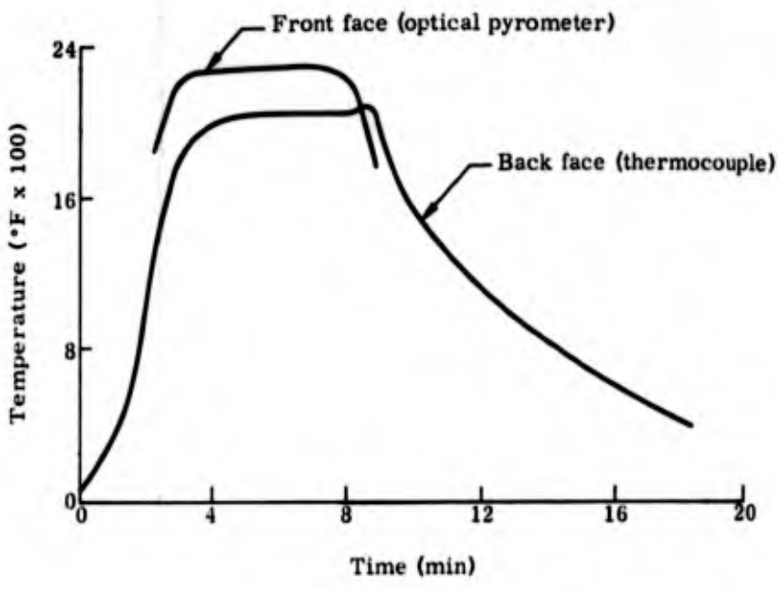

Fig. 156. Hot Gas Test, D-36
Shield Panel No. 2

MATERIAL Columbium alloy, D-36
PANEL NO. 5
TYPE OF TEST Hot gas flat heat shield
MAX TEST TEMP (AVG) 2270° F
TIME AT MAX TEMP 840 sec
TEST ANGLE 30 deg
DYNAMIC PRESSURE 144 psf

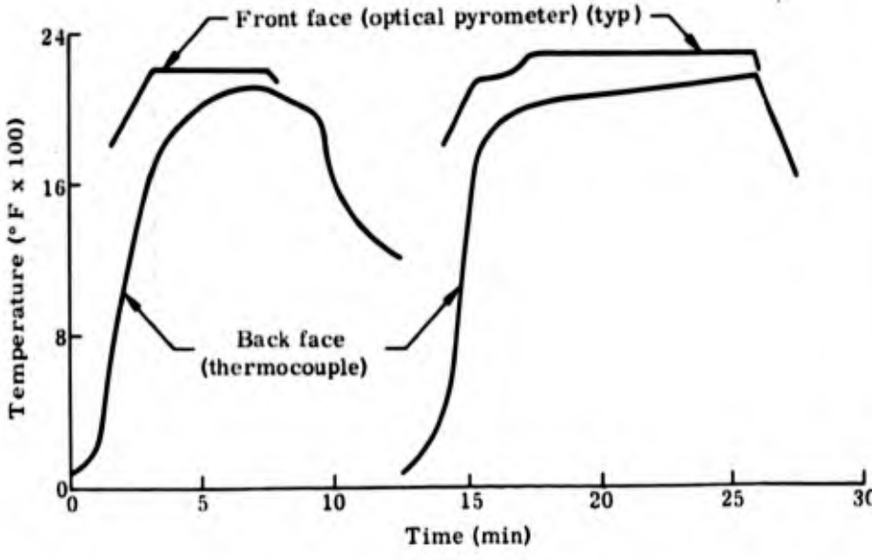

Fig. 157. Hot Gas Test, D-36 F
Panel No. 5

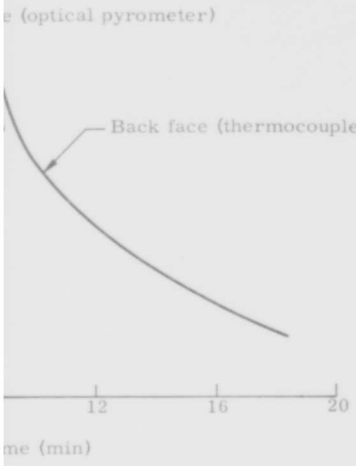

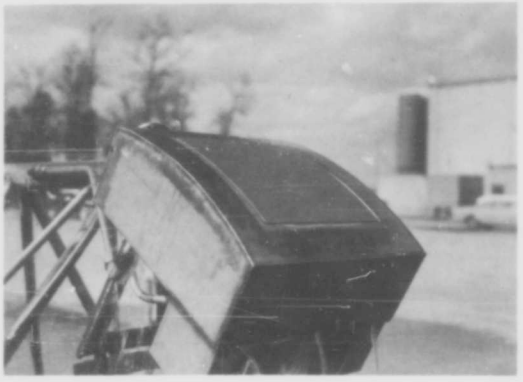

Fig. 156. Hot Gas Test, D-36 Curved Heat Shield Panel No. 2

DESCRIPTION OF PANEL FAILURE
No panel failure. Slight separations of the weld patches at the back face attachment points.

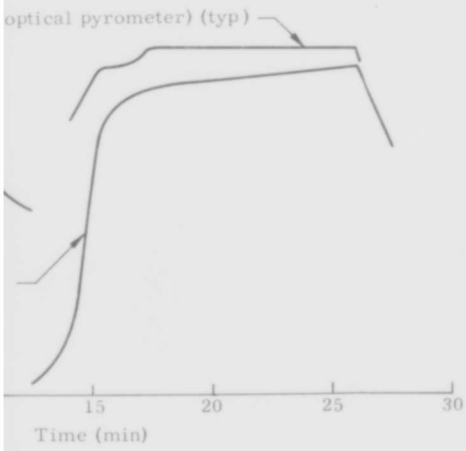

Fig. 157. Hot Gas Test, D-36 Flat Heat Shield Panel No. 5

DESCRIPTION OF PANEL FAILURE
No visible damage after one cycle. Slight separation of the upper left attachment patch after second cycle.

MATERIAL Columbium alloy, D-36
PANEL NO. 5
TYPE OF TEST Hot gas curved heat shield
MAX TEST TEMP (AVG) 2440° F
TIME AT MAX TEMP 1000 sec
TEST ANGLE 90 deg
DYNAMIC PRESSURE 250 psf

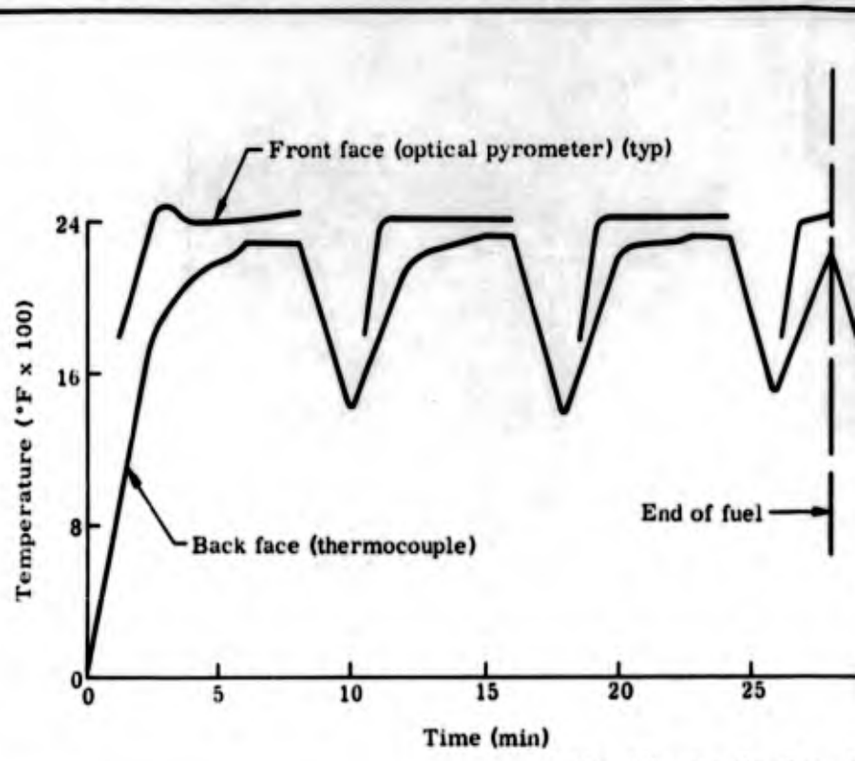

Fig. 158. Hot Gas Test, D
Shield Panel No

MATERIAL Columbium alloy, D-36
PANEL NO. 6
TYPE OF TEST Hot gas curved heat shield
MAX TEST TEMP (AVG) 2250° F
TIME ABOVE 2000° F 1320 sec
TEST ANGLE 90 deg
DYNAMIC PRESSURE 144 psf

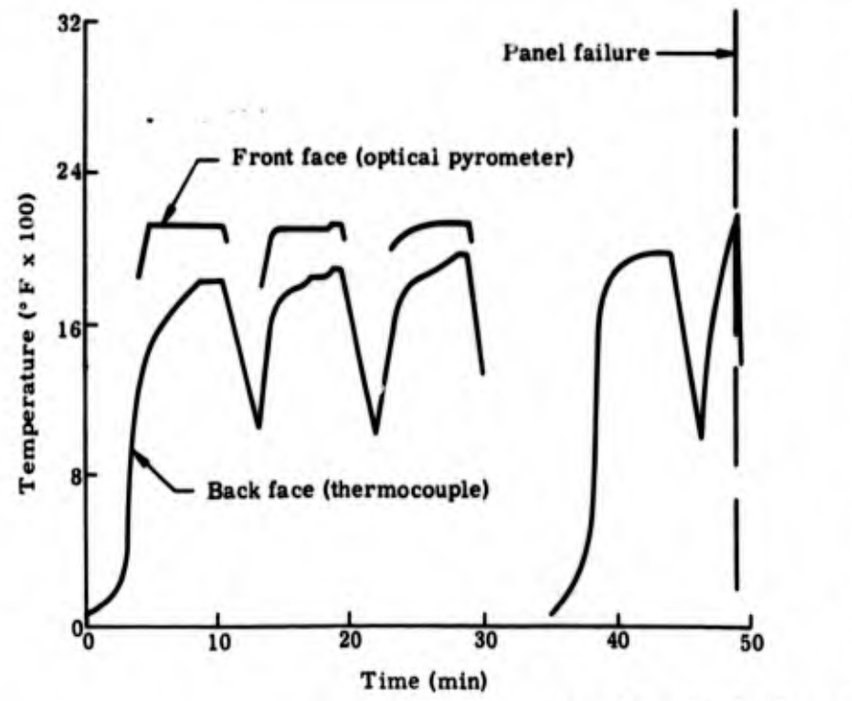

Fig. 159. Hot Gas Test, D
Shield Panel No

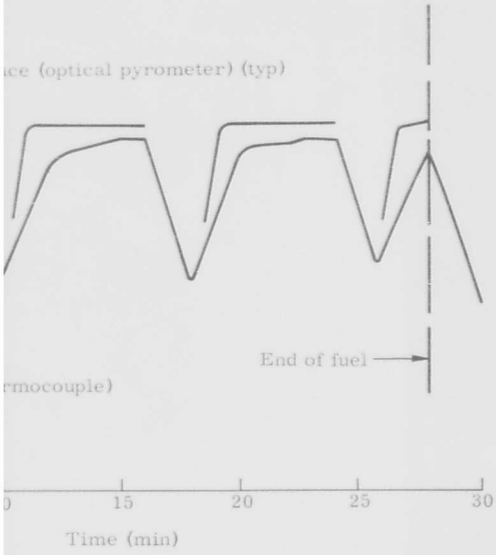

Fig. 158. Hot Gas Test, D-36 Curved Heat Shield Panel No. 5

DESCRIPTION OF PANEL FAILURE
Small surface cracks at upper left corner. Minor separation of attachment patches at upper right and lower left locations.

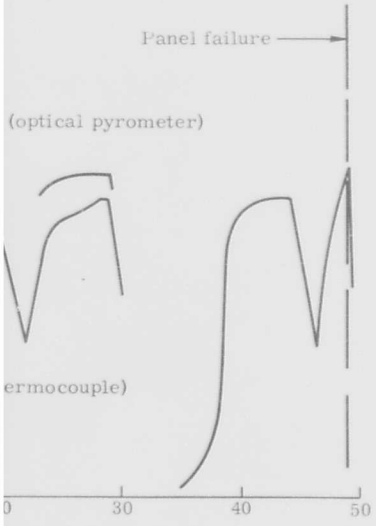

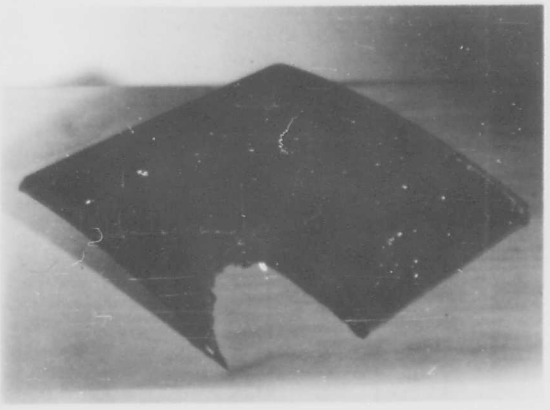

Fig. 159. Hot Gas Test, D-36 Curved Heat Shield Panel No. 6

DESCRIPTION OF PANEL FAILURE
Slight separation of upper right surface patch after three cycles. Failure of upper right surface patch during fifth cycle created local stagnation at the upper right corner which caused coating failure and subsequent severe oxidation of the exposed columbium.

MATERIAL Columbium alloy, D-36
PANEL NO. 11
TYPE OF TEST Radiant heat test of heat shield panel
MAX TEST TEMP 2600° F
TIME AT MAX TEMP 300 sec
FAILING LOAD
ULT STRESS
RENE JIG TEMP

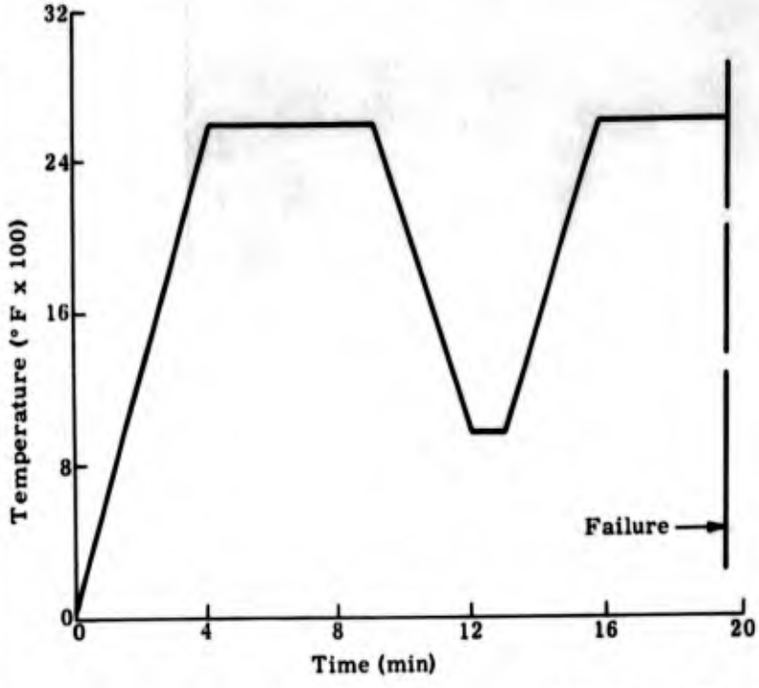

Fig. 160. Radiant Heat Test, D
Panel No. 11

MATERIAL Columbium alloy, D-36
PANEL NO. 4
TYPE OF TEST Radiant heat test of heat shield panel
MAX TEST TEMP 2400° F
TIME AT MAX TEMP 1800 sec
FAILING LOAD
ULT STRESS
RENÉ JIG TEMP

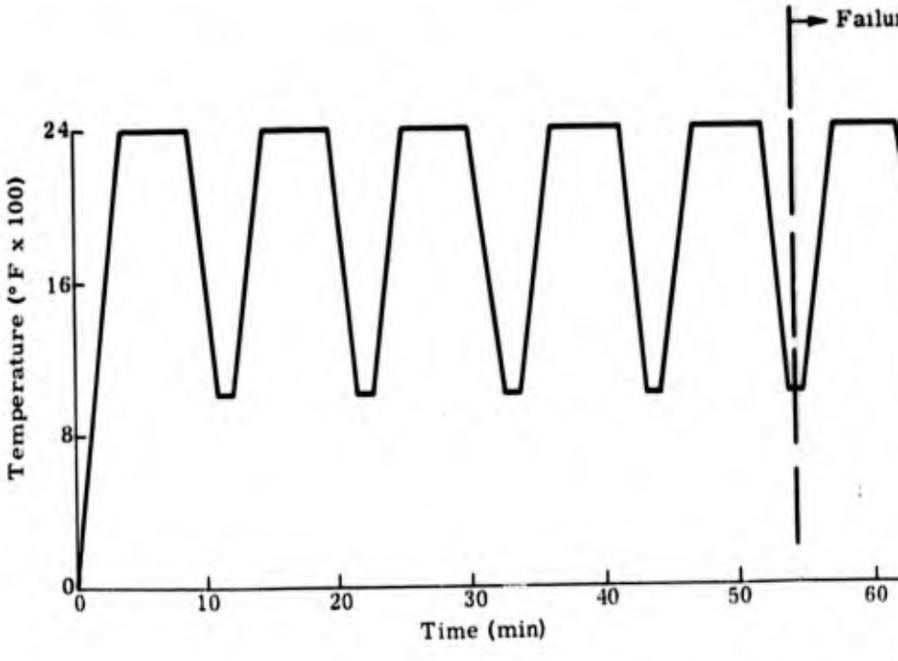

Fig. 161. Radiant Heat Test,
Panel No. 4

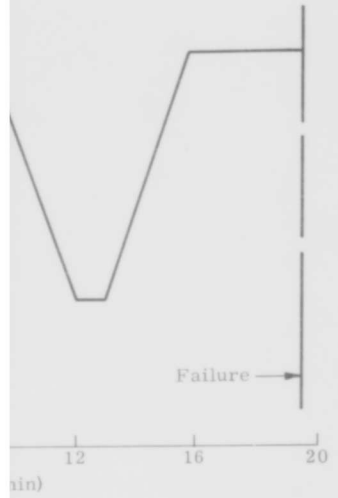

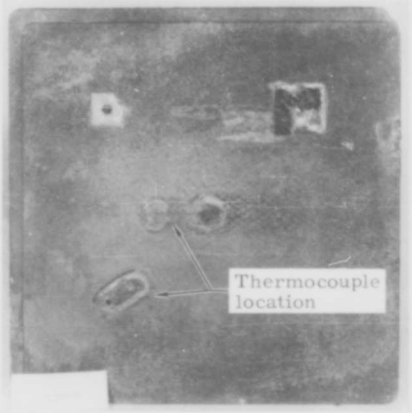

Fig. 160. Radiant Heat Test, D-36 Heat Shield Panel No. 11

DESCRIPTION OF PANEL FAILURE
Front face doubler at attachment clip access hole failed. Skin and core underneath doubler oxidized.

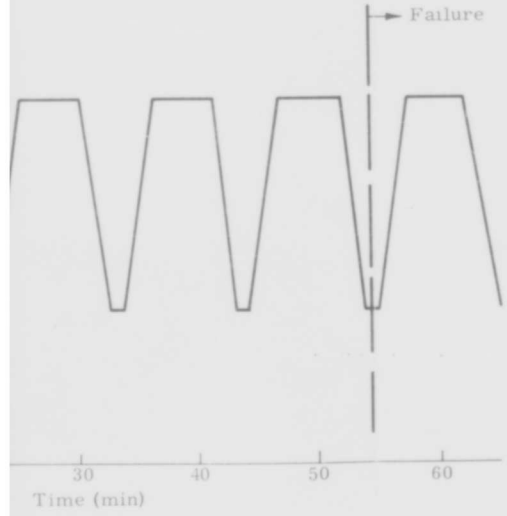

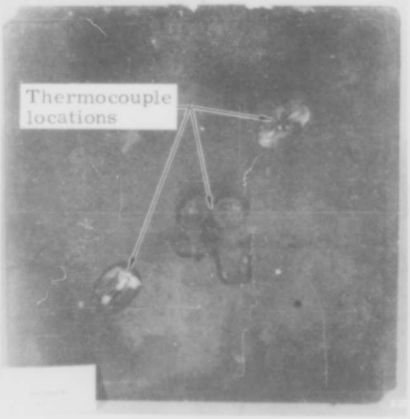

Fig. 161. Radiant Heat Test, D-36 Heat Shield Panel No. 4

DESCRIPTION OF PANEL FAILURE
Panel failed by oxidizing along edge where pans were joined by electron beam welding.

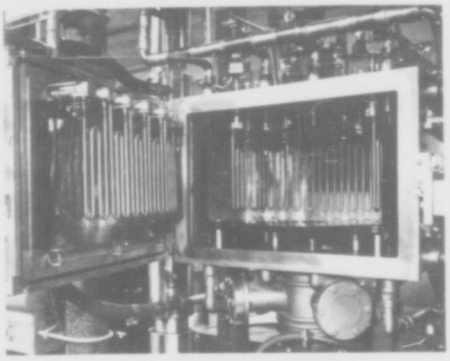

Fig. 162. High Temperature Vacuum Test Furnace

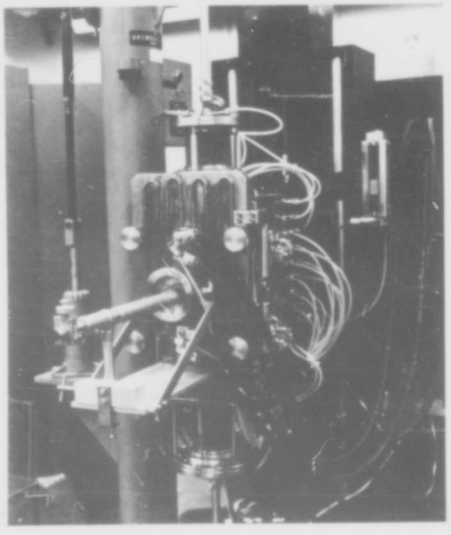

Fig. 163. High Temperature Vacuum Test Furnace--Creep Rack Test Arrangement

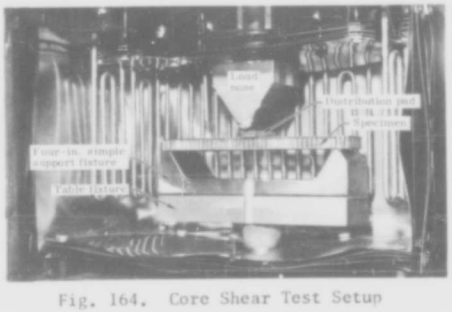

Fig. 164. Core Shear Test Setup

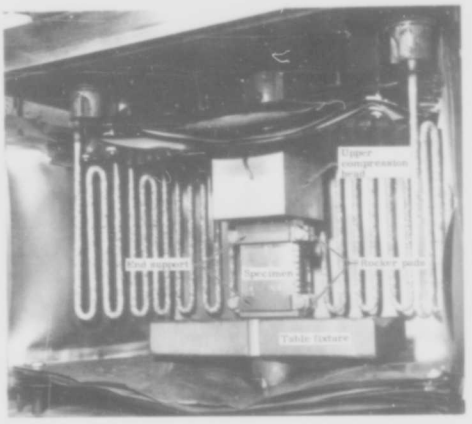

Fig. 165. Column Compression Test Setup

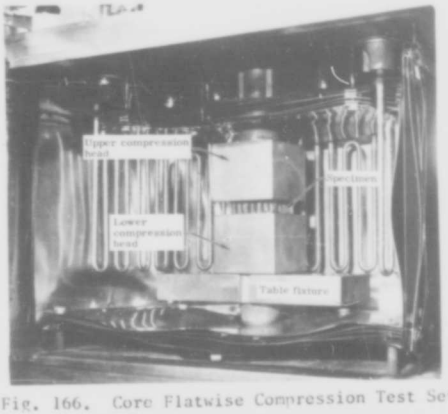

Fig. 166. Core Flatwise Compression Test Setup

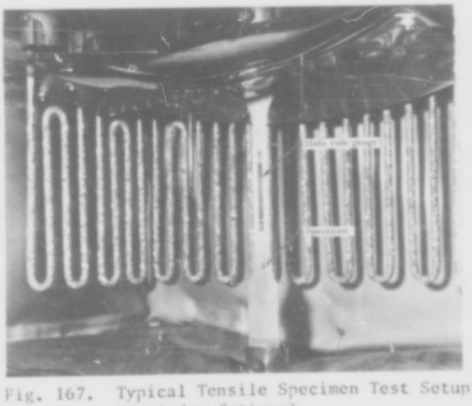

Fig. 167. Typical Tensile Specimen Test Setup (includes fatigue)

Fig. 168. Tensile Specimen Deflection Measuring System

tive displacements of the slides of the slide rule gage, while the other camera was used to record the needle movement of the test machine load dial (Fig. 169). These two cameras were synchronized with a timer so that the two readings were obtained at the same time. The two processed films were read frame by frame on a microfilm reader. The types of lenses and films for the various temperature levels were obtained from ASD TR 61-74 (Ref. 38).

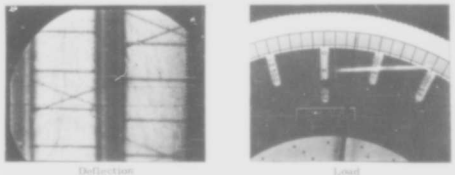

Fig. 169. Tensile Deflection--Load Optical Measurements

The specimen temperatures were obtained by using an optical pyrometer. The temperature readings were taken through the furnace sight port. An emissivity of unity was used since black body conditions prevailed (hole in an enclosed box).

The facing creep test deflections were determined by measuring the upper bellows flange movement with a deflectometer. Calibration tests were performed at elevated temperature with an optical system similar to the one previously described for the tensile ultimate tests. These tests proved the accuracy and reliability of the mechanical measuring system. The deflectometer output signal was automatically recorded on a Bristol chart recorder. The test temperature was obtained with a Pt;Pt-Rh (13%) thermocouple placed next to the specimen.

3. Specimen Preparation

The core properties specimens were obtained by cutting the unfailed portions of the tested structural panels (both materials) into the appropriate sizes (Fig. 170). Initially, a conventional friction band saw was used to cut the D-36 specimens. However, this

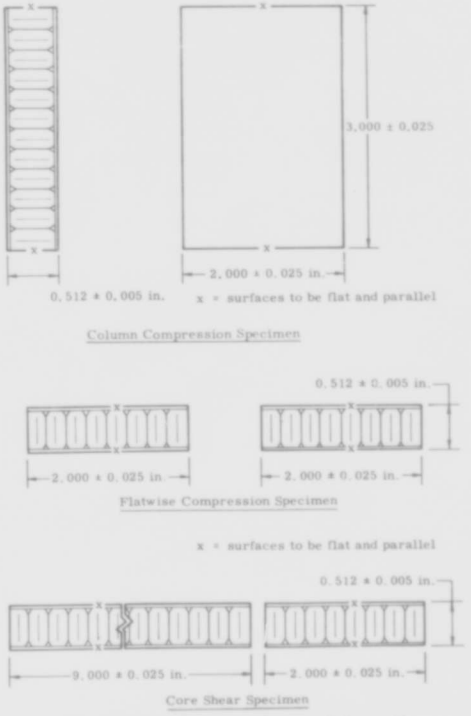

Fig. 170. Column Compression and Core Properties Specimen Configurations

operation damaged the core. A friction rubber wheel cutter was tried and proved to be successful for rough cutting the specimens (both materials). The specimens were then finished by grinding with an alumina (Al_2O_3) cup-wheel. Each of the specimens was tested at the same temperature as the panel from which it was obtained.

The tension specimens were fabricated in a manner that would reflect possible changes in strength due to the manufacturing processes used in making the structural and heat shield panels. Basically, three different specimens of each material were made:

Specimen Configuration	Panel Condition
Bare	As-received material
Brazed laminate	Panel after brazing
Coated brazed laminate	Panel after coating

All of these specimens had the same basic geometric dimensions (except for thickness). The laminates were fabricated by brazing two bare panel facing sheets together and then cutting out the specimens (Fig. 171). The coated specimens were fabricated in the same manner as the brazed laminates and then treated with the appropriate oxidation protective coating process (Cr-Ti-Si for D-36 and PFR-6 for TZM).

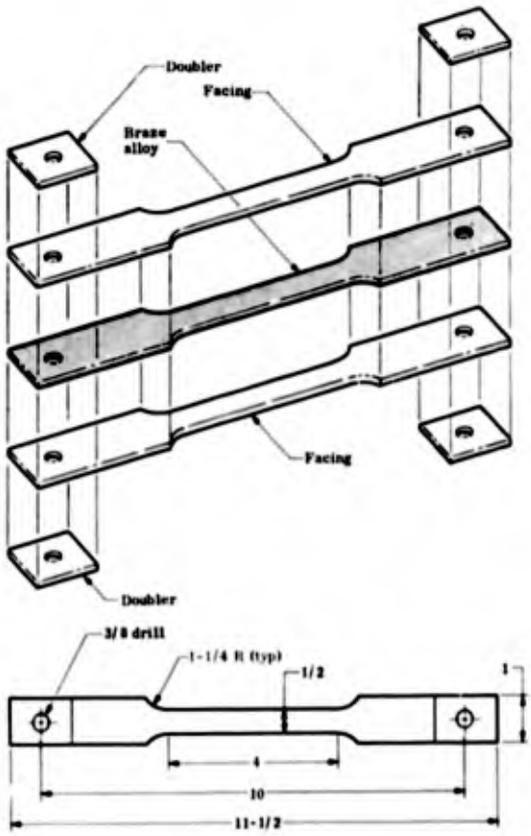

Fig. 171. Tensile Specimen Laminate for Small Specimen Tests

4. Test Procedures

In general, the small specimen tests were performed according to the following procedure:

(1) With the specimen properly mounted in the furnace, the chamber was pumped down to a pressure level of 10^{-5} to 10^{-6} torr.

(2) Power was applied to the elements and the chamber heated to the proper test temperature (chamber temperature was determined by a W-5Re versus W-26Re thermocouple).

(3) The test specimen was allowed to reach the test temperature, as determined by an optical pyrometer.

(4) The test load was applied at the prescribed rate (1000 psi/sec for all ultimate tests and 16 to 20 cycles/min for the fatigue tests) to the appropriate level.

(5) The specimen was cooled.

During the tests, several problems occurred that required changes in the load fixtures and/or methods of data acquisition.

During the column compression tests, several specimens exhibited premature end failures instead of the desired local instability failures. End failures occur when the braze or core strength at the ends of the specimen is not sufficient to withstand the local stress concentrations during load introduction. This problem was aggravated by improper machining or misalignment of the test specimens. To minimize these conditions, molybdenum end support members and rocker pads were used. An improper loading condition was created in the initial core shear tests by the small radius of the loading nose. Instead of failing the core in shear, the loading nose crushed the core at the contact line between the nose and the specimen facing. This situation was rectified by placing a 0.375-in. thick molybdenum plate between the loading nose and the specimen to distribute the test load.

During the tensile ultimate tests, the technique used for attaching the slide rule gages to the tension specimens caused premature failures. Initially, tantalum gage clamps were used but these proved to be unsatisfactory (see Subsection 2, Instrumentation). When using the Inconel gage blocks (for the lower temperature tests below 2000° F), the specimens usually failed at the gage clamp instead of between the clamps. Tack welding the gage to the specimen was also tried, but again, the failure occurred at the weld. Also, difficulty was encountered in welding the gages to the molybdenum specimens. No completely satisfactory method was obtained to attach the slide rule gages to the tensile specimens. Consequently, a two-stage procedure was established to obtain the desired test information. This consisted of instrumenting one set of specimens with slide rule gages and obtaining the modulus data; an identical set of specimens without the gages was tested for ultimate strength and percentage of elongation.

5. Test Results

The results of the D-36 and TZM core properties tests are presented in Chapter VIII, Section B. The following formulas were used to calculate the stresses and moduli:

Core shear:

$$F_s = P/b(h + c)$$

where

F_s = core shear strength (psi)

P = applied test load (lb)

b = width of specimen (in.)

h = specimen depth, uncoated (in.)

c = core depth (in.)

$$G_c = \frac{L_1}{4 A_c} \left[r_\ell^2 - 1\right] \left\{ \frac{1}{\frac{r_\ell^3}{(P/\Delta)_\ell} - \frac{1}{(P/\Delta)_{L_1}}} \right\}$$

where

G_c = modulus of rigidity (psi)

L_1 = length of longer span (in.)

ℓ = length of shorter span (in.)

$$A_c = b\left(\frac{t_f + t_c}{2}\right)$$

t_f = specimen facing thickness, uncoated (in.)

t_c = specimen core thickness (in.)

$r_\ell = L_1/\ell$

$(P/\Delta)_\ell$ = straight line slope of short span load deflection curve (lb/in.)

$(P/\Delta)_{L_1}$ = straight line slope of long span load deflection curve (lb/in.)

Column compression:

$$F_c = \frac{P}{2b\,(t_f + t_b)}$$

where

F_c = facing compression strength (psi)

t_b = braze alloy thickness (in.)

Flatwise compression:

$$F_G = P/bd$$

where

F_G = core compression strength (psi)

d = length of specimen (in.)

b = width of specimen (in.)

E_c = slope of stress-strain curve

where

E_c = core flatwise compression modulus (psi).

The results of the facing tensile tests are presented in Section VIII, Subsection B. The following formulas were used to calculate the stresses and moduli:

Facing tension:

Tension ultimate

$$F_t = P/A$$

where

F_t = tensile strength (psi)

$A = bt$

t = specimen thickness, uncoated (in.)

E = slope of stress-strain curve

where

E = Young's modulus (psi).

Typical specimen failures are shown in Figs. 172 through 174. In general, the specimens exhibited the following types of failures:

Specimen Configuration	Type of Failure
D-36 core shear	Shear failure
TZM core shear	Braze failure
D-36 column compression	Face wrinkling; intercellular dimpling (at higher temperatures); end and edge failures
TZM column compression	Braze failure
D-36 flatwise compression	Core wall buckling
TZM flatwise compression	Core wall buckling and fracturing
D-36 and TZM ultimate tension	Tension fracture
D-36 and TZM fatigue	Tension fracture; extreme elongation (at higher temperatures)
D-36 and TZM creep	Tension fracture; extreme elongation (at higher temperatures)

Fig. 172. Typical Specimen Failures--D-36 Columbium

Fig. 173. Typical Specimen Failures--TZM Molybdenum

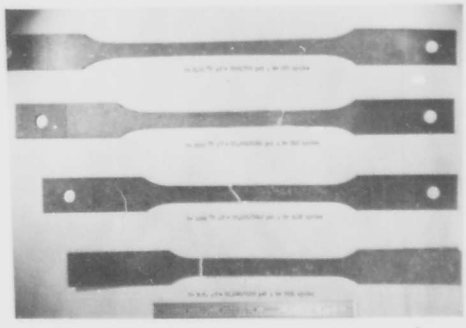

Fig. 174. D-36 Alloy Tensile Coupons

VII. ANALYSIS OF TEST RESULTS AND DESIGN PROCEDURES

A. DISCUSSION OF TEST RESULTS

1. D-36 Columbium

a. Structural panels

In the full panel test, it was necessary to use a servo-controlled hydraulic system to apply load to the panel. The deficiency of this arrangement was that the load application was dependent upon time alone and not upon deflection. This presents no problem as long as the test panel stresses were in the elastic range, but, when the panel started to yield or fail, the load application still continued. A dump switch was used to relieve the hydraulic pressure at a preset panel deformation to prevent this system follow-through from completely destroying a panel. The cutoff deformation selected was such that the panel stresses would be far into the plastic range before the test was stopped. Once the proper limiting deformation was selected, the test setup worked satisfactorily. All panels had failures when the deformation control had stopped the load application. Some of the failures were extended further than others. On this basis, some of the panel ultimate failing stresses might have been higher than others. However, the difference is considered small because, in the plastic region, the stress-strain curve is flat and a small difference in total strain makes an even smaller difference in applied stress. It is felt, therefore, that the maximum test loads are within 5% of ultimate.

The D-36 structural panel test results (Figs. 126 through 145) were uniform and consistent (Fig. 175). The panel strengths were in all cases higher than those predicted in the preliminary design effort of the program (Chapter IV). One of the purposes of this portion of the program was to determine why this occurred. The following sections review the facts and present conclusions concerning the causes of the conservative predictions.

The panel shear strengths were a consistently high percentage of the ultimate tensile strength, from 86.2% at room temperature to 100% at 2400° F. The failures of the shear test panels had to be classed a local instability, although they might be classed an ultimate material failure, since the failing stress was so far in the plastic

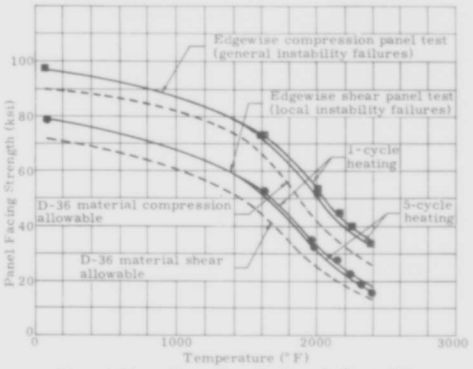

Fig. 175. Structural Panel Test Data

range. Also, some of the panels were as much as 5° out of square (because of the plastic deformation) before any failure occurred. Most of the panels had an intergranular tension failure in the tension corner.

In the room temperature shear test of the D-36 panel, failure occurred in a most unusual manner (Fig. 176), with the oxidation protective coating spalling off in a series of parallel lines across the panel. The uniformity of the spalling provided an excellent indication of the uniformity of stress distri-

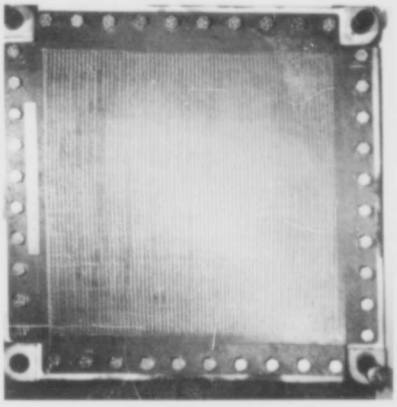

Fig. 176. Room Temperature D-36 Columbium Shear Test Panel Showing Lines Where Coating Spalled

bution in the panel. The orientation of the core ribbon direction provides an explanation as to why the coating spalled in the specific direction observed. The lines are perpendicular to the core ribbon direction and run along the core node attachment area. This is explained by considering two free body areas, one along the node area and the other along the cell-wall area, and then comparing the strength of the two.

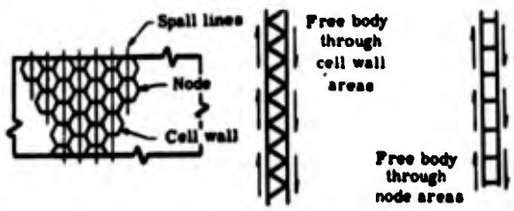

As can be seen from the free body diagram through the node areas, the straight nodes can rotate with a minimum of resistance, while the truss effect of the cell walls provides considerable resistance in the cell-wall area. The truss of the core actually carries part of the shear load, thereby causing initial yielding in the core node area.

The compression test panels failed in general instability in the plastic range. At the higher temperatures (2400° F) the panels deformed into a plastic bow, while at the lower temperatures the panels had a characteristic shear crimp. The compression panel consistently failed at a stress level higher than the ultimate tensile strength of the facing material. The facings were stressed far into the plastic range at the time of failure and some of the high temperature test panels had some intercellular dimpling.

Shear and compression tests were performed on panels which were subjected to a thermal gradient. In one set (shear test panel No. 7 and compression test panel No. 8) one face was held at 2400° F and the other face at 2200° F. In the other set (shear test panel No. 11 and compression test panel No. 7) one face was held at 2400° F and the other at 2000° F. This resulted in a 200° and a 400° F gradient on the panel during test. The panel failing stresses are plotted in Fig. 175 at the average temperature of the two faces. The gradient panel failing stresses fit precisely on the curve through the nongradient panel test data. It is concluded that the thermal stresses caused by these temperature differences did not affect the ultimate strength of the test panels. The thermal gradients in both the compression and shear test panels cause a convex deflection of the panel toward the hotter face. The initial thermal deflection evidently did not reduce the critical instability stresses, even though the compression panels failed in general instability in the plastic region.

The ultimate strengths from the D-36 columbium panel tests represent the maximum that these panels could withstand. A shear and a compression panel were evaluated in a cyclic load and heating test (Figs. 134 and 138). Since no particular vehicle load-time-temperature requirements were available, the ones utilized in these tests were arbitrarily chosen. The applied loads were selected at a level where structural failure of the panel was considered improbable. However, during the ninth loading cycle, a structural failure of the shear panel did occur. A special analysis was conducted to determine why the panel failed when the applied stresses were only a small percentage of the ultimate strength.

Considering the stresses induced by the temperature differential between the dissimilar jig and panel materials:

$$\Delta T = T_{jig} - T_{panel} \tag{11}$$

$$e_p = \alpha_p a (T_{2p} - T_1) \tag{12}$$

$$e_j = \alpha_j a (T_{2j} - T_1)$$

$$e = e_j - e_p = a (\alpha_j T_{2j} - \alpha_p T_{2p}) - T_1 a (\alpha_j - \alpha_p) \tag{13}$$

where subscripts j and p refer to jig and plate, and 1 and 2 refer to initial and terminal times, respectively (Fig. 177). The rigid body translation stresses of jig and plate are given by

$$\sigma_y = \sigma_x = \frac{eE'}{a(1-\mu)} = \frac{E'}{1-\mu} \left[(\alpha_j T_{2j} - \alpha_p T_{2p}) - T_1 (\alpha_j - \alpha_p) \right] \tag{14}$$

which gives a biaxial stress condition throughout the plate. Since the jig is obviously not infinitely rigid, we must consider the effect of its bending in our determination of stresses throughout the panel.

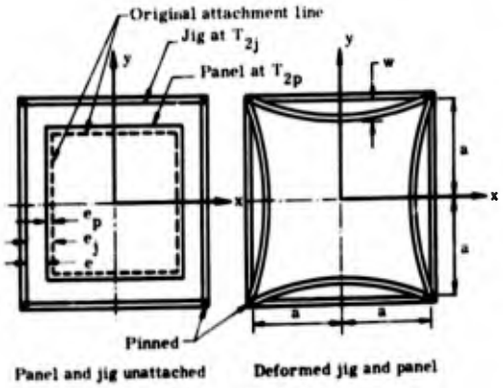

Fig. 177. Panel and Jig

By representing the deflection at the boundary due to bending by the Fourier series

$$\omega = \sum_{n=1,3,5,\ldots}^{\infty} a_n \cos \frac{n\pi x}{2a} \qquad (15)$$

and by prescribing the boundary stresses as

$$x = \pm a;\ \sigma_x = \frac{ke_x}{2t},\ \tau_{xy} = 0$$
$$y = \pm a;\ \sigma_y = \frac{ke_y}{2t},\ \tau_{yx} = 0 \qquad (16)$$

where

$$K = \frac{2E't}{a} \text{ (spring constant of plate)}$$

we may utilize Castigliano's Second Theorem of Least Work ($\delta U = 0$) to find the stresses in the panel due to jig bending. The strain energy in plates is given by

$$U = \frac{1}{2E} \iint_A \left\{ \sigma_x^2 + \sigma_y^2 - 2\mu\, \sigma_x \sigma_y + 2(1+\mu)\, \tau_{xy}^2 \right\} dx\, dy \qquad (17)$$

Converting to stress function form (assuming $\mu = 0$)

$$U = \frac{1}{2E} \iint_A \left\{ \left(\frac{\partial^2 \phi}{\partial y^2}\right)^2 + \left(\frac{\partial^2 \phi}{\partial x^2}\right)^2 + 2\left(\frac{\partial^2 \phi}{\partial x \partial y}\right)^2 \right\} dx\, dy \qquad (18)$$

where

$$\sigma_y = \frac{\partial^2 \phi}{\partial x^2};\ \sigma_x = \frac{\partial^2 \phi}{\partial y^2};\ \tau_{xy} = -\frac{\partial^2 \phi}{\partial x \partial y} \qquad (19)$$

The stress function ϕ must satisfy the prescribed boundary conditions (it already satisfies the equilibrium and compatibility equations).

$$\phi = \phi_0 + \sum_{i=1,2\ldots}^{\infty} C_i \phi_i \text{ or} \qquad (20)$$

taking the first constant

$$\phi = \int_P \int \int (F_1(y)\, dy)dy + \int_P \int \int (F_2(x)\, dx)dx + (x^2 - a^2)^2 (y^2 - a^2)^2 C_1 \qquad (21)$$

Substituting into Eq (19) and using the appropriate boundary conditions

$$\phi = \frac{k}{2t} \int\int (e_x dy)\, dy + \frac{k}{2t} \int\int (e_y dy)dy + (x^2 - a^2)^2 (y^2 - a^2)^2 C_1 \qquad (22)$$

where

$$e_y = \frac{q}{k} - \frac{(EI)_j}{k} \frac{d^4 \omega}{dx^4}$$

$$e_x = \frac{q}{k} - \frac{(EI)_j}{k} \frac{d^4 \omega}{dy^4}$$

but

$$q = k\omega \qquad (23)$$

making Eq (22)

$$\phi = \frac{an}{2t} \left[(EI)_j \left(\frac{n\pi}{2a}\right)^2 - k\left(\frac{2a}{n\pi}\right)^2 \right] \left[\cos \frac{n\pi x}{2a} + \cos \frac{n\pi y}{2a} \right] + (x^2 - a^2)^2 (y^2 - a^2)^2 C_1 \qquad (24)$$

Now performing $\frac{\partial U}{\partial C_1} = 0$, we find C_1

and from Eqs (14) and (19)

$$\sigma_y = \frac{eE'}{a(1-\mu)} + \frac{eE'\pi}{8(1-\mu)(EI)_j}\left[(EI)_j \frac{\pi^2}{4a^2} - E' t_f \frac{4a}{\pi^2}\right] \cdot \left[\frac{\pi a}{4}\cos\frac{\pi x}{2a} + \frac{1}{2a^5}(3x^2 - a^2)(y^2 - a^2)^2\right] \quad (25)$$

$$\sigma_x = \frac{eE'}{a(1-\mu)} + \frac{eE'\pi}{8(1-\mu)(EI)_j}\left[(EI)_j \frac{\pi^2}{4a^2} - E' t_f \frac{4a}{\pi^2}\right] \cdot \left[\frac{\pi a}{4}\cos\frac{\pi y}{2a} + \frac{1}{2a^5}(3y^2 - a^2)(x^2 - a^2)^2\right] \quad (26)$$

$$\tau_{xy} = \frac{\pi eE'}{4a^5(1-\mu)(EI)_j} xy(x^2 - a^2)(y^2 - a^2)\left[(EI)_j \frac{\pi^2}{4a^2} - \frac{4t_f a E'}{\pi^2}\right] \quad (27)$$

where the first term of the Fourier series is

$$a_1 = \frac{t_f eE' a^3}{4(1-\mu)(EI)_j}$$

which is the deflection due to bending of the center of the jig.

A point was chosen in the load-time-temperature history of the shear panel in question and the principal stresses calculated using the above formulas. Since the derivation considered an idealized temperature distribution and assumed thermally induced shear along panel edges to be zero, accuracy to the first Fourier and stress function coefficient was deemed sufficient. To obtain a more accurate solution, continuous principal stress histories at each point would be required, utilizing a more complete array of stress-strain curves.

Specifically, stresses were calculated in shear panel No. 12 at its point of failure (during its 9th load cycle or at the end of its 8th temperature cycle, t = 62 min). Resulting stress trajectories (Fig. 178) bear out that the panel was subjected to stresses much higher than the applied shear stresses. The failed panel had excessive permanent deformation in the corner and central regions as the stress contours would indicate; deformation of the jig showed that it indeed played an important part in causing stress concentrations in the heated panel. The conclusion is that thermal deformations induced a plastic condition in the panel while the mechanical shear load progressively deformed and failed it.

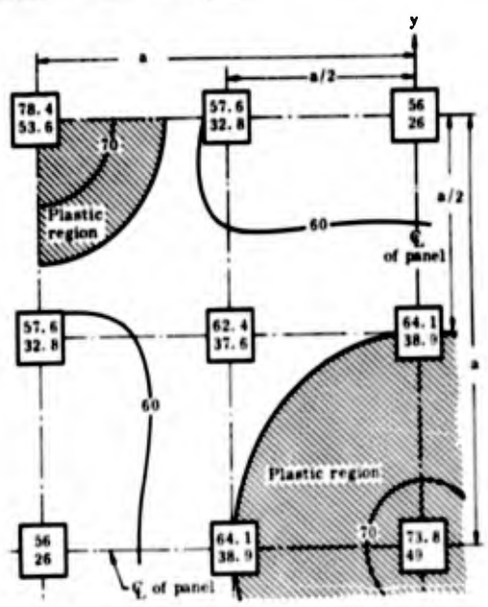

Fig. 178. Principal Stress Trajectories for Quarter Panel

Although the situation was not similarly analyzed, it is considered that the same conditions caused failure of the cyclic-load and temperature compression test panel (Fig. 138).

b. Heat shield panels

During the heat shield tests (Figs. 151 through 154 and 156 through 159) in the hot gas facility, the panels were subjected to a dynamic environment simulating that encountered during atmospheric re-entry. To

be able to test the panel at the highest temperature possible in the facility, it was necessary to allow the dynamic pressure to increase to a level higher than the design capabilities of the panels. This was necessary because the facility temperature capabilities are directly proportional to the dynamic pressure. During a 2550° to 2600° F panel test (Flat D-36 heat shield No. 7), the adverse pressure caused a lower edge of the panel to protrude above the panel holder. This protrusion created a turbulent area in the boundary layer, resulting in increased heat transfer in the area. The local temperature increased to above 2800° F and, after two minutes at this temperature, the coating failed, resulting in a catastrophic failure of the panel. A set of four pictures showing the progression of this failure is shown in Fig. 179. Once the panel coating failed, half the panel was gone in 4 to 8 seconds.

During all of the heat shield tests, hot spots or tails were observed streaming from the access tube holes. These tails were about 100° to 200° F hotter than the remainder of the panel. In some of the other panels, the outer face sealing details also caused hot spots to appear on the panel facing.

Two important conclusions were obvious as a result of these heat shield tests: (1) the service temperature of the panel systems must be limited to a temperature at which local hot spots will not exceed the capabilities of the oxidation protective coating and (2) the outer surfaces and joints should be as smooth and free from discontinuities as possible to prevent hot spots.

Some of the intergranular weld cracks that occurred during the installation of the sealing details opened up during the application of the Cr-Ti-Si coating. The cracks along the edges of the panels were covered by the coating and were not extended or enlarged.

The enlarged cracks on the inner face sealing details caused the final failures of the two heat shield panels that were tested in the quartz lamp facility. The panels that were tested in the hot gas facility were not obviously affected by the cracks in the inner sealing details. However, it is considered that if the outer face sealing details had been free of defects, some of the panels would have lasted longer before failure.

c. Small specimens

The D-36 columbium small specimen test results which are summarized and treated in detail in Section B of Chapter VII are within the normal scatter range for honeycomb tests of this type. The flatwise compression and shear tests were consistent and the test techniques were satisfactory.

The small specimen column compression tests were not as consistent as the panel edgewise compression tests, with the results showing considerable scatter (Fig. 180). In general, small column compression specimens should have strengths equal to or stronger than those of the panel tests; however, when testing thin-skinned specimens that have been cut from honeycomb panels, the unsupported cut edges can become a problem. In some cases, the thin unsupported edges buckle early, then propagate a premature failure into the rest of the specimen. In bonded honeycomb and low temperature brazed specimen tests, the edges of the small specimens are filled or potted with some plastic or ceramic compound. This provides support along the edges and prevents premature failures. However, in the high temperature vacuum test, there are no materials available to support the edges which will withstand the test conditions. As a result of these premature edge failures, the 1600° and 2000° F specimen data are scattered, and the 2400° F specimen data are considerably lower than the panel test data. Because of these testing problems and the large scatter, the compression strengths obtained from these tests were not used to determine the material compression strengths. Instead, the test panel compression strengths were utilized.

The beam test to determine the core shear strength and modulus was used because the high temperature test requirements make it extremely difficult to use the plate shear method (Ref. 39). The beam test is not as good as the plate shear test because of the fixturing problems involved and the normally larger scatter in the test data. The test setup and the procedure must be accurately controlled to obtain good results because the modulus calculation (Section IV) is based on the difference between the square of the slope of the long span load-deflection curve and the square of the slope of the short span load-deflection curve. This is usually a small difference between two large numbers squared, which results in considerable scatter in the test results because of seemingly minor test procedure variances. The test data that were obviously questionable were not considered in determining the averages and allowables.

The tensile test was satisfactory, with results within the normal expected scatter

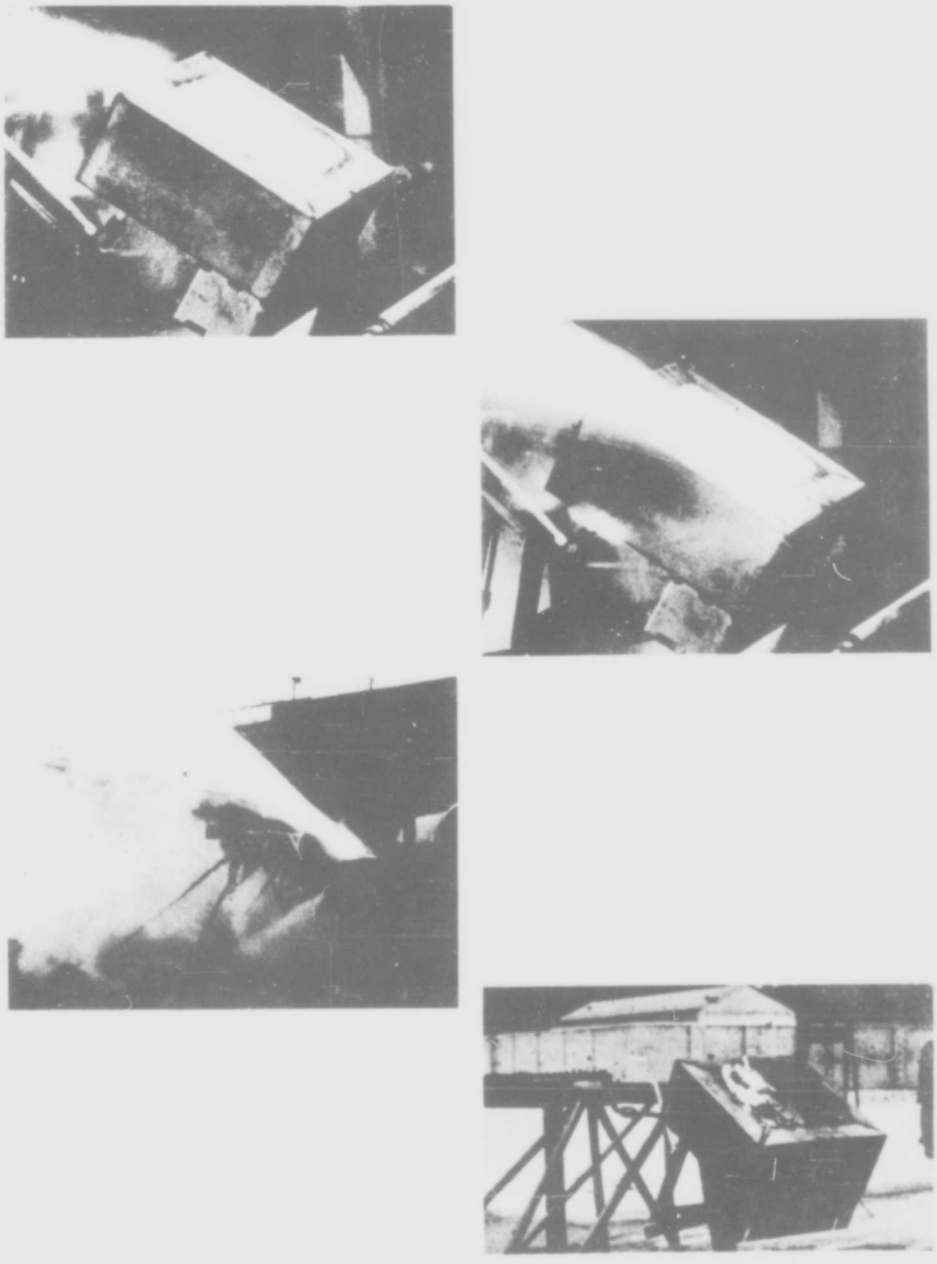

Fig. 179. Progression of Failure in D-36 Heat Shield Panel No. 7

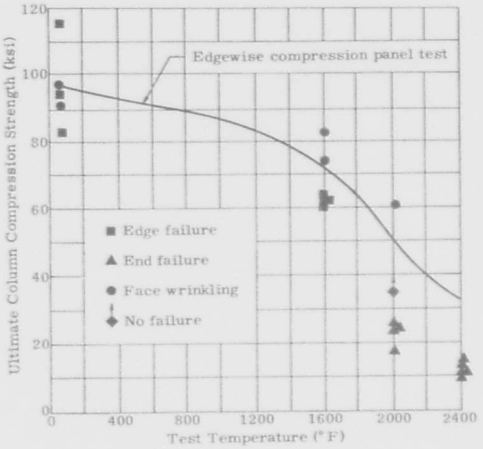

Fig. 180. D-36 Columbium Small Specimen Column Compression Strength Versus Temperature

range. Some of the ultimate tensile tests, in which the tantalum slide rule gages were used for modulus of elasticity determinations, failed through the area where the gages were spot-welded to the specimens. The failure stresses of some of these tests were consequently low and were not included in the specimen average.

The high elongation of D-36 at 2400° F caused the vacuum furnace bellows assembly to bottom-out during static test without failing the specimen. Also, a short gage length had to be machined on the creep specimens to prevent bottoming of the bellows before the desired results were obtained. In addition, the 2400° F tensile-tensile fatigue tests were stopped because of the excessive creep that was occurring in the test specimens.

The brazed laminate tensile specimens apparently performed their required task very successfully. At room temperature there were distinct strength differences in the three types of specimens (as received, as brazed, and as-brazed-plus-coated). However, at elevated temperatures, these differences disappeared.

The tensile specimen strengths were low, compared to the high strengths obtained in the panel test. The average strengths obtained from these tensile tests were about the same as the panel shear strengths. For ductile material, the shear strength is usually about one-half the tensile strength.

The fractures of the D-36 tensile specimens were different from those normally found in ductile materials. The entire gage length of the specimens yielded until failure, with almost no necking at the point of fracture. The elongation of the room temperature, 1600°, and 2000° F test specimens was very low for columbium alloys (Fig. 181). The 2400° F specimens exhibited good elongations. The behavior was like a brittle failure phenomenon.

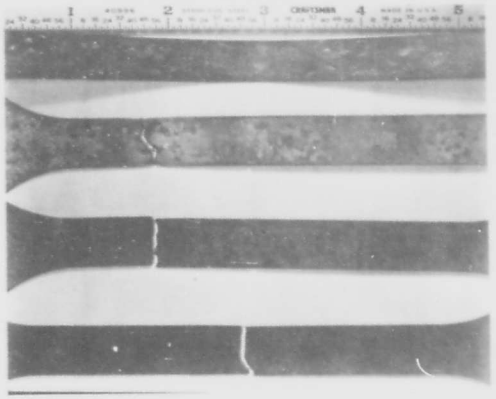

Fig. 181. D-36 Alloy Coated Laminate Tensile Coupons Tested at: (a) 2400° F, (b) 2000° F, (c) 1600° F and (d) Room or Ambient Temperature

A metallographic evaluation of the microstructure of the brazed laminate tensile specimen fractures was made to determine the types of fractures that occurred. At the lower temperatures, the ultimate fractures were predominately transcrystalline but some intercrystalline fractures were visible (Figs. 182 through 185). At the higher temperatures, the ultimate fractures were predominately intercrystalline with only a few transcrystalline cracks visible. Examination indicated the presence of considerable precipitate, particularly at the grain boundaries. Evidently, during the braze and coating cycles, grain growth was extreme and, as a result, the precipitate was concentrated on the relatively few grain boundaries that remained. This can result in low grain boundary cohesive strength and is considered the source of the specimen fracture (page 258 of Ref. 40). This was substantiated in the metallographic study, where numerous small grain boundary cracks are visible on the test specimens in areas removed from the fracture (Fig. 186). No indication of slip planes within the metal grains was visible.

NOTE:

Path of fracture is both transcrystalline and intercrystalline. (75X)

Fig. 182. Cross Section of D-36 Alloy Tensile Coupon Tested at Room Temperature Showing Profile of Fracture and Metallographic Structure

NOTE:

Path of fracture is both transcrystalline and intercrystalline. (75X)

Fig. 183. Cross Section of D-36 Alloy Tensile Coupon Tested at 1600° F Showing Profile of Fracture and Metallographic Structure

NOTE:

Path of fracture is both intercrystalline and transcrystalline. (75X)

Fig. 184. Cross Section of D-36 Alloy Tensile Coupon Tested at 2000° F Showing Profile of Fracture and Metallographic Structure

NOTE:

Path of fracture is both intercrystalline and transcrystalline. (75X)

Fig. 185. Cross Section of D-36 Alloy Tensile Coupon Tested at 2400° F Showing Profile of Fracture and Metallographic Structure

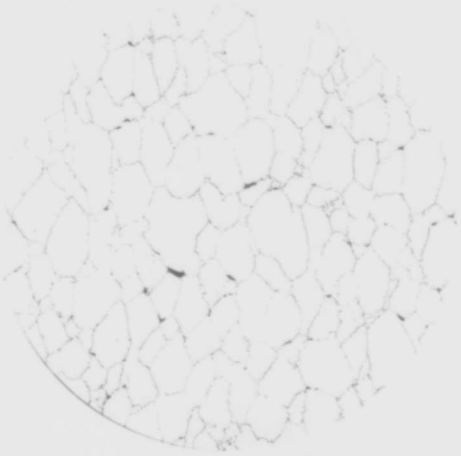

NOTE:

Coupon was not pulled to total fracture.
(75X)

Fig. 186. Cross Section of D-36 Alloy Tensile Coupon Tested at 2400° F Showing Characteristics of Metallographic Structure After Plastic Deformation

The fracture mechanism, as previously described, is very aptly explained by Freudental in his book on "The Inelastic Behavior of Engineering Materials and Structures" (Ref. 41). He states:

> If, . . . , the rate of energy dissipation within the intercrystalline and distorted crystal regions is of the same, or of a higher, order of magnitude as the rate of energy application, the deformation is concentrated within the regions, which therefore appear soft. Their cohesion is gradually destroyed by the cumulative effects of relaxation under load and separation. The deterioration of the intercrystalline cohesion under sustained or slowly applied load extends over the entire specimen since the rotation and relative motion of the crystals along the intercrystalline boundaries is not localized in the regions of highest stress, as it is in the case of plastic deformation following the sudden breakdown of the grain boundaries under a rapidly applied load (at the elevated temperatures the rapidly applied load tensile specimens failed similar to this description for the sustained or slowly applied load). The observed decrease in overall density of the material and its appearance under the microscope suggest that the disintegration of the intercrystalline regions is followed by the appearance of microscopic cracks at or near the crystal boundaries which, during a later stage, spread into the neighboring crystal.

A good example of the decrease in density and disintegration of the intercrystalline regions that Freudental describes can be seen in the tensile specimens shown in Fig. 187.

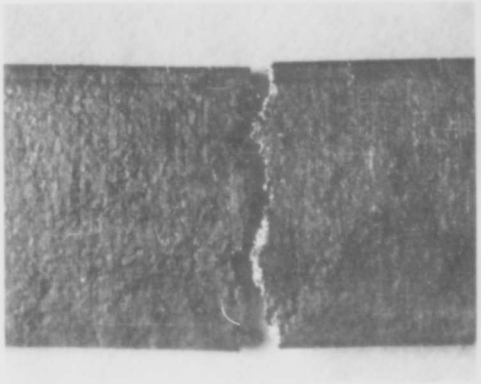

Fig. 187. D-36 Alloy Bare Laminate Tensile Coupon Tested at 1600° F

Based on brittle fracture theory, the relationships of the tensile, shear, and compression strengths are rational. In the shear test, once the principal tensile stress reaches the critical level, as determined by the axial tensile test, fracture will occur. However, since the compression test produces no tensile stresses, the material is ductile in compression. Ductile behavior in compression justifies the compression panel test strength being higher than the shear panel strengths. In the region between shear and compression there is a transition between brittle fractures and ductile failures. Under biaxial compressive loading, a ductile theory of failure will apply (such as the Maximum Strain Energy of Distortion Theory, or, more conservatively, the Maximum Principal Stress Theory). For biaxial tensile loading, it appears necessary to use a brittle failure theory (such as the Maximum Total Stress Theory).

It is considered that a ductile theory is applicable to define the stress level at which yielding begins. However, since only the yield strength of material in tension is

known, the shape of the curves in compression and shear cannot be established. As a result, no attempt was made to plot a curve for this condition.

The D-36 structural panel test results were higher than those predicted in the preliminary design and analysis study, as previously noted. These predicted strengths were based on uncoated tensile specimens with the material in the recrystallized condition (1 hour at 2200° F). In this study, the material was assumed to be ductile with the compression strength equal to the tensile strength and the shear strength equal to 50% of the tensile strength. Information on the compression and shear strengths of the D-36 was not available at the time of the panel design, and no new information has become available. The room temperature tensile strength of the brazed and coated material was about 14% higher than that used in preliminary studies. As explained before, the panel shear strengths are equal to facing tensile strength and the compression strengths are even higher. It is possible that some hardening or strengthening may have occurred. This can only be speculated, since initial strengths in compression and shear are not known.

2. TZM Molybdenum

a. Structural panels

Only a few TZM panel tests were performed because of the difficulty in sealing the panels and in welding the load application strips to the shear test panels. Additional tests that were planned were abandoned when two of the panels blew apart during heating. These panels had small braze voids at the edges of the panels (the edges of these panels were not sealed by electron beam welding). When the panels were heated, the entrapped air in the void area expanded faster than it could escape, thus subjecting the core-facing intersection to a peeling stress large enough to fail the rest of the brazed area. An important observation from these tests was that the honeycomb panels must be sealed at a sufficiently low pressure so that expansion of any entrapped gases, upon heating the panels, will not generate a pressure high enough to fail the panel if any small braze voids exist. Because they did not blow apart, the remaining panels were sealed obviously during the braze operation.

The TZM-Haynes 25 braze joints were extremely brittle below about 1600° F. One panel that was tested at 1600° F had a braze joint failure at a very low stress level. A metallographic study of the braze joint indicated that considerable solid-state diffusion alloying had occurred and resulted in the formation of a brittle intermetallic at the braze-alloy to base-metal interface (Fig. 188). This evidently occurred during the high temperature diffusion treatment cycle utilized in the application of the oxidation protective coating.

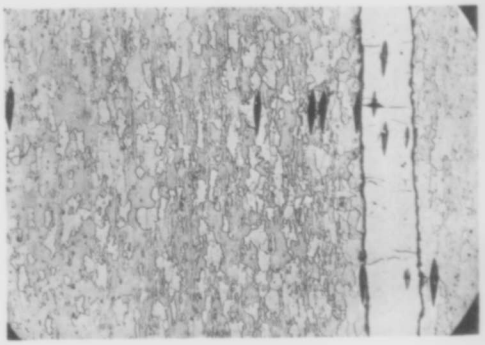

NOTE:

Photomicrograph showing the brittle intermetallic at braze alloy-to-metal interface. (130X)

Fig. 188. TZM Molybdenum-Haynes 25 Braze Joint After Coating Process

b. Small specimen test

The high temperature tests (1600°, 2000°, and 2300° F) of the TZM small specimen were very successful. The test results were consistent and in general higher than expected from preliminary data. However, the room temperature tests of the coated TZM panels were completely unsuccessful, with the brittle braze joints failing at very low stress levels. The data were scattered and unusable.

In an attempt to obtain honeycomb core properties at temperatures below 1600° F, specimens were cut from a panel that was not coated. The braze-alloy to base-metal joints in these specimens were still ductile and could be loaded at lower temperatures without brittle fracture. These specimens were tested at 400° and 800° F and provided satisfactory results.

The brazed-coated specimens exhibited brittle-type failures, with the core fracturing during the test. In most instances the core shear strengths obtained from the

specimen tests reflected only braze failures. The as-brazed specimens had failures typical of ductile material with the core crushing in compression and wrinkling in shear.

The 1600°, 2000° and 2300° F small specimen column compression test results were higher than expected, with about the normal amount of scatter for TZM specimens (Fig. 189). The specimens failed in face wrinkling with the braze failing and the facing buckling away from the core. These results were considerably more successful than the D-36 small columns; the primary reason for this is considered to be the greater stiffness of the TZM.

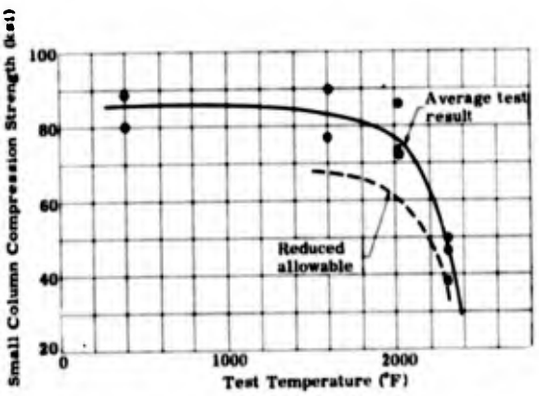

Fig. 189. TZM Molybdenum--Small Column Compression Strength Versus Test Temperature

Considerable difficulty was encountered in the TZM tensile tests (ultimate and fatigue). The brazed and coated-brazed specimens were extremely brittle, and many specimens were prematurely damaged during installation. Also approximately 1/4 of the coated specimens were lost during the coating operation. Several of the fatigue test specimens were prematurely failed during the initial test load balancing. Consequently, a limited number of datum points were acquired.

B. MATERIAL PROPERTIES

The panel and small specimen test data were reduced to provide mechanical property data on the panel strengths, facing strength and moduli, and the honeycomb core strength and moduli. Plots of the various data versus test temperature are presented in this subsection on the basis of material and type of test.

1. D-36 Columbium

a. Panel properties

A plot of the compression and shear panel test results is shown in Fig. 175. The plotted stresses were calculated on the basis of material thickness plus braze alloy thickness (0.002 in. per skin) before coating. This was done because of the difficulty in nondestructively ascertaining the base metal and diffusion layer thickness after coating. The braze alloy was considered as a load-carrying part of the skin because of the alloying that occurs between the braze alloy and the base metal during the brazing process, and the fact that the elastic modulus of the titanium brazing alloy is almost identical to that of D-36 columbium. Under these conditions, the braze alloy must carry an equal share of the load.

The five cycle heating had a very small but consistent effect on the panel strengths. The strengths of the five cycle panels were about 2 to 4% lower than those of the one-cycle panels.

All of the panels except for one of each type (shear and compression) were loaded only once. The ultimate strengths shown in Fig. 175 represent a maximum that these panel systems could be expected to withstand. For actual vehicle application, the short duration flight loads could safely be applied to some reduced load level but for long duration flight loads, such as internal vehicle pressurization and thermal stresses, the allowable load level should be based on the creep strength of the facing material.

Shown with the test data are curves representing material allowable stresses for shear and compression. These are based on an arbitrary reduction of the test data. These allowables are to be used for determining the required facing thickness to resist edgewise compression and shear loads.

b. Facing materials

The tensile properties of D-36 were evaluated for these material conditions: (1) as-received, (2) as-brazed and (3) as-brazed-plus-coated (Figs. 190 through 194). The three conditions were evaluated to show the effects which the brazing and coating cycles had on the mechanical properties of D-36. The tensile properties of the coated specimens were based on the material thickness before coating. Special tensile specimens (Fig. 171) were used to show the effect of

both the braze alloy and the coating. The tensile data represent a one-cycle load-temperature test of the material.

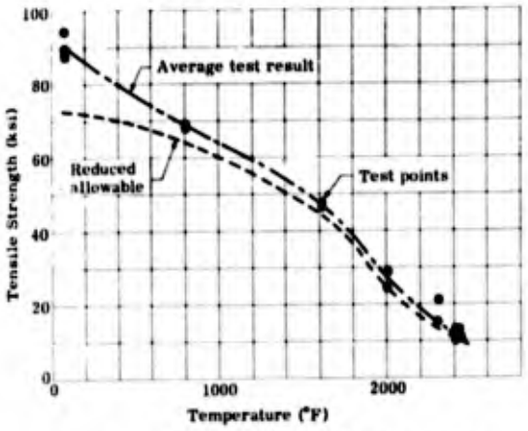

Fig. 190. Tensile Properties Versus Test Temperature--Brazed Plus Coated D-36 Columbium

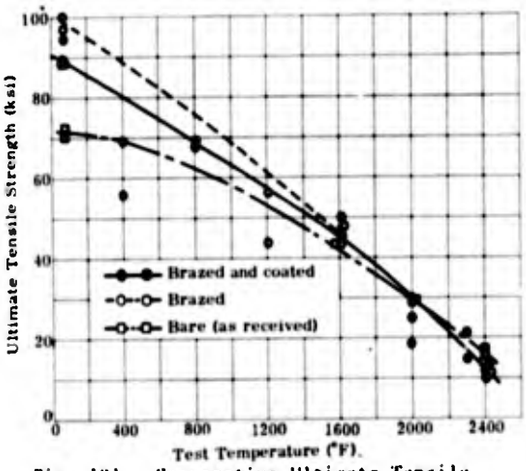

Fig. 191. Comparative Ultimate Tensile Strength Versus Temperature for D-36 Columbium Composites

Shown on the test data plots are curves representing the averages. On the as-brazed-plus-coated plot is a curve representing a reduced allowable stress (Fig. 190). The data were arbitrarily reduced to provide an allowable stress curve which is 5% below the lowest test point. Because of the types of failure that occurred and the apparent relationship between the tensile strengths and the shear panel test results, the tensile allowables for the brazed and coated laminates were made the same as the material shear allowables.

High load-limited cycle-fatigue strengths of as-brazed and as-brazed-plus-coated D-36

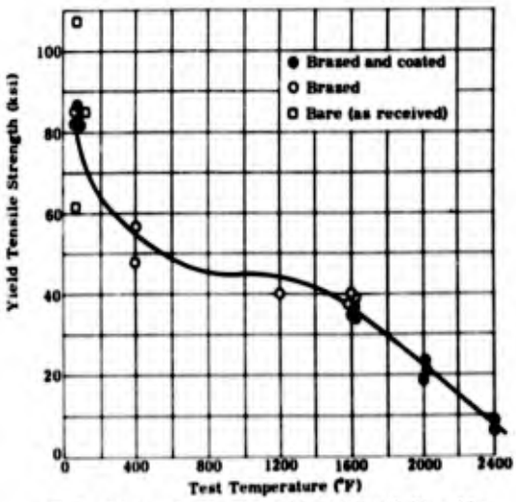

Fig. 192. D-36 Columbium Yield Tensile Strength Versus Temperature

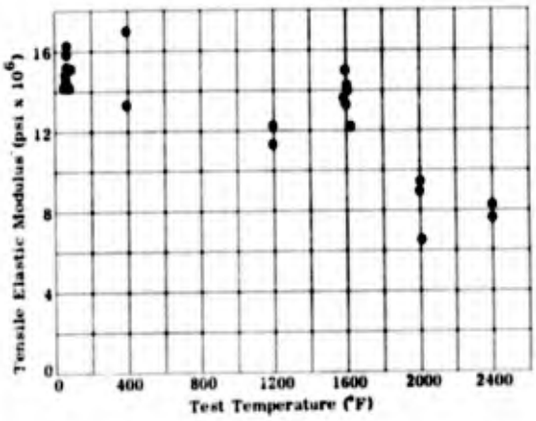

Fig. 193. D-36 Columbium Tensile Elastic Modulus Versus Temperature

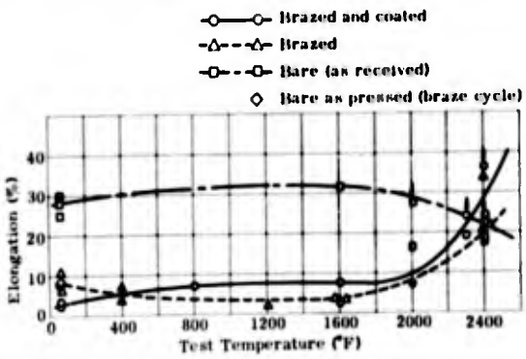

Fig. 194. D-36 Columbium--Percent Elongation Versus Temperature; Ultimate Tensile Test

were evaluated at room and elevated temperatures. S-N curves for the two material conditions are shown in Fig. 195. The stress

levels for the test were chosen to limit the test life to approximately 10,000 cycles.

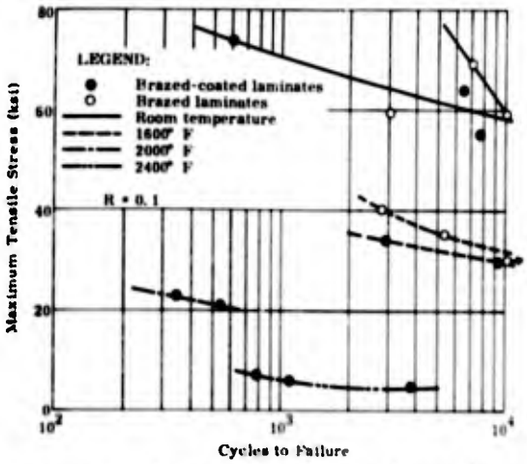

Fig. 195. Fatigue Test Results for D-36 Columbium Specimens

High load-short time-creep strengths of as-brazed and as-brazed-plus-coated D-36 were evaluated at elevated temperatures. Figure 196 shows a plot of stress rupture strength versus time, with curves at various temperatures. The only difference in the two material conditions occurs at the higher stress levels and short time periods. As the stresses become lower and the times longer there was no distinguishable difference in the two materials. Figures 197 and 198 show a plot of stress versus time, at several strain levels and temperatures. Again, the only distinguishable differences occur at high stress level-short time periods. The creep rupture strength of the D-36 columbium at the elevated temperatures is very low and the creep rate is high at relatively nominal stress levels.

c. Honeycomb core

The properties of D-36 honeycomb core were evaluated with small specimen tests at room and elevated temperatures to 2400° F. These data were required to provide sufficient design information for honeycomb sandwich panels.

The flatwise compression strength test results versus temperature are shown in Fig. 199. Shown on this plot is a curve representing the flatwise compression strength predicted in the preliminary design and analysis study phase of the program (Section IV). The curve is in reasonable agreement with the actual test data. A median curve and a reduced allowable curve are also shown. The allowable curve is arbitrarily reduced at least 5% below the lowest test point of each temperature. This was necessary since the number of tests at each point are insufficient to allow a statistical reduction.

The flatwise compression modulus test results versus temperature are shown in Fig. 200. Shown on this plot is a curve representing the flatwise compression modulus predicted in the preliminary design and analysis study (Section IV). The predicted moduli were considerably higher than the actual test results. In this initial study, a reduction factor of 0.4 was used; from examination of the test results a factor of 0.2 would have been better. A median curve and a reduced allowable curve are shown.

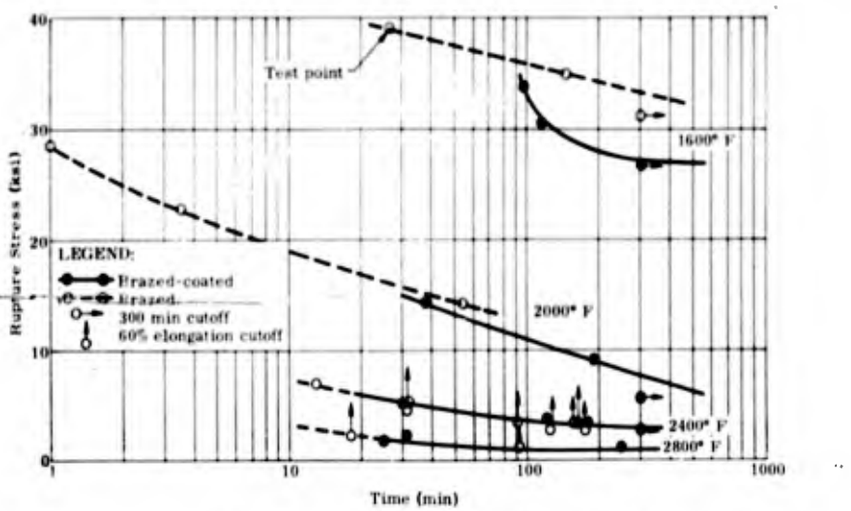

Fig. 196. D-36 Columbium Creep Rupture Strength

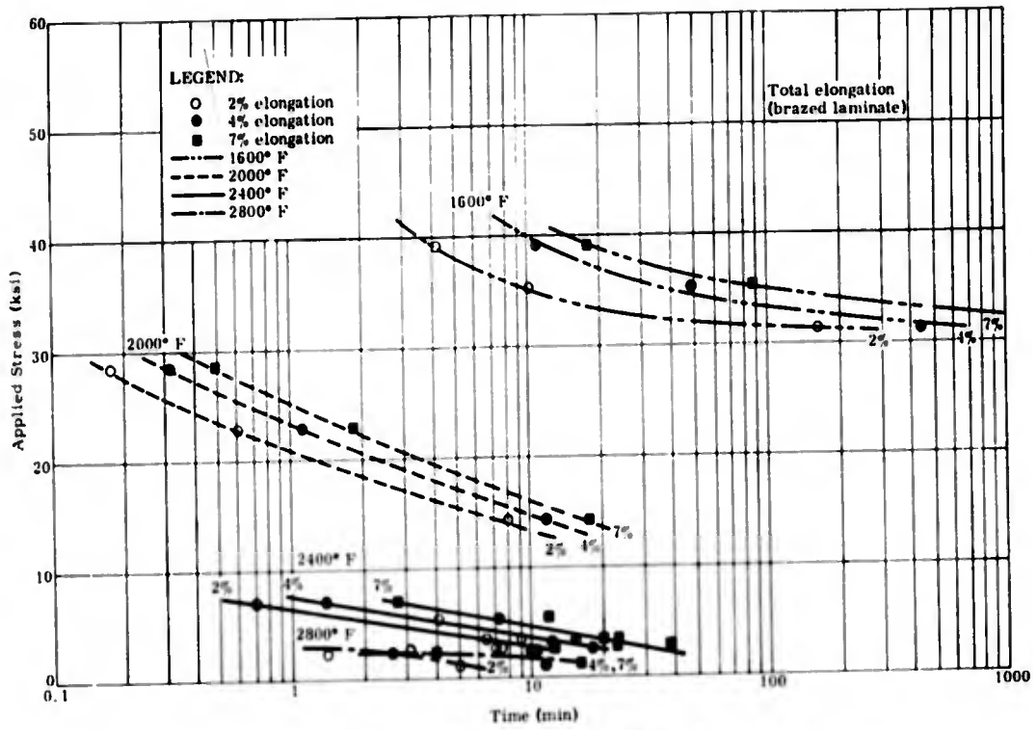

Fig. 197. Creep Rate for D-36 Columbium Brazed Laminate Specimens

The shear strength test results versus temperature are shown in Fig. 201. Shown on this plot is a curve representing the core shear strength predicted in the preliminary design and analysis study phase of the program (Section IV). The curve provides a good estimate of the actual test data at room temperature and at the high temperatures, but at the intermediate temperatures the test results are lower than predicted. A median curve and a reduced allowable curve are also shown. The allowable curve is arbitrarily reduced at least 5% below the lowest test point at each temperature, again because of the limited number of test points.

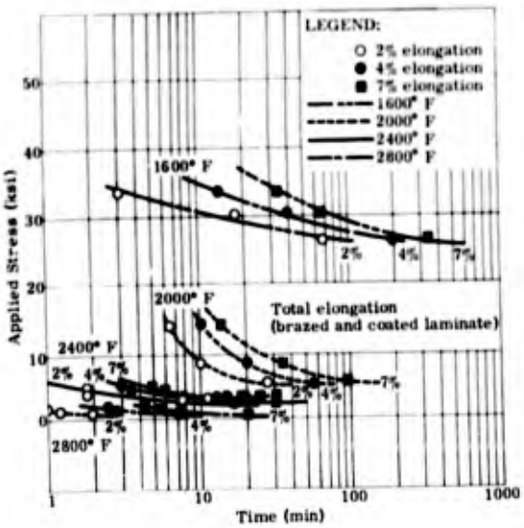

Fig. 198. Creep Rate for D-36 Columbium Brazed and Coated Laminate Specimens

The shear modulus test results versus temperature are shown in Fig. 202. Shown on this plot is a curve representing the core shear moduli predicted in the preliminary design and analysis study phase of the program (Section IV). The curve provides an approximate estimate of the actual test data and is slightly lower than all the test results. A median curve and a reduced allowable curve are also shown. The allowable curve is based on an arbitrary reduction because of the limited number of test points.

2. TZM Molybdenum

a. Facing properties

The tensile properties of TZM were evaluated for three material conditions: (1) as-received, (2) as-brazed and (3) as-brazed-plus coated (Figs. 203 through 206). The three conditions were evaluated to show the effects of the braze and coating cycles on the mechanical properties of TZM. The tensile strengths of the coated tensile specimens are based on the material thickness before coating. Special tensile specimens were used to

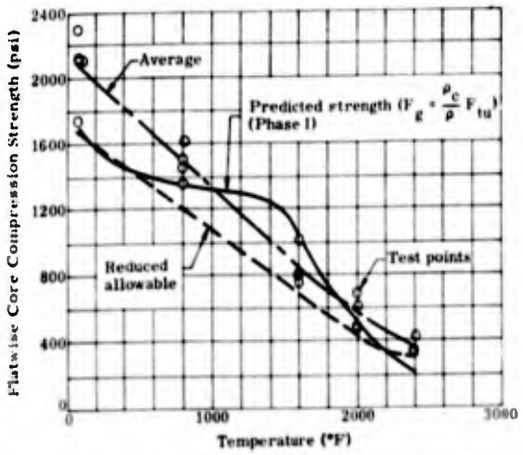

Fig. 199. D-36 Columbium Flatwise Core Compressive Strength Versus Temperature

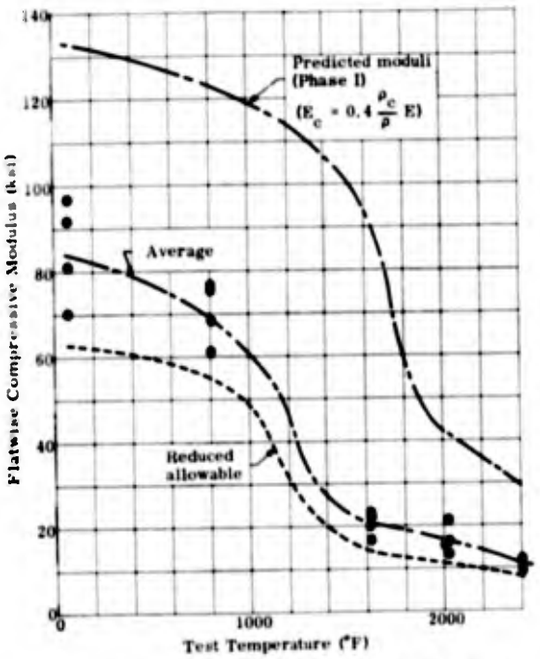

Fig. 200. D-36 Honeycomb Core Flatwise Compression Modulus Versus Temperature

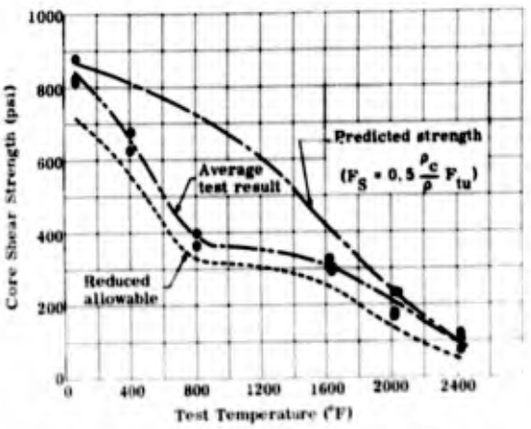

Fig. 201. D-36 Columbium--Honeycomb Core Shear Strength Versus Temperature

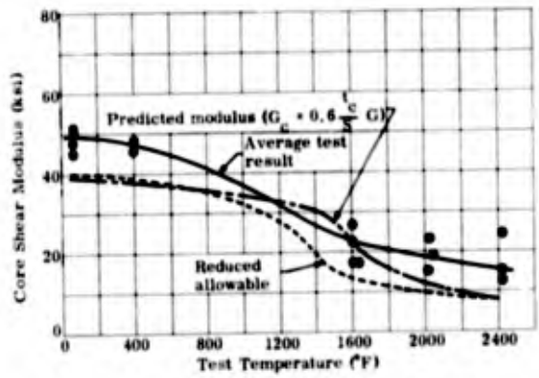

Fig. 202. D-36, Columbium--Core Shear Modulus Versus Temperature

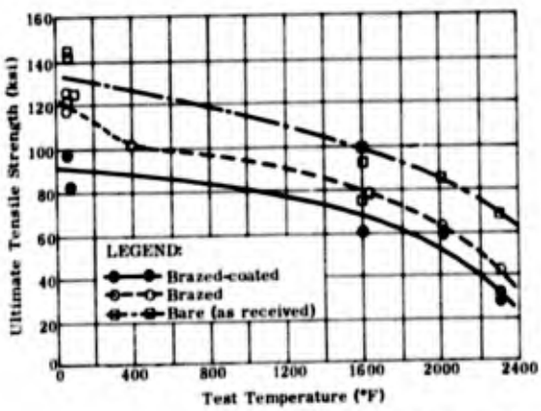

Fig. 203. TZM Molybdenum Ultimate Tensile Strength Versus Temperature

show the effects of both the braze alloy and coating. The tensile data represent a one-cycle load-temperature test of the material.

High load-short time creep strength of the as-brazed and the as-brazed-plus-coated TZM were evaluated at elevated temperatures. Figure 207 shows a plot of the rupture stresses versus time at various temperatures. The two material conditions produced radical differences in both creep rate and creep rupture strength. The 1600° F coated specimens were so brittle that they failed during loading. Figures 208 and 209 show the creep rate at various load levels versus temperature and time.

Because of the coating and testing problems previously described, no useful fatigue

data were obtained for TZM, and no S-N curve is presented in this report.

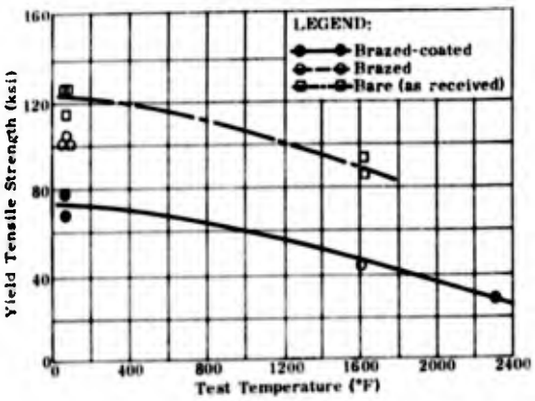

Fig. 204. TZM Molybdenum Yield Tensile Strength Versus Temperature

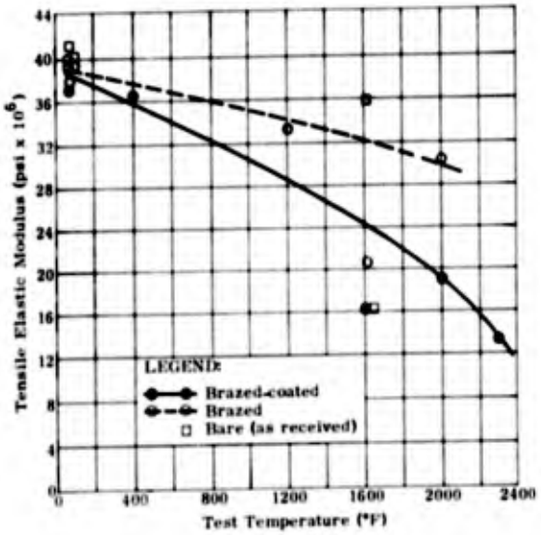

Fig. 205. TZM Molybdenum Tensile Elastic Modulus Versus Temperature

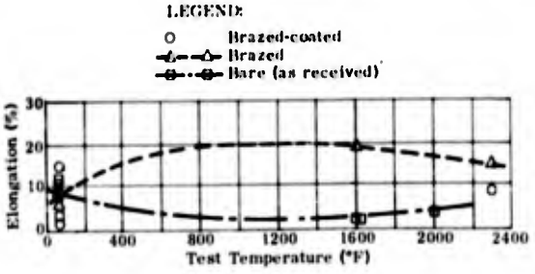

Fig. 206. TZM Molybdenum--Percent Elongation Versus Temperature; Ultimate Tensile Test

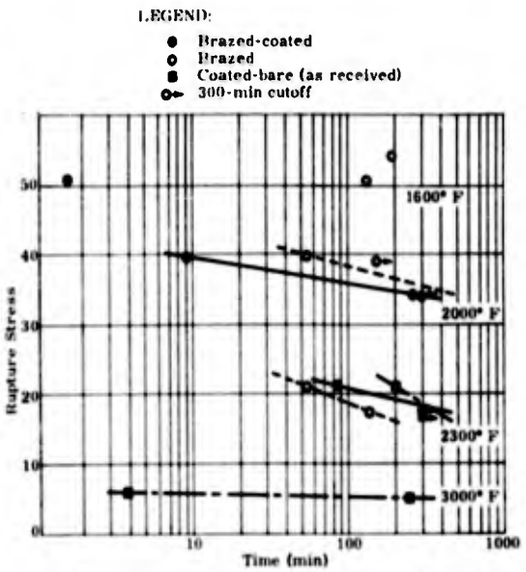

Fig. 207. TZM Molybdenum Creep Rupture Strength

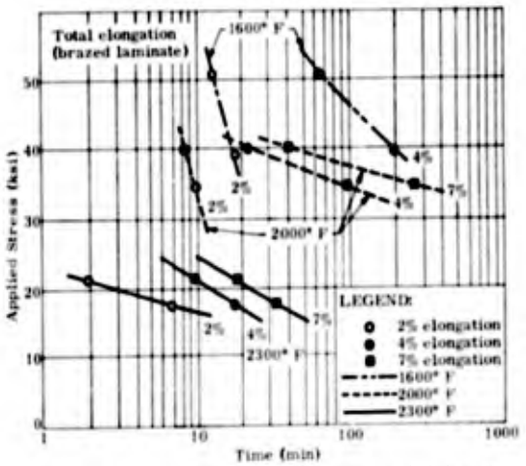

Fig. 208. Creep Rate for TZM Molybdenum Brazed Laminate Specimens

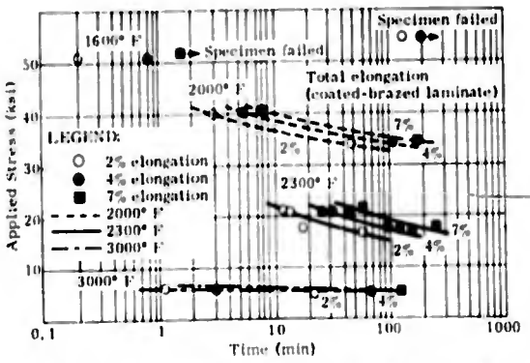

Fig. 209. Creep Rate for TZM Molybdenum Coated and Brazed Laminate Specimens

The small column compression test results can be used to determine a facing compression allowable for TZM (Fig. 189). However, since the braze strength has a primary effect on the compression strength of a honeycomb sandwich panel, these allowables should be used with reservations until new braze systems are similarly evaluated.

b. Honeycomb core

The properties of TZM honeycomb core were evaluated with the small specimen tests to provide further design information on TZM core. Because of the brittleness of the braze joints, it was impossible to determine accurate core properties at temperatures below 1600° F for the brazed and coated panels. Tests were performed on specimens cut from the coated panel at 1600°, 2000° and 2300° F. The strengths are reasonably consistent at these temperatures and are considered to represent feasible design strengths. The properties at 400° and 800° F were obtained from specimens cut from uncoated panels.

The flatwise compression strength test results versus temperature are shown in Fig. 210. A curve is shown on this plot representing the flatwise compression strength predicted in the preliminary design and analysis study phase of the program (Section IV). The predicted values from the equation are about 30% conservative. A median and a reduced allowable curve are also shown in Fig. 210. For D-36, the allowable curve is based on an arbitrary reduction of the test data, because of the limited number of test points.

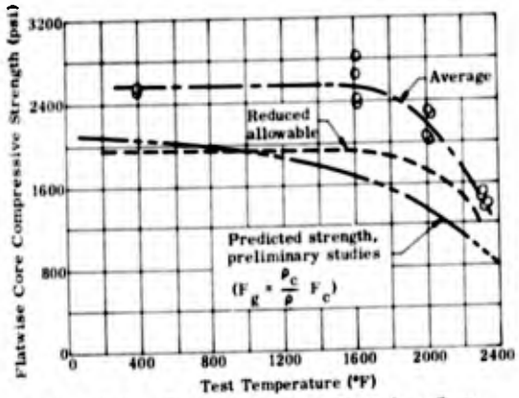

Fig. 210. TZM Molybdenum Flatwise Core Compressive Strength Versus Temperature

The flatwise compression modulus test results versus temperature are plotted in Fig. 211. The preliminary prediction was about six times higher than the test data. A modified equation of $E_c = \frac{1}{15} \frac{\rho c}{\rho}$ will predict the data with reasonable accuracy. There was considerable scatter in the test data because of the brittleness of the core and braze alloy. A median curve and an arbitrary reduced allowable are also shown on the curve.

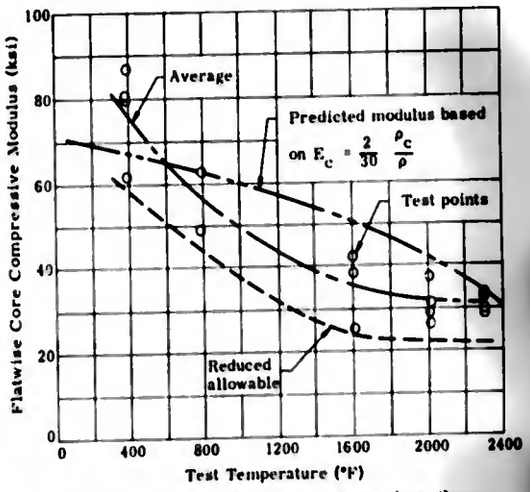

Fig. 211. TZM Molybdenum Flatwise Core Compressive Modulus Versus Temperature

The shear strength test results versus temperature are shown in Fig. 212 which also presents a curve representing the shear strength predicted in the preliminary design and analysis study (Section IV). The predicted core properties are about twice as high as the test data. A median and an allowables curve are also shown. The 400° and 800° F core shear allowables are based on specimens cut from the uncoated panel.

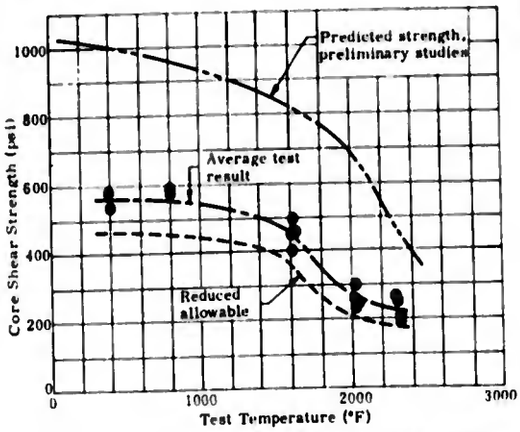

Fig. 212. TZM Molybdenum Honeycomb Core Shear Strength Versus Temperature

An arbitrary reduction of the available test data was used to establish honeycomb core allowables.

The shear modulus test results versus temperature are shown in Fig. 213. A curve is shown on this plot representing the shear modulus predicted in the preliminary design and analysis study (Section IV). The prediction equation provides a reasonable estimate of the test data. A median and an allowable curve are shown. The 400° and 800° F core shear allowables are based on specimens cut from the uncoated panel. Again, the allowables were based on an arbitrary reduction of the test data. There was considerable scatter in the test data at all temperatures.

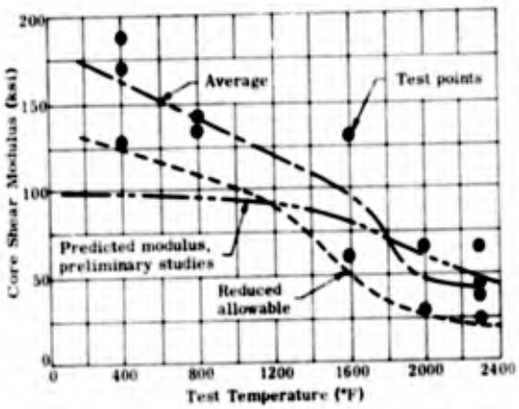

Fig. 213. TZM Molybdenum Core Shear Modulus Versus Temperature

C. CORRELATION OF TEST RESULTS WITH DESIGN ANALYSIS PROCEDURES

A comparison was made of the panel test results versus the predicted design strengths utilizing the formulas in MIL-HDBK-23, "Composite Construction for Flight Vehicles," Part III. The facing properties and the honeycomb core strengths obtained from the small specimen tests were utilized. To calculate the predicted design strength, these calculated data were then compared with the actual panel test strengths.

1. D-36 Columbium

a. General instability

The critical general instability stress is given by the formula

$$\frac{F_{cr}}{E'} = \frac{\pi^2 K}{4\lambda}\left(\frac{h}{b}\right)^2 . \qquad (7)$$

The critical compression instability stresses predicted by Eq (7) are lower than the critical stresses determined by the panel test (Fig. 214). This occurs because the effective modulus, E', used in the equation is based on the stress-strain curves obtained from the tensile test. Because of this, the predicted maximum critical compressive stress can never be more than just above tensile yield stress. The best result would be obtained if an E' based on compression stress-strain curves could be used; however, these values were not determined during this test program because of the unavailability of satisfactory instrumentation and test methods. Attempts to obtain stress-strain curves from the small edgewise compression specimens were unsuccessful.

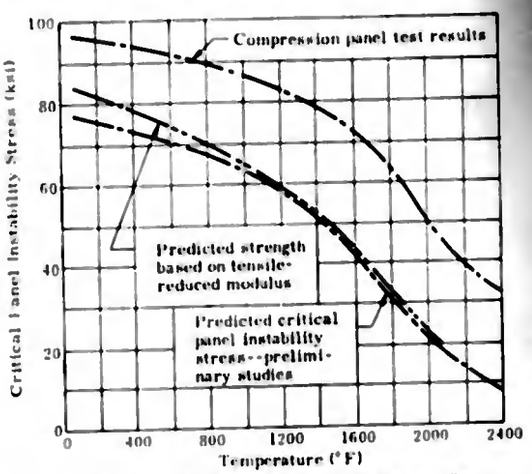

Fig. 214. Comparison of D-36 Panel Test Data with Critical Panel Instability Stresses

Modification of Eq (7) to provide an accurate prediction of the test data cannot be accomplished unless a different form is used for effective modulus, E'. One method is to use an elastic modulus instead of the reduced modulus for E'. However, the required core thickness predicted with an elastic modulus will be less than actually needed to stabilize the panel. Another method is to plot an empirical F_c versus $\frac{F_c\lambda}{E'}$ curve where the upper portion of the curve is made to fit the panel test data (Fig. 215). This method should accurately predict the core thickness required to stabilize the panel. By using: (1) a straight line (semilog paper) between the material cutoff point and the tensile portions of the curve, (2) a constant value of F_c above the material cutoff point and (3) the reduced allowable for the material cutoff point, the empirical relationship for E'

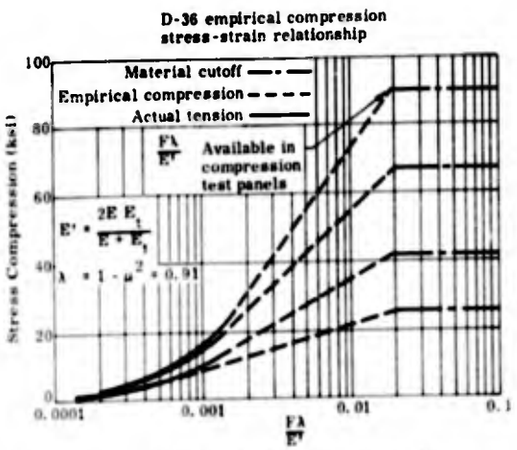

Fig. 215. Effective Modulus Curve Based on Empirical Compressive Modulus

will give conservative results when compared to panel test data. For even more conservative results, an F_c versus $\frac{F_c \lambda}{E'}$ based on the tensile stress-strain curves could be used (Fig. 216).

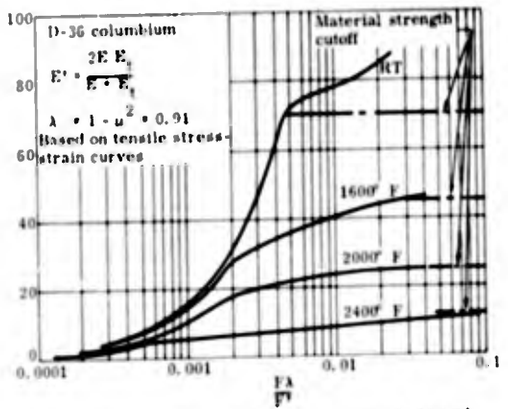

Fig. 216. Effective Modulus Curve Based on Tensile Stress-Strain Curves

For general instability design of panels in shear, the E' based on the tensile stress-strain curves must be used.

b. Intercellular dimpling

The design formula for intercellular dimpling is

$$\frac{F_c}{E'} = \frac{2}{\lambda}\left(\frac{t_f}{S}\right)^2$$

where for the test panels, $t_f = 0.014$ in. (considering the 0.002-in. braze alloy) and S = 0.1875 in. This equation is empirical and represents a stress level at which dimpling will not occur. The calculated value of F_c critical and the panel test results versus temperature are shown in Fig. 217. The predicted critical crimpling strengths are considerably lower than the compression panel test strengths, when an E' based on the tensile stress-strain curves is used. However, if the empirical E' relationship is used, the predicted critical strengths are just below the compression panel test strengths. By using the tensile stress-strain curve for E', an accurate prediction can be made for critical dimpling stress for the shear test panels.

c. Face wrinkling

The design formula that best represents the critical face wrinkling stress is based on Hoff's elastic energy solution for a plate on an elastic foundation (Ref. 42), or

$$F_{cw} = K \sqrt[3]{E_c G_c E'} \qquad (28)$$

where K is an empirical constant. A value of 0.85 is the best value of K for stainless steel sandwich (17-7PH and PH15-7Mo). Since no value has previously been established for D-36 columbium, trial values of 0.7 to 0.9 were used for K.

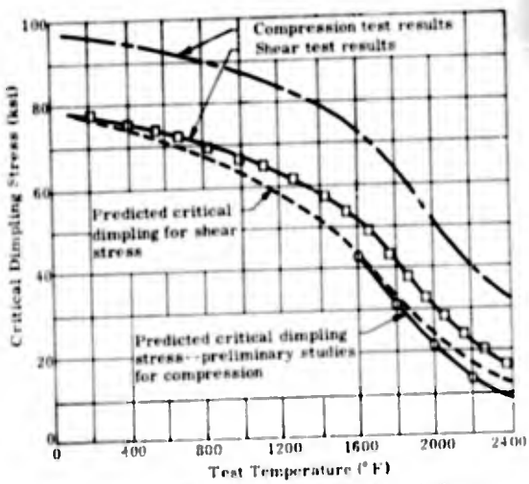

Fig. 217. Comparison of D-36 Panel Test Data with Critical Dimpling Stress

Equation 28 cannot be solved directly since E' is dependent upon the stress (F_{cw}) and all terms are dependent upon temperature. A solution was obtained graphically (Fig. 218). Shown on this plot are different curves for values of K from 0.7 to 0.9.

The compression panel test results are shown on the same plot as the critical face

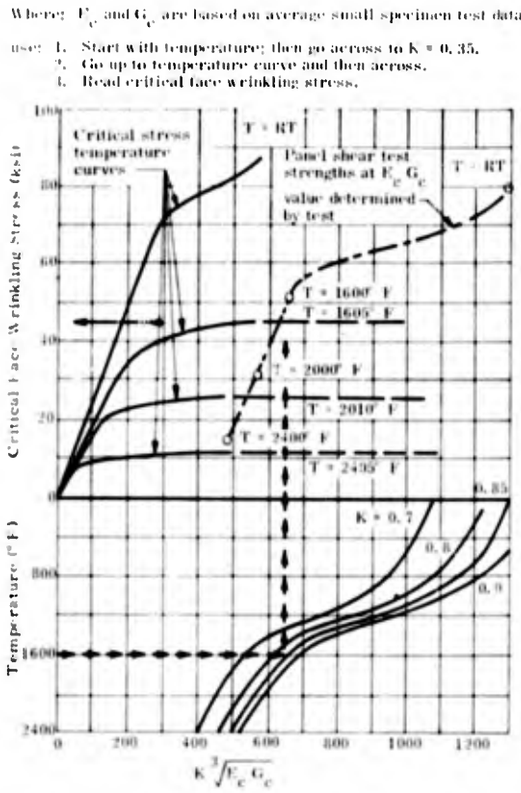

Fig. 218. Comparison of D-36 Panel Test Data with Critical Face Wrinkling Strengths

wrinkling stress. Using an E' based on the tensile stress-strain curves, the predicted critical wrinkling stress is low when compared to the compression test panel strengths and reasonably close when compared to the shear test panel strengths. The empirical E' provides the best means for predicting the critical compressive face wrinkling stress. A K = 0.85 appears reasonable for D-36 columbium.

D. RECOMMENDED DESIGN PROCEDURES

This section presents basic honeycomb design procedures, utilizing the material properties obtained in the test program and the procedures recommended by MIL-HDBK-23, "Composite Construction for Flight Vehicles," Part III. Design curves and procedures in MIL-HDBK-23 have not been reproduced in this section, but are referenced when required. The primary purpose is to present design curves utilizing the material properties. The procedures are applicable to both TZM and D-36, unless noted.

1. Selection of Facing Thickness

The selected panel facing should be thick enough to withstand the limit design load without yielding and the ultimate design load without failure. The material tensile allowables for ultimate strengths are shown in Figs. 189 and 203. These can be used directly to determine the required panel facing thickness for axial tension.

The D-36 columbium allowable axial compression stress used to determine required facing thickness should be no larger than that given in Fig. 175. Before this allowable is used, checks should be made to show that the critical local and general instability stresses are equal or higher. This can be accomplished with the procedures defined in Subsections 2 and 3 of this section.

The interaction curve provided in Fig. 219 is recommended for D-36 columbium. This curve is possibly conservative in the regions of biaxial compression or tension; for designs in this region, it is recommended that special biaxial tests be performed. This curve represents critical material and configuration allowables and should be used only when the critical instability stresses are higher.

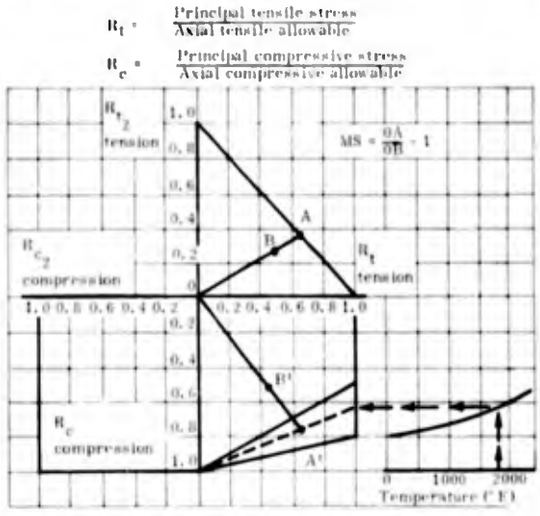

Fig. 219. Interaction Curve for D-36 Columbium Sandwich Panels

The TZM panel strengths can be approximated by utilizing the tensile strengths shown in Fig. 203. However, it is recommended that supplementary tests be performed with the selected braze alloy before final design approval. For combined load, the Maximum Shear Stress Theory of Failure

(Ref. 43) should predict the ultimate material strength satisfactorily. No design allowables should be utilized that are stronger than the critical instability stresses.

In high temperature panel systems, the thermal stresses during transient heating should not be higher than the short-time creep rupture strength of the facing material, and the steady-state temperature thermal stresses should produce only negligible creep during the thermal life of the vehicle. Thermal stresses lower than facing material creep rupture strength will not cause fracture but can cause excessive permanent structural deformation.

2. General Instability

The honeycomb core must be thick enough and have a high enough shear modulus to prevent general buckling of the panel. The formula for critical general instability stress of a honeycomb panel with similar isotropic facings is

$$F_{cr_{1,2}} = \frac{\pi^2 K}{4} \frac{t_1 t_2}{(t_1 + t_2)^2} \left(\frac{h}{b}\right)^2 \frac{E'_{1,2}}{\lambda} \quad (29)$$

where

t_1 and t_2 = panel facing thickness.

Because E' is proportional to F_{cr}, the equation is usually transformed to

$$\frac{F_{cr_{1,2}}^{\lambda}}{E'_{1,2}} = \frac{\pi^2 K}{4} \frac{t_1 t_2}{(t_1 + t_2)^2} \left(\frac{h}{b}\right)^2 \quad (30)$$

Design nomographs for solution of the above equation are presented in Part III of MIL-HDBK-23. These provide a general solution of the equation for both shear and compression instability, with various edge support conditions and for isotropic and orthotropic cores. The nomographs are presented in such a manner that they can be used with any materials. The required material properties are G_c, E', μ and F_c/E'. To simplify the solution of this equation for D-36 and TZM, two curves, in addition to the G_c versus temperature curve (Fig. 202), were prepared. These are $F_c\lambda/E'$ versus N_x/t_f (Fig. 220) and $F_s\lambda/E'$ versus N_{xy}/t (Fig. 221), with individual curves for various temperatures. They can be used along with the procedures in Chapters II and III, Part III of MIL-HDBK-23, to determine the required h and G_c to prevent panel buckling.

To determine critical general instability stresses for panels under combined loads, the procedures in Forrest Product Laboratory Report Nos. 1857 and 1859 can be utilized (Refs. 44 and 45).

3. Local Instability

A. Dimpling

The facings must have a honeycomb core cell size such that dimpling of the facings into the core cells will not occur at the facing stress caused by limit load, where the critical dimpling stress is given by

$$F_{cr} = 2 \frac{E'}{\lambda} \left(\frac{t_f}{S}\right)^2 \quad (8)$$

This equation is usually written in the form

where

t_f = facing thickness

S = cell size

$\lambda = 1 - \mu^2$ (μ = Poisson's ratio).

A nomograph was made for use in determining the critical honeycomb cell size from the edgewise facing load, thickness and temperature.

To find the critical cell size, the nomograph is entered with N_{xy}/t_f (Fig. 220) or N_x/t_f (Fig. 221) and temperature, and followed through with Fig. 222, as marked to determine cell size s. If critical cell size is between the standard sizes (1/8, 3/16 and 1/4 in.), the next smaller standard size is recommended. If a size less than 1/8 in. is required, then a new required facing thickness, based on the 1/8-in. cell size, should be used. To determine the margin of safety with the cell size. and facing thickness, the nomograph can be used in reverse.

b. Face wrinkling

The core must be stiff enough, and the sandwich flatwise tensile strength and core flatwise compressive strength must be great enough, so that face wrinkling will not occur. The critical facing stress at which wrinkling of thin facings will occur can be calculated with the equation

$$F_{cw} = 0.85 \sqrt[3]{E' E_c G_c} \quad . \quad (28)$$

This empirical formula does not include direct strength parameters for the core and

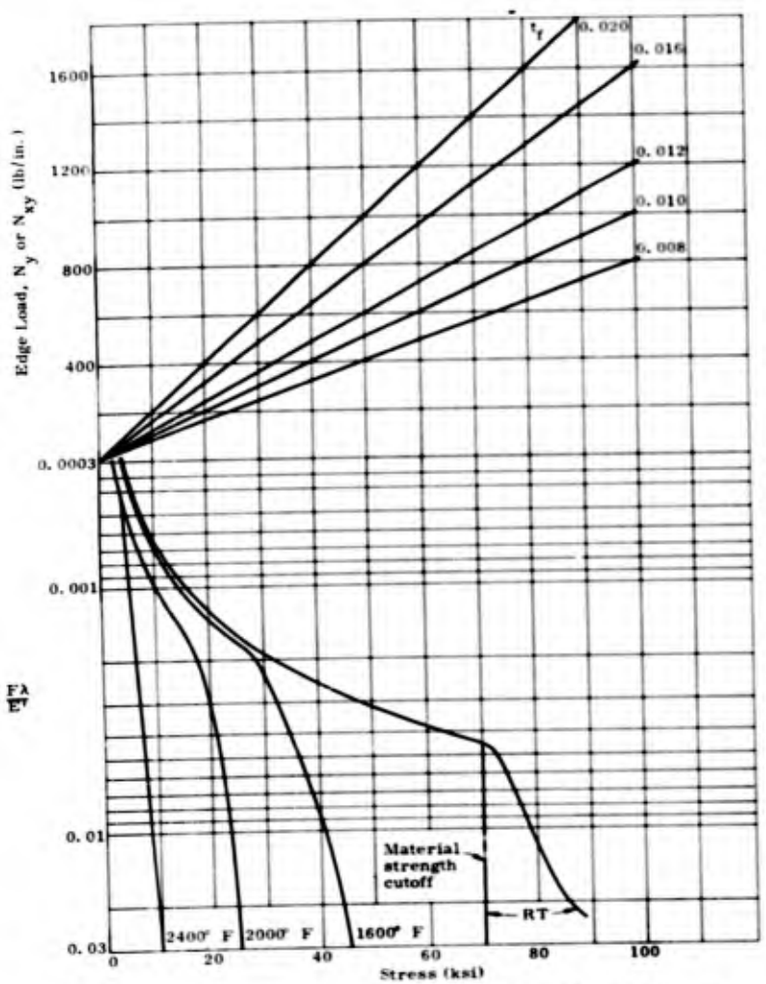

Fig. 220. B-36 Columbium Plasticity Correction Curve--Tension and Shear

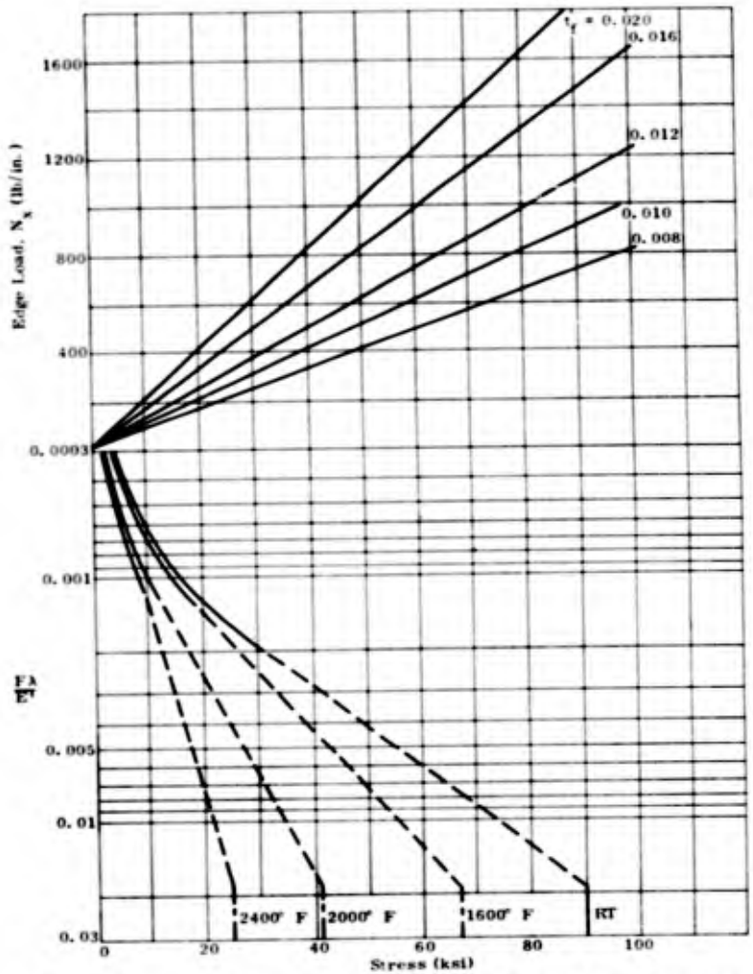

Fig. 221. B-36 Columbium Plasticity Corrective Curve--Compression

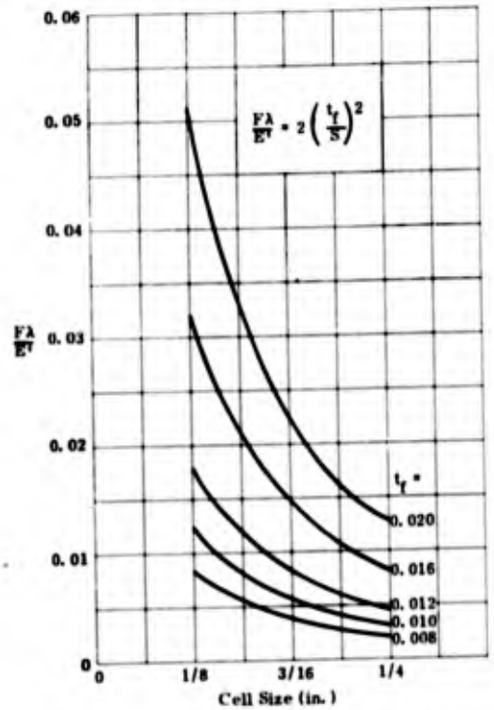

Fig. 222. Maximum Facing Stress at Which Dimpling Will Not Occur

the braze joints, but the core strength is accounted for with the proportional parameters E_cG_c. For brazed sandwich construction, the braze fillet strength is stronger than the core and, for most cases, can be neglected.

To aid in the solution of the formula for sandwich panel design, special nomographs were plotted (Figs. 223 and 224). With the edgewise compression or shear load and the design temperature known, the required core moduli can be found, or inversely, with the core moduli and temperature known, the critical edgewise compression load can be determined.

It is recommended that small edgewise compression specimens be tested before the final design is approved, if a core density lower than that used in this program is selected.

4. Heat Shield Panel Design

An analysis procedure for the heat shield panels was developed in the preliminary design and analysis phase of the program (Appendix B). The nomographs developed as part of this study can be used to determine the required facing thickness. The core strength requirements can be determined once the panel design load and support clip configuration have been determined. Appendix F also presents a method for determining panel deflections due to a thermal gradient through the panel and due to applied loads.

5. Honeycomb Core Strengths

Design allowables for the 3/16-in. cell, 0.002-in. foil thickness honeycomb cores of both TZM and D-36 were determined from the small specimen test data (Figs. 199 through 202 and 210 through 213). The strengths for honeycomb cores other than 3/16-0.002-in. core can be determined with the prediction equations used in the preliminary design and analysis phase of the program. However, if a core having a density less than 8 lb/cu ft or higher than 12 lb/cu ft is used, it is recommended that small specimen tests be used to check out these properties.

6. General Design Restrictions

Refractory metal honeycomb sandwich panels should be designed for sealing of all joints and entries into core area either by brazing or welding. Before brazing alone is used to seal the joint, it is recommended that the compatibility of the coating and braze alloy be evaluated at elevated temperatures. Even when a compatible braze alloy is used, the joints should still be designed so that they can be sealed by welding, if required. This is recommended to provide capabilities of repair in case of braze voids or pin holes that might allow air to enter the honeycomb core area.

A nonperforated core should be utilized to prevent air that might enter from filling the entire panel. The panels must be sealed in a vacuum or at reduced pressures to prevent adverse internal pressure buildup during high temperature exposure.

The outer surface discontinuities must be held to an absolute minimum to prevent unnecessary hot spots on the panels. Depth and width of edge slots should be kept to a minimum. The panels should be designed to minimize deflection during the critical periods of aerodynamic heating.

7. Optimum Panel Design

For each honeycomb panel design application (size and temperature), there is an optimum core density, facing thickness and panel thickness which represent a minimum weight structure capable of resisting the design loads. Consider, for instance, a hypothetical design problem where the panels must stand with an inplane compressive load of

NOTE: For 3/16--0.002 inch thick foil core use temperature correction curve, for other cores use E_c and G_c curves

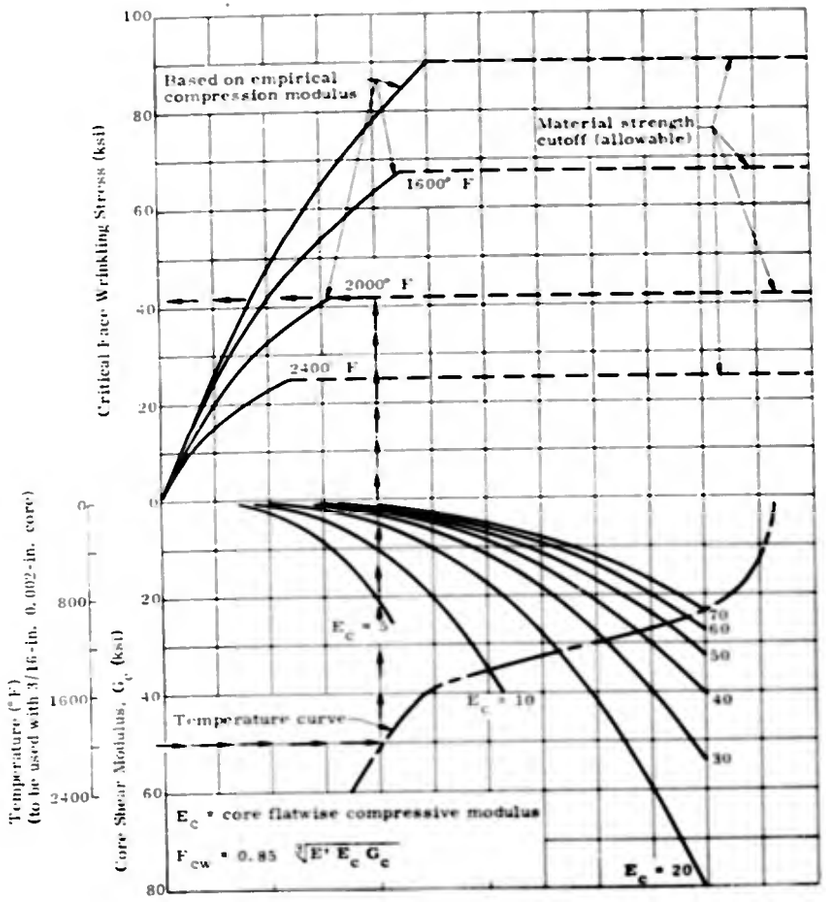

Fig. 223. Nomograph for Determining Critical F_{cw}: D-36 Columbium--Compression

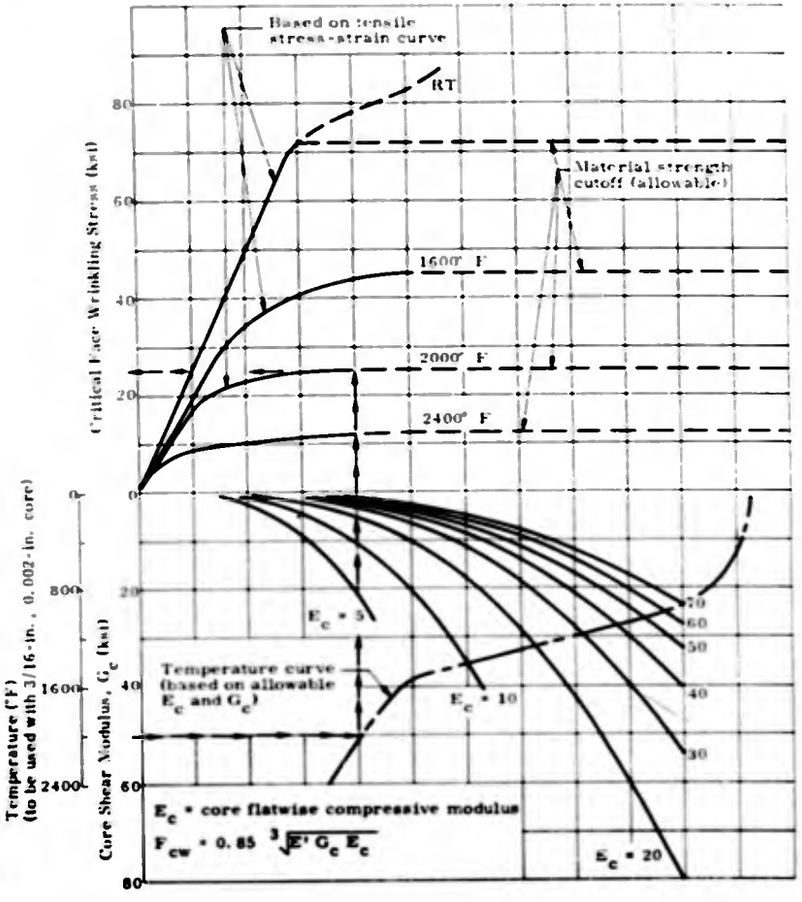

Fig. 224. Nomograph for Determining Critical F_{cw}: D-36 Columbium--Shear

N_{x_1} at RT, N_{x_2} at 2000° F and N_{x_3} at 2400° F. A panel under these conditions can be critical in three modes of failure: intercellular dimpling, face wrinkling and general instability. Since the critical dimpling stress is dependent upon cell size, it can be varied without affecting the panel weight, by allowing the core density to remain constant while changing the t_c/s ratio. This means that unless the facings are less than 0.008 in. thick, the critical dimpling stress does not enter into the optimum panel design configuration except for determining cell size. The face wrinkling stress is dependent upon the core stiffness and the facing stiffness. This is a function of core density and the stress level in the facings. Only in core density does it affect panel weight, and this has only a negligible effect on the optimum panel thickness, as will be explained later. The general instability equation, which is primarily a function of h^2, has the greatest effect on the optimum panel configuration.

The general instability equation can be used to determine the optimum panel thickness; however, it does not lend itself to a simple solution, since it must be solved iteratively because of the dependency of K and E on the facing stress. By making certain simplifying assumptions concerning K, the equation can be solved with reasonable accuracy. This is accomplished by assuming $G_c = \alpha$, which results in a value of K which is dependent upon the panel edge support condition only. The equation for strength to weight is

$$N_x = \frac{\pi^2 K E'}{4\lambda t_f}\left(\frac{h}{b}\right)^2 \quad \text{at } T = RT,$$

2000° F, 2400° F

The simplest solution to this equation is found by first plotting the solution to

$$\frac{N_x}{W} = \frac{\frac{\pi^2 K E'}{4\lambda t_f}\left(\frac{h}{b}\right)^2}{2t_f\rho_f + h\rho_c}.$$

on a coordinate axis with N_x versus h and curves for several pertinent t_f's. Then this curve is basically divided by the panel weight

$$W = 2t_f\rho_f + h\rho_c.$$

In this study the weight of the braze alloy is neglected since it is constant for both cases. The optimum panel is obtained by picking a value of h at the highest point of the curve, so that an h, t_f combination provides an equal or higher N_x capability. This should be evaluated at each of the separate design temperatures to attain the most severe panel design conditions.

Once t_f and h are obtained by this method, they can be put back in the critical instability equation and a new critical N_x value obtained. In this solution the proper value of G_c is used in determining K. This new N_x value can be compared with that obtained from the optimum design procedure to determine if any iterations of the procedure are required.

In using a plasticity correction factor, E', in the general instability equation, the other factors within their normal variance have an insignificant effect on the critical panel instability stress. The optimum panel thickness usually occurs at a facing stress equal to yield stress of the material. Any small modifications in core density to obtain the required critical instability stress or face wrinkling produce a negligible effect on the optimum panel thickness.

8. Analysis of Thermal Gradient Through Honeycomb Panels

With a heating cycle to the outer surface of a honeycomb panel, it is desired to determine the thermal gradient between the outer and inner faces of the panel. A procedure developed by Swann and Pittman (Refs. 46 and 47) was used to analyze the problem. This is a method for determining the effective thermal conductivity at the panel's mean temperature during steady-state conditions.

To utilize the above method for transient heating conditions, steady-state conditions were assumed to exist during small successive time intervals. The effective thermal conductivity used includes the three modes of heat transfer: radiation, conduction, and convection. With the panel configuration given, and an inside surface temperature at the end of a time interval assumed, the effective thermal conductivity during that time interval was determined. With this effective thermal conductivity,

the inside surface temperature was calculated by using a genneral heat balance equation until the assumed and calculated values of the inside surface temperature agreed. Then an inside surface temperature at the end of the next time increment was assumed, etc.

A solution of the equation was obtained by taking an outer face temperature (T_o) at each 0.5-second time interval, and assuming a mean temperature and an inner face temperature (T_{i_2}). The following equations were used to determine $\bar{T}_o$ and $\bar{T}_{i_2}$.

$$\bar{T}_o = \left(\frac{\sigma e L}{K \Delta A}\right)^{1/3} T_o$$

$$\bar{T}_{i2} = \left(\frac{\sigma e L}{K \Delta A}\right)^{1/3} T_{i2}$$

These were substituted into

$$\frac{Ke}{K\Delta A} = 1.0 + 0.664\,(\lambda + 0.3)^{-0.69}\, e^{1.63(1 + \lambda)^{-0.89}} \left(T_o^2 + T_{i2}^2\right)\left(\bar{T}_o + \bar{T}_{i2}\right)$$

where $\lambda = \frac{L}{D}$ (L = thickness of panel and D = cell diameter). From this equation and the material properties, the effective conductivity Ke was calculated. The heat flow through the panel was then determined with

$$q = \frac{Ke}{L}\,(T_o - T_{i2})$$

Now with the calculated heat flow through the panel based on assumed T_{i_2}, a new T_{i_2} was calculated with the heat balance equation and this heat flow, or

$$q\Delta t = We\,(C_p)\,(T_{i2} - T_{i2})$$

where

We = weight of core (lb/sq ft) plus weight of inner face (lb/sq ft)

T_{i_1} = temperature of inner surface at beginning of the time increment

T_{i_2} = temperature of inner surface at end of the time increment.

The new T_{i_2} was then compared to the assumed value. This process was then repeated until the proper agreement was obtained.

This solution was programmed for the IBM 1620 computer (flow diagram shown, pg 140) and two example problems were evaluated. One was the case of a panel at a steady-state temperature of 2440° F which was heated at a rate of 50° F/sec to 2750° F, then held at this temperature 10 seconds and cooled at a rate of 15° F/sec for 32 seconds (Figs. 225 and 226). In the other, the panel was heated from room temperature to 3000° F at the rate of 400° F/sec (Figs. 227 and 228). Different curves which represent temperatures caused by different panel thicknesses are indicated on these figures.

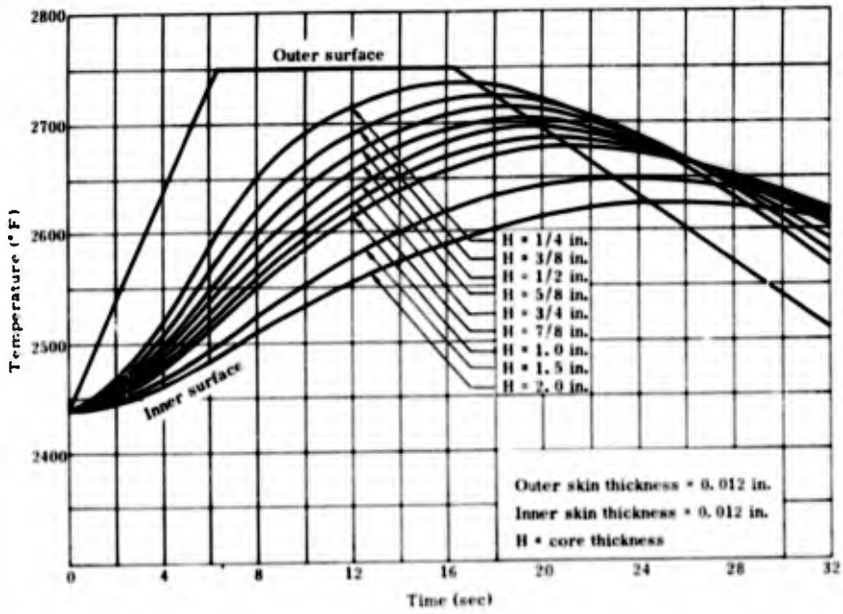

Fig. 225. Outer and Inner Surface Temperatures of Molybdenum Honeycomb During a Thermal Shock

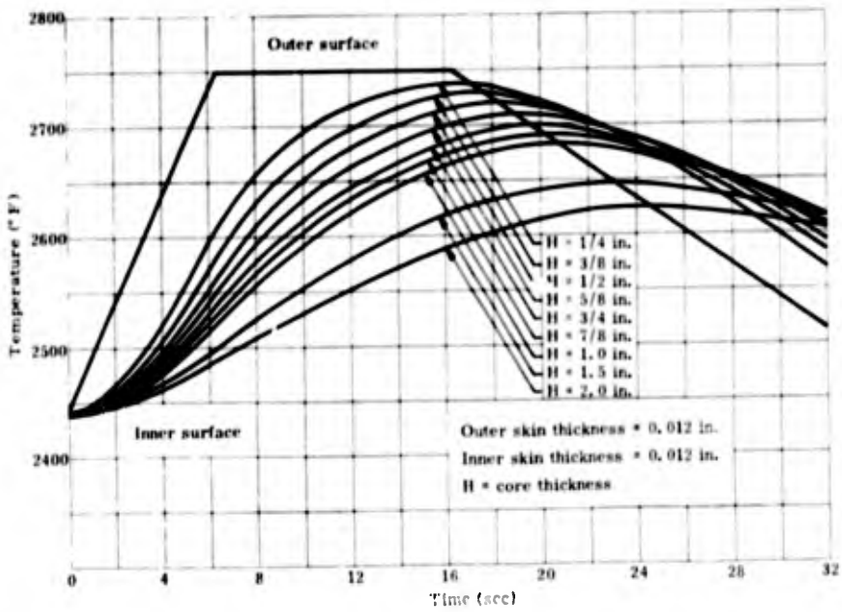

Fig. 226. Outer and Inner Surface Temperatures of Columbium Honeycomb During a Thermal Shock

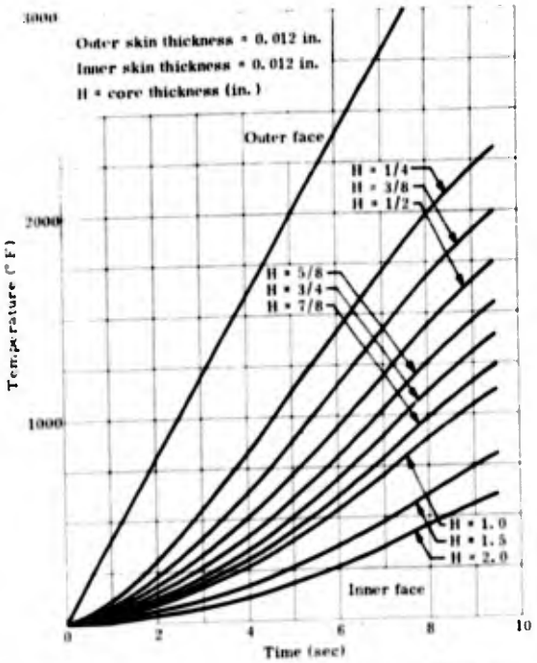

Fig. 227. Outer and Inner Surface Temperature of Molybdenum Honeycomb During a Thermal Shock

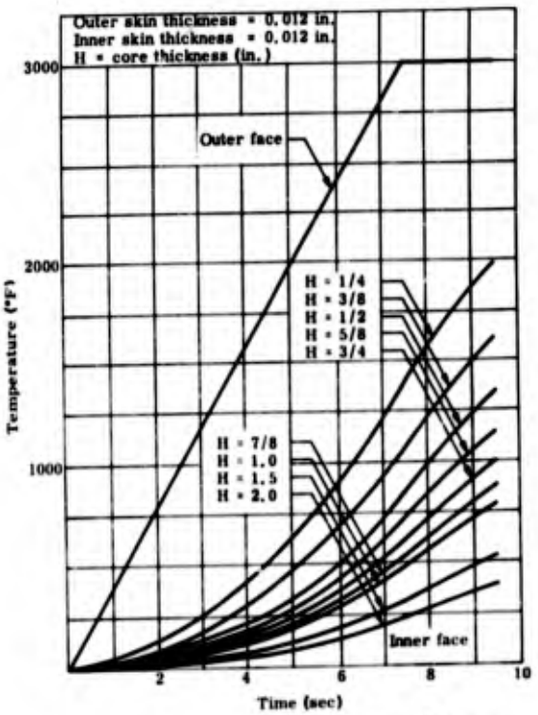

Fig. 228. Outer and Inner Surface Temperature of Columbium Honeycomb During a Thermal Shock

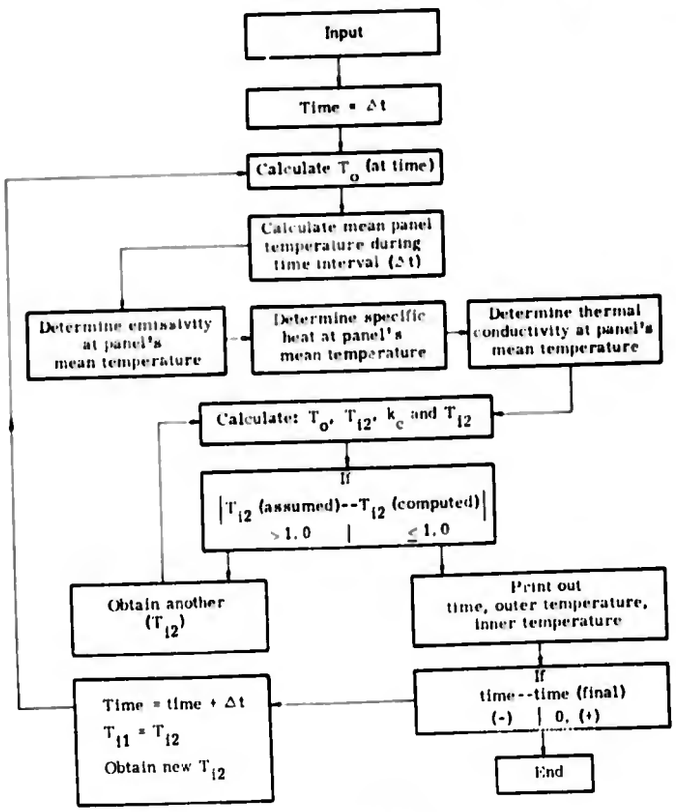

Flow Diagram

VIII. SPECIAL FLIGHT PANELS

In addition to the development investigation of the materials, design, analysis and fabrication of refractory metal honeycomb panels, which comprised by far the greater portion of the program, an experimental panel system for use as a radiation heat shield on a proposed re-entry vehicle was constructed. This system consisted of two D-36 columbium honeycomb panels with the necessary fairing strips, attachment details and instrumentation for flight application. Although the primary design, analyses and fabrication procedures used in the manufacture of this panel system were developed as a result of the basic investigation portion of the program, there were several innovations in both design and fabrication.

A. PANEL SYSTEM DESIGN

Since the primary function of the panel system was to be thermal protection rather than structural application, a modular stand-off panel arrangement was selected as the basic foundation for the panel system design (Fig. 229). For simplicity, since special edge designs were required, the flat structural panel (Dwg No. SK 46841, Appendix A) was utilized as the panel configuration for the two-panel systems. However, 0.010-in. facings were used for the experimental panels, instead of the 0.012-in. structural panel facings, to reduce panel weight (Dwg No. SK 46915, Appendix A).

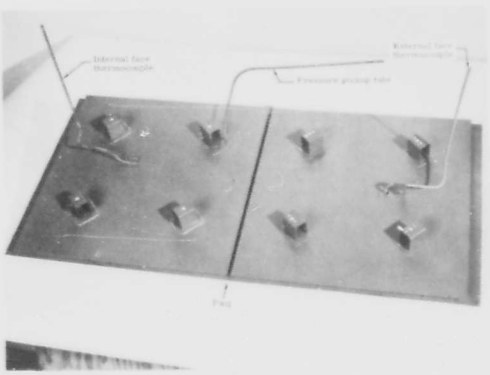

Fig. 229. Experimental Panel System

To satisfy the stand-off mounting arrangement, 0.025-in. U-shaped legs were provided for attachment of the panels to the substructure of the proposed vehicle. Four attachment legs per panel were used, which were located on 6-in. centers (approximately on the panel quarter points). Each leg was oriented at a 45-deg angle to the panel centerlines to allow the panel to thermally expand with a minimum of restraint.

Fairing strips were used on the panels to provide an aerodynamically smooth external surface and to prevent the hot boundary layer gases from entering the installation area behind the panel. This was necessary because, in a modular heat shield arrangement, gaps exist between the panels. These gaps provide for the thermal expansion of the panels when heated. A gap of 0.2 in. was allowed between the two panels since each panel expanded approximately 0.108 in. upon heating to 2000° F (representative temperature). A stepped fairing strip was attached to one of the panels to fill the gap between the two experimental panels. An integral fairing strip was incorporated on the forward external face of both panels by stepping the extended U-channel facing flange. The outboard edge fairing strips were initially conceived as extensions of the outside facing of the panels. However, these had to be removed when warpage problems were encountered during the coating operation (discussed in detail in Section C, Panel System Fabrication).

Provisions for measuring pressure and temperature were incorporated in the panel system. A columbium (Cb-1Zr) pressure pickup tube (0.156-in. OD, 0.017-in. wall) was attached to the external face of the -19 panel to provide for the pressure measuring requirement. Because of the problems associated with attaching thermocouples to coated surfaces (Chapter VII), a mechanical attachment method was used for both thermocouples. The external face thermocouple installation for the -9 panel was accomplished by inserting a 0.250-in. OD columbium tube between the two faces of the panel. The sheath thermocouple could then be inserted into the tube with the measuring junction contacting the panel external face. The thermocouple was held in place by a "scissor" thermocouple holder attached to the inner face (Fig. 230). The inside face thermocouple installation on the -19 panel was of the same design as that used on the SK 46843 heat shield panel. Both thermocouples were placed in the same relative positions on the respective panels so that the thermal gradient

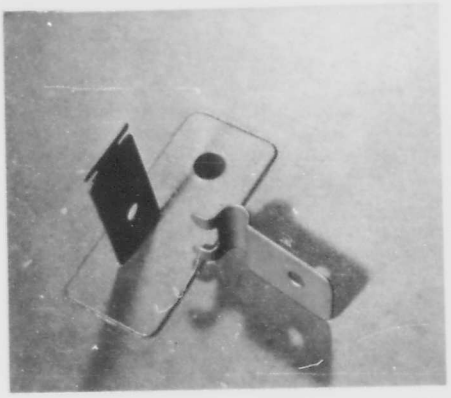

Fig. 230. External Face Thermocouple Holder

through the panels could be determined. It was assumed that the same thermal environment would be imposed on both panels.

B. PANEL SYSTEM ANALYSIS

To qualify the panel system for flight-worthiness, structural and thermal analyses were performed. Representative trajectories for a high lift-to-drag re-entry vehicle were used to obtain the structural and thermal inputs. The structural analysis consisted of determining the margins of safety of the critical areas of the panels, which were:

Environment		
Air Load	Temperature (°F)	Critical Area
4.5 psi (compression)	600	Facing at attachment clip; core at attachment clip; attachment clip.
2.0 psi (tension)	600	Facing at attachment clip; attachment clip.
1.0 psi (tension)	2250	Facing at attachment clip; attachment clip.
28 lb-in. (handling torque)		Nut plate installation; attachment clip.

All of the margins of safety for these critical elements were quite high and the panel system was considered structurally satisfactory.

A low angle-of-attack trajectory was selected for the thermal analysis because it would provide the maximum thermal energy input to the panel system and, consequently, the maximum vehicle substructure temperatures. The thermal analysis was accomplished by converting the equilibrium wall temperature to a hot wall heating rate versus time, so that the heat sink effect of the panels would be represented. This heating rate was imposed upon the panel system and analyzed with a four-dimensional transient heat transfer program (Ref. 48).

Two panel areas were analyzed--one at the attachment leg, the other at an area removed from the attachment leg. A two-dimensional analysis was accomplished at the attachment leg, and a one-dimensional analysis was performed for the isolated area. Figures 231 and 232 depict the resultant outer face and inner support temperatures for the low angle-of-attack trajectory.

The maximum substructure temperature

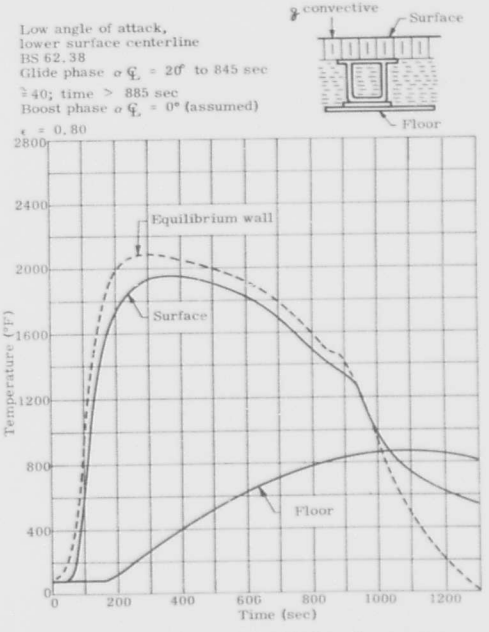

Fig. 231. Maximum Q Condition Temperature Distribution with Clip

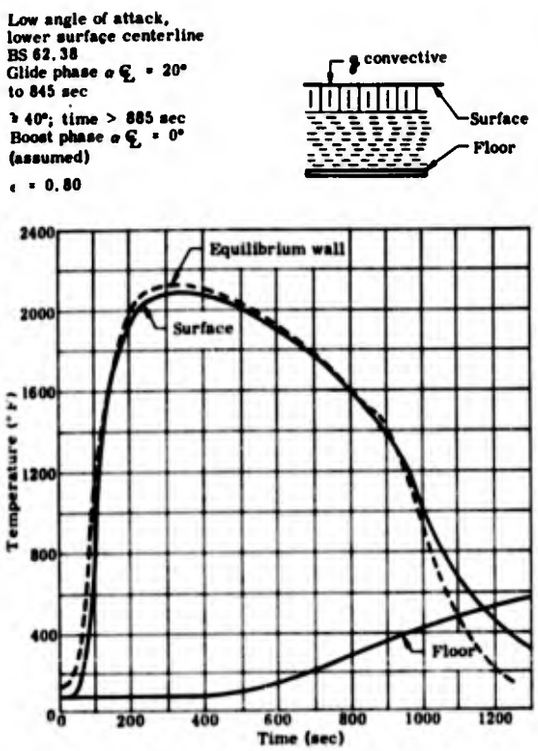

Fig. 232. Maximum Q Condition Temperature Distribution Without Clip

during the glide portion of the flight was 860° F at 1050 sec. The analysis is conservative to the extent that it does not consider the heat loss from the floor to the internal structure and equipment.

C. PANEL SYSTEM FABRICATION

The general philosophy was to accomplish as much of the panel assembly as possible during and before the panel brazing operation, to eliminate the post-braze welding problems experienced during the earlier fabrication efforts on the structural and heat shield panels.

Prior to brazing, the necessary panel details were made. The only innovation in the basic panel detail preparation was that the external facing and U-channel flange edges were brake-formed to simulate the forward fairing strip. The thermocouple insert tube and holder and the attachment legs were assembled and electron beam welded. The pressure tube was electron beam welded to the external skin of the -19 panel.

The brazing operation for the experimental panels was unique in that two braze alloy systems were used instead of the usual one. A 60% Cr-40% Ti powder was used around all of the exposed edges of the panels. This was done to ensure compatibility of the coating and the braze alloy, thus eliminating the requirement for electron beam weld sealing of the braze joints (the Cr-Ti powder is the same as that used in the initial step of the Cr-Ti-Si coating process). B-120 VCA titanium braze alloy was used to braze the remaining areas. Minor difficulty was incurred, because of the varying grain size of the Cr-Ti powder, which caused small voids in the edge braze. However, this was easily remedied by finely crushing the powder. Another important feature of the two-braze alloy system was that edge gaps that were created by layup misalignments, irregularities, etc., could easily be filled by rebrazing with the Cr-Ti powder at lower temperatures (Cr-Ti powder flows at 2550° F), or sealed by electron beam welding.

The brazing of the panels encompassed the final assembly of the panel system. The external face thermocouple installation on the -19 panel, the panel attachment legs and the pressure tube were installed by brazing. Consequently, the only operations remaining, after panel brazing, were the electron beam welding of the thermocouple holder to the -9 panel and the electron beam welding of the center fairing strip to the -9 panel. After these operations were accomplished, the panels were cleaned and readied for application of the oxidation protective coating.

D. PANEL SYSTEM COATING

The Cr-Ti-Si oxidation protective coating was used on the experimental panels. Generally, the results of the coating process were satisfactory, with one exception. The outboard extensions (fairings) of panel external faces were warped after the coating operation. This was caused by the relatively severe thermal environment of the coating process (Cr-Ti stage: 8 hr at 2300° F; Si stage: 4 hr at 2000° F) on the unsupported edges of the thin facings (0.010-in. thick).

To determine a suitable repair for the warped facing extensions, a recoating study was performed. Basically, the approach was to remove the edges and recoat. Two coating techniques were considered. One was to recoat the panels with just the silicide portion of the Cr-Ti-Si process, since the panel system operating temperature was to be 2300° F maximum. The other was to coat just the exposed edge of the facing with the LB-2 slurry coating process (Cr-Al-Si). This coating process is much less severe than the Cr-Ti-Si process, since the maxi-

mum coating temperature is 1950° F for only one hour. Previously, Cr-Ti-Si coated specimens with exposed edges were recoated by both processes and subjected to oxidation tests at temperatures to 2400° F. Both recoating processes worked satisfactorily, with each exhibiting a small failure on one specimen after a one-hour exposure at 2400° F. Other specimens from both processes lasted two hours at 2400° F. After considering both coating processes, the LB-2 coating was selected to recoat the panel edges, because it involved a less severe thermal environment and could be applied locally.

After the panel edges were recoated, the panel systems were delivered to the Manufacturing Technology Division at ASD.

IX. CONCLUSIONS

This section presents significant conclusions in the areas of panel design, fabrication and testing that were a result of this investigation.

D-36 columbium honeycomb sandwich panels suitable for re-entry vehicle applications can be designed and fabricated for use up to 2400° F. While the structural panel strengths are consistent, the low creep strength of the alloy tends to limit the structural application of this material above 2300° F. The heat shield panels exhibited a short time capability at 2600° F. However, the operational temperatures must be kept sufficiently low so that local hot spots will not exceed the protection capabilities of the coatings. Surface irregularities in the panels or between the mold lines of adjacent panels cause hot spots and must be minimized.

Recrystallization characteristics of the TZM molybdenum alloy seriously restrict the fabrication capabilities of this alloy for high temperature re-entry vehicle application. Because of embrittlement, the structural integrity is destroyed. Suitable braze alloys require development that will not recrystallize TZM during the brazing cycle, yet have adequate high temperature strength for vehicle application. These braze alloys must be compatible with TZM and the oxidation protective coating during coating application and subsequent service exposure. Until such braze alloys can be developed, brazed TZM panels cannot be fabricated satisfactorily by any of the techniques explored during this investigation. Haynes 25 is unsatisfactory as a braze alloy for TZM. The 2550° F brazing temperature is generally too high to avoid recrystallization of TZM in thin sheet gages. Even where the amount of recrystallization can be held to tolerable levels, subsequent diffusion alloying occurs during coating application and service exposure, which results in the formation of brittle intermetallic phases at braze alloy-TZM interfaces.

Cracking of high restraint weldments in TZM molybdenum for edge sealing could not be eliminated. While the initial TZM requirement is the development of suitable brazing alloys, it is evident that, until improved molybdenum alloys and welding techniques are also developed, acceptable panel configurations are limited to those in which welding is not involved or, at the most, held to tolerable minimums.

B-120 VCA brazements on D-36 columbium exhibit excellent strength and ductility at temperatures up to 2600° F. No braze failures were observed in panel or small specimen tests. Heating of D-36 columbium to 3000° F or above for periods of 5 to 15 minutes, as required for brazing with titanium or titanium-based alloys (B-120 VCA), produces excessive grain growth and grain boundary weakening, which appear responsible for intergranular cracking during weld sealing operations and for the fracture characteristics encountered in test. This imposes definite restrictions on panel configurations that can be fabricated satisfactorily for vehicle application. The acceptable configurations are limited to those in which all welding operations are accomplished prior to brazing, as demonstrated in two experimental flight test panels that were fabricated. The brazing cycle increased the room temperature ultimate tensile strength of the D-36, but this effect disappeared at elevated temperature.

Thompson-Ramo-Wooldridge Cr-Ti-Si provided a satisfactory oxidation-protective coating for the D-36 panel tests. No visible coating defects were found on the panels, and no obvious failures occurred because of poor coating performance. It should be noted that the Cr-Ti-Si coating process lowers the room temperature ultimate tensile strength of the coated tensile specimens when compared to the brazed specimens. Also, inelastic panel stresses at temperatures below 1600° F cause spalling of the Cr-Ti-Si coating on D-36 columbium and must be avoided in panel design for vehicle application.

Insufficient tests were conducted to evaluate the performance of the Pfaudler PFR-6 coating on the TZM panels. This coating did perform satisfactorily on TZM bolts and nuts which were used in the shear testing of D-36 structural panels.

D-36 columbium honeycomb core can be produced with generally conventional techniques, employing resistance welding to join the corrugated core material and standard sawing and belt sanding methods to finish the core. Electron beam welding, diamond blade sawing and hot belt sanding are required to process TZM core.

TZM molybdenum and D-36 columbium thin sheet details can be marformed with the addition of special overlay and underlay

techniques and proper lubrication. The D-36 material can be formed at room temperature, but the TZM material required heating to 300° F with specially heated dies.

The practical use of hard refractory metal tooling for successful vacuum brazing of refractory metal honeycomb sandwich panels was demonstrated. However, extreme care must be used in maintaining close tolerances with regard to facing flatness and detail fabrication, since the metal braze tools cannot compensate for these deficiencies.

The D-36 heat shield panels withstood the dynamic thermal environment (hot gas) about half as long as those subjected to the static thermal environment (radiant), thus indicating that panel life as predicted by radiant test is approximately one-half of the life predicated by the hot gas facility tests.

Thermal stresses in honeycomb panels do not appear to affect ultimate panel strengths for single-cycle loading. However, if sustained for long periods at high temperatures, they can produce excessive inelastic deformations in structures which are made of low creep strength materials, such as D-36 columbium. Thermal stresses can, when coupled with applied cyclic loads, produce premature fatigue failures.

Above 2000° F, creep strength is more important than fatigue strength for design. Most of the 2400° F tensile-tensile fatigue test specimens creeped to the maximum elongation possible in the test setup without fracturing.

Fixturing and methods utilized for the small specimen tests were generally satisfactory, but special specimens are needed to obtain more uniform results on the small column compression tests, and improved strain measuring techniques are required for measuring stress-strain relationships of coated tensile specimens above 2000° F.

MIL-HDBK-23 design procedures for sandwich panels are satisfactory when actual material properties generated in the program are used. In general, core properties could be predicted from material properties on the basis of simplified empirical formulas.

X. REFERENCES

1. Houch, J. A., "Physical and Mechanical Properties of Commercial Molybdenum-Base Alloys," Defense Metals Information Center, DMIC Report No. 140, Columbus 1, Ohio, 30 November 1960.

2. "Physical and Mechanical Properties of Columbium-Base Alloys," DMIC Report No. 125, February 1960.

3. "High-Temperature Fasteners," Contract AF33(616)-8104, Republic Aviation Company, ESRD7-4 and ESRD7-7 Quarterly Reports, 10 September 1961.

4. Refractomet Division, Universal-Cyclops Steel Corporation, Molybdenum Specifications, Mill Products, 20 March 1961 to 28 November 1961.

5. Gentry, W. O. and Michael, A. B., "Properties of Some Columbium-Rich Alloys in Columbium-Tantalum-Tungsten-Zirconium System," Fansteel Metallurgical Corporation, North Chicago, Illinois, 26 April 1961.

6. "Refractory Metal Structural Development Program," Part I--Refractory Metal and Development, Part II--Coating Studies and Application, Contract No. AF33(616)-6578, Project Nos. 1368 and 7381, Task Nos. 13719 and 73810, McDonnell Aircraft Corporation, General Electric Company.

7. "Research on Workable Refractory Alloys of Tungsten, Tantalum, Molybdenum and Columbium," Crucible Steel Company of America, Central Research Laboratory, Cambridge, Massachusetts, WADC TR 61-134, May 1961.

8. Lement, B. S., Thomas, D. A., Weissmann, S. and others, "Substructure and Mechanical Properties of Refractory Metals," Manufacturing Laboratories, Inc., Cambridge, Massachusetts, WADC TR 61-181, August 1961.

9. Semchyshen, M. and Barr, R. W., "Extrusion and Mechanical Properties of some Molybdenum- and Tungsten-Base Alloys," Climax Molybdenum Company of Michigan, ASD TR 61-163, June 1961.

10. Climax Molybdenum Corporation, Molybdenum-0.5 Ti and TZM Alloy Specifications.

11. E. I. duPont deNemours, D-14, D-31 and D-36 Alloy Data Sheets, 1961.

12. Private Communications- Fansteel Metallurgical Corporation, FS-82 Alloy.

13. Westinghouse Electric Corporation, B-33, B-66 and B-77 Alloy Data Sheets.

14. Haynes Stellite Company, Haynes Refractory Metal and Alloys, October 1961.

15. Suggested High Strength TZM Specification, Climax Molybdenum Corporation, 21 August 1961.

16. Private Communications--Haynes Stellite Company, Cb-752.

17. Barr, R. W. and Semchyshen, M., "Stress-Strain Curves for Wrought Molybdenum Alloys," Climax Molybdenum Company, New York, N. Y., December 1959.

18. Jefferys, R. A. and Gadd, J. D., "Development and Evaluation of High Temperature Protective Coatings for Columbium Alloys," Part I--Coating Development, ASD TR 61-66, Part I, May 1961, Part II, June 1961.

19. Krier, C. A., "Coatings for the Protection of Refractory Metals from Oxidation," DMIC Report No. 162, 24 November 1961.

20. "Review of Recent Developments on Oxidation-Resistant Coatings for Refractory Metals," DMIC Memorandum No. 120, 31 July 1961.

21. Chao, P. J., Payne, B. S., Jr. and Priest, D. K., "Development of a Cementation Coating Process for High-Temperature Protection of Molybdenum," Contract No. AF33(616)-7192, ASD TR 61-241, June 1961.

22. "Elevated-Temperature Mechanical Properties and Oxidation Resistance of Columbium and its Alloys," DMIC Memorandum No. 8, 4 February 1959.

23. "Coatings for the Protection of Refractory Metal from Oxidation," DMIC Report No. 162, 24 November, 1961.

24. "Review of Recent Developments on Oxidation-Resistant Coatings for Refractory Metals," DMIC Memorandum No. 137.

25. Chao, P. J., Zupan, J. and Priest, D. K., "Recent Development of Oxidation-Resistant Coating of Pfaudler," TR61-15, 14 July 1961.

26. Lawthers, D. D. and Sama, L., "Aluminide and Beryllide Protective Coatings for Tantalum," Sylcor Division, Sylvania Electric Products, Inc., 26 April 1961.

27. Lawthers, D. D. and Sama, L., "High Temperature Oxidation-Resistant Coatings for Tantalum-Base Alloys," Sylcor Division, Sylvania Electric Products, Inc., ASD TR 61-233, Contract AF33(616)-7462, Project No. 7351, Task No. 73512.

28. Aves, W. L., Jr., Bourland, G. W., Featherston, A. B., Forcht, B. A. and O'Kelly, K. P., Vought Astronautics Division, Chance-Vought Corporation, "Diffusion Coating Process for Columbium-Base Alloys," Contract No. AF33(616)-7896, August 1961.

29. Jefferys, R. A. and Gadd, J. D., "Development and Evaluation of High Temperature Protective Coatings for Columbium Alloys, Part II- Coating Evaluation, Thompson-Ramo-Wooldridge, Inc., Contract No. AF33(616)-7215, 30 June 1961.

30. National Symposium on Ceramics and Composites, Coatings and Solid Bodies, Society of Aerospace Materials and Process Engineers, Dayton, Ohio, 14 and 15 November 1961.

31. Anthony, F. M., "Design Fabrication and Testing of a Molybdenum Alloy Outer Wall Heat Shield," Dallas, Texas--Refractory Composites Working Group, 8 to 10 August 1961.

32. Dukes, W. H., Gosden, G. E., Kappelt, G. F. and Mirti, A. E., "Manufacturing Methods for Insulated and Cooled Double-Wall Structures," Final Technical Engineering Report ASD TR 61-7-799, Contract No. AF33(600)-40100, May 1961.

33. Bredzs, N., Ruoy, J. and Schwartzbart, H., "Development of Partially Volatile Brazing Filler Alloys for High Temperature Applications and Resistance to Oxidation," WADD TR 59-404, Part II, June 1961.

34. Armstrong, R., "Exo-Reactant Nickel Base Structural Adhesives," Quarterly Progress Report No. 3, prepared under Navy Bureau of Naval Weapons Contract Now61-0308-c, October 1961.

35. "Development of Low Temperature Brazing of Tungsten for High Temperature Service," Solar Aircraft Company, Interim Reports 1, 2 and 4, prepared under Navy Bureau of Naval Weapons Contract No. 61-0414-c.

36. Hansen, M., "Constitution of Binary Alloys," McGraw-Hill Book Company, 2nd Edition, 1958.

37. Milewski, C. and Robertson, A., "Heating Rate Investigation--Martin 14-Inch Hot Gas Facility," RM-144, Martin Company, Baltimore 3, Maryland, March 1963.

38. "Development of Methods and Instruments for Mechanical Evaluation of Refractory Materials at Very High Temperatures," Battelle Memorial Institute, ASD TR 61-74, May 1961.

39. MIL-STD-401A, Sandwich Constructions and Core Materials, General Test Methods, 15 June 1956.

40. McLean, D., "Mechanical Properties of Metals," John Wiley & Sons, Inc., New York, 1962.

41. Freudenthal, A. M., "The Inelastic Behavior of Engineering Materials and Structures," p 382, John Wiley & Sons, Inc., New York, 1950.

42. Hoff, N. J. and Mantner, S. E., "The Buckling of Sandwich-Type Panels," Polytechnic Institute of Brooklyn, Skydyne, Inc., Journal of Aeronautical Sciences, Vol. 12, 1945.

43. Nadai, A., "Theory of Flow and Fracture of Solids," McGraw-Hill Book Company, Inc., New York, 1950.

44. Kimel, R. W., "Elastic Buckling of a Simply Supported Rectangular Sandwich Panel Subjected to Combined Bending, Compression and Shear," Report No. 1859, Forrest Products Laboratory USDA, November 1956.

X. REFERENCES

1. Houch, J. A., "Physical and Mechanical Properties of Commercial Molybdenum-Base Alloys," Defense Metals Information Center, DMIC Report No. 140, Columbus 1, Ohio, 30 November 1960.

2. "Physical and Mechanical Properties of Columbium-Base Alloys," DMIC Report No. 125, February 1960.

3. "High-Temperature Fasteners," Contract AF33(616)-8104, Republic Aviation Company, ESRD7-4 and ESRD7-7 Quarterly Reports, 10 September 1961.

4. Refractomet Division, Universal-Cyclops Steel Corporation, Molybdenum Specifications, Mill Products, 20 March 1961 to 28 November 1961.

5. Gentry, W. O. and Michael, A. B., "Properties of Some Columbium-Rich Alloys in Columbium-Tantalum-Tungsten-Zirconium System," Fansteel Metallurgical Corporation, North Chicago, Illinois, 26 April 1961.

6. "Refractory Metal Structural Development Program," Part I--Refractory Metal and Development, Part II--Coating Studies and Application, Contract No. AF33(616)-6578, Project Nos. 1368 and 7381, Task Nos. 13719 and 73810, McDonnell Aircraft Corporation, General Electric Company.

7. "Research on Workable Refractory Alloys of Tungsten, Tantalum, Molybdenum and Columbium," Crucible Steel Company of America, Central Research Laboratory, Cambridge, Massachusetts, WADC TR 61-134, May 1961.

8. Lement, B. S., Thomas, D. A., Weissmann, S. and others, "Substructure and Mechanical Properties of Refractory Metals," Manufacturing Laboratories, Inc., Cambridge, Massachusetts, WADC TR 61-181, August 1961.

9. Semchyshen, M. and Barr, R. W., "Extrusion and Mechanical Properties of some Molybdenum- and Tungsten-Base Alloys," Climax Molybdenum Company of Michigan, ASD TR 61-163, June 1961.

10. Climax Molybdenum Corporation, Molybdenum-0.5 Ti and TZM Alloy Specifications.

11. E. I. duPont deNemours, D-14, D-31 and D-36 Alloy Data Sheets, 1961.

12. Private Communications- Fansteel Metallurgical Corporation, FS-82 Alloy.

13. Westinghouse Electric Corporation, B-33, B-63 and B-77 Alloy Data Sheets.

14. Haynes Stellite Company, Haynes Refractory Metal and Alloys, October 1961.

15. Suggested High Strength TZM Specification, Climax Molybdenum Corporation, 21 August 1961.

16. Private Communications--Haynes Stellite Company, Cb-752.

17. Barr, R. W. and Semchyshen, M., "Stress-Strain Curves for Wrought Molybdenum Alloys," Climax Molybdenum Company, New York, N. Y., December 1959.

18. Jefferys, R. A. and Gadd, J. D., "Development and Evaluation of High Temperature Protective Coatings for Columbium Alloys," Part I--Coating Development, ASD TR 61-66, Part I, May 1961, Part II, June 1961.

19. Krier, C. A., "Coatings for the Protection of Refractory Metals from Oxidation," DMIC Report No. 162, 24 November 1961.

20. "Review of Recent Developments on Oxidation-Resistant Coatings for Refractory Metals," DMIC Memorandum No. 120, 31 July 1961.

21. Chao, P. J., Payne, B. S., Jr. and Priest, D. K., "Development of a Cementation Coating Process for High-Temperature Protection of Molybdenum," Contract No. AF33(616)-7192, ASD TR 61-241, June 1961.

22. "Elevated-Temperature Mechanical Properties and Oxidation Resistance of Columbium and its Alloys," DMIC Memorandum No. 8, 4 February 1959.

23. "Coatings for the Protection of Refractory Metal from Oxidation," DMIC Report No. 162, 24 November, 1961.

24. "Review of Recent Developments on Oxidation-Resistant Coatings for Refractory Metals," DMIC Memorandum No. 137.

25. Chao, P. J., Zupan, J. and Priest, D. K., "Recent Development of Oxidation-Resistant Coating of Pfaudler," TR61-15, 14 July 1961.

26. Lawthers, D. D. and Sama, L., "Aluminide and Beryllide Protective Coatings for Tantalum," Sylcor Division, Sylvania Electric Products, Inc., 26 April 1961.

27. Lawthers, D. D. and Sama, L., "High Temperature Oxidation-Resistant Coatings for Tantalum-Base Alloys," Sylcor Division, Sylvania Electric Products, Inc., ASD TR 61-233, Contract AF33(616)-7462, Project No. 7351, Task No. 73512.

28. Aves, W. L., Jr., Bourland, G. W., Featherston, A. B., Forcht, B. A. and O'Kelly, K. P., Vought Astronautics Division, Chance-Vought Corporation, "Diffusion Coating Process for Columbium-Base Alloys," Contract No. AF33(616)-7896, August 1961.

29. Jefferys, R. A. and Gadd, J. D., "Development and Evaluation of High Temperature Protective Coatings for Columbium Alloys, Part II- Coating Evaluation, Thompson-Ramo-Wooldridge, Inc., Contract No. AF33(616)-7215, 30 June 1961.

30. National Symposium on Ceramics and Composites, Coatings and Solid Bodies, Society of Aerospace Materials and Process Engineers, Dayton, Ohio, 14 and 15 November 1961.

31. Anthony, F. M., "Design Fabrication and Testing of a Molybdenum Alloy Outer Wall Heat Shield," Dallas, Texas--Refractory Composites Working Group, 8 to 10 August 1961.

32. Dukes, W. H., Gosden, G. E., Kappelt, G. F. and Mirti, A. E., "Manufacturing Methods for Insulated and Cooled Double-Wall Structures," Final Technical Engineering Report ASD TR 61-7-799, Contract No. AF33(600)-40100, May 1961.

33. Bredzs, N., Ruoy, J. and Schwartzbart, H., "Development of Partially Volatile Brazing Filler Alloys for High Temperature Applications and Resistance to Oxidation," WADD TR 59-404, Part II, June 1961.

34. Armstrong, R., "Exo-Reactant Nickel Base Structural Adhesives," Quarterly Progress Report No. 3, prepared under Navy Bureau of Naval Weapons Contract Now61-0308-c, October 1961.

35. "Development of Low Temperature Brazing of Tungsten for High Temperature Service," Solar Aircraft Company, Interim Reports 1, 2 and 4, prepared under Navy Bureau of Naval Weapons Contract No. 61-0414-c.

36. Hansen, M., "Constitution of Binary Alloys," McGraw-Hill Book Company, 2nd Edition, 1958.

37. Milewski, C. and Robertson, A., "Heating Rate Investigation--Martin 14-Inch Hot Gas Facility," RM-144, Martin Company, Baltimore 3, Maryland, March 1963.

38. "Development of Methods and Instruments for Mechanical Evaluation of Refractory Materials at Very High Temperatures," Battelle Memorial Institute, ASD TR 61-74, May 1961.

39. MIL-STD-401A, Sandwich Constructions and Core Materials, General Test Methods, 15 June 1956.

40. McLean, D., "Mechanical Properties of Metals," John Wiley & Sons, Inc., New York, 1962.

41. Freudenthal, A. M., "The Inelastic Behavior of Engineering Materials and Structures," p 382, John Wiley & Sons, Inc., New York, 1950.

42. Hoff, N. J. and Mantner, S. E., "The Buckling of Sandwich-Type Panels," Polytechnic Institute of Brooklyn, Skydyne, Inc., Journal of Aeronautical Sciences, Vol. 12, 1945.

43. Nadai, A., "Theory of Flow and Fracture of Solids," McGraw-Hill Book Company, Inc., New York, 1950.

44. Kimel, R. W., "Elastic Buckling of a Simply Supported Rectangular Sandwich Panel Subjected to Combined Bending, Compression and Shear," Report No. 1859, Forrest Products Laboratory USDA, November 1956.

45. Kimel, R. W., "Elastic Buckling of a Simply Supported Rectangular Sandwich Panel Subjected to Combined Edgewise Bending and Compression," Report No. 1857, Forrest Products Laboratory, USDA, November 1956.

46. Swann, R. T., "Calculated Effective Thermal Conductivities of Honeycomb Sandwich Panels," NASA TR D-171, December 1959.

47. Swann, R. T. and Pittman, C. M., "Analysis of Effective Thermal Conductivities of Honeycomb and Corrugated-Core Sandwich Panels," NASA TR D-714, April 1961.

48. Sallis, D. and Boogar, E. R., "Transient Heating Digital Analysis for Structural Design," RM-63, Martin Company, Baltimore 3, Maryland, December 1960.

APPENDIX A

REFRACTORY METAL HONEYCOMB TEST PANELS

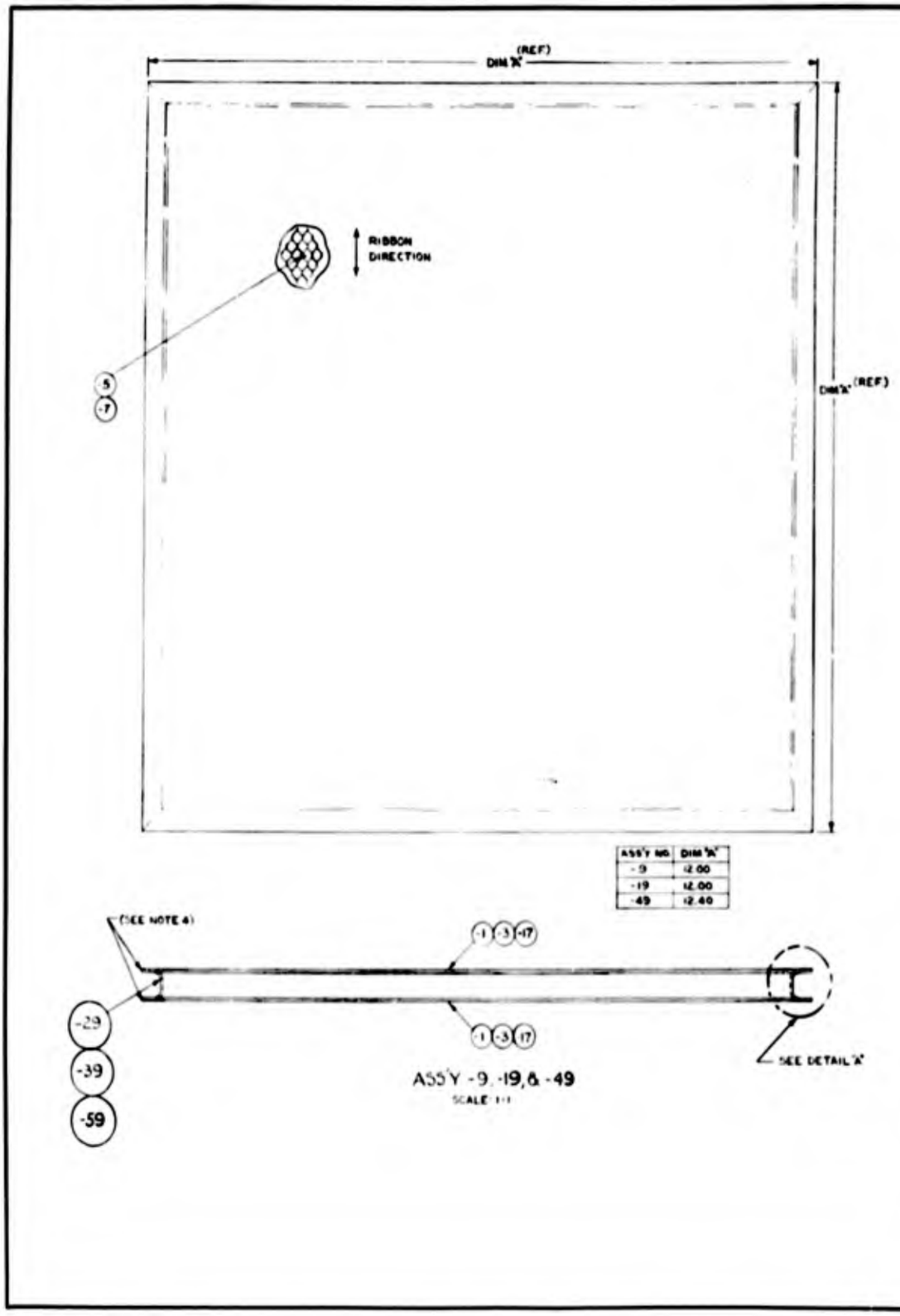
DIM 'A' (REF)
RIBBON DIRECTION
5
-7
DIM 'A' (REF)
ASS'Y NO. | DIM 'A'
-9 | 12.00
-19 | 12.00
-49 | 12.40
(SEE NOTE 4)
-1 -3 -17
-29
-39
-59
SEE DETAIL 'A'
ASS'Y -9, -19, & -49
SCALE 1:1
SK-46041

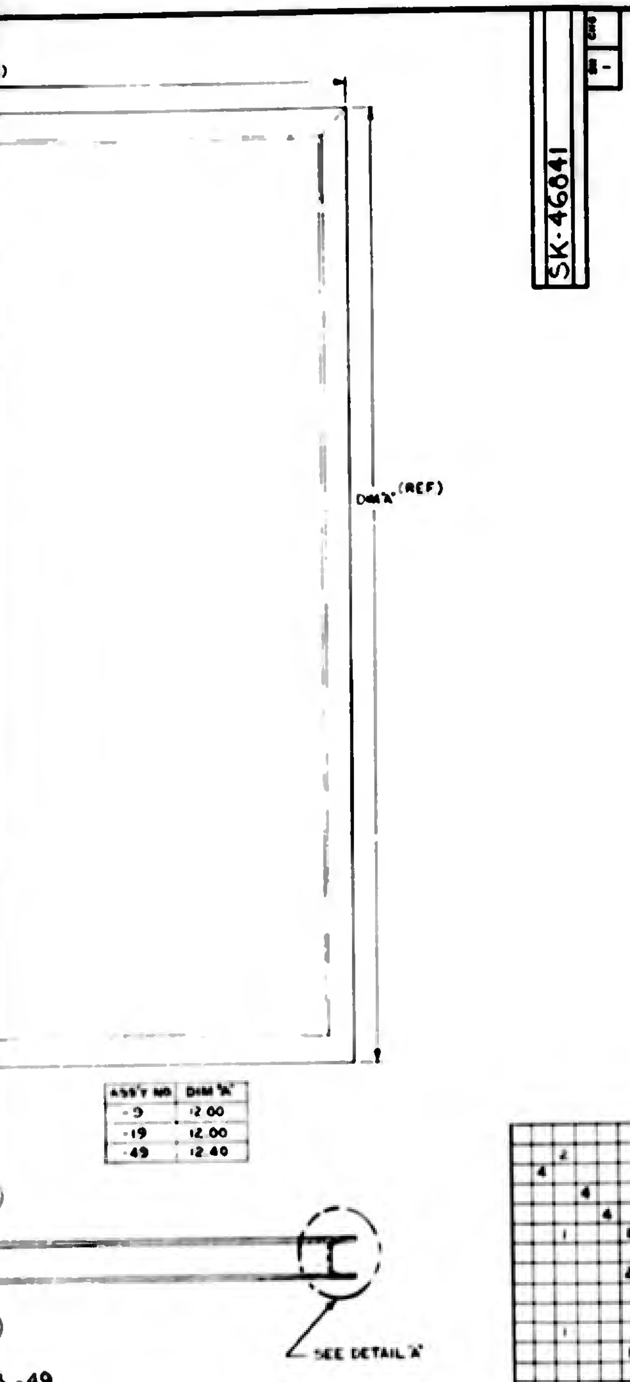

ASS'Y NO	DIM 'A'
-9	12.00
-19	12.00
-49	12.40

REVISIONS				
SYM	ZONE	DESCRIPTION	DATE	APPROVED
A		REVISE NOTES - ADD -49		

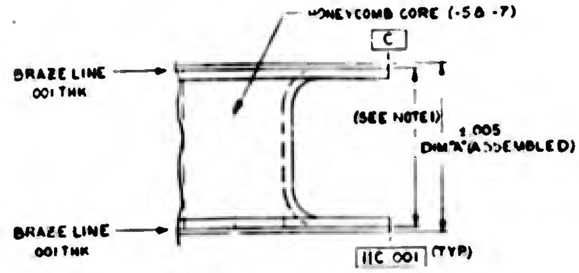

DETAIL 'A'
SCALE 4:1

ASS'Y NO	DIM 'A'
-9	.512
-19	.512
-49	.508

NOTES:
1. HONEYCOMB (-5 & -7) MUST MATCH CHANNEL ASSY'S (-29, -39, -59) WITHIN ±.0015.
2. MINIMUM BEND RADII WILL BE EXPERIMENTALLY DETERMINED UPON RECEIPT OF MATERIALS.
3. FRAMES TO BE HERMETICALLY SEALED BY WELDING (ELECTRON BEAM.)
4. SKINS TO BE WELDED TO FRAME ASSY'S AT EXTERNAL EDGES FOR HERMETICAL SEAL (ALL AROUND) (AFTER BRAZING). (ELECTRON BEAM)
5. HONEYCOMB CORE TO BE SIZED TO INSIDE DIMS OF FRAME ASSY.

FOR ENGR. REF ONLY

-59	-49	-39	-29	-19	-9	PART NO.	DESCRIPTION	STOCK SIZE	MATERIAL OR VENDOR	MATERIAL SPECIFICATION
	2					-17	SKIN	.010 x 12⅝ x 12⅝	Cb ALLOY "D-36	MMS-1691
4						-15	CHANNEL	.025 x 1⅛ x 12⅝	Cb ALLOY "D-36	MMS-1691
		4				-13	CHANNEL	.025 x 1½ x 12¼	Cb ALLOY, "D-36	[illegible]
			4			-11	CHANNEL	.025 x 1½ x 12¼	TZM MOLY ALLOY	[illegible]
	1			1		-7	HONEYCOMB CORE	.002 x ¼ CELL	Cb ALLOY, "D-36	[illegible]
					1	-5	HONEYCOMB CORE	.002 x ¼ CELL	TZM MOLY ALLOY	[illegible]
				2		-3	SKIN	.012 x 12¼ x 12¼	Cb ALLOY, "D-36	[illegible]
					2	-1	SKIN	.012 x 12¼ x 12¼	TZM MOLY ALLOY	[illegible]
	1					-59	ASS'Y, FRAME			
				1		-39	ASS'Y, FRAME			
					1	-29	ASS'Y, FRAME			

LIST OF MATERIAL

DASH NUMBER	NEXT ASSY	QTY. REQD
-49	SK-46915	4
-19		13
-9		13

UNLESS OTHERWISE SPECIFIED DIMENSIONS ARE IN INCHES AND ARE AFTER PLATING.
TOLERANCES ON: FRACTIONS ± 1/32; DECIMALS .X ± .1, .XX ± .03, .XXX ± .010; ANGLES ± 1/2°
MACHINED SURFACES REF. MIL-STD-10 ✓
MIL-I-8500 STATUS: INTERCHANGEABLE / REPLACEABLE / UNCONTROLLED

DRAWN BY HUGHES, DEPT. 2560, DATE 12-18-61

THE MARTIN COMPANY, BALTIMORE, MARYLAND

TEST PANEL
REFRACTORY METALS HONEYCOMB

CODE IDENT NO. 38597 — SIZE D — SK-46841
SHEET 1 OF 2

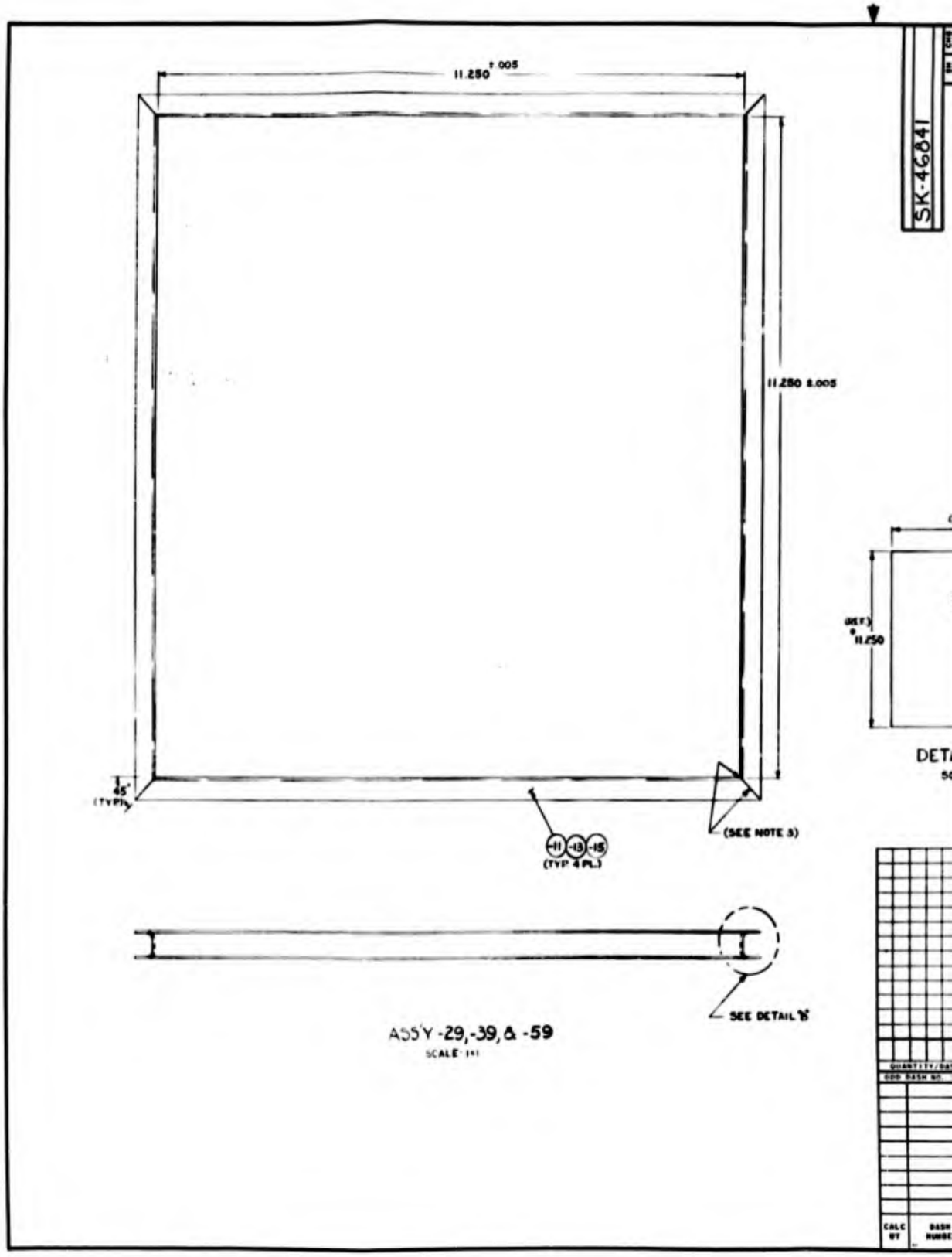
11.250 +.005
11.250 ±.005
SK-46841
45°
(TYP)
-11
-13
-15
(TYP 4 PL.)
(SEE NOTE 3)
SEE DETAIL 'B'
ASS'Y -29, -39, & -59
SCALE: 1=1

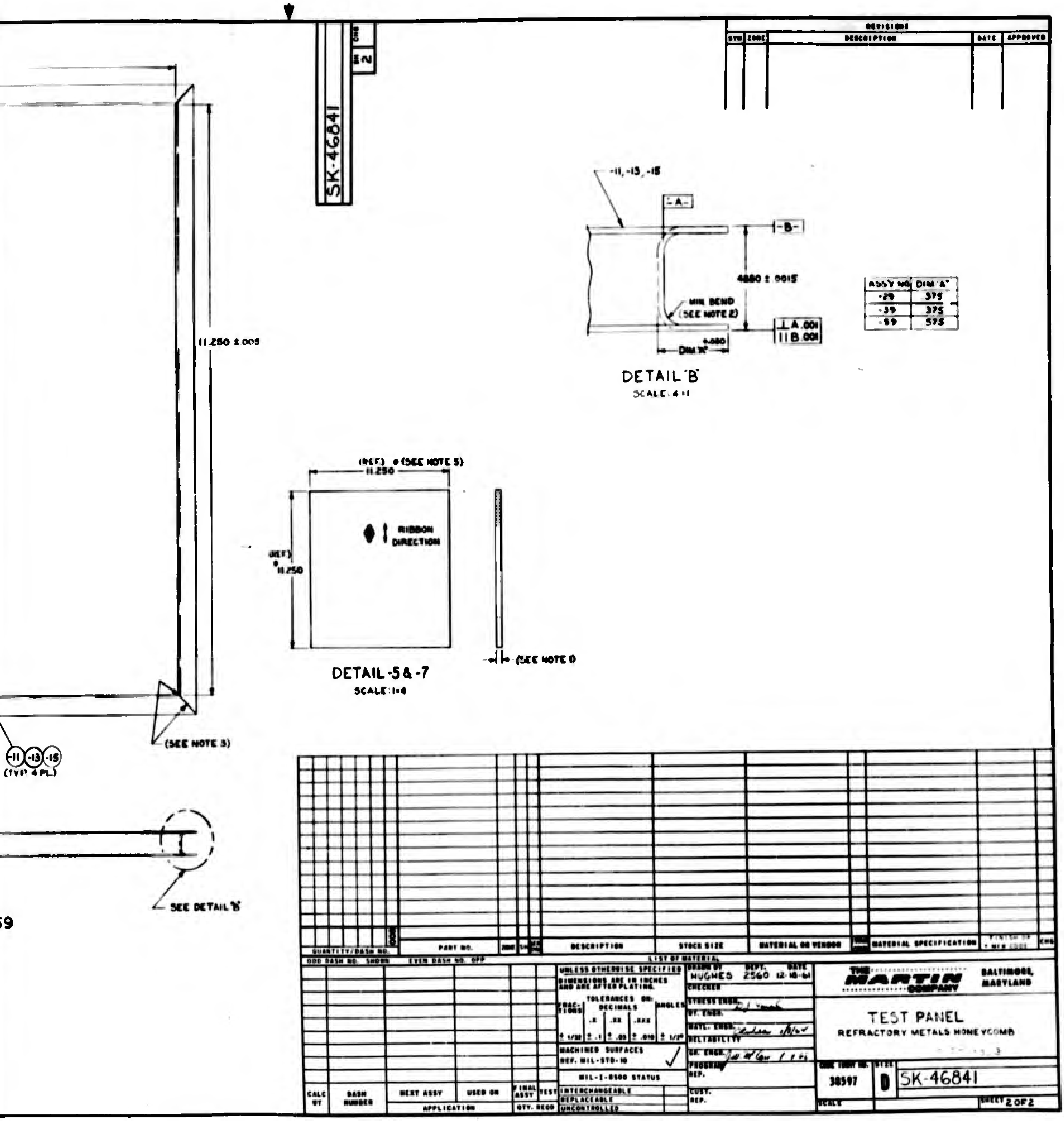
SK-46841
2
REVISIONS
SYM
ZONE
DESCRIPTION
DATE
APPROVED
-11, -13, -15
-A-
-B-
.4880 ± .0015
MIN. BEND (SEE NOTE 2)
⊥ A .001
‖ B .001
DIM "A"
DETAIL 'B'
SCALE: 4=1
ASSY NO. | DIM "A"
-29 | .375
-39 | .375
-59 | .575
11.250 ±.005
(REF) ⌀ (SEE NOTE 5)
11.250
RIBBON DIRECTION
(REF) ⌀ 11.250
(SEE NOTE 1)
DETAIL -5 & -7
SCALE: 1=4
(SEE NOTE 5)
-11 -13 -15
(TYP 4 PL)
SEE DETAIL 'B'
QUANTITY/DASH NO.
ODD DASH NO. SHOWN
EVEN DASH NO. OPP
PART NO.
DESCRIPTION
STOCK SIZE
MATERIAL OR VENDOR
MATERIAL SPECIFICATION
LIST OF MATERIAL
UNLESS OTHERWISE SPECIFIED DIMENSIONS ARE IN INCHES AND ARE AFTER PLATING.
TOLERANCES ON:
FRACTIONS
DECIMALS
ANGLES
MACHINED SURFACES REF. MIL-STD-10
MIL-I-6500 STATUS
DRAWN BY HUGHES
DEPT. 2560
DATE 12-18-61
CHECKER
STRESS ENGR.
WT. ENGR.
MATL. ENGR.
RELIABILITY
GR. ENGR.
PROGRAM
CUST.
THE MARTIN COMPANY
BALTIMORE, MARYLAND
TEST PANEL
REFRACTORY METALS HONEYCOMB
38597
D
SK-46841
SCALE
SHEET 2 OF 2
CALC BY
DASH NUMBER
NEXT ASSY
USED ON
APPLICATION
FINAL ASSY
TEST
QTY. REQD
INTERCHANGEABLE
REPLACEABLE
UNCONTROLLED

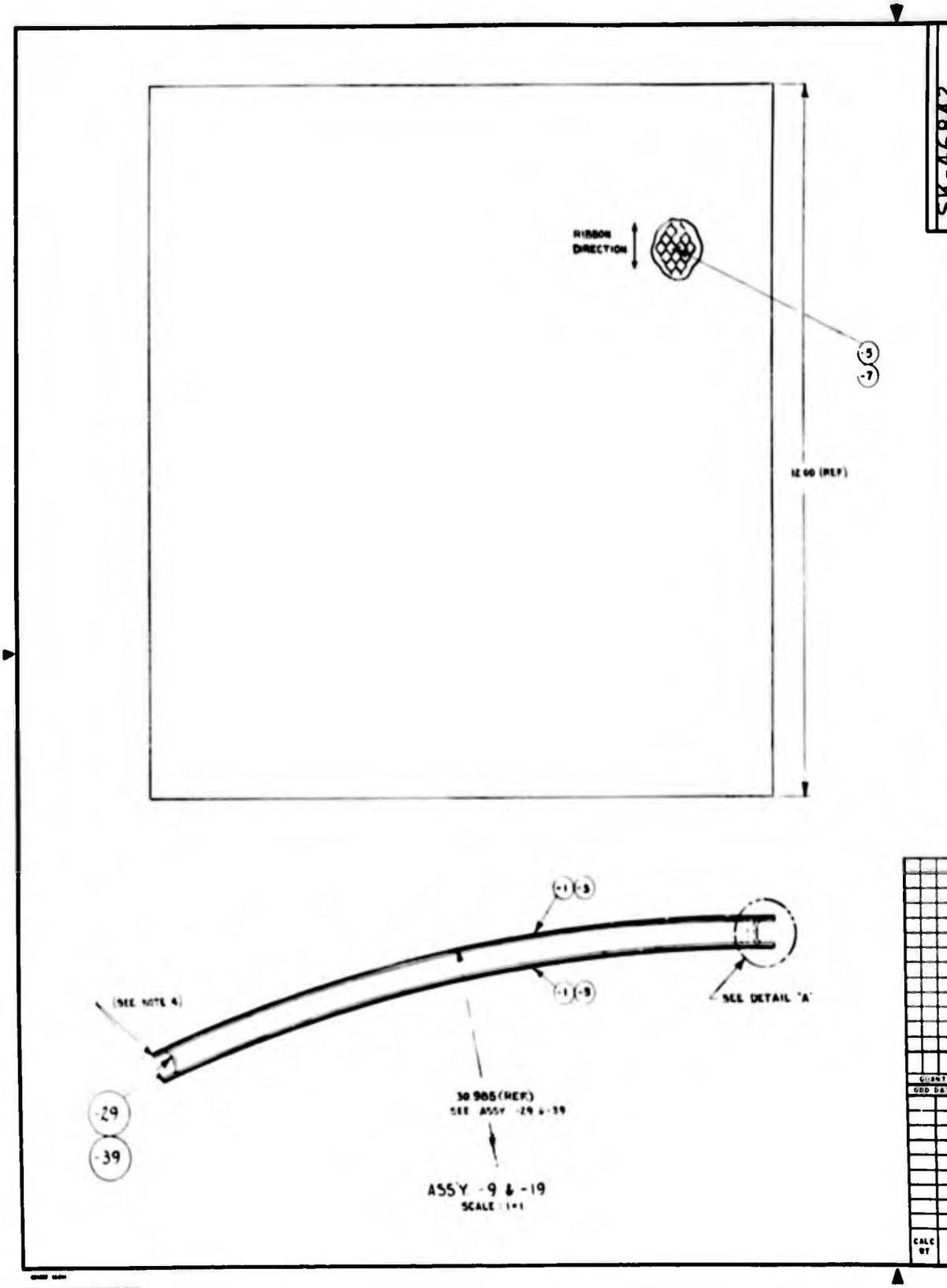
RIBBON DIRECTION
-3
-7
12.00 (REF)
-1 -5
-1 -5
(SEE NOTE 4)
SEE DETAIL 'A'
30.985 (REF)
SEE ASSY -29 & -39
-29
-39
ASSY -9 & -19
SCALE 1=1

SK-46842

REVISIONS				
SYM	ZONE	DESCRIPTION	DATE	APPROVED
A		REVISE NOTES	5/26/62	

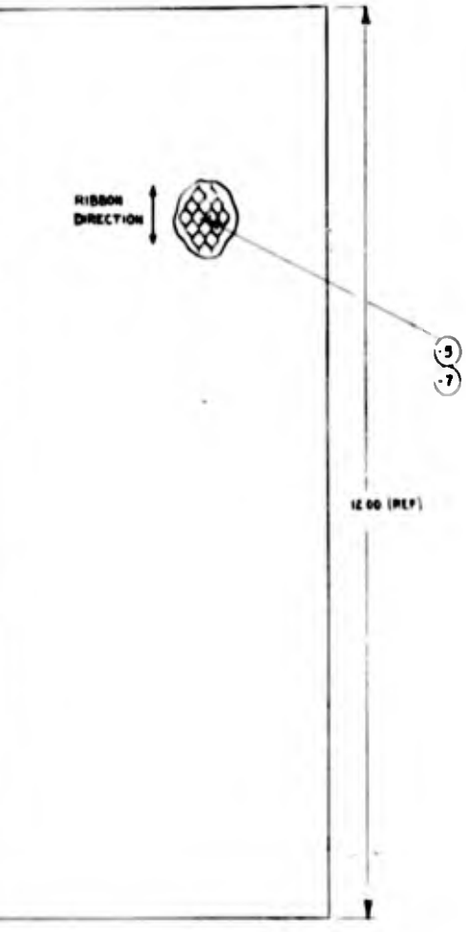

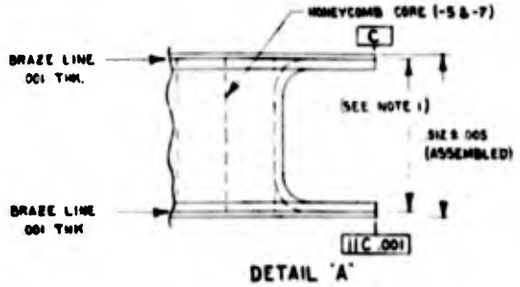

DETAIL "A"
SCALE 4:1

NOTES:
1. HONEYCOMB (-5 & -7) MUST MATCH CHANNEL ASSY'S (-29 & -39) RESP WITHIN ± .001"
2. MINIMUM BEND RADII WILL BE EXPERIMENTALLY DETERMINED UPON RECEIPT OF MATERIALS
3. FRAMES TO BE HERMETICALLY SEALED BY WELDING (ELECTRON BEAM)
4. SKINS TO BE WELDED TO FRAME ASSY'S AT EXTERNAL EDGES FOR HERMETICAL SEAL (ALL AROUND) (AFTER BRAZING) (ELECTRON BEAM)
5. HONEYCOMB CORE TO BE SIZED TO INSIDE DIMS OF FRAME ASSY
6. CURVED SURFACES MUST MATCH BRAZING FIXTURE WITHIN ±.001".

-19
1

(F)
-29 & -39

QUANTITY/DASH NO.					PART NO.	ZONE	SYM	MS NO.	DESCRIPTION	STOCK SIZE	MATERIAL OR VENDOR	MATERIAL SPECIFICATION	FINISH OR MFR CODE	CHG
		2			-17				CHANNEL	.025 x 1 1/2 x 12 1/8	Cb ALLOY, "D-36	MMS 1691		
			2		-15				CHANNEL	.025 x 1 1/2 x 12 1/8	TEM MOLY ALLOY	MMS 1633		
		2			-13				CHANNEL	.025 x 1 1/2 x 12 1/8	Cb ALLOY, "D-36	MMS 1691		
			2		-11				CHANNEL	.025 x 1 1/2 x 12 1/8	TEM MOLY ALLOY	MMS 1633		
				1	-7				HONEYCOMB CORE	.002 x 3/16 CELL	Cb ALLOY, "D-36	MMS 1691		
					-5				HONEYCOMB CORE	.002 x 3/16 CELL	TEM MOLY ALLOY	MMS 1633		
			2		-3				SKIN	.012 x 12 1/8 x 12 1/8	Cb ALLOY, "D-36	MMS 1691		
				2	-1				SKIN	.012 x 12 1/8 x 12 1/8	TEM MOLY ALLOY	MMS 1633		
				1	-39				ASSY, FRAME					
				1	-29				ASSY, FRAME					

ODD DASH NO. SHOWN — EVEN DASH NO. OPP — LIST OF MATERIAL

UNLESS OTHERWISE SPECIFIED DIMENSIONS ARE IN INCHES AND ARE AFTER PLATING.
TOLERANCES ON: FRACTIONS ± 1/32 | DECIMALS .X ± .1, .XX ± .03, .XXX ± .010 | ANGLES ± 1/2°
MACHINED SURFACES REF. MIL-STD-10 ✓
MIL-I-8500 STATUS
INTERCHANGEABLE
REPLACEABLE
UNCONTROLLED

CALC BY	DASH NUMBER	NEXT ASSY	USED ON	FINAL ASSY	TEST
	-19			13	
	-9			13	
		APPLICATION		QTY. REQD	

DRAWN BY: WICHOREK — DEPT.: 2560 — DATE: 12-20-61
CHECKED
STRESS ENGR.
QUAL. ENGR.
MATL. ENGR.
RELIABILITY
SR. ENGR.
PROGRAM REP.
CUSTY. REP.

THE MARTIN COMPANY — BALTIMORE, MARYLAND

TEST PANEL
REFRACTORY METALS HONEYCOMB
ST PT 9363

CODE IDENT NO. 38597 — SIZE D — SK-46842 — SCALE — SHEET 1 OF 2

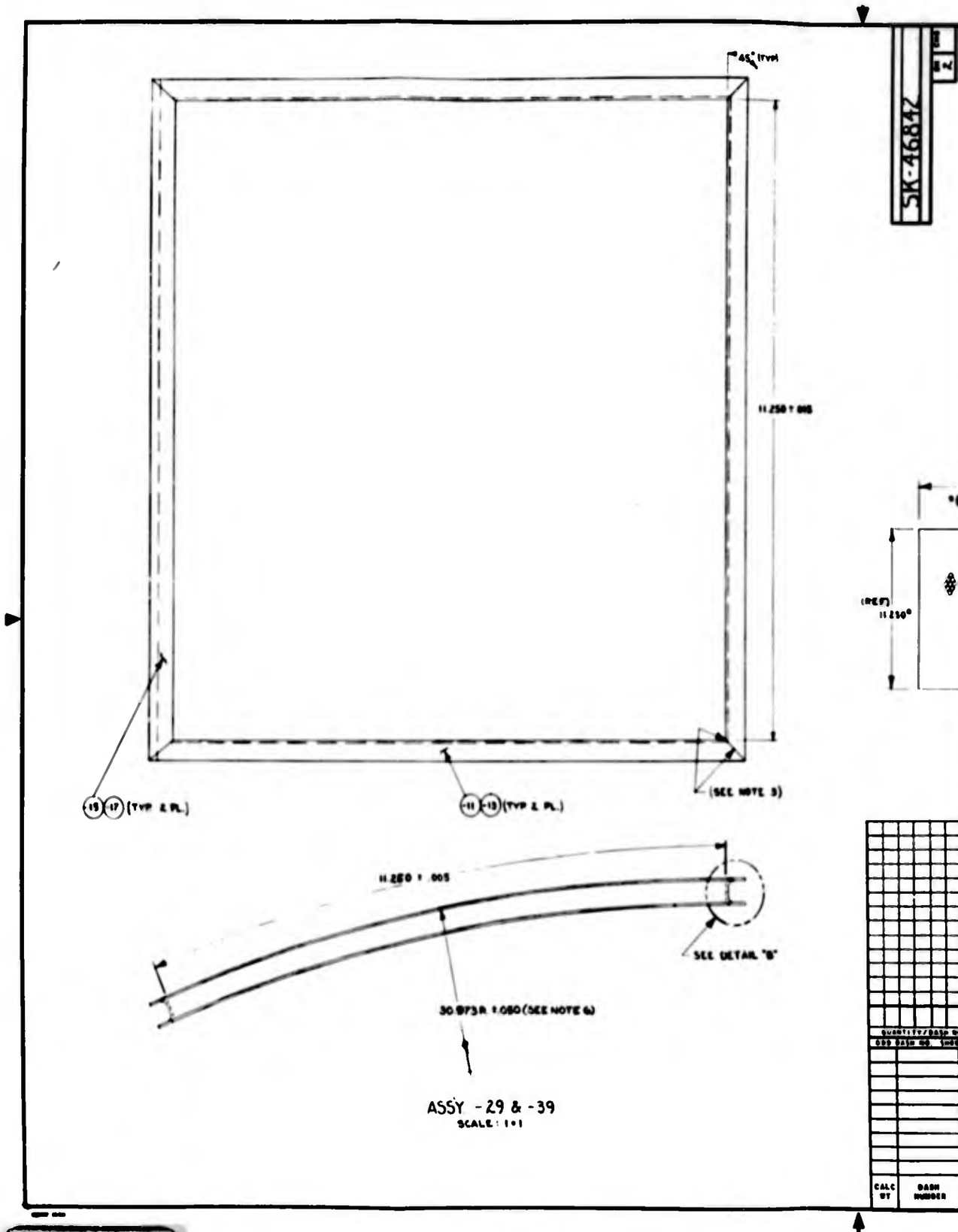
SK-46842
45° (TYP)
11.250 ± .005
(REF)
11.250"
(SEE NOTE 3)
-19 -17 (TYP 2 PL.)
-11 -13 (TYP 2 PL.)
11.250 ± .005
SEE DETAIL "B"
30.973 R ± .050 (SEE NOTE 6)
ASSY -29 & -39
SCALE: 1=1
CALC BY
DASH NUMBER

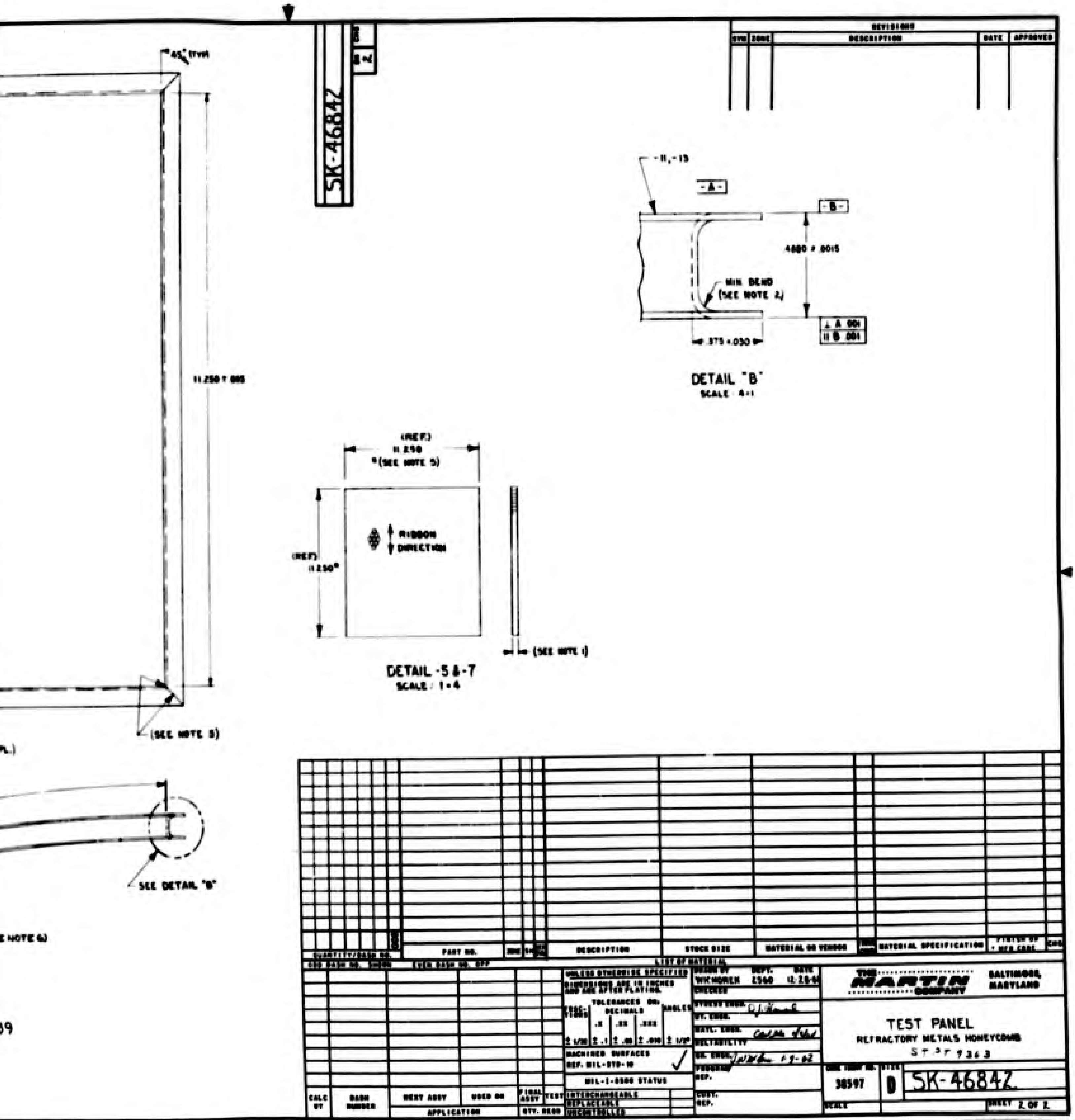
SK-46842
REVISIONS
SYM ZONE DESCRIPTION DATE APPROVED
45° (TYP)
11.250 ± .005
(SEE NOTE 3)
SEE DETAIL "B"
-11, -13
-A-
-B-
.4880 ± .0015
MIN BEND (SEE NOTE 2)
.375 ± .030
DETAIL "B"
SCALE 4:1
(REF.) 11.250 *(SEE NOTE 5)
RIBBON DIRECTION
(REF.) 11.250*
(SEE NOTE 1)
DETAIL -5 & -7
SCALE 1:4
QUANTITY/DASH NO.
PART NO.
DESCRIPTION
STOCK SIZE
MATERIAL OR VENDOR
MATERIAL SPECIFICATION
LIST OF MATERIAL
APPLICATION
NEXT ASSY
USED ON
UNLESS OTHERWISE SPECIFIED DIMENSIONS ARE IN INCHES AND ARE AFTER PLATING.
TOLERANCES ON:
DECIMALS
ANGLES
MACHINED SURFACES REF. MIL-STD-10
MIL-I-6000 STATUS
INTERCHANGEABLE
REPLACEABLE
DRAWN BY WICHOREK
DEPT. 2560
THE MARTIN COMPANY
BALTIMORE, MARYLAND
TEST PANEL
REFRACTORY METALS HONEYCOMB
38597
D
SK-46842
SHEET 2 OF 2

v

2

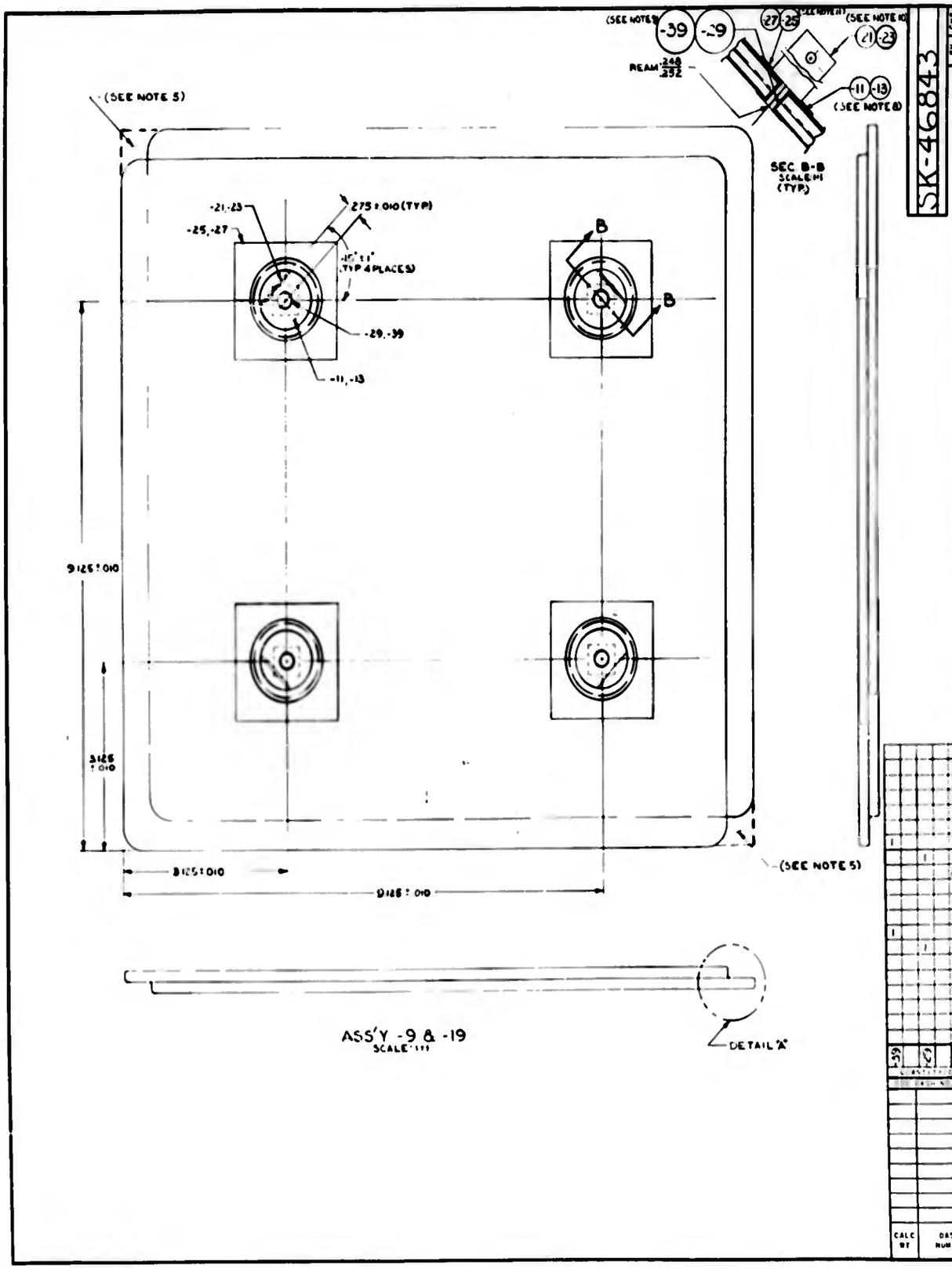
SK-46843
(SEE NOTE 5)
-39
-29
-27
-25
(SEE NOTE 10)
-21
-23
REAM .248 .252
-11
-13
(SEE NOTE 8)
SEC B-B
SCALE:1
(TYP)
-21,-23
-25,-27
.275 ± .010 (TYP)
.15 ± .1
TYP 4 PLACES)
B
B
-29,-39
-11,-13
9.125 ± .010
3.125 ± .010
3.125 ± .010
9.125 ± .010
(SEE NOTE 5)
ASS'Y -9 & -19
SCALE: 1:1
DETAIL 'A'
CALC BY

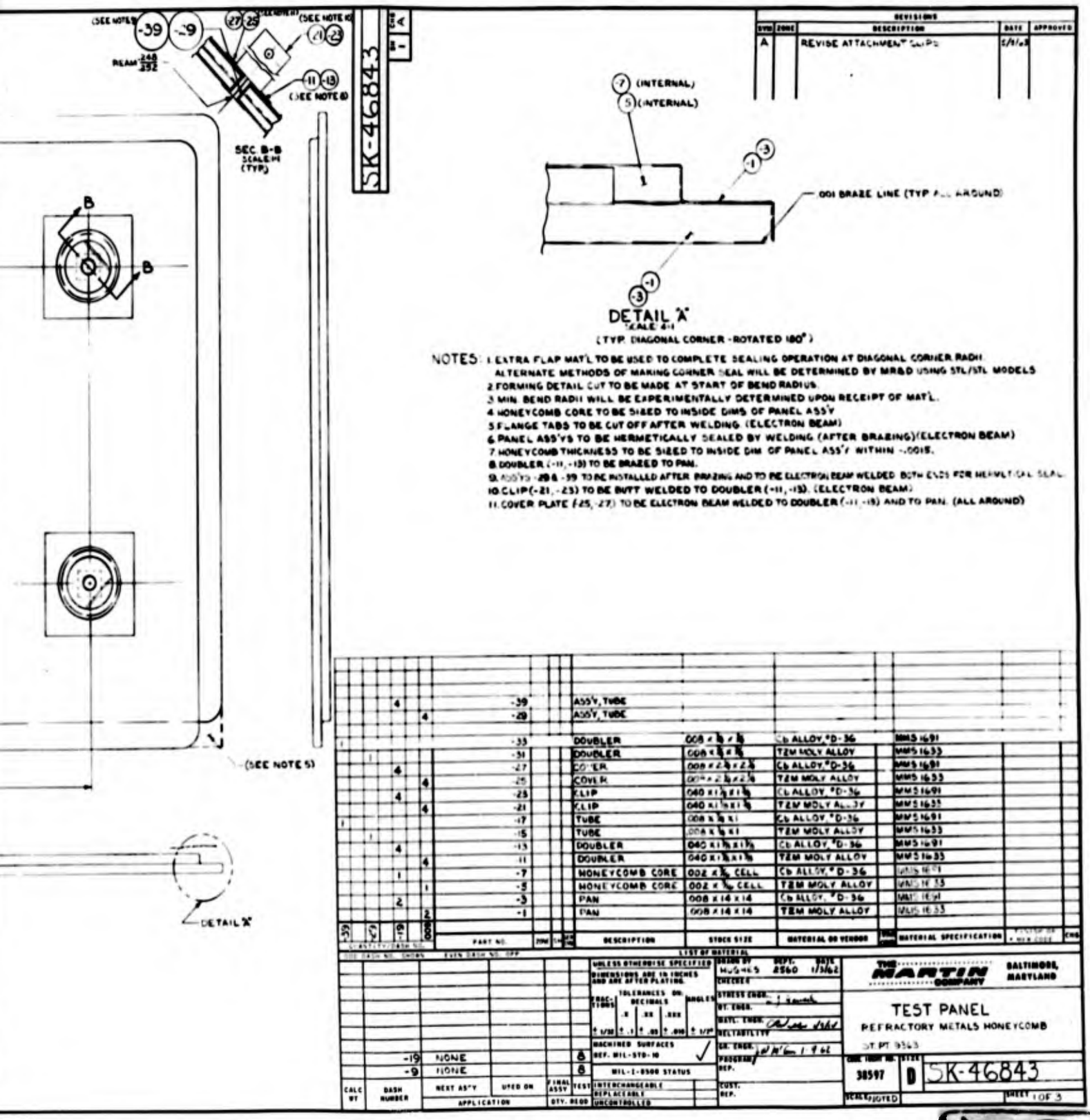

REVISIONS				
DASH	ZONE	DESCRIPTION	DATE	APPROVED
A		REVISE ATTACHMENT SKIPS	5/31/62	

NOTES:
1. EXTRA FLAP MAT'L TO BE USED TO COMPLETE SEALING OPERATION AT DIAGONAL CORNER RADII. ALTERNATE METHODS OF MAKING CORNER SEAL WILL BE DETERMINED BY MR&D USING STL/STL MODELS
2. FORMING DETAIL CUT TO BE MADE AT START OF BEND RADIUS.
3. MIN. BEND RADII WILL BE EXPERIMENTALLY DETERMINED UPON RECEIPT OF MAT'L.
4. HONEYCOMB CORE TO BE SIZED TO INSIDE DIMS. OF PANEL ASS'Y
5. FLANGE TABS TO BE CUT OFF AFTER WELDING (ELECTRON BEAM)
6. PANEL ASS'YS TO BE HERMETICALLY SEALED BY WELDING (AFTER BRAZING)(ELECTRON BEAM)
7. HONEYCOMB THICKNESS TO BE SIZED TO INSIDE DIM. OF PANEL ASS'Y WITHIN ±.0015.
8. DOUBLER (-11, -13) TO BE BRAZED TO PAN.
9. ASS'YS -29 & -39 TO BE INSTALLED AFTER BRAZING AND TO BE ELECTRON BEAM WELDED BOTH ENDS FOR HERMETICAL SEAL.
10. CLIP (-21, -23) TO BE BUTT WELDED TO DOUBLER (-11, -13). (ELECTRON BEAM)
11. COVER PLATE (-25, -27) TO BE ELECTRON BEAM WELDED TO DOUBLER (-11, -13) AND TO PAN. (ALL AROUND)

CALC QT	DASH NUMBER	NEXT ASS'Y APPLICATION	USED ON	FINAL ASS'Y QTY. REQD	TEST
	-39	ASS'Y, TUBE		4	
	-29	ASS'Y, TUBE		4	
	-33	DOUBLER	.008 x ½ x ½	Cb ALLOY, *D-36	MMS 1691
	-31	DOUBLER	.008 x ½ x ½	TZM MOLY ALLOY	MMS 1633
4	-27	COVER	.008 x 2½ x 2½	Cb ALLOY, *D-36	MMS 1691
4	-25	COVER	.008 x 2½ x 2½	TZM MOLY ALLOY	MMS 1633
4	-23	CLIP	.040 x 1½ x 1½	Cb ALLOY, *D-36	MMS 1691
4	-21	CLIP	.040 x 1½ x 1½	TZM MOLY ALLOY	MMS 1633
1	-17	TUBE	.008 x ½ x 1	Cb ALLOY, *D-36	MMS 1691
1	-15	TUBE	.008 x ½ x 1	TZM MOLY ALLOY	MMS 1633
4	-13	DOUBLER	.040 x 1½ x 1½	Cb ALLOY, *D-36	MMS 1691
4	11	DOUBLER	.040 x 1½ x 1½	TZM MOLY ALLOY	MMS 1633
1	-7	HONEYCOMB CORE	.002 x ⅝ CELL	Cb ALLOY, *D-36	MMS 1691
1	-5	HONEYCOMB CORE	.002 x ⅝ CELL	TZM MOLY ALLOY	MMS 1633
2	-3	PAN	.008 x 14 x 14	Cb ALLOY, *D-36	MMS 1691
2	-1	PAN	.008 x 14 x 14	TZM MOLY ALLOY	MMS 1633
	-19	NONE		8	
	-9	NONE		8	

LIST OF MATERIAL

UNLESS OTHERWISE SPECIFIED
DIMENSIONS ARE IN INCHES AND ARE AFTER PLATING.
TOLERANCES ON: DECIMALS .X ±.1, .XX ±.05, .XXX ±.010; ANGLES ±1°; FRACTIONS ±1/32
MACHINED SURFACES REF. MIL-STD-10
MIL-I-8500 STATUS
INTERCHANGEABLE
REPLACEABLE
UNCONTROLLED

DESIGN BY HUGHES DEPT. 2560 DATE 1/3/62
CHECKED
STRESS ENGR.
DT. ENGR.
MATL. ENGR.
RELIABILITY
QA. ENGR. 12 M'Gee 1 '62
PROGRAM REP.
CUST. REP.

THE MARTIN COMPANY BALTIMORE, MARYLAND

TEST PANEL
REFRACTORY METALS HONEYCOMB
ST PT 9563

CODE IDENT NO. 38597 SIZE D SK-46843
SCALE QUOTED SHEET 1 OF 3

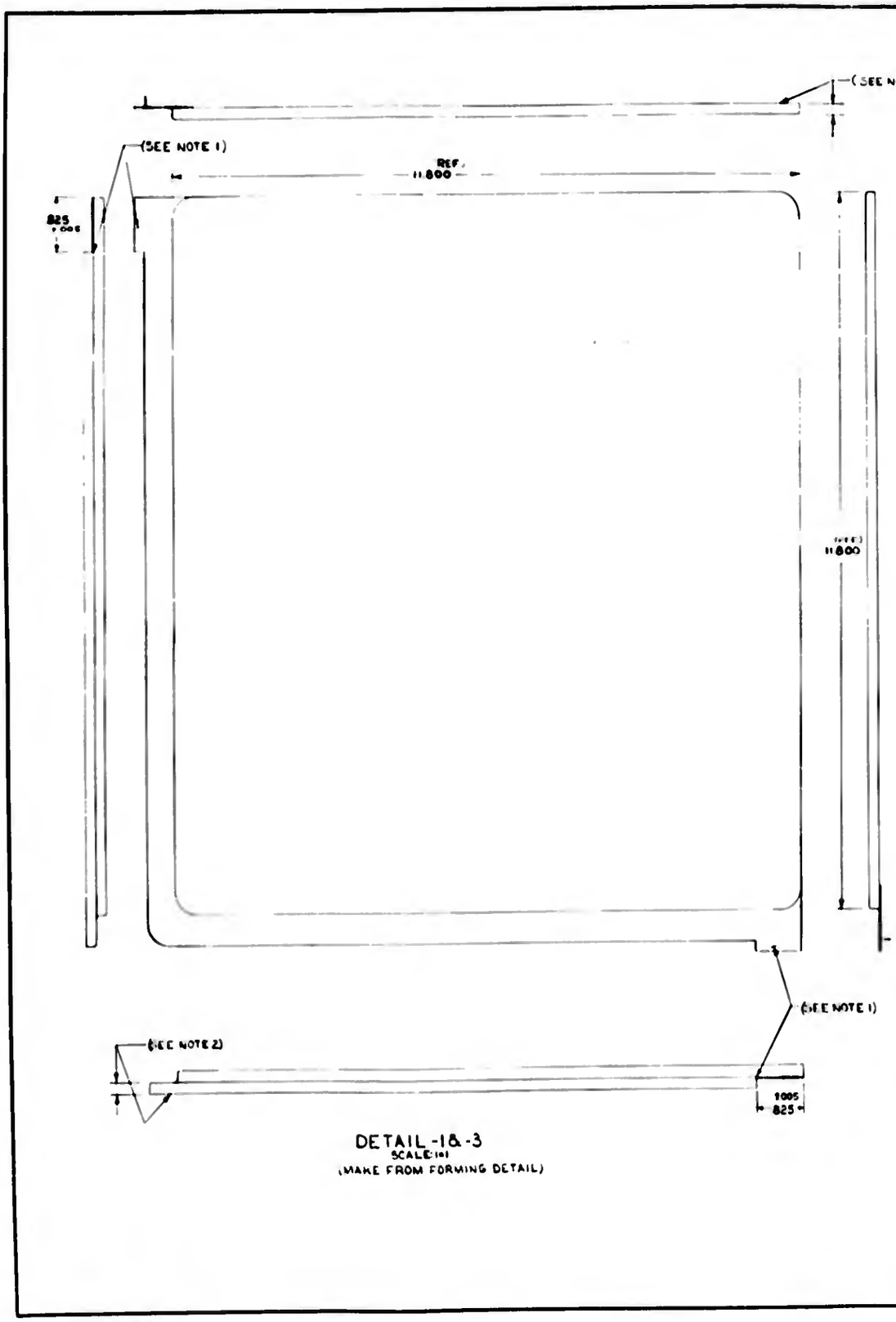

DETAIL-18-3
SCALE: 1:01
(MAKE FROM FORMING DETAIL)

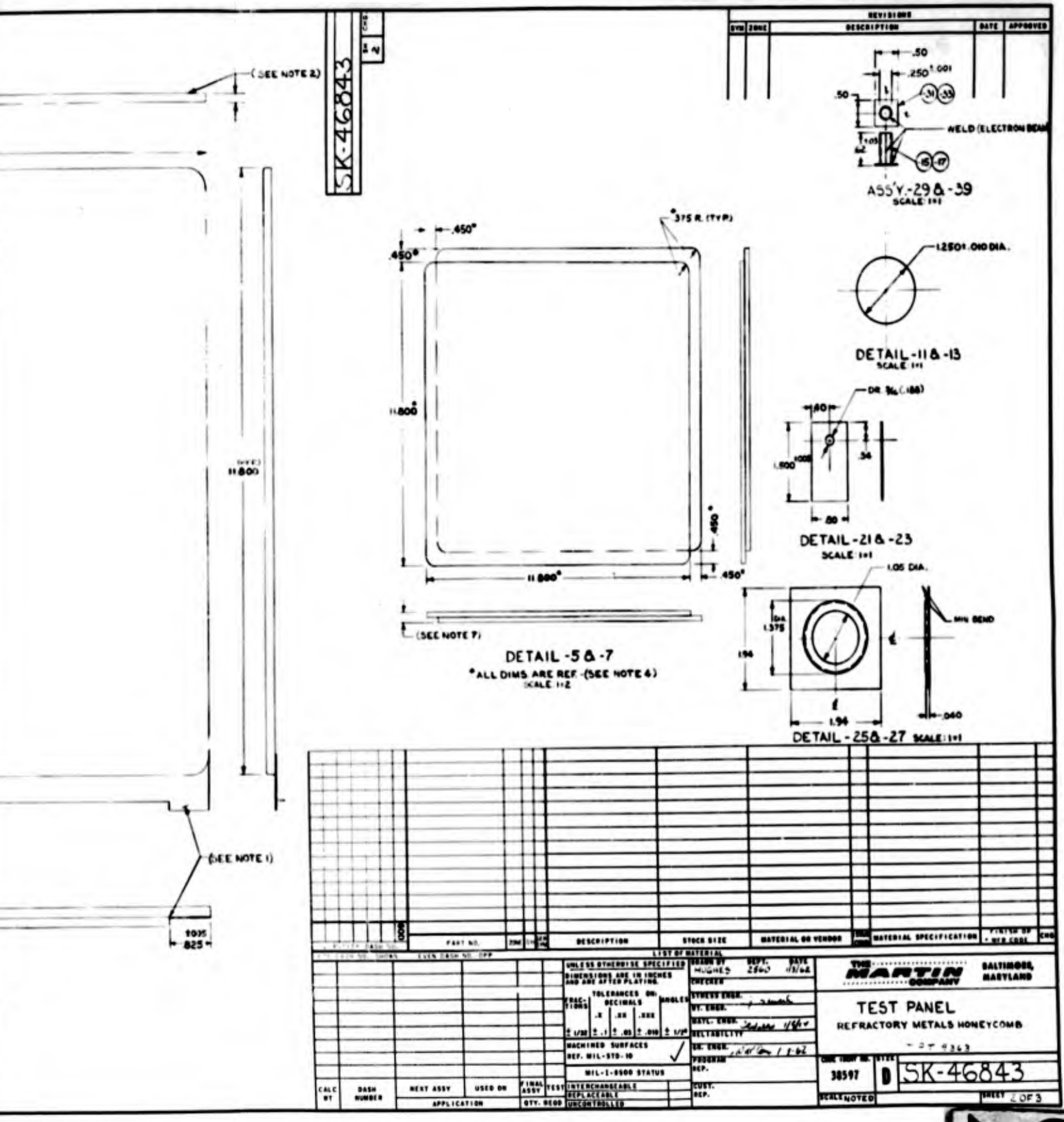
SK-46843
(SEE NOTE 2)
11.800
(SEE NOTE 1)
1.935
.825
REVISIONS
ZONE
DESCRIPTION
DATE
APPROVED
.50
.250 +.001
WELD (ELECTRON BEAM)
ASS'Y.-29 & -39
SCALE 1=1
.375 R. (TYP.)
.450
11.800
(SEE NOTE 7)
DETAIL -5 & -7
*ALL DIMS ARE REF. (SEE NOTE 4)
SCALE 1=2
1.250±.010 DIA.
DETAIL -11 & -13
SCALE 1=1
DR. 3/16 (.188)
.60
1.500
.34
.80
DETAIL -21 & -23
SCALE 1=1
1.05 DIA.
1.375
1.94
MIN BEND
.040
DETAIL -25 & -27 SCALE 1=1
ZONE
PART NO.
DESCRIPTION
STOCK SIZE
MATERIAL OR VENDOR
MATERIAL SPECIFICATION
LIST OF MATERIAL
UNLESS OTHERWISE SPECIFIED
DIMENSIONS ARE IN INCHES AND ARE AFTER PLATING.
TOLERANCES ON DECIMALS
FRACTIONS
ANGLES
MACHINED SURFACES
REF. MIL-STD-10
MIL-I-8500 STATUS
INTERCHANGEABLE
REPLACEABLE
UNCONTROLLED
DESIGN BY
HUGHES
DEPT. 2540
DATE 1/31/64
CHECKER
STRESS ENGR.
PT. ENGR.
MATL. ENGR.
RELIABILITY
SR. ENGR.
PROGRAM DEP.
CUST. REP.
THE MARTIN COMPANY
BALTIMORE, MARYLAND
TEST PANEL
REFRACTORY METALS HONEYCOMB
CONT. ACCT. NO.
38597
SIZE
D
SK-46843
SCALE NOTED
SHEET 2 OF 3
CALC BY
DASH NUMBER
NEXT ASSY
USED ON
APPLICATION
FINAL ASSY
QTY. REQD
TEST

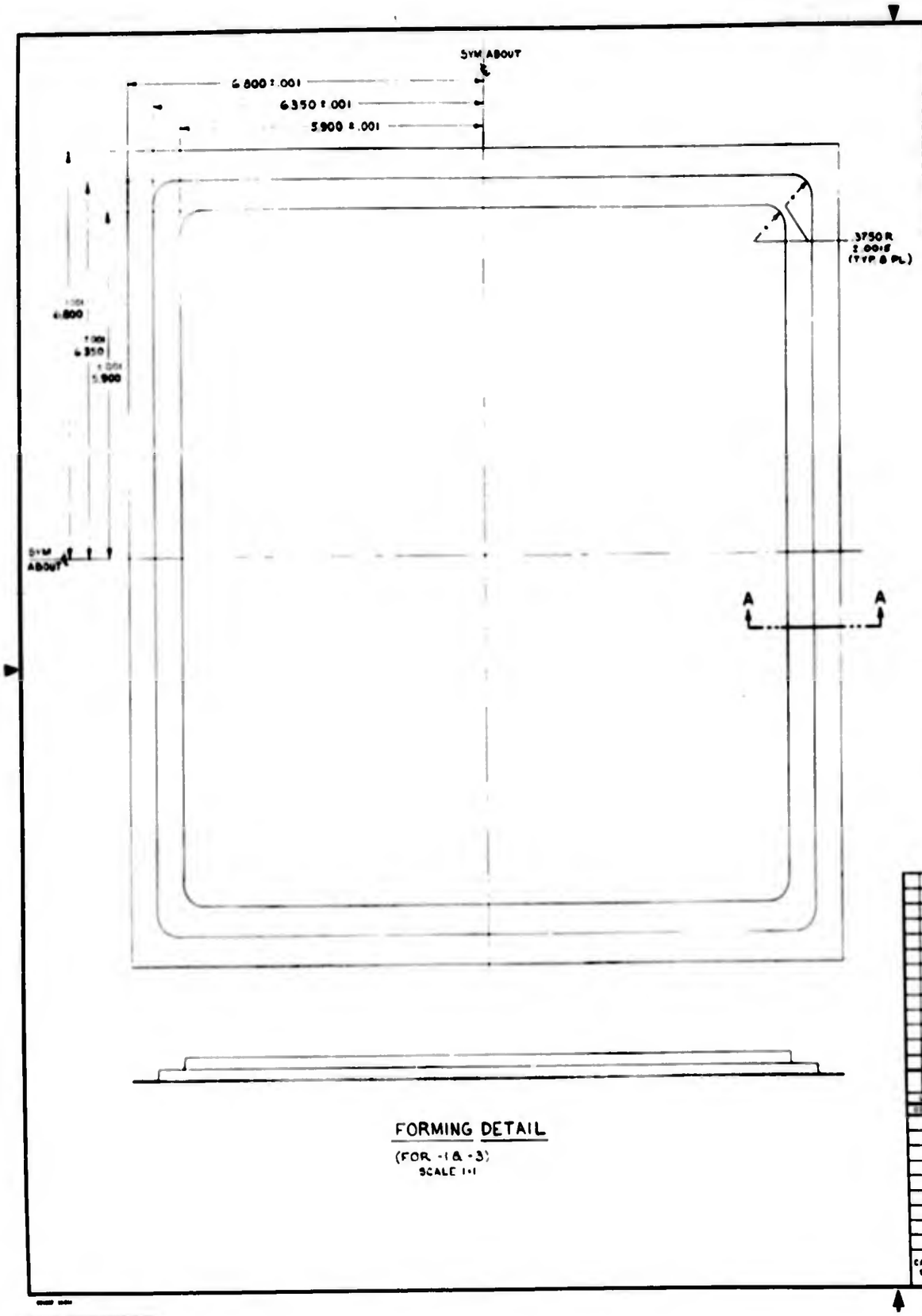

FORMING DETAIL

(FOR -1 & -3)
SCALE 1=1

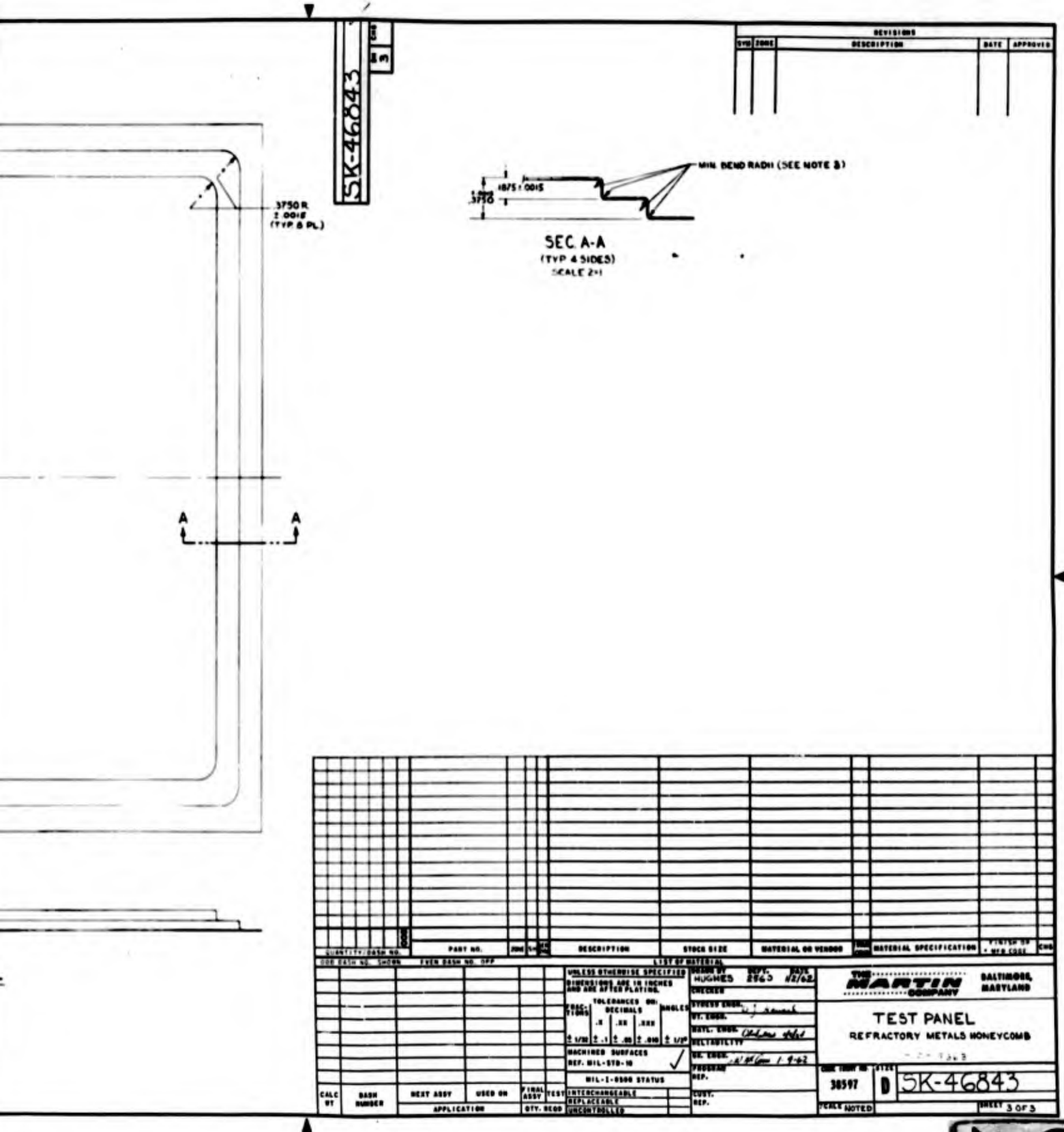
SK-46843
SHT 3
REVISIONS
ZONE
DESCRIPTION
DATE
APPROVED
MIN. BEND RADII (SEE NOTE 8)
.1875 ± .0015
.3750
SEC A-A
(TYP 4 SIDES)
SCALE 2:1
.3750 R
± .0015
(TYP 8 PL)
A
A
PART NO.
DESCRIPTION
STOCK SIZE
MATERIAL OR VENDOR
MATERIAL SPECIFICATION
UNLESS OTHERWISE SPECIFIED
DIMENSIONS ARE IN INCHES AND ARE AFTER PLATING.
TOLERANCES ON: DECIMALS
ANGLES
MACHINED SURFACES
REF. MIL-STD-10
MIL-I-8500 STATUS
INTERCHANGEABLE
REPLACEABLE
UNCONTROLLED
DESIGN BY
HUGHES
DEPT.
2963
DATE
4/2/62
CHECKER
STRESS ENGR.
WT. ENGR.
MATL. ENGR.
RELIABILITY
QA. ENGR.
PROGRAM REP.
CUST. REP.
THE MARTIN COMPANY
BALTIMORE, MARYLAND
TEST PANEL
REFRACTORY METALS HONEYCOMB
CODE IDENT NO.
30597
SIZE
D
SK-46843
SCALE NOTED
SHEET 3 OF 3
CALC QT
DASH NUMBER
NEXT ASSY
USED ON
APPLICATION
FINAL ASSY
TEST
QTY. REQD

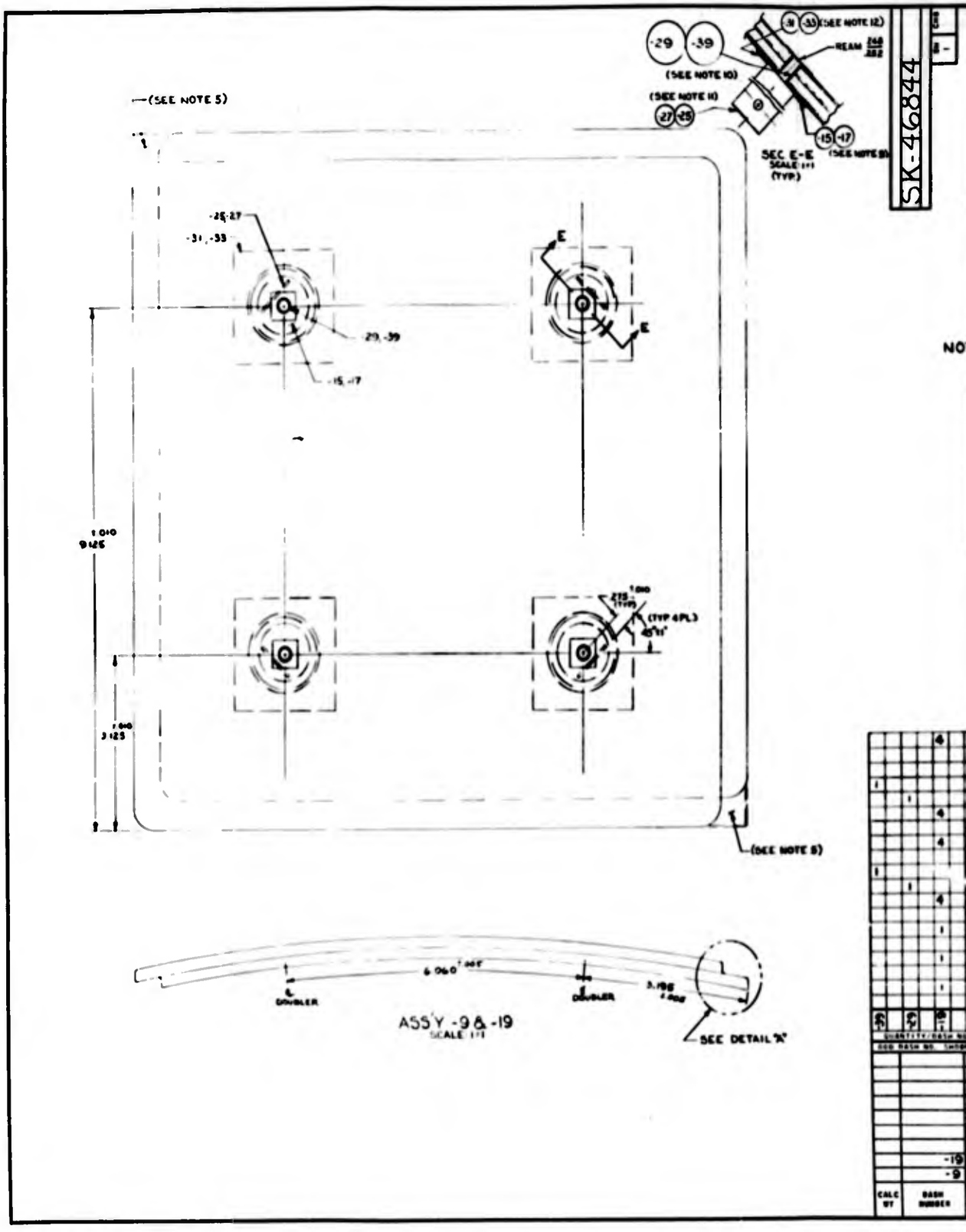
SK-46844
(SEE NOTE 5)
-29
-39
(SEE NOTE 10)
(SEE NOTE 11)
-27
-25
-31
-33
(SEE NOTE 12)
REAM
-15
-17
SEC E-E
SCALE: 1/1
(TYP.)
-25,-27
-31,-33
-29,-39
-15,-17
E
E
1.010
0.125
1.000
.270
(TYP)
(TYP 6 PL)
45°
1.010
0.125
(SEE NOTE 5)
6.060
DOUBLER
DOUBLER
ASSY -9 & -19
SCALE 1/1
SEE DETAIL "A"
-19
-9
CALC
BY
DASH
NUMBER

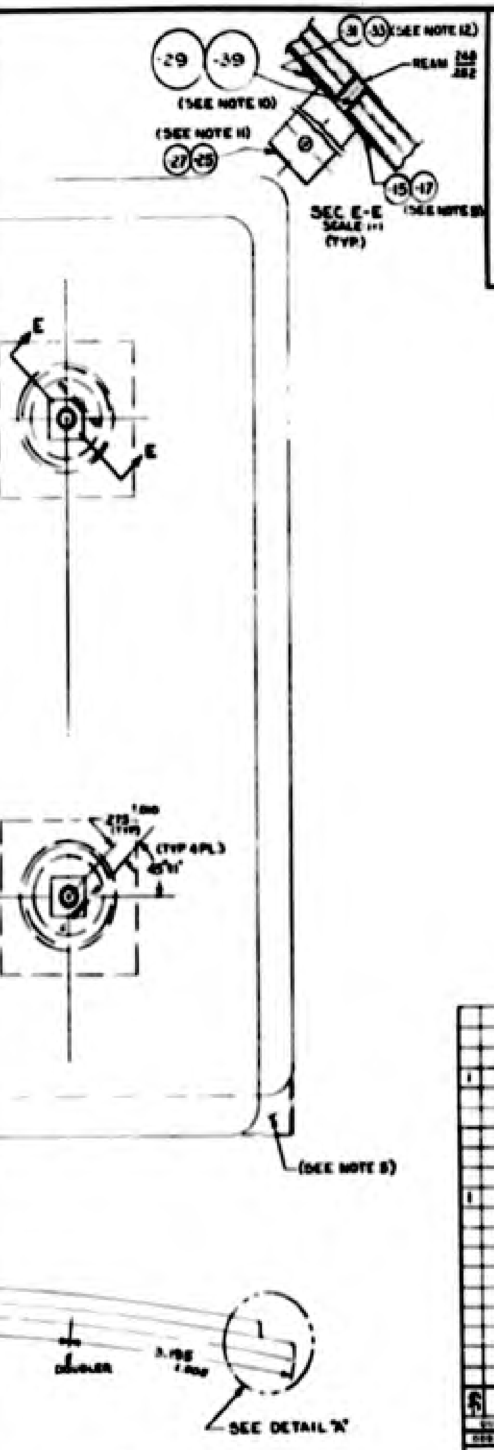

5K-46844

REVISIONS				
SYM	ZONE	DESCRIPTION	DATE	APPROVED
A		REVISE ATTACHMENT CLIPS	6/6/63	

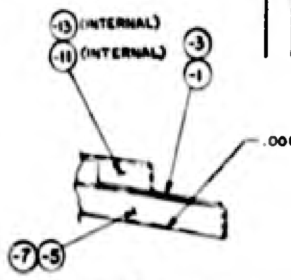

DETAIL "A"
SCALE: 2:1
(SIM ASS'Y DIAGONAL CORNER)

NOTES:
1. EXTRA FLAP MAT'L TO BE USED TO COMPLETE SEALING OPERATION AT DIAGONAL CORNER RADII. ALTERNATE METHODS OF MAKING CORNER SEAL WILL BE DETERMINED BY MR&D USING STL/STL MODELS.
2. FORMING DETAIL CUT TO BE MADE AT START OF BEND RADIUS.
3. MIN BEND RADII WILL BE EXPERIMENTALLY DETERMINED UPON RECEIPT OF MAT'L.
4. HONEYCOMB CORE TO BE SIZED TO INSIDE DIMS. OF PANEL ASS'Y.
5. FLANGE TABS TO BE CUT OFF AFTER WELDING (ELECTRON BEAM)
6. PANEL ASS'YS TO BE HERMETICALLY SEALED BY WELDING (AFTER BRAZING) (ELECTRON BEAM)
7. HONEYCOMB THICKNESS TO BE SIZED TO INSIDE DIMS OF PANEL ASS'Y WITHIN -.0015
8. CURVED SURFACES MUST MATCH BRAZING FIXTURE WITHIN ±.0015
9. DOUBLER (-15, -17) TO BE BRAZED TO PAN.
10. ASSY'S -29 & -39 TO BE INSTALLED AFTER BRAZING AND TO BE ELECTRON BEAM WELDED BOTH ENDS FOR HERMETICAL SEAL.
11. CLIP (-25, -27) TO BE BUTT WELDED TO DOUBLER (-15, -17) (ELECTRON BEAM)
12. COVER PLATE (-31, -33) TO BE ELECTRON BEAM WELDED TO DOUBLER (-15, -17) AND TO PAN (ALL AROUND)

-39	-29	-19	-9	PART NO.	DESCRIPTION	STOCK SIZE	MATERIAL OR VENDOR	MATERIAL SPECIFICATION
		4			ASS'Y TUBE			
			4		ASS'Y TUBE			
1				-37	DOUBLER	.008 x [illegible] x [illegible]	Cb ALLOY, #D-36	MMS1691
	1			-35	DOUBLER	.008 x [illegible] x [illegible]	TZM MOLY ALLOY	MMS1633
		4		-33	COVER	.008 x 2[illegible] x 2[illegible]	Cb ALLOY, #D-36	MMS1691
			4	-31	COVER	.008 x 2[illegible] x 2[illegible]	TZM MOLY ALLOY	MMS1633
		4		-27	CLIP	.040 x 1[illegible] x 1[illegible]	Cb ALLOY, #D-36	MMS1691
			4	-25	CLIP	.040 x 1[illegible] x 1[illegible]	TZM MOLY ALLOY	MMS1633
1				-23	TUBE	.008 x [illegible] x 1	Cb ALLOY, #D-36	MMS1691
	1			-21	TUBE	.008 x [illegible] x 1	TZM MOLY ALLOY	MMS1633
		4		-17	DOUBLER	.040 x 1[illegible] x 1[illegible]	Cb ALLOY, #D-36	MMS1691
			4	-15	DOUBLER	.040 x 1[illegible] x 1[illegible]	TZM MOLY ALLOY	MMS1633
		1		-13	HONEYCOMB CORE	.002 x 3/16 CELL	Cb ALLOY #D-36	MMS1691
			1	-11	HONEYCOMB CORE	.002 x 3/16 CELL	TZM MOLY ALLOY	MMS1633
		1		-7	PAN	.008 x 14 x 14	Cb ALLOY #D-36	MMS1691
			1	-5	PAN		TZM MOLY ALLOY	MMS1633
		1		-3	PAN		Cb ALLOY, #D-36	MMS1691
			1	-1	PAN	.008 x 14 x 14	TZM MOLY ALLOY	MMS1633

QUANTITY/DASH NO. — ODD DASH NO. SHOWN — EVEN DASH NO. OPP — LIST OF MATERIAL

DASH NUMBER	NEXT ASSY	USED ON	FINAL ASSY	TEST
-19	NONE		8	
-9	NONE		8	

APPLICATION

UNLESS OTHERWISE SPECIFIED DIMENSIONS ARE IN INCHES AND ARE AFTER PLATING.

DRAWN BY: WICHOREK — DEPT. 2560 — DATE 1/3/62

THE MARTIN COMPANY — BALTIMORE, MARYLAND

TEST PANEL
REFRACTORY METALS HONEYCOMB
ST PT 9363

CODE IDENT NO. 38597 — SIZE D — 5K-46844

SCALE NOTED — SHEET 1 OF 5

SK-46844

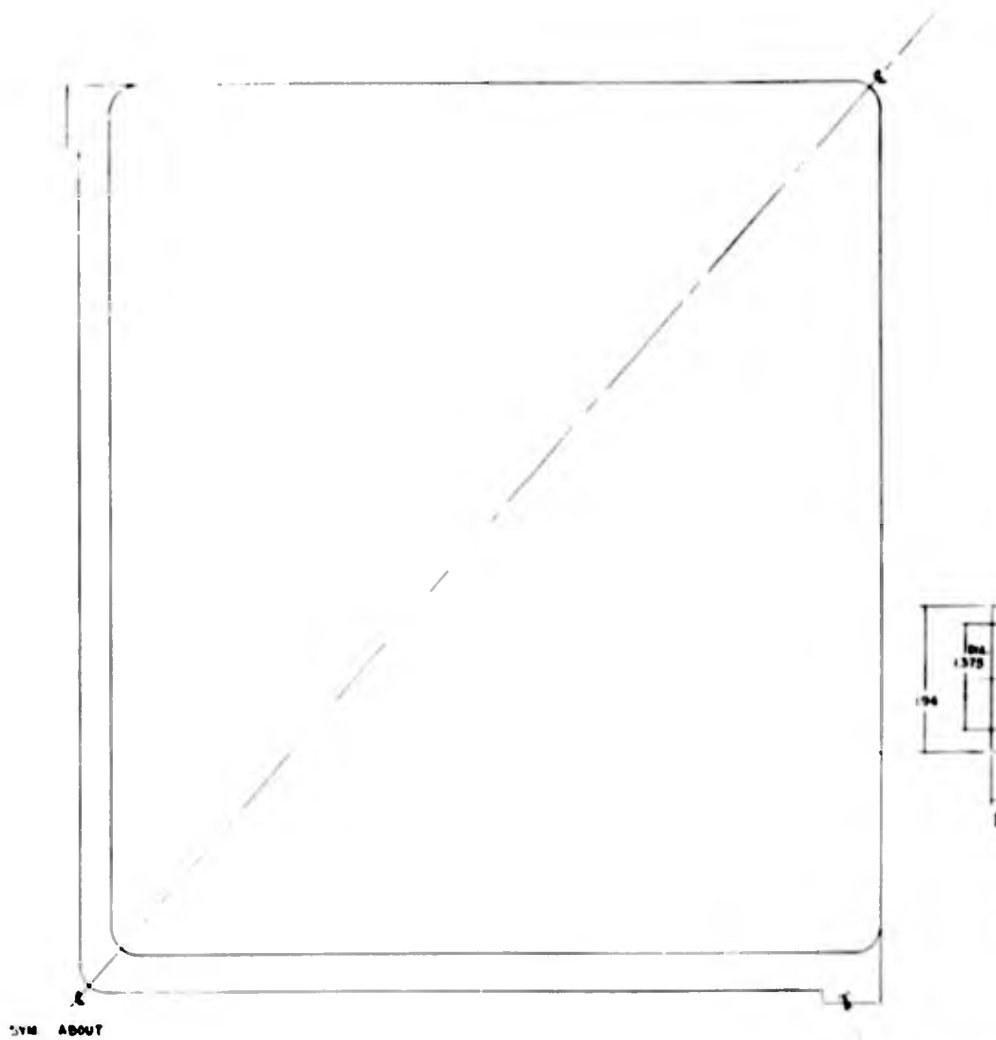

DETAIL -1 & -3
SCALE 1:1
(MAKE FROM FORMING DETAIL)

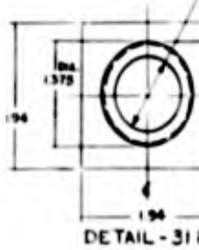

DETAIL - 31
SCALE

CALC
BY

x

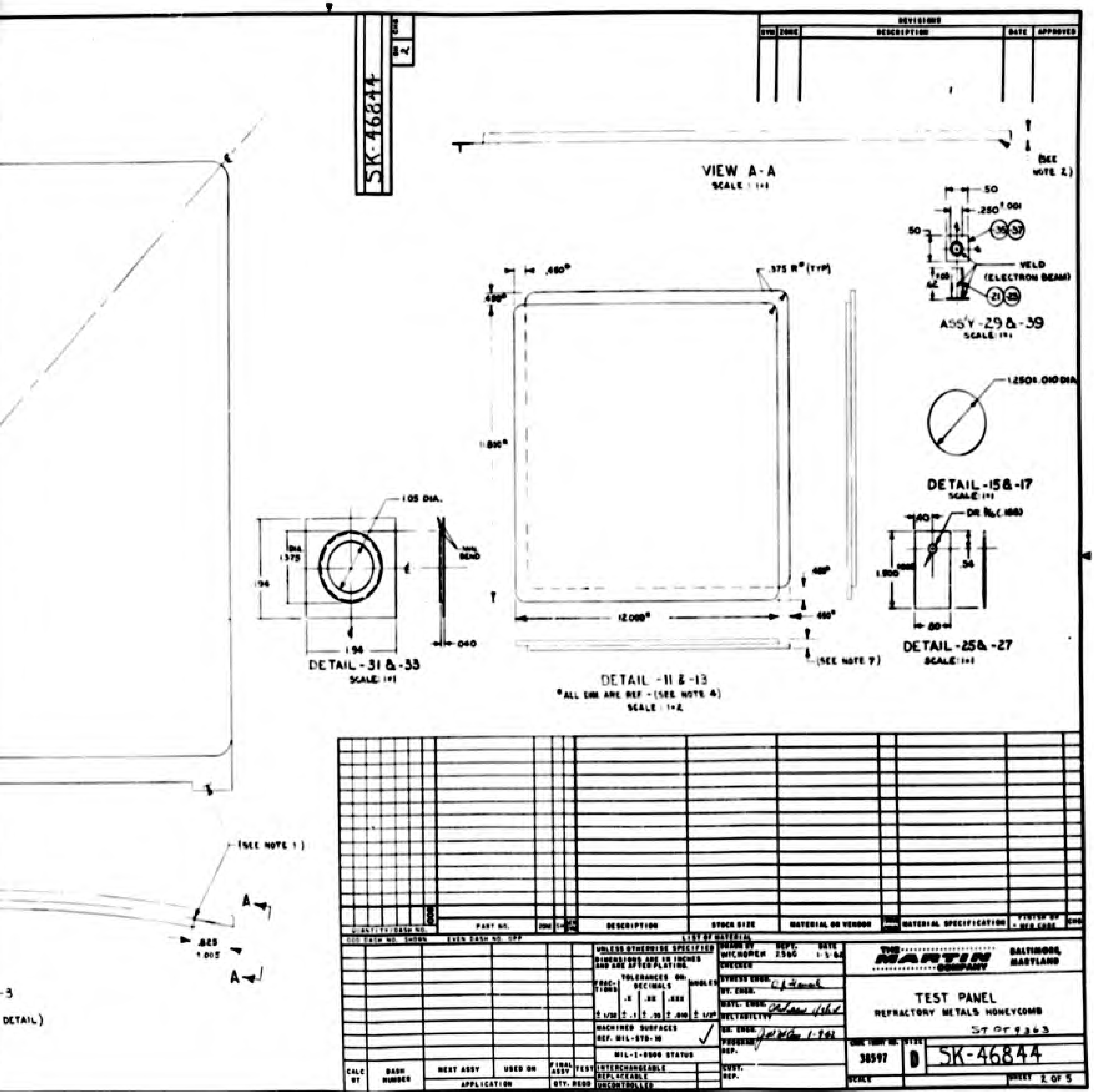
SK-46844
REVISIONS
VIEW A-A
SCALE : 1=1
(SEE NOTE 2)
ASS'Y -29 & -39
WELD (ELECTRON BEAM)
.375 R* (TYP)
DETAIL -15 & -17
DETAIL -25 & -27
DETAIL -31 & -33
105 DIA.
DETAIL -11 & -13
*ALL DIM ARE REF - (SEE NOTE 4)
SCALE : 1=2
12.000*
(SEE NOTE 7)
(SEE NOTE 1)
A
DETAIL)
PART NO.
DESCRIPTION
STOCK SIZE
MATERIAL OR VENDOR
MATERIAL SPECIFICATION
LIST OF MATERIAL
APPLICATION
NEXT ASSY
USED ON
UNLESS OTHERWISE SPECIFIED DIMENSIONS ARE IN INCHES
TOLERANCES ON:
MIL-I-8500 STATUS
INTERCHANGEABLE
REPLACEABLE
UNCONTROLLED
THE MARTIN COMPANY
BALTIMORE, MARYLAND
TEST PANEL
REFRACTORY METALS HONEYCOMB
38597
D
SK-46844
2 OF 5

2

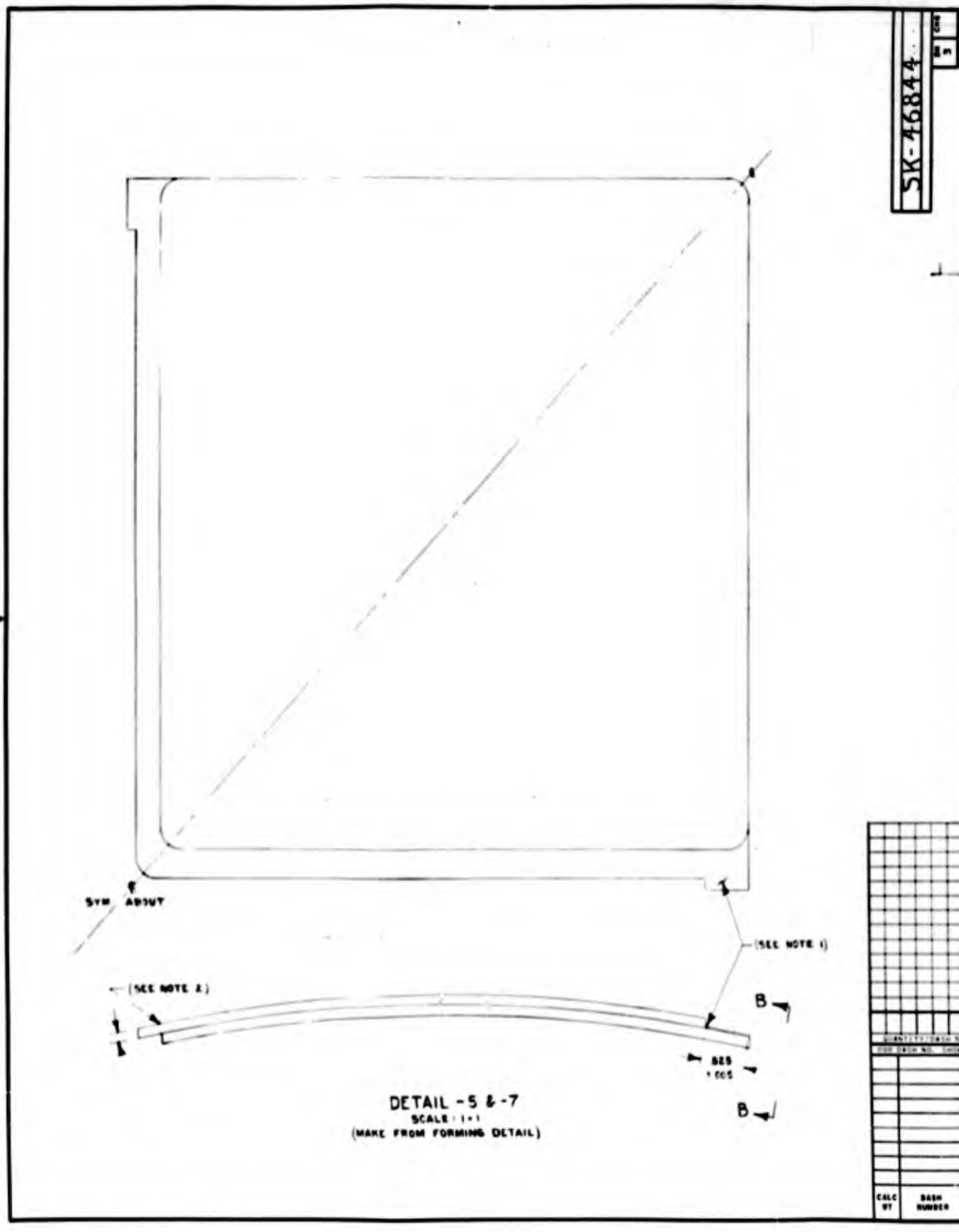
SK-46844
SYM ABOUT
(SEE NOTE 1)
(SEE NOTE 2)
B
B
DETAIL -5 & -7
SCALE : 1 : 1
(MAKE FROM FORMING DETAIL)

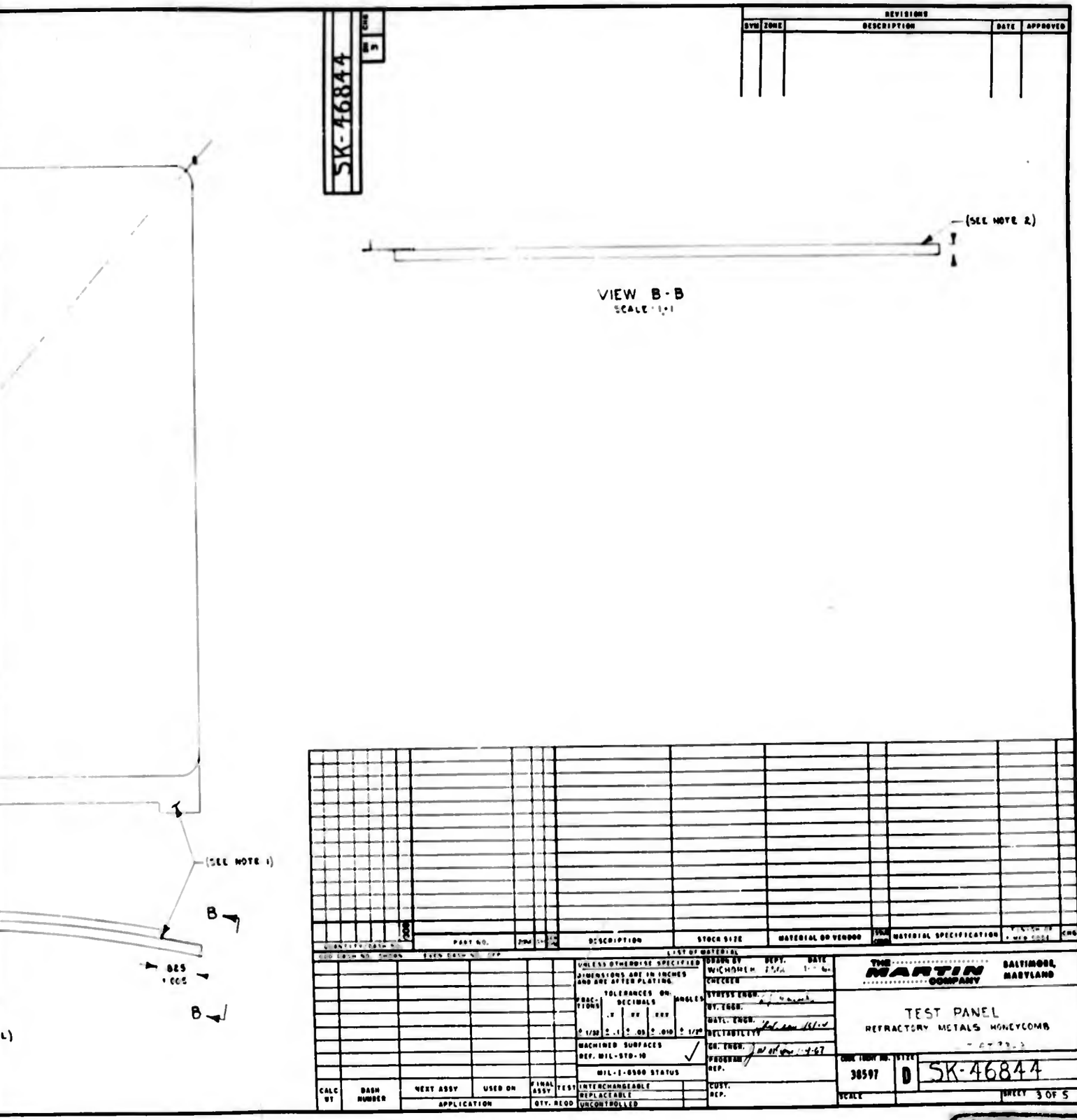
SK-46844
REVISIONS
SYM
ZONE
DESCRIPTION
DATE
APPROVED
(SEE NOTE 2)
VIEW B-B
SCALE 1:1
(SEE NOTE 1)
B
B
.865
.005
PART NO.
DESCRIPTION
STOCK SIZE
MATERIAL OR VENDOR
MATERIAL SPECIFICATION
LIST OF MATERIAL
UNLESS OTHERWISE SPECIFIED
DIMENSIONS ARE IN INCHES AND ARE AFTER PLATING
TOLERANCES ON:
FRACTIONS
DECIMALS
.X
.XX
.XXX
ANGLES
± 1/32
± .1
± .03
± .010
± 1/2°
MACHINED SURFACES
REF. MIL-STD-10
MIL-I-8500 STATUS
INTERCHANGEABLE
REPLACEABLE
UNCONTROLLED
DRAWN BY
WICHMEN
DEPT.
DATE
CHECKED
STRESS ENGR.
QT. ENGR.
MATL. ENGR.
RELIABILITY
GR. ENGR.
PROGRAM REP.
CUST. REP.
THE MARTIN COMPANY
BALTIMORE, MARYLAND
TEST PANEL
REFRACTORY METALS HONEYCOMB
CODE IDENT NO.
38597
SIZE
D
SK-46844
SCALE
SHEET 3 OF 5
CALC WT
DASH NUMBER
NEXT ASSY
USED ON
APPLICATION
FINAL ASSY
TEST
QTY. REQD

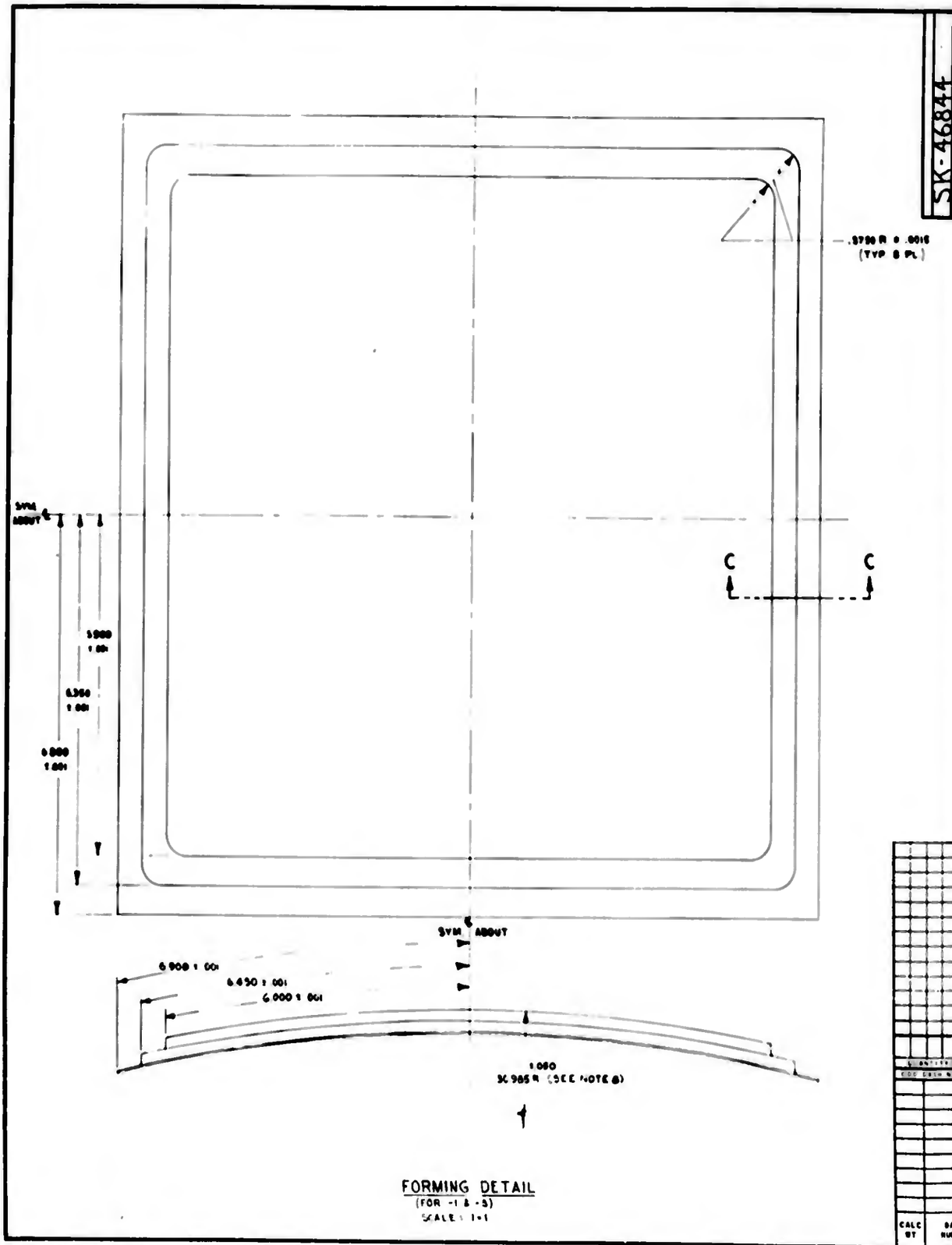
SK-46844
.9750 R ± .0015
(TYP 8 PL)
C
C
SYM
ABOUT
5.900
± .001
6.350
± .001
6.800
± .001
SYM ABOUT
6.900 ± .001
6.650 ± .001
6.000 ± .001
1.050
30.985 R (SEE NOTE 6)
FORMING DETAIL
(FOR -1 & -3)
SCALE: 1=1
CALC
BY

SK-46844

SHT 4

REVISIONS				
SYM	ZONE	DESCRIPTION	DATE	APPROVED

SEC C-C
(TYP 4 SIDES)
SCALE 2=1

DETAIL

QUANTITY/DASH NO.	PART NO.	ZONE	SYM	DESCRIPTION	STOCK SIZE	MATERIAL OR VENDOR	SYM	MATERIAL SPECIFICATION	FINISH OR HEAT CODE	CHG
USED DASH NO. SHOWN	DASH NO. SHOWN			LIST OF MATERIAL						

UNLESS OTHERWISE SPECIFIED
DIMENSIONS ARE IN INCHES
AND ARE AFTER PLATING.
TOLERANCES ON DECIMALS
FRACTIONS | .X ± .1 | .XX ± .03 | .XXX ± .010 | ANGLES ± 1/2°
MACHINED SURFACES
REF. MIL-STD-10
MIL-I-8500 STATUS
INTERCHANGEABLE
REPLACEABLE
UNCONTROLLED

DESIGN BY W.C. HOPLER DEPT. 2560 DATE 1-3-62
CHECKED
STRESS ENGR.
BY. ENGR.
MATL. ENGR.
RELIABILITY
ENGR.
PROGRAM MGR.
DEP.
CUST. REP.

THE MARTIN COMPANY BALTIMORE, MARYLAND

TEST PANEL
REFRACTORY METALS HONEYCOMB
PT 9363

CODE IDENT NO. 38597 SIZE D SK-46844
SCALE SHEET 4 OF 5

CALC BY	DASH NUMBER	NEXT ASSY	USED ON	FINAL ASSY	TEST
		APPLICATION		QTY. REQD	

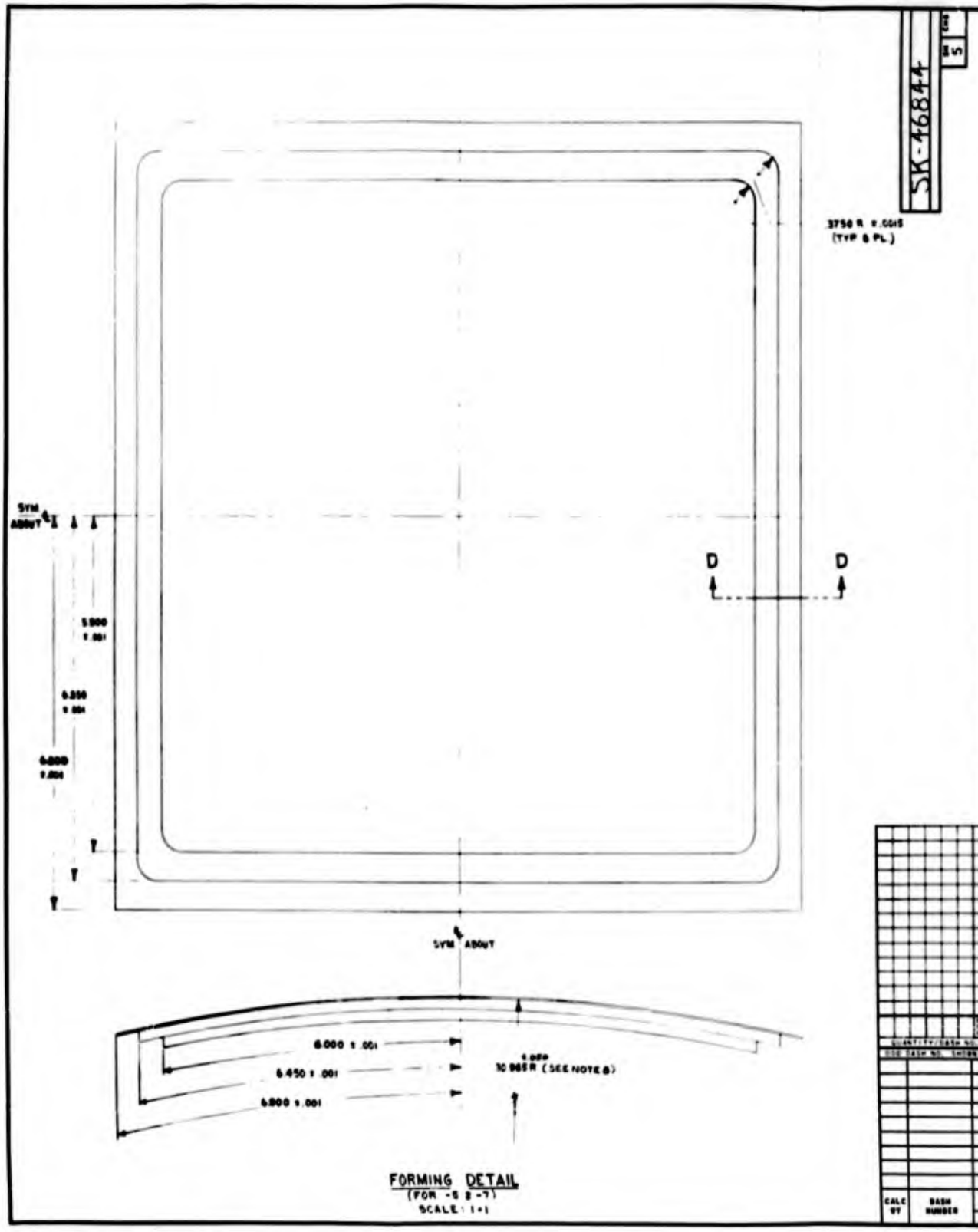
SK-46844
.3750 R ± .005
(TYP 8 PL)
SYM ABOUT
D
D
5.500 ± .001
6.250 ± .001
6.000 ± .001
SYM ABOUT
6.000 ± .001
6.450 ± .001
6.900 ± .001
10.965 R (SEE NOTE 8)
FORMING DETAIL
(FOR -5 & -7)
SCALE 1=1
CALC BY
DASH NUMBER

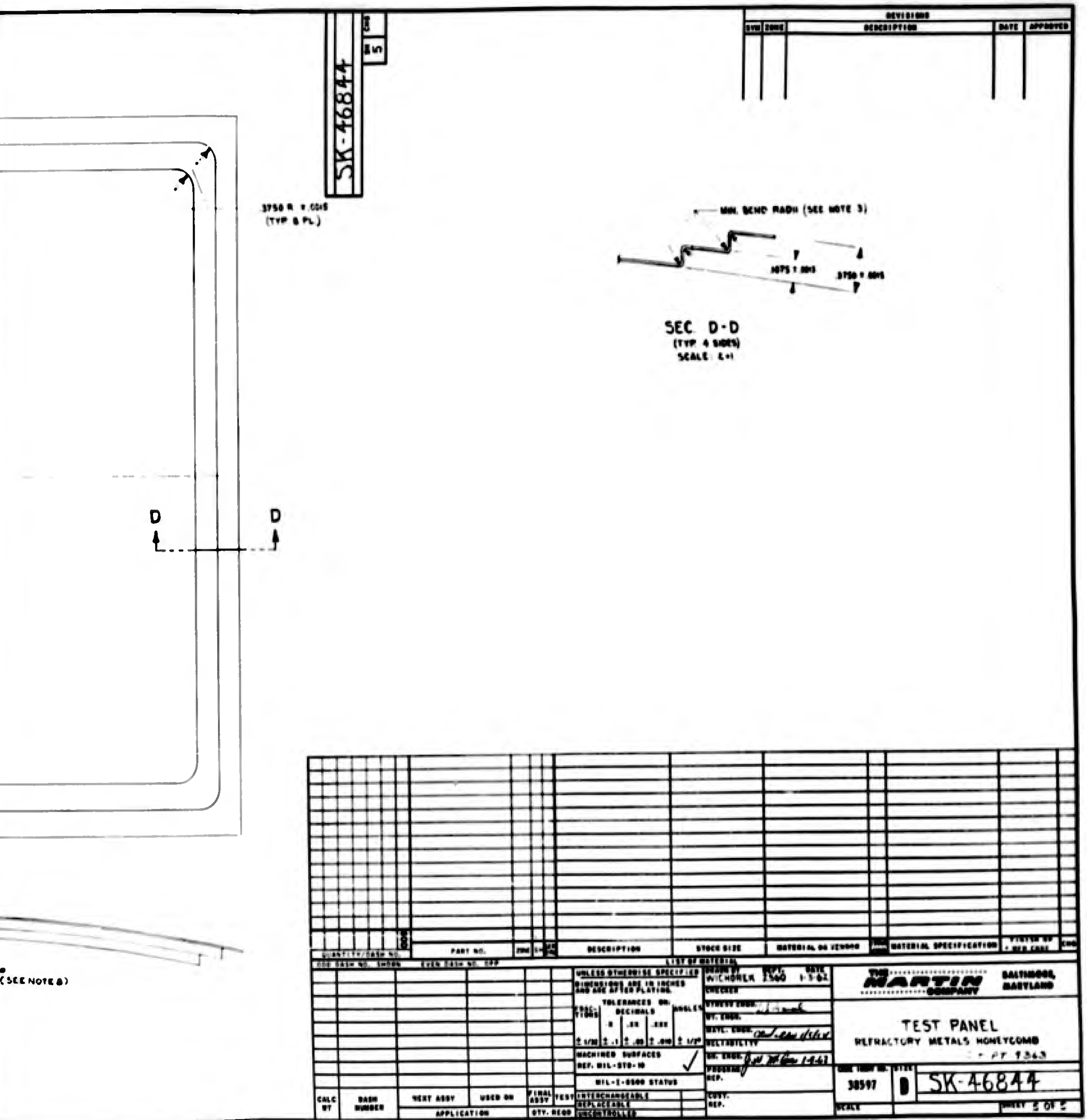
SK-46844
REVISIONS
.3750 R ±.0015 (TYP 8 PL.)
MIN. BEND RADII (SEE NOTE 3)
SEC D-D
(TYP 4 SIDES)
D
D
(SEE NOTE 8)
LIST OF MATERIAL
DESCRIPTION
STOCK SIZE
MATERIAL SPECIFICATION
UNLESS OTHERWISE SPECIFIED
DIMENSIONS ARE IN INCHES AND ARE AFTER PLATING.
TOLERANCES ON:
DECIMALS
ANGLES
MACHINED SURFACES
REF. MIL-STD-10
WICHOREK 2560
CHECKER
THE MARTIN COMPANY
BALTIMORE, MARYLAND
TEST PANEL
REFRACTORY METALS HONEYCOMB
38597
D
SK-46844
SCALE
SHEET 5 OF 5

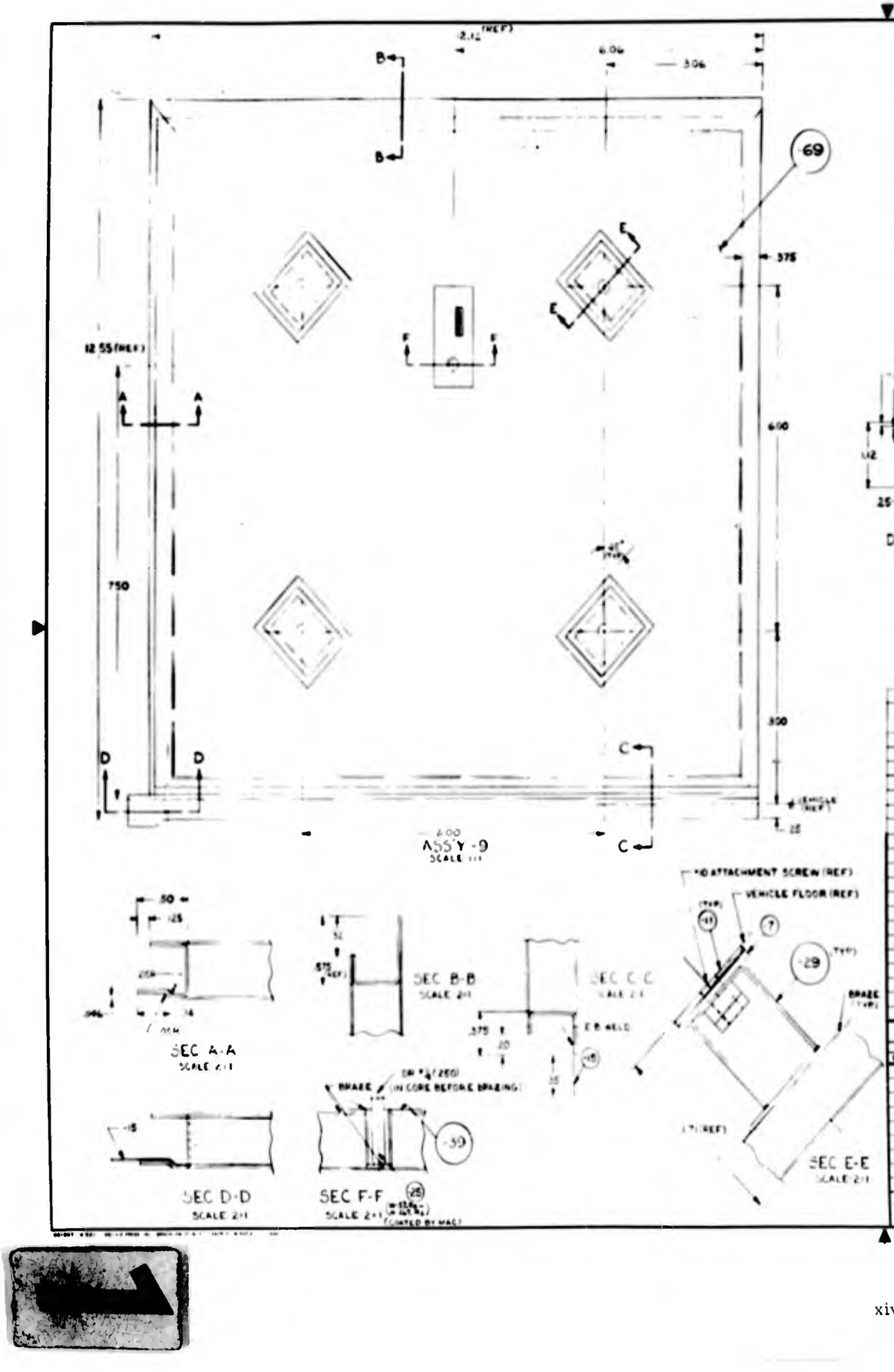
12.55 (REF)
6.06
3.06
69
375
600
750
300
25
50
ASSY -9
SCALE 1:1
DETAIL -2
SCALE 1:1
SEC A-A
SCALE 2:1
SEC B-B
SCALE 2:1
SEC C-C
SCALE 2:1
SEC D-D
SCALE 2:1
SEC F-F
SCALE 2:1
SEC E-E
SCALE 2:1
BRAZE
VEHICLE FLOOR (REF)
-29
-39

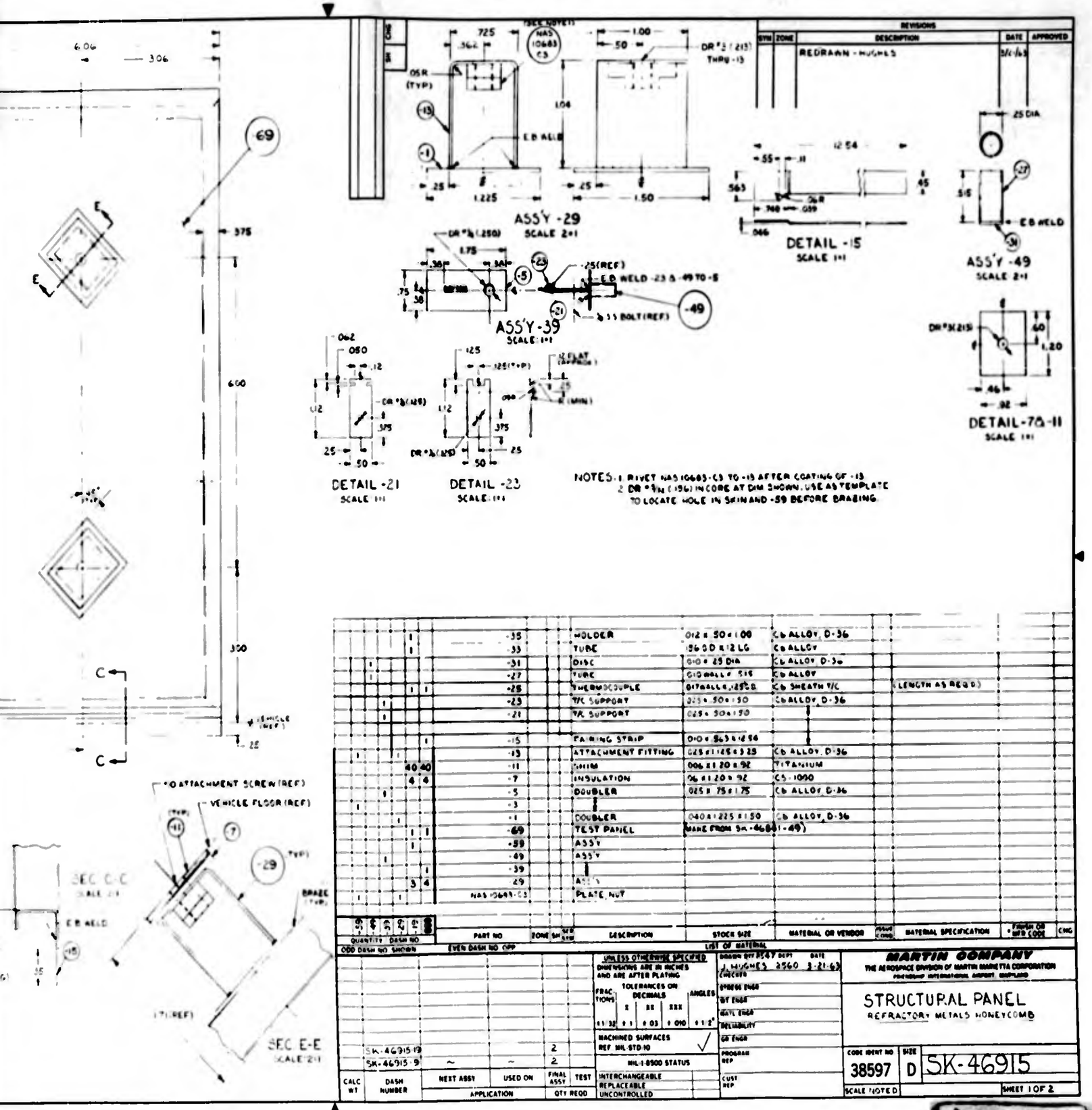

REVISIONS				
SYM	ZONE	DESCRIPTION	DATE	APPROVED
		REDRAWN - HUGHES	3/21/63	

QUANTITY DASH NO						PART NO	ZONE	SYM	DESCRIPTION	STOCK SIZE	MATERIAL OR VENDOR	MATERIAL SPECIFICATION
					-35				HOLDER	.012 x .50 x 1.00	Cb ALLOY D-36	
					-33				TUBE	.156 OD x .12 LG	Cb ALLOY	
					-31				DISC	.010 x .25 DIA	Cb ALLOY D-36	
					-27				TUBE	.010 WALL x .515	Cb ALLOY	
					-25				THERMOCOUPLE	.010 WALL x .125 OD	Cb SHEATH Y/C	(LENGTH AS REQ'D)
					-23				Y/C SUPPORT	.025 x .50 x 1.50	Cb ALLOY D-36	
					-21				Y/R SUPPORT	.025 x .50 x 1.50		
					-15				PA RING STRIP	.010 x .563 x 1.56		
					-13				ATTACHMENT FITTING	.025 x 1.125 x 3.25	Cb ALLOY D-36	
					-11				SKIN	.006 x 1.20 x .92	TITANIUM	
					-7				INSULATION	.06 x 1.20 x .92	C5-1000	
					-5				DOUBLER	.025 x .75 x 1.75	Cb ALLOY D-36	
					-3							
					-1				DOUBLER	.040 x 1.225 x 1.50	Cb ALLOY D-36	
					-69				TEST PANEL	(MAKE FROM SK-46841-49)		
					-59				ASS'Y			
					-49				ASS'Y			
					-39				ASS'Y			
					-29				ASS'Y			
3	4				NAS 1069-C3				PLATE NUT			

ODD DASH NO SHOWN — EVEN DASH NO OPP — LIST OF MATERIAL

CALC WT	DASH NUMBER	NEXT ASSY	USED ON	FINAL ASSY	TEST
	SK-46915-19			2	
	SK-46915-9	~	~	2	
		APPLICATION		QTY REQD	

UNLESS OTHERWISE SPECIFIED
DIMENSIONS ARE IN INCHES AND ARE AFTER PLATING
TOLERANCES ON FRACTIONS ±1/32, DECIMALS X ±.1, XX ±.03, XXX ±.010, ANGLES ±1°
MACHINED SURFACES REF MIL-STD-10 ✓
MIL-I-8500 STATUS
INTERCHANGEABLE
REPLACEABLE
UNCONTROLLED

DRAWN BY J.S.Y DEPT 2560 DATE 3-21-63
J. HUGHES
CHECKED
STRESS ENGR
QT ENGR
QA/L ENGR
RELIABILITY
QR ENGR
PROGRAM REP
CUST REP

MARTIN COMPANY
THE AEROSPACE DIVISION OF MARTIN MARIETTA CORPORATION
DENVER INTERNATIONAL AIRPORT, COLORADO

STRUCTURAL PANEL
REFRACTORY METALS HONEYCOMB

CODE IDENT NO	SIZE	
38597	D	SK-46915
SCALE NOTED		SHEET 1 OF 2

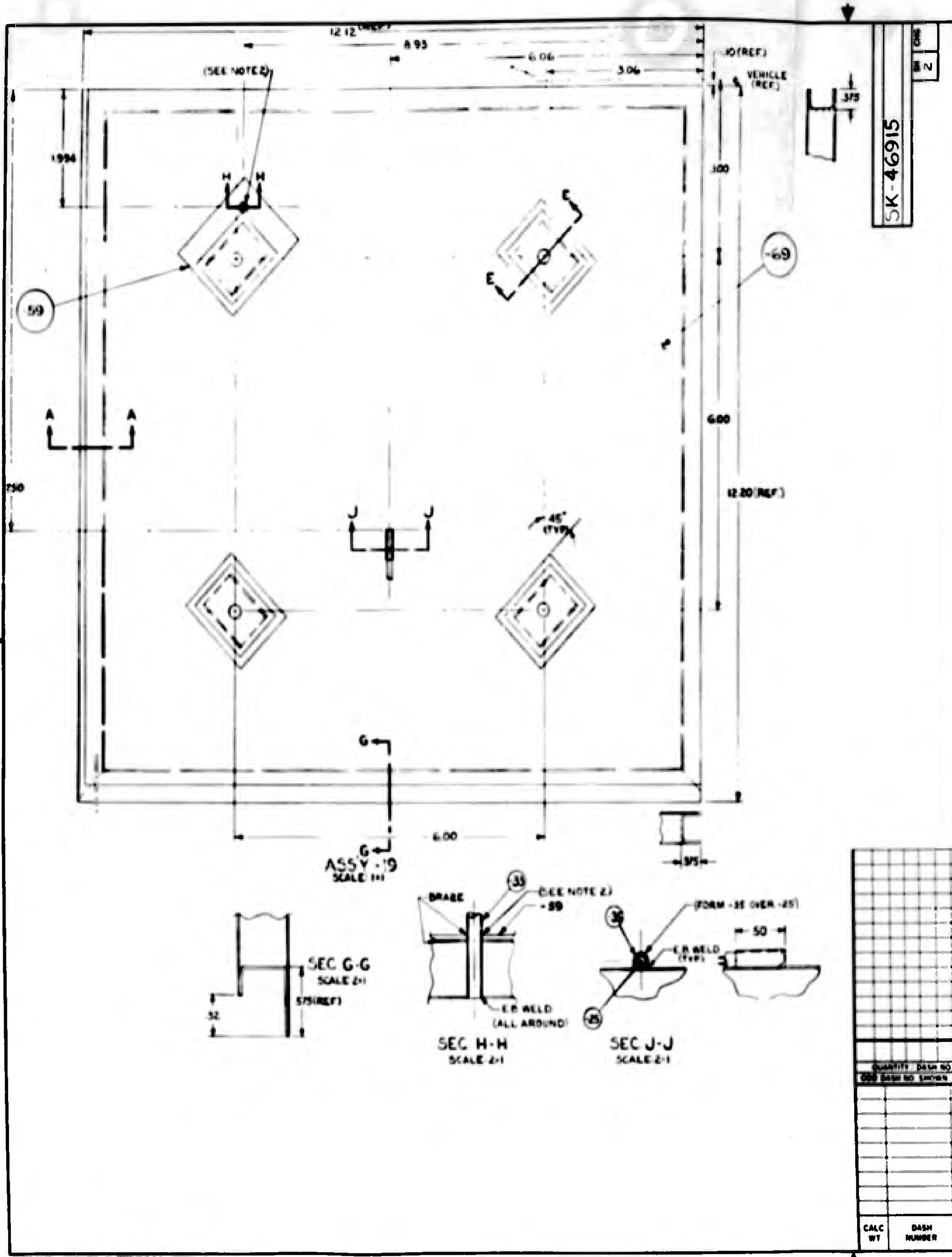
SK-46915
(SEE NOTE 2)
VEHICLE (REF)
12.20 (REF)
ASSY -19
SCALE 1:1
SEC G-G
SCALE 2:1
575(REF)
BRAZE
(SEE NOTE 2)
E.B WELD (ALL AROUND)
SEC H-H
SCALE 2:1
(FORM -35 OVER -25)
E.B WELD (TYP)
SEC J-J
SCALE 2:1
CALC WT
DASH NUMBER

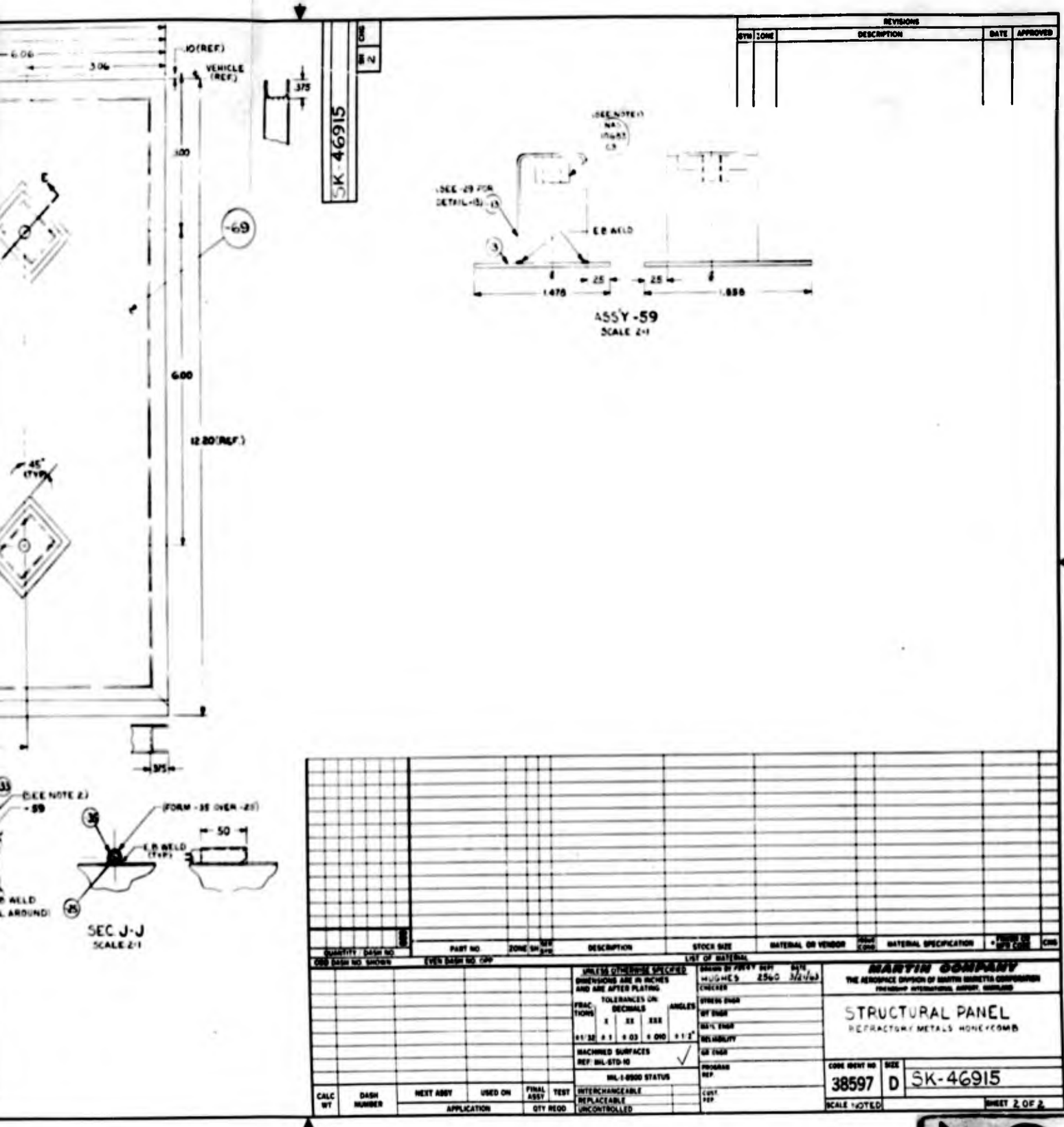
SK-46915
REVISIONS
DESCRIPTION
DATE
APPROVED
ASSY -59
SCALE 2:1
SEC J-J
SCALE 2:1
MARTIN COMPANY
STRUCTURAL PANEL
REFRACTORY METALS HONEYCOMB
38597
D
SK-46915
SCALE NOTED
SHEET 2 OF 2

APPENDIX B

HEAT SHIELD PANEL ANALYSIS

One of the more promising concepts for the design of an order skin of an aerospace vehicle is that of the non-structural heat shield which is composed of a number of discrete panels. Each of these panels is supported from the structural skin of the vehicle on equally spaced posts which hold the panel parallel to the structural skin and serve to transmit the local aerodynamic pressure loads from the heat shield panel to the structure. The posts are light-weight and provide a path of high thermal resistance. The individual heat shield panels are separated sufficiently from each other to permit their free thermal expansion. These discontinuities preclude the carrying of structural bending or shearing loads in the heat shield.

This study was made specifically for honeycomb core sandwich panels, but it is adaptable to similar types of isotropic or nearly isotropic heat shield panels. A typical heat shield assembly is shown in Fig. B-1.

1. Method of Analysis

The numerous solutions which are available for the analysis of plates with simply supported or clamped edges are not directly applicable to a plate on post supports. In the case of simply supported or clamped edge sandwich panels, the deflection analysis and stress analysis may readily be performed according to Ref. B-1. There is no such method available for the post-supported sandwich panel in which the core shear flexibility is taken into account. This report provides an approximate method of solution for a post-supported sandwich panel with isotropic core and facings.

The deflection of a solid plate is ordinarily calculated by means of the solution of the following plate partial differential equation of equilibrium (Ref. B-2, Eq 103):

$$\nabla^4 w = \frac{\partial^4 w}{\partial x^4} + 2\frac{\partial^4 w}{\partial x^2 \partial y^2} + \frac{\partial^4 w}{\partial y^4} = \frac{q}{D} \quad \text{(B-1)}$$

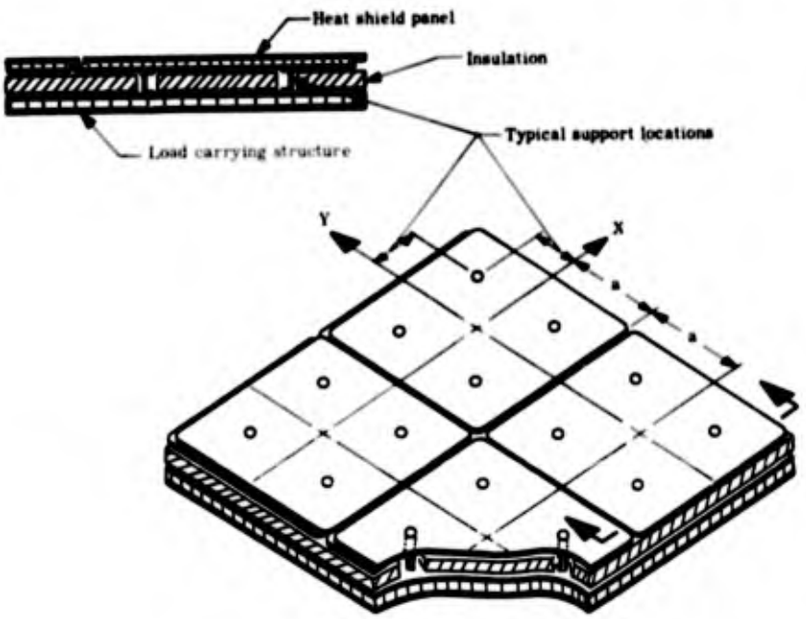

Fig. B-1. Typical Heat Shield Arrangement

This equation does not account for the effect of transverse shear deformation such as that encountered in sandwich plate analysis. Equation (B-1) is appropriate for a "solid" plate in which the transverse shear flexibility is assumed to be negligible. The solution of Eq (B-1) in conjunction with the appropriate boundary condition equations has been employed for many practical solid plate applications (Ref. B-2). However, if the effect of transverse core shear flexibility is included in the development of plate equations, a formidable sixth-order partial differential equation of equilibrium is obtained. Equations for the analysis of plates with finite shear stiffness and orthotropic properties are presented in Ref. B-3. Equation (B-1a) is the basic equation from Ref. B-3 for comparison with Eq (B-1).

$$\frac{1}{2}\frac{D'_{xy}D'_x}{D_{Q_y}}\frac{\partial^6 w}{\partial x^6} + \frac{1}{2}\frac{D'_{xy}D'_y}{D_{Q_x}}\frac{\partial^6 w}{\partial y^6}$$

$$+\left(\frac{1}{2}\frac{D'_{xy}D'_x}{D_{Q_x}} + \frac{D'_xD'_y - \frac{1}{2}D'_{xy}D'_x\mu_y - \frac{1}{2}D'_{xy}D'_y\mu_x}{D_{Q_y}}\right)\frac{\partial^6 w}{\partial x^4\partial y^2}$$

$$+\left(\frac{1}{2}\frac{D'_{xy}D'_y}{D_{Q_y}} + \frac{D'_yD'_x - \frac{1}{2}D'_{xy}D'_y\mu_x - \frac{1}{2}D'_{xy}D'_x\mu_y}{D_{Q_x}}\right)\frac{\partial^6 w}{\partial y^4\partial x^2}$$

$$-\left(2D'_{xy}\left(1-\mu_x\mu_y\right) + D'_x\mu_y + D'_y\mu_x\right)\frac{\partial^4 w}{\partial x^2\partial y^2}$$

$$- D'_x\frac{\partial^4 w}{\partial x^4} - D'_y\frac{\partial^4 w}{\partial y^4} = -\left(1-\mu_x\mu_y\right)q. \qquad \text{(B-1a)}$$

The solution of Eq (B-1a) would be difficult even for a simply supported, uniformly loaded sandwich plate. The fact that most sandwich plate solutions are based upon approximate energy methods testifies to the difficulty of directly integrating the sixth-order partial differential Eq (B-1a). The additional complexity of post supports further dictates against any attempt to use Eq (B-1a) in this brief study.

Instead, an approximate method is used in which a correction for shear deflection is applied to the deflection calculated for a post-supported square flat "solid" plate with a uniform load. The effect of core shear flexibility upon simply supported, uniformly loaded square or circular flat sandwich plates is readily determined from Ref. B-1. The midpoint deflection for either a square or circular plate accordingly is approximated by the equation

$$w = w_0\,(1 + 1.25V) \qquad \text{(B-2)}$$

where w_0 is the maximum deflection at the center of the corresponding solid plate. The symbol V represents the well-known ratio $\pi^2\,D/a^2U$ of sandwich theory (Ref. B-1, page 53).

A method of "solid" plate deflection analysis using Eq (B-1) is presented in this report. The deflections w_0 thus calculated may be corrected according to Eq (B-2) to provide an approximate deflection analysis for the post-supported sandwich plate. A deflection test will be performed on a sandwich panel heat shield assembly, which will provide a check on the validity of using Eq (B-2) for a post-supported plate.

It can be shown (Refs. B-1 and B-4) that the core shear flexibility has negligible effect upon the bending stress in the facings of a simply supported, uniformly loaded rectangular sandwich plate with isotropic core properties. Therefore, it is suggested that the heat shield facing stresses be calculated from the bending deflections as calculated for a "solid" post-supported plate. This approximation is not recommended, however, in the case of a sandwich panel whose core properties are not essentially isotropic.

2. Finite Difference Method

It is frequently possible to solve Eq (B-1) approximately by finite difference methods (Refs. B-2, B-5 and B-6). The deflections are calculated

at a finite number of equally spaced grid points. The plate bending moments are expressed in terms of calculated deflections by finite difference approximations to the moment equations

$$M_x = -D\left(\frac{\partial^2 w}{\partial x^2} + \mu \frac{\partial^2 w}{\partial y^2}\right) \qquad \text{(B-3a)}$$

and

$$M_y = -D\left(\frac{\partial^2 w}{\partial y^2} + \mu \frac{\partial^2 w}{\partial x^2}\right) \qquad \text{(B-3b)}$$

The grid point numbering system of Ref. B-5 is used and is illustrated in Fig. B-2. It is only necessary to consider one-half of one quadrant of the plate because of its symmetry about the diagonal lines and the centerlines. If the plate half-length a is divided into n spaces, then the grid spacing λ is equal to $\frac{a}{n}$. In Fig. B-2, n = 6, so $\lambda = \frac{a}{6}$.

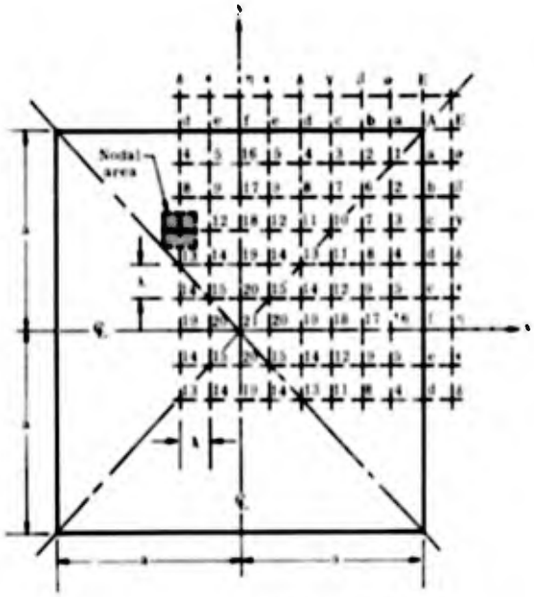

Fig. B-2. Typical System of Numbering Finite Difference Grid Points on a Square Heat Shield

It is convenient to adopt a standard nodal point numbering system to be used in the writing of finite difference approximations to the plate equations. The numbering system of Ref. B-7 is illustrated in Fig. B-3.

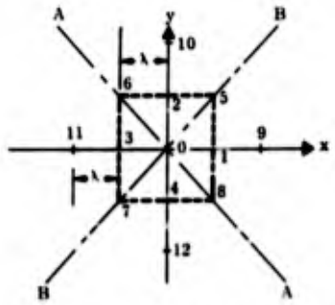

Fig. B-3. Numbering System Used in Writing Finite Difference Equations for a Typical Point "0"

The finite difference approximations to some of the more commonly used partial derivatives are copies from Ref. B-7, in conjunction with the numbering convention of Fig. B-3.

$$\left(\frac{\partial w}{\partial x}\right)_0 = \frac{w_1 - w_3}{2\lambda} \qquad \text{(B-4)}$$

$$\left(\frac{\partial w}{\partial y}\right)_0 = \frac{w_2 - w_4}{2\lambda} \qquad \text{(B-5)}$$

$$\left(\frac{\partial^2 w}{\partial x^2}\right)_0 = \frac{w_1 - 2w_0 + w_3}{\lambda^2} \qquad \text{(B-6)}$$

$$\left(\frac{\partial^2 w}{\partial y^2}\right)_0 = \frac{w_2 - 2w_0 + w_4}{\lambda^2} \qquad \text{(B-7)}$$

$$(\nabla^2 w)_0 = \frac{\partial^2 w}{\partial x^2} + \frac{\partial^2 w}{\partial y^2} = \frac{w_1 + w_2 + w_3 + w_4 - 4w_0}{\lambda^2} \qquad \text{(B-8)}$$

$$\left(\frac{\partial^2 w}{\partial x\, \partial y}\right)_0 = \frac{1}{4\lambda^2}\left(w_5 - w_6 + w_7 - w_8\right) \qquad \text{(B-9)}$$

$$\left(\frac{\partial^3 w}{\partial y\, \partial x^2}\right)_0 = \frac{1}{2\lambda^3}\left(w_5 - 2w_2 + w_6 - w_8 + 2w_4 - w_7\right) \qquad \text{(B-10)}$$

$$(\nabla^4 w)_0 = \frac{\partial^4 w}{\partial x^4} + 2\frac{\partial^4 w}{\partial x^2 \partial y^2} + \frac{\partial^4 w}{\partial y^4} = \frac{1}{\lambda^4}\left(20w_0 - 8\left(w_1 + w_2 + w_3 + w_4\right)\right.$$

$$+ 2\left(w_5 + w_6 + w_7 + w_8\right)$$
$$+ w_9 + w_{10} + w_{11} + w_{12}\Big) \qquad \text{(B-11)}$$

Equation (B-1) is written in the finite difference form of Eq (B-11) as

$$20 w_0 - 8\left(w_1 + w_2 + w_3 + w_4\right)$$
$$+ 2\left(w_5 + w_6 + w_7 + w_8\right)$$
$$+ w_9 + w_{10} + w_{11} + w_{12} = \frac{q\lambda^4}{D}. \qquad \text{(B-12)}$$

Equation (B-12) is directly applicable to each of the internal plate points numbered 6 through 21 of Fig. B-2. The points E, α, β, etc., are fictitious points external to the plate proper. The equations for these points and for the edge points must be written subject to the appropriate boundary conditions.

The lateral load corresponding to each internal point is $q\lambda^2$, that is, the load intensity q times the area λ^2. An exception is made, however, at the point on the diagonal, upon which the plate is supported. The support reaction is $-qa^2$ for each of the four equally loaded supports. Therefore, the net load on the supported node is $q(\lambda^2 - a^2) = q\lambda^2(1 - n^2)$. The equation corresponding to the supported point is written as

$$20 w_0 - 8\left(w_1 + w_2 + w_3 + w_4\right)$$
$$+ 2\left(w_5 + w_6 + w_7 + w_8\right)$$
$$+ w_9 + w_{10} + w_{11} + w_{12} = \frac{q\lambda^2(1 - n^2)}{D}. \qquad \text{(B-13)}$$

Two boundary conditions are used at the free edges for the writing of the equations for each edge point. The moment normal to the free edge is equal to zero so that at the edge (y = +a)

$$\frac{\partial^2 w}{\partial y^2} + \mu \frac{\partial^2 w}{\partial x^2} = 0. \qquad \text{(B-14)}$$

The second boundary equation at a free edge, such as the edge (y = +a), states that the edge shear loading is zero, that is,

$$\frac{\partial^3 w}{\partial y^3} + (2 - \mu)\frac{\partial^3 w}{\partial y\, \partial x^2} =$$
$$\frac{\partial}{\partial y}\nabla^2 w + (1 - \mu)\frac{\partial^3 w}{\partial y\, \partial x^2} = 0. \qquad \text{(B-15)}$$

The numbering system of Fig. B-3 is shown in Fig. B-4 as applied to a typical point 0 at the edge.

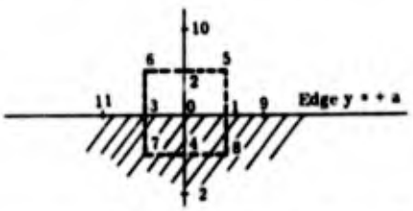

Fig. B-4. Numbering for a Typical Nodal Point 0 on a Free Edge

Equations (B-14) and (B-15) are written in finite difference form using Fig. B-4 and Eqs (B-4) through (B-11) as

$$\frac{\partial^2 w}{\partial y^2} + \mu \frac{\partial^2 w}{\partial x^2} =$$
$$\frac{w_2 + w_4 - 2w_0 + \mu\left(w_1 - 2w_0 + w_3\right)}{\lambda^2} = 0 \qquad \text{(B-16)}$$

and

$$-4w_2 + 4w_4 + w_5 + w_6 - w_7 - w_8 + w_{10} - w_{12}$$
$$+ (1 - \mu)\left(-2w_2 + 2w_4 + w_5 + w_6 - w_7 - w_8\right) = 0. \qquad \text{(B-17)}$$

Note that Eq (B-17) includes the deflection w_{10} of point 10, which is two grid distances from the edge in Fig. B-4. The plate equilibrium equation, Eq (B-12), also includes w_{10}. It is therefore necessary to eliminate w_{10} between Eqs (B-12) and (B-17) to arrive at the second equation for each edge point. The resulting equation is

$$-2(1+\mu)w_2 + \mu w_5 + \mu w_6 + (2\mu - 14)w_4$$
$$+ (4 - \mu)w_8 + (4 - \mu)w_7$$

$$-8w_1 - 8w_3 + w_9 + w_{11} + 2w_{12}$$

$$+ 20w_0 = q\lambda^4/D. \qquad \text{(B-18)}$$

The corner point A of Fig. B-2 receives special treatment due to the fact that both M_x and M_y equal zero at A. In terms of the numbering of Fig. B-3,

$$\frac{\partial^2 w}{\partial x^2} = \frac{w_1 + w_3 - w_0}{\lambda^2} = 0 \qquad \text{(B-19a)}$$

and

$$\frac{\partial^2 w}{\partial y^2} = \frac{w_2 + w_4 - w_0}{\lambda^2} = 0. \qquad \text{(B-19b)}$$

In the case of the square plate of Fig. B-2, either Eq (B-19a) or (B-19b) results in the equation

$$w_E - 2w_A + w_a = 0. \qquad \text{(B-20)}$$

There must be as many equations as there are unknown deflections. The final equation serves the purpose of relating the deflections to a convenient plane of reference by the specification that the deflection is zero at the supported (nth) point, that is,

$$w_n = 0. \qquad \text{(B-21)}$$

One of of Eqs (B-12), (B-13), (B-16), (B-18), (B-20) or (B-21) is written for each of the grid points.

The method presented in Chapter IV of Ref. B-6 uses a slightly different method of applying the boundary conditions from that used here. The author (Ref. B-6) uses the alternative form of the equilibrium equation

$$\frac{\partial^2 M_x}{\partial x^2} - 2\frac{\partial^2 M_{xy}}{\partial x\,\partial y} + \frac{\partial^2 M_y}{\partial y^2} = -q \qquad \text{(B-21a)}$$

instead of Eq (B-1).

3. Sample Analysis of Heat Shield Panel

Four sample plate problems have been worked for the purpose of analyzing the post-supported heat shield panel. The four cases are identical except for the location of the post supports. Each quadrant of the plate is divided into the grid system of Fig. B-2. The support point is at one of the points, 13, 10, 6 or 1, for each of the four cases. The nondimensional coordinates of the support points for the four cases are, respectively (cf. Fig. B-2):

$$\frac{x}{a} = \frac{y}{a} = 0.333,\ 0.500,\ 0.667 \text{ or } 0.833.$$

Several of the 35 equations are written for the case in which the support is at point 6 in order to demonstrate the procedure. Equation (B-12) is used to write the following expression for point 8 which is a typical internal point.

$$2w_3 - 8w_4 + 2w_5 + w_6 - 8w_7 + 20w_8 - 8w_9 + 2w_{10}$$

$$- 8w_{11} + 2w_{12} + w_{13} + w_{17} + w_d = \frac{q\lambda^4}{D}. \qquad \text{(B-22)}$$

Points equally spaced on either side of the centerlines and diagonal lines have equal deflections. This is shown symbolically in Fig. B-2 by the use of identical numbering of corresponding "reflection" points. The equation for the support point 6 is obtained from Eq (B-13) as

$$2w_1 - 16w_2 + 4w_3 + 20w_6 - 16w_7 + 2w_8 + 2w_{10}$$

$$+ 2w_b = -35\, q\lambda^4/D. \qquad \text{(B-23)}$$

A value of $\mu = 0.3$ is assumed, and Eqs (B-16) and (B-18) are used to write the following equations for a typical edge point c

$$-w_3 - 0.3w_b + 2.6w_c - 0.3w_d - w_\gamma = 0 \qquad \text{(B-24)}$$

and

$$3.7w_2 - 13.4w_3 + 3.7w_4 + 2w_7 + w_a - 8w_b + 20w_c$$

$$- 8w_d + w_e + 0.3w_\beta - 2.6w_\gamma + 0.3w_\delta = q\lambda^4/D.$$

$$\text{(B-25)}$$

Equation (B-20) is used for the corner point A and Eq (B-21) for the supported point 6.

Thirty-five equations typified by Eqs (B-22), (B-23), (B-24) and (B-25) are written for each of the four cases. The four sets of equations corresponding to the four cases have been solved for the 35 unknown deflections w by means of IBM 7090 program JB004. The results are presented and discussed in the next section.

4. Results and Discussion of Analysis

The deflections which have been calculated for each of the four example cases are presented in Table B-1 for the grid system of Fig. B-2.

Figures B-5 through B-8 are contour plots of the deflections of the four cases presented in Table B-1. The corner and center deflections are the largest due to the nature of the post support method. Because of their importance in design, the corner and center deflections (points A and 21) are plotted in Fig. B-9 as a function of the distance of the supports from the center of the heat shield. The four cases analyzed in this report do not include the one in which the heat shield is supported at the four corners A. However, the case of a corner-supported, uniformly loaded square plate is presented in Ref. B-2 (page 220). The midplate deflection from Ref. B-2 is included in Fig. B-9 of this report.

TABLE B-1

Deflection of Post-Supported Square Plate

Dimensionless Deflections

Grid Point	Support at Point 13 $\frac{x}{a} = \frac{y}{a} = 0.333$	Support at Point 10 $\frac{x}{a} = \frac{y}{a} = 0.500$	Support at Point 6 $\frac{x}{a} = \frac{y}{a} = 0.667$	Support at Point 1 $\frac{x}{a} = \frac{y}{a} = 0.833$
1	0.08210	0.02138	-0.01606	0.00000
2	0.06815	0.01609	-0.00730	0.03279
3	0.05551	0.01213	0.00392	0.06289
4	0.04550	0.01045	0.01441	0.08671
5	0.03929	0.01012	0.02167	0.10192
6	0.05356	0.01018	0.00000	0.06100
7	0.04007	0.00561	0.01159	0.08713
8	0.02934	0.00454	0.02199	0.10800
9	0.02301	0.00480	0.02898	0.12136
10	0.02535	0.00000	0.02144	0.10968
11	0.01345	-0.00326	0.03053	0.12784
12	0.00726	0.00083	0.03678	0.13957
13	0.00000	-0.00110	0.03837	0.14191
14	-0.00550	-0.00084	0.04380	0.15432
15	-0.01208	-0.00116	0.04865	0.16407
16	0.03721	0.01014	0.02425	0.10720
17	0.02097	0.00503	0.03144	0.12603
18	0.00539	0.00123	0.03899	0.14370
19	-0.00710	-0.00080	0.04573	0.15806
20	-0.01405	-0.00113	0.05039	0.16742
21	-0.01619	-0.00119	0.05206	0.17067
a	0.09636	0.02700	-0.02406	-0.02900
b	0.08274	0.02200	-0.01443	0.00632
c	0.07051	0.01825	-0.00298	0.03970
d	0.06084	0.01636	0.00782	0.06646
e	0.05473	0.01576	0.01539	0.08362
f	0.05267	0.01566	0.01810	0.08952
A	0.11046	0.03246	-0.03262	-0.06039

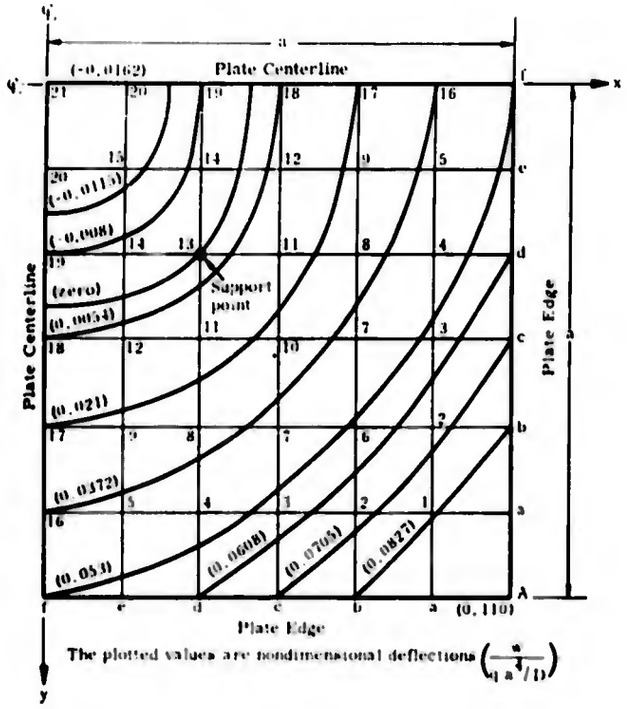

Fig. B-5. Contour Lines of Plate Deflections on a Quadrant of a Square Plate

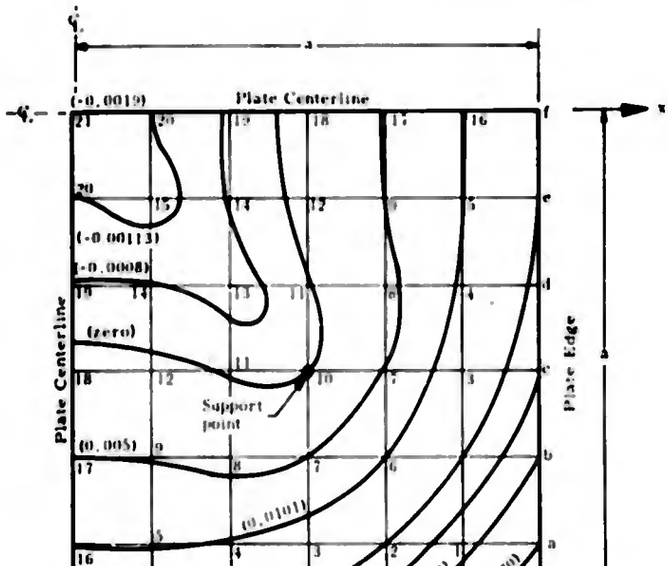

Fig. B-6. Contour Lines of Plate Deflections on a Quadrant of a Square Plate

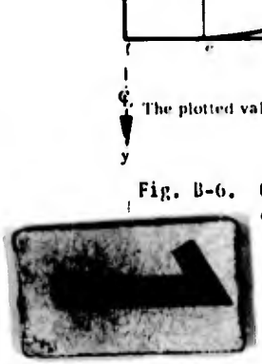

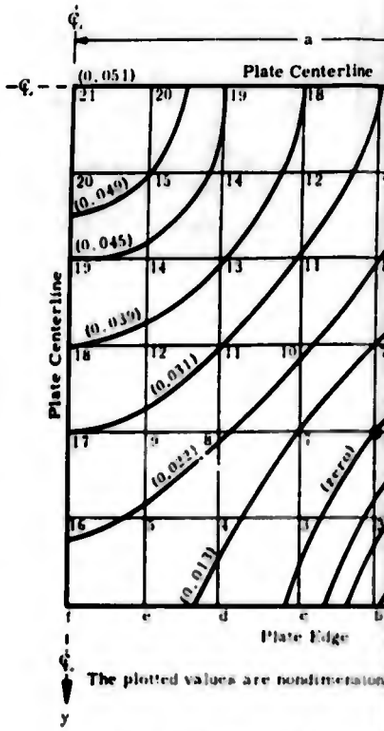

Fig. B-7. Contour Lines of
on a Quadrant of

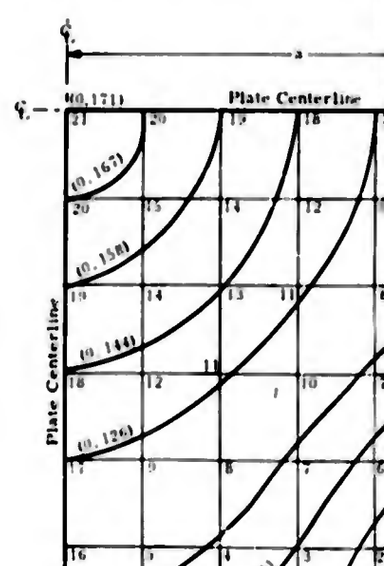

Fig. B-8. Contour Lines of
on a Quadrant of

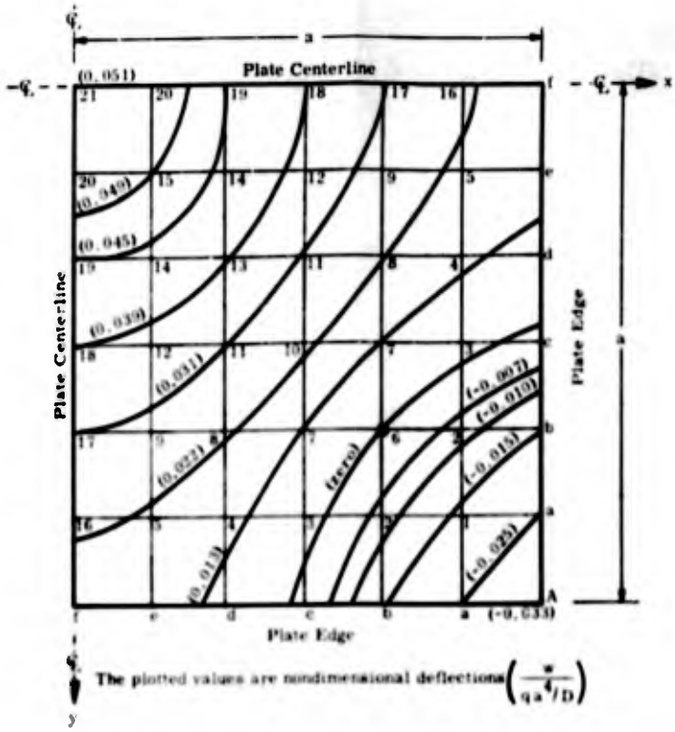

Fig. B-7. Contour Lines of Plate Deflections on a Quadrant of a Square Plate

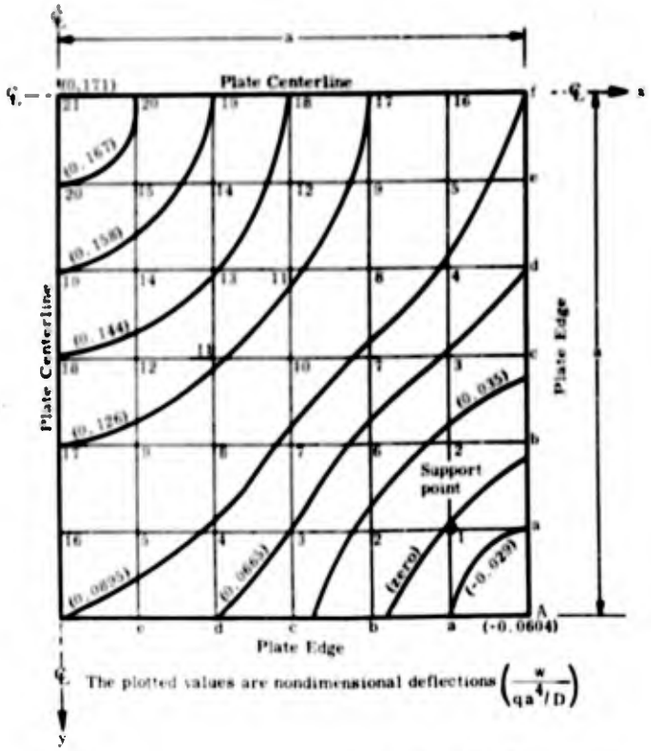

Fig. B-8. Contour Lines of Plate Deflections on a Quadrant of a Square Plate

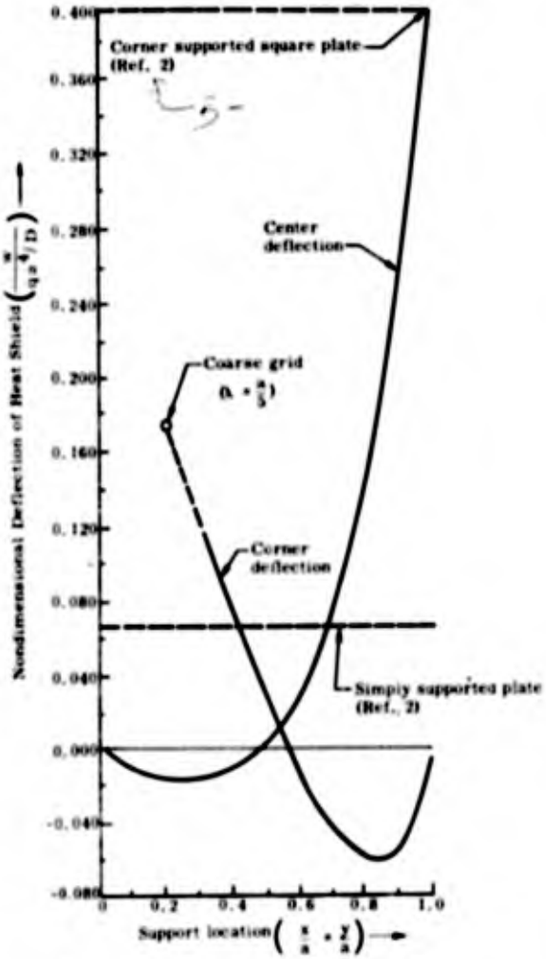

Fig. B-9. Deflection Versus Support Locations

A coarser grid ($\lambda = a/5$) also has been used with the supports at x/a = y/a = 0.2, 0.4, 0.6 and 0.8. The deflections thus calculated for the center and corner of the plate fall almost exactly on the curves of Fig. B-9. In fact, one of the points on the corner deflection curve of Fig. B-9 is seen to be taken from the coarser grid solution.

It is necessary that the bending moments be calculated so that the bending stresses for the facings may be calculated. Equation (B-3), which expresses the moment in terms of deflections, is readily written in finite difference form by means of Eqs (B-6) and (B-7), and with reference to the typical numbering convention of Fig. B-3.

$$M_x = -\frac{D}{\lambda^2}\left(w_1 - 2w_0 + w_3 + \mu\left(w_2 - 2w_0 + w_4\right)\right) \quad \text{(B-26)}$$

$$M_y = -\frac{D}{\lambda^2}\left(w_2 - 2w_0 + w_4 + \mu\left(w_1 - 2w_0 + w_3\right)\right) \quad \text{(B-27)}$$

The theory of plates (Ref. B-2, page 40) discusses the "Mohr's Circle" method of determining the bending moments at a point in a plate. This method permits the determination of the bending and twisting moments in any other direction if the moments corresponding to the principal directions are known.

The moments at the center of the plate are the same in all directions and are therefore obtained directly by the use of Eq (B-26) or (B-27).

The deflection pattern in the area adjacent to the supports does not result in calculated moments which satisfy the Mohr's Circle relationship. This probably is due to the combination of effects of the relatively coarse grid and the singularity introduced by the post support.

Since the bending moment in the diagonal direction corresponding to the "overhanging" corner is of considerable importance in the heat shield analysis, Eq (B-3) is directly written in finite form for the diagonal direction.

The equation is written for the directions A-A and B-B of Fig. B-3 by means of Eqs (B-3), (B-6) and (B-7) as

$$M_{A\text{-}A} = -\frac{D}{(1.414\lambda)^2}\left(w_8 - 2w_0 + w_6 + \mu\left(w_5 - 2w_0 + w_7\right)\right) \quad \text{(B-28)}$$

$$M_{B\text{-}B} = -\frac{D}{(1.414\lambda)^2}\left(w_5 - 2w_0 + w_7 + \mu\left(w_8 - 2w_0 + w_6\right)\right). \quad \text{(B-29)}$$

Equations (B-26) through (B-29) are used to calculate bending moments from the deflections given in Table B-1 for the four cases. The moments thus calculated are plotted versus support location in Fig. B-10 for several critical regions of the heat shield. The moment at the center (point 21) of the heat shield is the same in all directions. The moment parallel to the edge is plotted for point f at the centerline. The "overhanging" bending moment is plotted at the support point for the diagonal direction. The center and edge bending moments for the case of corner supports are taken from Ref. B-2 and are included in Fig. B-10.

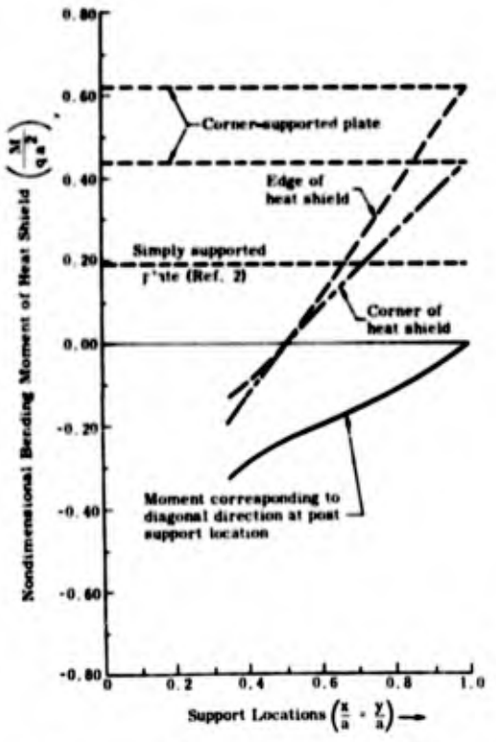

Fig. B-10. Plate Bending Moments Versus Support Locations

The curves of maximum deflections and moments in Figs. B-9 and B-10 provide a means of selecting a suitable support location. The midpoint deflection of a simply supported, uniformly loaded square plate is indicated in Fig. B-9 by the dashed line. It is seen in Fig. B-9 that for the support at x/a = 0.6, the corner deflection is essentially zero. The corner and center deflections are equal to each other for the case where the supports are at X/a = 0.55. In either case, the deflections are less than half that of the center of a simply supported square plate of the same size.

The midpoint bending moment of a simply supported, uniformly loaded square plate is shown in Fig. B-10 by the dashed line. The "overhang" moment at the support is essentially the same as the maximum bending moment of the simply supported plate when the support is in the range of x/a = 0.55 to 0.6. The moments at the center and edge of the heat shield, with supports in the range x/a = 0.55 to 0.6, are approximately half that of the simply supported plate.

As a result of the study of maximum deflections and moments, it is apparent that the placement of supports at x/a = 0.6 provides a compromise in which the deflections and moments are equal to or less than the maximum deflection and maximum moment of a simply supported square plate of the same size. The effect of transverse shear in causing additional deflection is evaluated approximately by the use of Eq (B-2).

The maximum bending moment is the "overhang" moment at the support. This moment is seen from Fig. B-10 to be equal to

$$M = -0.191\, qa^2 \qquad \text{(B-30)}$$

when the support is at the location

$$x/a = y/a = 0.6.$$

The bending stress in the facings is

$$\sigma = \frac{M}{t_i h} . \qquad \text{(B-31)}$$

The stress is tensile in the outer facing and compressive in the inner facing for a positive surface pressure "q."

Equation (B-31) and Fig. B-10 have been used to develop the nomograph of Fig. B-11. This figure provides a convenient method for the calculation of the maximum bending stress in the facings at the support. It is seen in Fig. B-10 that, for support locations outboard of point 6, the bending moment along the center of the edge of the heat shield is greater than at the support. The graphical solution of Eq (B-31) is provided in Fig. B-12 for the maximum bending stress at the edge.

5. Thermal Deflection

There is no exact analysis for thermal deflection of a sandwich panel on post supports. The method presented here is an approximation based upon several simplifying assumptions.

It is assumed that the core has a shear rigidity which is large enough to cause the plate to assume a spherical thermal curvature just as a solid plate would do. It is assumed that there is no temperature variation in the planes of the facings, but the facings are at two different temperatures, T_o and T_i. The subscripts designate the outer and inner facings. It is assumed that the restraints to thermal curvature offered by the flexible supports and the edge members are negligible.

An equation for the thermal deflection of a plate is readily obtained from Ref. B-8 (page 173) with the aid of Fig. B-13, as follows:

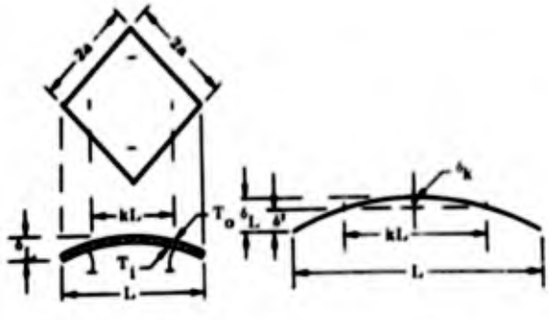

Fig. B-13. Thermal Deflection of Post-Supported Heat Shield

The deflection δ_L is given by the expression

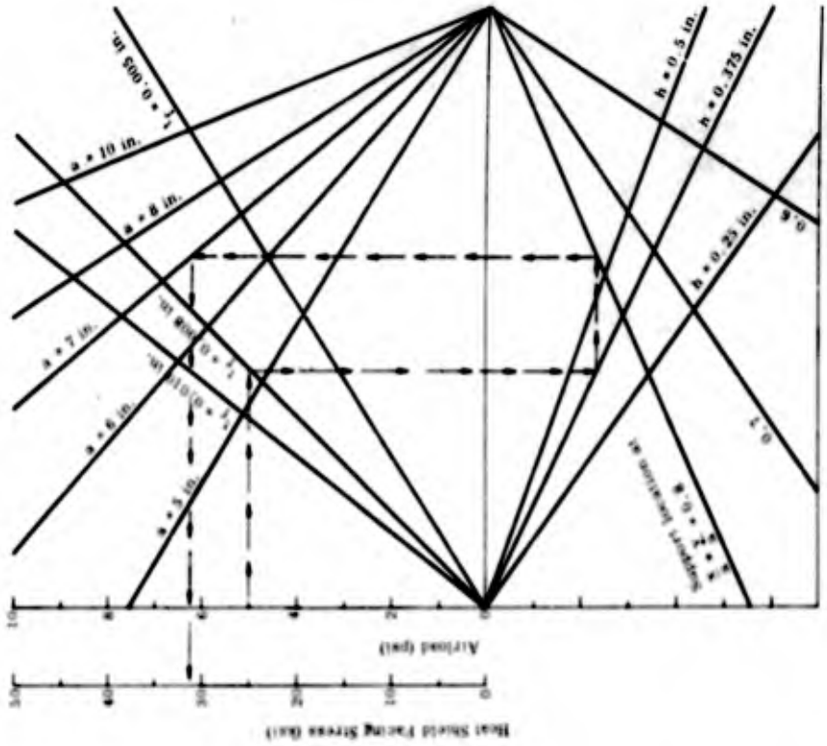

Fig. B-12. Heat Shield--Plate Bending Stress at Edge of Plate

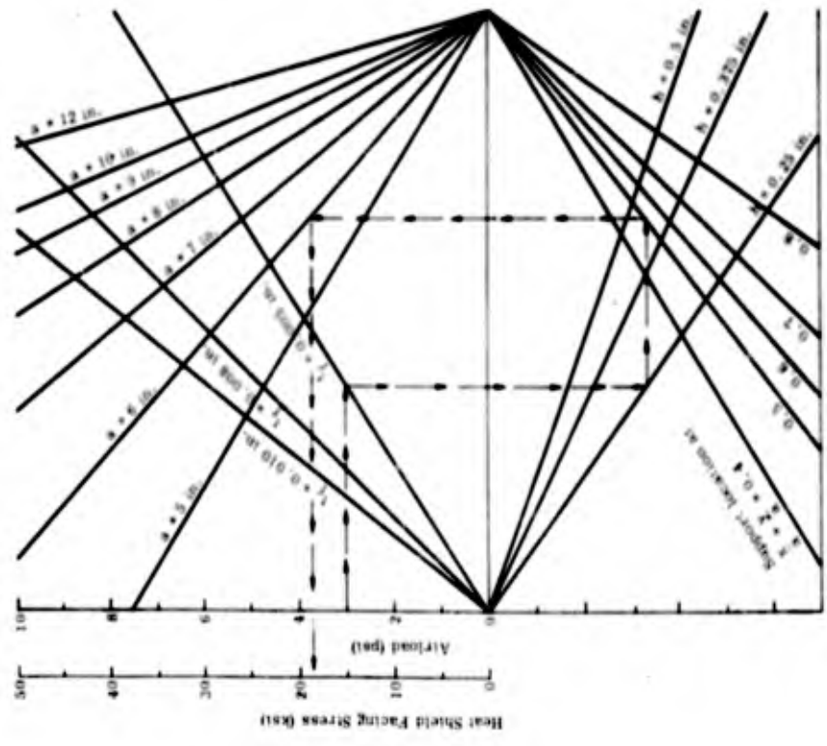

Fig. B-11. Heat Shield--Plate Bending Stress in Facing at Support Location

$$\delta_L = -\frac{M_T L^2 (1-\mu^2)}{8 EI (1+\mu)} \qquad \text{(B-32)}$$

where the thermal moment is

$$M_T = \frac{EI\alpha (T_o - T_i)}{h} . \qquad \text{(B-33)}$$

The substitution of M_T into Eq (B-32) results in the deflection expression

$$\delta_L = -\frac{\alpha (T_o - T_i)(1-\mu) L^2}{8h} . \qquad \text{(B-34)}$$

The deflection δ_L in terms of a is

$$\delta_L = -\frac{\alpha (T_o - T_i)(1-\mu) (1.414\, 2a)^2}{8h} \cdot \frac{\alpha (T_o - T_i)(1-\mu) a^2}{h} . \qquad \text{(B-35)}$$

The midpoint deflection δ_k is

$$\delta_k = k^2 \delta_L = -\frac{\alpha (T_o - T_i)(1-\mu) k^2 a^2}{h} . \qquad \text{(B-36)}$$

The corner deflection δ' is

$$\delta' = -(1-k^2)\delta_L = \frac{\alpha (T_o - T_i)(1-\mu)(1-k^2) a^2}{h} . \qquad \text{(B-37)}$$

The deflection equations do not take into account the temperature variations of the properties μ, E and α. It is suggested that properties be used which are the average of the values of the inner and outer facing to permit an approximate solution to be obtained.

In the case where the supports are at x/a = 0.6 and k = 0.6, the thermal deflections at the center and corner are found from Eqs (B-36) and (B-37) to be

$$\delta_k = -0.36 \frac{\alpha (T_o - T_i)(1-\mu) a^2}{h} \qquad \text{(B-38)}$$

and

$$\delta' = 0.64 \frac{\alpha (T_o - T_i)(1-\mu) a^2}{h} \qquad \text{(B-39)}$$

It is interesting to compare the maximum thermal deflections (Eqs (B-38) and (B-39)) of the post-supported heat shield with the midpoint thermal deflection of a simply supported square solid plate as analyzed in Ref. B-2 (page 164). The equation from Ref. B-2 is

$$w_m = -\frac{0.585\alpha (T_o - T_i)(1+\mu) 16a^2}{a^2 h} \qquad \text{(B-40)}$$

If μ is assumed to equal 0.3, the thermal deflection of Eq (B-40) becomes

$$w_m = -\frac{0.392\alpha (T_o - T_i) a^2}{h} . \qquad \text{(B-41)}$$

The center and corner deflections of the heat shield with supports at x/a = y/a = 0.6 similarly are found from Eqs (B-38) and (B-39) to be

$$\delta_k = -\frac{0.252\alpha (T_o - T_i) a^2}{h} \qquad \text{(B-42)}$$

and

$$\delta' = \frac{0.448\alpha (T_o - T_i) a^2}{h} . \qquad \text{(B-43)}$$

It is seen that the heat shield midpoint thermal deflection is less than that of the corresponding simply supported plate. However, the heat shield corner thermal deflection is 14% higher than the midpoint deflection of the simply supported plate.

LIST OF SYMBOLS

A	Area
a	Half-length of side of square plate
D	Plate rigidity $\left(\frac{EI}{1-\mu^2}\right)$ (per inch)
D'_x, D'_y	Orthotropic plate rigidity with unrestrained anticlastic curvature $\left(D'_x = -M_x \frac{\partial^2 w}{\partial x^2}\right)$
D'_{xy}	Twisting stiffness $\left(D'_{xy} = M_{xy} \Big/ \frac{\partial^2 w}{\partial x \partial y}\right)$
D_{Q_x}, D_{Q_y}	Transverse shear stiffness of plate
E	Young's modulus of elasticity
f	Stress
h	Sandwich panel thickness
I	Moment of inertia (per inch)
i	Subscript for "inner"
k	Nondimensional distance from center of heat shield to support location
M	Bending moment (per inch)
n	Number of divisions of plate quadrant
o	Subscript for "outer"
q	Distributed surface load on heat shield (psi)
T	Temperature (°F)
t	Thickness of sandwich panel facing
U	Transverse shear stiffness of sandwich panel core
w	Deflection of heat shield
α	Linear coefficient of thermal expansion $\left(\frac{\text{in.}}{\text{in.-°F}}\right)$
λ	Grid spacing (see Fig. B-2)
δ	Thermal deflection of heat shield
μ	Poisson's ratio
σ	Stress (psi)

REFERENCES

B-1. Anonymous, ANC-23, Part II, "Sandwich Construction for Aircra't," 2nd ed., 1955.

B-2. Timoshenko, S. and Woinowsky-Krieger, S., "Theory of Plates and Shells," 2nd ed., New York: McGraw-Hill Book Co., Inc., 1959.

B-3. Libove, C. and Batdorf, S. B., "A General Small Deflection Theory for Flat Sandwich Plates," NACA Report 899, 1948.

B-4. Raville, Milton E., "Deflection and Stresses in a Uniformly Loaded, Simply Supported, Rectangular Sandwich Plate," Forest Products Laboratory Report No. 1847, December 1955.

B-5. Holl, D. L., "Analysis of Plate Examples by Difference Methods and the Superposition Principle," Journal of Applied Mechanics, September 1936, pp A-81 to A-90.

B-6. William, D., "Theory of Aircraft Structures," 1st ed., London: Edward Arnold Ltd., 1960.

B-7. Shaw, F. S., "An Introduction to Relaxation Methods," 1st ed., New York: Dover Publications, 1953.

B-8. Gatewood, B. E., "Thermal Stresses," 1st ed., New York: McGraw-Hill Book Co., Inc., 1957.

B-9. McCown, J. W., Wilks, C. R. and Gagola, L. J., "Manufacturing Methods and Design Procedures of Brazed Refractory Metal Honeycomb Sandwich Panels," Contract No. AF33(657)-7276 ASD Project No. 7-937, Martin Marietta Corporation (Martin ER 12249).

APPENDIX C

THERMAL STRESS ANALYSIS OF SHEAR TEST PANELS

A relatively heavy René 41 superalloy edge fixture frame will be used to impose the edge shear loading condition upon the square sandwich panel specimen, as discussed in Section G and with a general arrangement similar to that shown in Fig. C-1. In addition to the difference in materials between the fixture frame and the sandwich facings, there is also a temperature differential associated with the elevated temperature shear test. Consequently, there are compressive thermal stresses in the sandwich facing during heating up and tensile thermal stresses during cooling down.

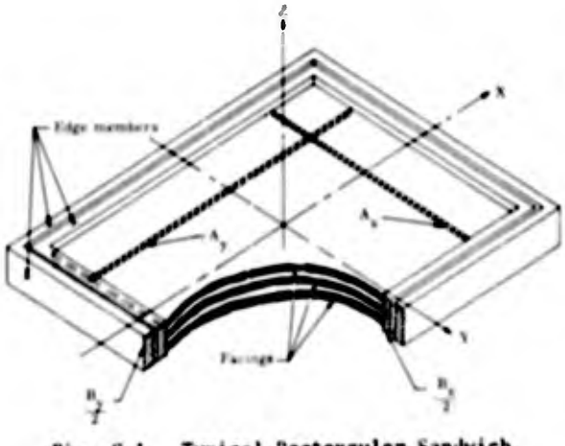

Fig. C-1. Typical Rectangular Sandwich Assembly of Flat Facings and Straight Edge Members

Figures C-2 and C-3 are provided as a means of setting safe limits on relative facing and fixture temperatures to prevent thermal stress damage during heating and cooling of the test specimens. Figure C-2 is for TZM molybdenum panels and Fig. C-3 is for D-36 columbium panels. The facing temperature should fall within the shaded area between the upper and lower limiting lines for any given temperature of the fixture frame. The upper line represents a compressive stress limitation and the lower line a tensile stress limitation for the material of the facing at its corresponding temperature. As an example of the use of the charts, consider the case of a D-36 columbium specimen when the shear test fixture frame is at 900° F. It may be seen in Fig. C-3 that the facing temperature should be within the range of temperatures from 1100° to 1870° F.

The charts are constructed on the assumptions that both facings of the panel are at the same uniform temperature and that the outer edge of the panel is at the same temperature as the fixture frame. The limiting thermal stresses in the facing have been established at 50% of tensile yield for a compressive limit and 70% of tensile yield for a tensile limit. The tensile yield is taken as the 0.1% "offset" yield from the available curves of tensile stress versus strain at various temperatures.

The thermal stress equation used for the construction of Figs. C-2 and C-3 for the shear test setup is:

$$\sigma_1 = \left(\frac{E_1}{1-\mu_1}\right)\left\{\frac{-(\alpha_1\Delta T_1)(A_2E_2+A_3E_3)+(A_2E_2\alpha_2+A_3E_3\alpha_3)\Delta T_3}{\left(\frac{A_1E_1}{1-\mu_1}\right)+(A_2E_2+A_3E_3)}\right\} \quad \text{(C-1)}$$

where

σ_1 = thermal stress in the facings (the subscript "1" applies to the facings; "2" to the outer edge of the specimen; and "3" to the fixture frame).

ΔT = difference between the actual temperature and 70° F (T - 70° F) (ΔT_2 is assumed to be equal to ΔT_3).

A_1 = cross-sectional area of both facings taken together.

A_2 = cross-sectional area of two opposite edges of the test panel.

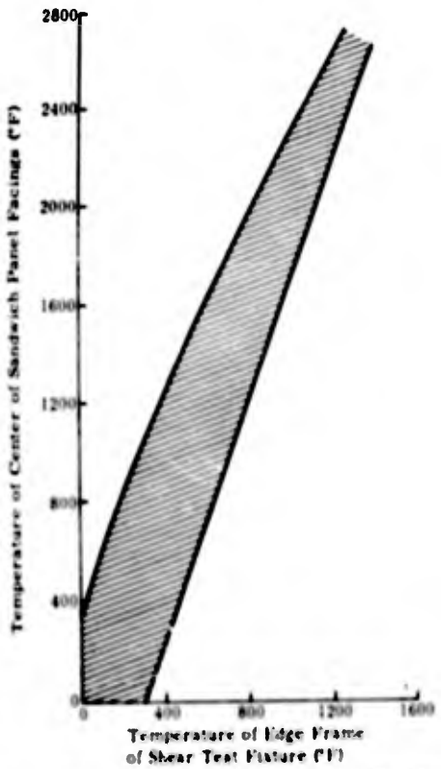

Fig. C-2. Control Chart for Use During Heating and Cooling of T24 Shear Test Panels

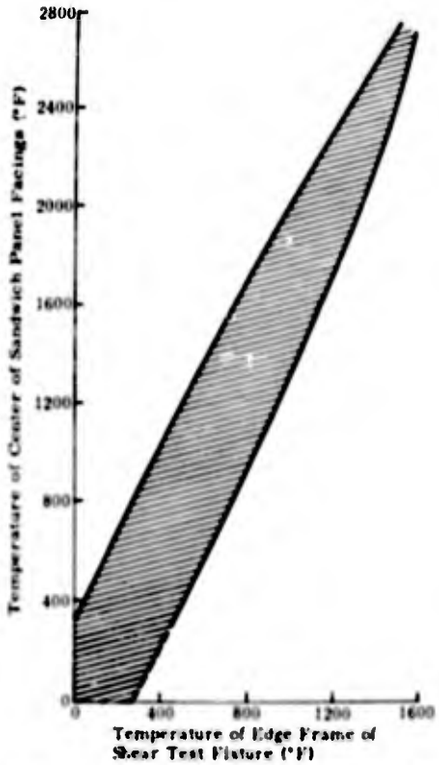

Fig. C-3. Control Chart for Use During Heating and Cooling of B-56 Shear Test Panels

A_3 = cross-sectional area of two opposite fixture frames.

The properties E, α and μ (defined at end of Appendix B) in Eq (C-1) vary with temperature. If equations were known which describe each property as a function of T_1 and T_3, then Eq (C-1) could be written accordingly with functions of T_1 and T_3 substituted for E, α and μ. In the absence of such functional descriptions of the properties it is convenient to solve the problem by the following trial-and-error method:

A value of facing temperature equal to T_1 is selected. The corresponding facing properties and allowable stresses are determined and inserted into Eq (C-1). A trial value of frame temperature T_3 is selected. The corresponding edge and frame properties E_2, α_2, E_3 and μ_3 are substituted together with ΔT_3 into Eq (C-1). The resulting calculated value of σ_1 is compared with the allowable stress, and then the process is repeated for successive trial values of ΔT_3 until a value is found which gives the correct σ_1. The lines enclosing the shaded areas of Figs. C-2 and C-3 represent plots of T_1 versus T_3 as determined by this method.

Equation (C-1) for the shear test setup is a relatively simple special case of the more general problem of a flat rectangular assembly composed of an indefinite number of facings and edge members.

The following analysis applies to this generalized problem but is restricted to a nonbending case with thermal and geometrical symmetry with respect to the three principal planes which contain the centerlines of the assembly (cf. Fig. C-1). It is assumed further that:

(1) Hooke's law applies.

(2) The temperature of each member is uniform.

(3) Each edge (longitudinal) member has half of its area on opposing sides of the assembly. This assures a condition of symmetry and precludes thermal bending.

(4) The edge members do not bend; therefore, the facings remain rectangular with straight edges.

(5) Stress is zero at room temperature.

The following symbols are used:

ΔT_i = difference between the actual temperature and 70° F (T_i - 70° F)

A_{xi}, A_{yi} = cross-sectional areas of facings (cf. Fig. C-1)

B_{xi}, B_{yi} = cross-sectional areas of edge members (cf. Fig. C-1)

i, n, p, q = subscripts are employed as follows: (i = 1,2, . . . , n) apply to facings; (i = n + 1, n + 2, . . ., p) apply to edge members which are parallel to the x-direction; (i = p + 1, p + 2, . . . , q) apply to edge members which are parallel to the y-direction.

The equilibrium equations require that, in the absence of external loads, the summation of the forces in either the x- or y-direction is equal to zero. That is:

$$\sum_{i=1}^{i=p} F_x = \sum_{i=1}^{i=n} \sigma_{xi} A_{xi} + \sum_{i=n+1}^{i=p} \sigma_{xi} B_{xi} = 0 \qquad \text{(C-2)}$$

and

$$\sum_{i=1}^{i=q} F_y = \sum_{i=1}^{i=n} \sigma_{yi} A_{yi} + \sum_{i=p+1}^{i=q} \sigma_{yi} B_{yi} = 0. \qquad \text{(C-3)}$$

The compatibility condition states that the total strains of all members parallel to the x-axis are equal to one another. Similarly, all strains in the y-direction are equal. The condition is written in equation form as

$$\epsilon_{x1} = \epsilon_{x2} = \epsilon_{x3} = \cdots = \epsilon_{xp} = \epsilon_x \qquad \text{(C-4)}$$

and

$$\epsilon_{y1} = \epsilon_{y2} = \epsilon_{y3} = \cdots = \epsilon_{yq} = \epsilon_y. \qquad \text{(C-5)}$$

The stress-strain equations, including thermal effects, are

$$\sigma_x = \frac{E}{1-\mu^2}\left(\epsilon_x + \mu\,\epsilon_y\right) - \frac{E\alpha\Delta T}{1-\mu} \qquad \text{(C-6)}$$

and

$$\sigma_y = \frac{E}{1-\mu^2}\left(\epsilon_y + \mu\,\epsilon_x\right) - \frac{E\alpha\Delta T}{1-\mu} \qquad \text{(C-7)}$$

for the facings, and

$$\sigma_x = E\,\epsilon_x - E\alpha\Delta T \qquad \text{(C-8)}$$

and

$$\sigma_y = E\,\epsilon_y - E\alpha\Delta T \qquad \text{(C-9)}$$

for the edge members.

The unknown strains ϵ_x and ϵ_y are readily evaluated by the simultaneous solution of Eqs (C-2) and (C-3) with the substitution of the stress Eqs (C-6) (C-7), (C-8) and (C-9).

The resulting total strain equations are

$$\epsilon_x = \frac{RV - UW}{RQ - SU} \qquad \text{(C-10)}$$

and

$$\epsilon_y = \frac{QW - SV}{RQ - SU} \qquad \text{(C-11)}$$

where

$$R = \sum_{i=1}^{i=n}\left(\frac{EA}{1-\mu^2}\right)_i + \sum_{i=p+1}^{i=q}\left(EB_y\right)_i \qquad \text{(C-12)}$$

$$S = \sum_{i=1}^{i=n}\left(\frac{\mu EA}{1-\mu^2}\right)_i \qquad \text{(C-13)}$$

$$W = \sum_{i=1}^{i=n} \left(\frac{E\alpha TA_y}{1-\mu}\right)_i + \sum_{i=p+1}^{i=q} \left(E\alpha \Delta T B_y\right)_i \quad \text{(C-14)}$$

$$Q = \sum_{i=1}^{i=n} \left(\frac{EA_x}{1-\mu^2}\right)_i + \sum_{i=n+1}^{i=p} \left(EB_x\right)_i \quad \text{(C-15)}$$

$$U = \sum_{i=1}^{i=n} \left(\frac{\mu EA_x}{1-\mu^2}\right)_i \quad \text{(C-16)}$$

$$V = \sum_{i=1}^{i=n} \left(\frac{E\alpha TA_x}{1-\mu}\right)_i + \sum_{i=n+1}^{i=p} \left(E\alpha \Delta T B_x\right)_i \quad \text{(C-17)}$$

The thermal stress in either the facings or the edge members is obtained from Eqs (C-6), (C-7), (C-8) or (C-9) with values of ϵ_x and ϵ_y from Eqs (C-10) and (C-11). The stress equations developed here are general enough to be usable in a considerable number of problems similar to the shear test assembly analyzed in this report. In the case of the shear test assembly, the panel is square and all edges are assumed to be identical. It follows that

$$R = Q = \left(\frac{EA}{1-\mu^2}\right)_1 + (EB)_2 + (EB)_3 \quad \text{(C-18)}$$

$$V = W = \left(\frac{E\alpha\Delta TA}{1-\mu}\right)_1 + (E\alpha B\Delta T)_2 + (E\alpha B\Delta T)_3 \quad \text{(C-19)}$$

and

$$U = S = \left(\frac{\mu EA}{1-\mu^2}\right)_1. \quad \text{(C-20)}$$

With the further assumption that $T_2 = T_3$ and with the substitution of A_2 for B_2 and A_3 for B_3 into the facing stress equation, Eq (C-1) is obtained for the shear test assembly.

UNCLASSIFIED